

THE UNIVERSITY OF HULL

**EVALUATION AND ANALYSIS OF WEAR IN
PROGRESSIVE CAVITY PUMPS**

being a thesis submitted for the Degree of

Doctor of Philosophy

in the University of Hull

by

Lucy Victoria Whittaker

B.Sc., UMIST

September 2003

WARNING

This document contains Mono Pumps Ltd's confidential and trade secret information, and is given to the receiver in confidence. The receiver accepts the document in confidence and agrees that, except with Mono Pumps Ltd's prior expressed written permission, it will (1) not use or disclose to others the document or any copy thereof or the confidential trade secret information contained therein: (2) not copy or reproduced the document whole, or part: and (3) upon completion of the need to retain the document, or upon demand, return the document, all copies thereof and all material copied therefrom.

*Success is the reward
of
perseverance*

Progressive cavity pumps are used in the transportation of slurries. The pumping element consists of a single helical rotor, which intermeshes with a double helical resilient stator, to create the moving cavities that transport the slurry. Both components suffer from wear, at different rates, due to relative sliding movement of the rotor to the stator, and the presence of the abrasives carried within the slurry. For a pump manufacturer to remain active in the market they must provide the customer with optimised material selection, for both wearing parts, at a competitive price.

Wear is not an intrinsic material property and its value is dependent upon the conditions within each individual tribological system. In order to improve or optimise the wear life of a system, it is first vital to understand the complexity of the mechanisms that generate the material loss. This thesis achieves this goal, with specific reference to a pumping system, by analysing the wear mechanisms of the pumping element components in progressive cavity pumps and evaluating how the wear severity changes with the system parameters. The in-depth study has enabled a new wear model to be proposed which describes how the behaviour of the abrasive particles contribute to the wearing process, in the pumping element of a progressive cavity pump.

Hard particle laboratory wear tests were reviewed and assessed to determine their suitability for assessing the wear performance of rotor and stator materials. It was concluded that no one standard laboratory test was suitable and recommendations are given for two tribometers which specifically meet the tribological needs of the pumping system.

Without the poor, unpredictable performances of Manchester City FC, in the late 1990's. I would never have met Allan Matthews and been talked into starting my Ph.D. So thanks to them and to Allan, for not only his role as my supervisor, but for being lenient with the truth, on that fateful day, on what the next four years of my life would entail !

I am indebted to Mono Pumps Ltd. for providing the opportunity of an exciting, whilst extremely challenging, problem for me to study and the funding, support and, most importantly, time to enable me to complete, what has been an ambition since my teenage years. I'd like to give particular thanks to Gareth Thomas, Chris Griffiths, John Drane, Bill Yates, Jim Mellor, Rob Pastore, Paula Edwards and Rachel Munton for their individual contributions and support.

A huge thank you of support to my husband Kevin, Ali, parents, sister Sue, Paul, and Bruv, particularly in the final year, when things became quite intense, stress levels ran high and I sounded like a broken record as I became totally absorbed in writing my thesis. And thanks to the patience of my friends who I thought of often but gave little time to during my studies.

A special thank you to Dave Winder, of Sulzer Metco, for his lateral thinking in our brain storming sessions in the early days, his constant moral support and supply of coated samples. The tireless assistance, patience and chat of Gary Robinson, that I, like many other students, have to thank for ensuring we had great quality photographs for our theses and providing technical support. And finally to CT, for his infectious enthusiasm and inspirational espresso breaks.

	<u>Page No.</u>
Chapter 1 Introduction	1
Chapter 2 Fundamentals of progressive cavity pumps	
2.1 <i>Operating principles</i>	8
2.2 <i>Pumping element geometry</i>	13
2.3 <i>Stator loads</i>	13
2.3.1 <i>Drive shaft loads</i>	13
2.3.2 <i>Rotor loads</i>	13
2.4 <i>Interference fit between the rotor and stator</i>	15
2.5 <i>Slurry velocities within the pumping element</i>	18
2.5.1 <i>Fluid velocity</i>	19
2.5.2 <i>Particle velocity</i>	19
2.6 <i>Influence of operating parameters</i>	20
2.6.1 <i>Discharge pressure</i>	20
2.6.2 <i>Speed</i>	21
2.7 <i>Rotor and stator material selection</i>	21
2.7.1 <i>Rotor surfaces</i>	21
2.7.2 <i>Stator materials</i>	23
2.8 <i>Slurry characteristics</i>	24
2.9 <i>References</i>	24
Chapter 3 Wear by hard particles	
3.1 <i>Introduction</i>	26
3.2 <i>Wear by abrasive slurries</i>	28
3.2.1 <i>Abrasion by plastic deformation</i>	29
3.2.2 <i>Solid particle erosion</i>	34
3.2.3 <i>Wear by brittle fracture</i>	38
3.2.4 <i>Factors influencing wear</i>	41
3.3 <i>Rubber abrasion and wear</i>	48
3.3.1 <i>Dry abrasion</i>	49
3.3.2 <i>Abrasion of rubber under wet conditions</i>	52
3.3.3 <i>Erosion of rubber</i>	55

	<u>Page No.</u>
3.4 <i>Hardness relationships between contact surfaces and abrasive particles</i>	56
3.5 <i>References</i>	61
Chapter 4 An appraisal of hard particle laboratory wear tests	
4.1 <i>Introduction</i>	65
4.2 <i>Hard particle laboratory wear tests</i>	65
4.2.1 <i>ASTM G65, G105 & B611 Wheel abrasion tests</i>	66
4.2.2 <i>Micro-scale abrasion test</i>	74
4.2.3 <i>ASTM G75 Miller abrasion test</i>	79
4.2.4 <i>ASTM G132 Pin abrasion test</i>	82
4.2.5 <i>Rotating-Oscillating-Sliding tribometer</i>	85
4.2.6 <i>Slurry erosion tests</i>	87
4.3 <i>References</i>	92
Chapter 5 Design and validation on the simulated ‘in-service’ wear test rig	
5.1 <i>Introduction</i>	95
5.2 <i>Design criteria</i>	95
5.2.1 <i>Wear rig configuration</i>	96
5.2.2 <i>Design problems</i>	97
5.3 <i>Test conditions</i>	98
5.3.1 <i>Contact conditions</i>	98
5.3.2 <i>Acceleration of service conditions</i>	99
5.3.3 <i>Standard test conditions</i>	100
5.3.4 <i>System parameters</i>	100
5.3.5 <i>Monitoring of system variables</i>	104
5.4 <i>Interpretation of test results</i>	104
5.4.1 <i>Assessment of surface damage to rotors</i>	105
5.4.2 <i>Assessment of surface damage to stators</i>	108
5.5 <i>Evaluation of particle loading conditions</i>	111
5.6 <i>Evaluation of the lubrication film thickness</i>	113
5.7 <i>References</i>	114

	<u>Page No.</u>
Chapter 6 Modelling the tribological system of the pumping element	
6.1 <i>The wear system in the pumping element</i>	115
6.1.1 <i>Characteristic wear features in the stator</i>	115
6.1.2 <i>Characteristic rotor wear features</i>	121
6.1.3 <i>Effect of particle size</i>	125
6.2 <i>Comparison with existing wear theories and models</i>	130
6.3 <i>Influence of system parameters</i>	132
6.3.1 <i>Velocities within the pumping element</i>	132
6.3.2 <i>Differential pressure across the length of the pumping element</i>	138
6.3.3 <i>Contact pressure between the rotor and stator</i>	142
6.3.4 <i>Rotor surface properties</i>	146
6.4 <i>References</i>	149
Chapter 7 Comparison of the wear system in the pumping element to standard hard particle laboratory wear tests	
7.1 <i>Introduction</i>	151
7.1.1 <i>Wet rubber wheel abrasion test</i>	152
7.1.2 <i>Micro-scale abrasion test using a hardened steel ball and a resilient rubber ball</i>	153
7.1.3 <i>Slurry jet erosion test</i>	154
7.2 <i>Evaluation of lubrication conditions of the abrasion tests</i>	156
7.2.1 <i>Wet rubber wheel abrasion test</i>	157
7.2.2 <i>Micro-scale abrasion test</i>	158
7.3 <i>Effect of contact velocity</i>	164
7.4 <i>Wet rubber wheel abrasion test results</i>	165
7.4.1 <i>Comparison of wear mechanisms with the pumping element</i>	166
7.4.2 <i>Ranking of rotor coatings</i>	169
7.4.3 <i>Versatility of test apparatus</i>	173
7.5 <i>Micro-scale abrasion test results</i>	174
7.5.1 <i>Comparison of wear mechanisms with the pumping element</i>	174
7.5.2 <i>Ranking of rotor coatings</i>	174
7.5.3 <i>Versatility of test apparatus</i>	175

	<u>Page No.</u>
7.6 <i>Slurry jet erosion test results</i>	178
7.6.1 <i>Simulate of type 'a' stator wear regime</i>	178
7.6.2 <i>Comparison of wear mechanism with the pumping element</i>	178
7.6.3 <i>Ranking of rotor coatings</i>	180
7.6.4 <i>Versatility of test apparatus</i>	182
7.7 <i>Criteria for two new tribometers</i>	183
7.7.1 <i>Test criteria for the assessment of stator materials</i>	184
7.7.2 <i>Test criteria for the assessment of rotor materials</i>	184
7.7.3 <i>Assessment of 'real' slurries</i>	185
7.8 <i>References</i>	186
Chapter 8 Conclusion & Recommendations for further work	
8.1 <i>Conclusion</i>	187
8.2 <i>Recommendations for further work</i>	189
8.2.1 <i>Development of the wear model for progressive cavity pumps</i>	189
8.2.2 <i>Development of the tribometers</i>	190
Appendix	
A (a): <i>Example of profile of a stator from the Mitutoyo CHN1008 co-ordinate measuring machine</i>	191
(b): <i>Example of an AutoCAD drawing for determining the major and minor dimensions of the stator</i>	191
B <i>Data for calculating the particle loading conditions</i>	192

An introduction to tribological testing

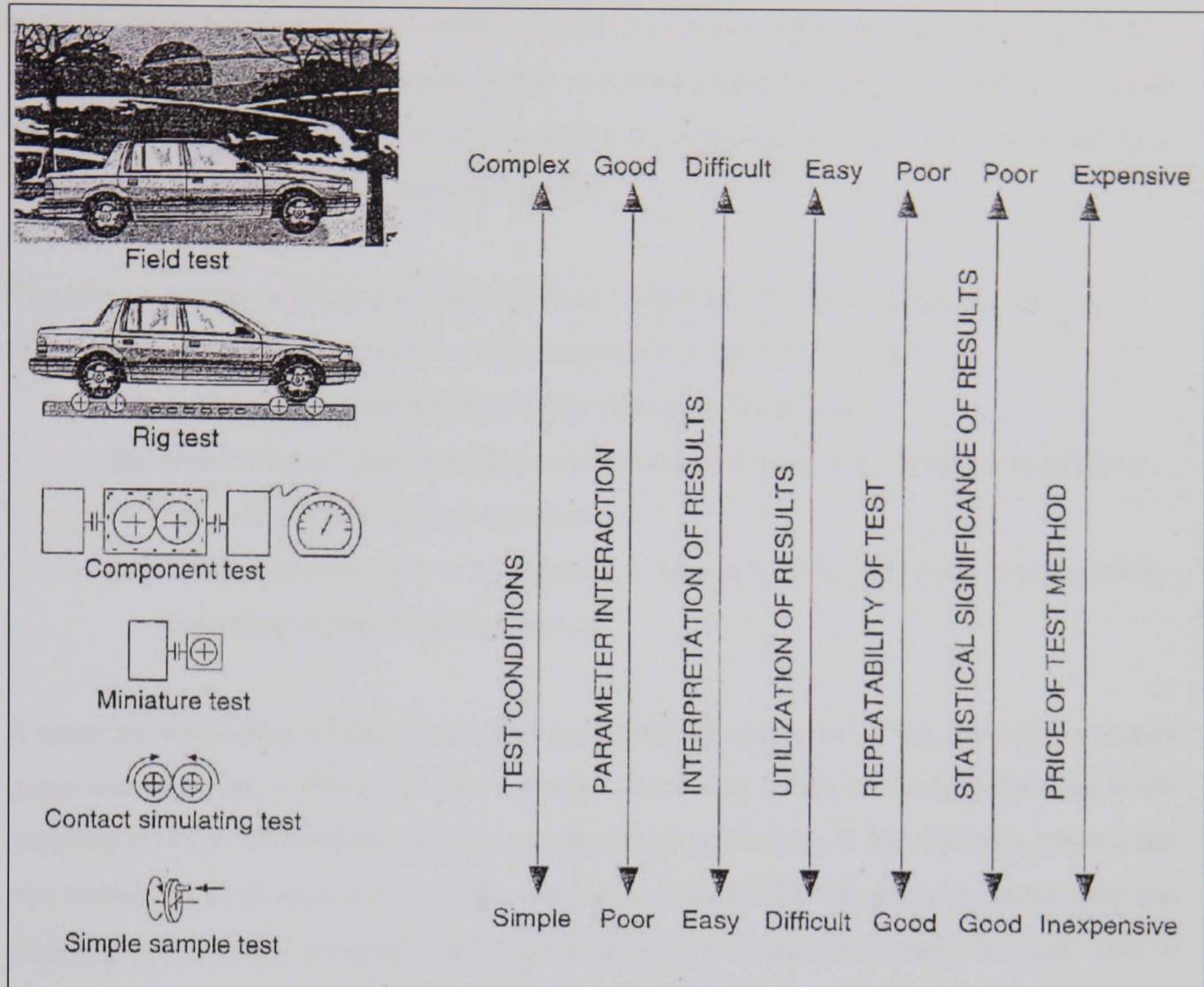
The technology of progressive cavity pumps has been around for over 60 years. However, knowledge and understanding of the unique wear behaviour within the pumping element of this type of positive displacement pump is very limited. That which is known is based upon empirical data, and the lack of understanding, after all these years, emphasises the complexity of the wear system involved.

One of the main features of progressive cavity pumps is the interference fit between the rotor and stator and the resultant wear which prevails. Wear rates vary dramatically depending upon the type of abrasive being pumped. The pumping element of progressive cavity pumps consists of a one start helix rotor turning inside a two start helix stationary resilient tube, known as a stator. Slurry is transported from the inlet to the outlet within the sealed capsulisms which are created from the geometry of the two components. In order to prevent the slurry slipping backwards, an interference fit must exist between the rotor and stator to create the seal lines. The action of the rotor rubbing against the resilient stator material generates a hydrodynamic film using the fluid that is being pumped. The lubrication film is essential to prevent the catastrophic effects of frictional heat between the two rubbing components. However the negative side of using the slurry as the lubricant is when it contains hard abrasive particles. Along with the fluid, the abrasive particles also pass through the seal lines and drastically reduce the life of the rotors and stators. To compensate, rotors and stators are manufactured from or coated with wear resistant materials. A common choice of rotor surface is electro-deposited hard chromium plate which is generally considered as the industrial standard for slurry applications, such as primary sewage sludge pumping and mineral processing. Other alternatives available on the market are hardened tool steels, nitrided steels, solid ceramics and thermally sprayed coatings. The stators need to be resilient, so the choice of materials tends to favour rubbers and polymers, and often abrasion resistance has to be balanced against chemical compatibility.

The impetus behind this study was the proactive desire of one progressive cavity pump manufacturer to obtain an edge on the competition, essential in today's highly competitive world markets. The company wanted to significantly reduce their development lead times of new wear resistant coatings for their rotors in order to expand their potential market into applications where traditionally the wear life capability of the pumps was unacceptable.

Their approach entailed the testing of individual coated rotors in a closed pump loop, pumping a silica sand slurry and recording the performance of the pump until the flow rate fell by 15%. Pre- and post-performance testing were required to then determine whether the fall was due to wear of the coating and/or the elastomeric stator. This engineering approach was not only time consuming but labour intensive and as thermal spray technology advanced to produce reliable wear resistant coatings such as tungsten carbide as replacements for hard chromium plate, the duration of the wear tests began to run into months for the assessment of a single coating. In an increasingly competitive market these types of leads times for new products were unacceptable.

To study or evaluate a wear system, the analysis must be conducted under the same tribological conditions as the service application. However, analysis within actual industrial tribological systems can be extremely time consuming, costly and frequently impractical. Accelerated tribological testing of components can be performed by increasing load, speed, contact pressure, temperature or rate of contamination, or by decreasing the lubricant viscosity or additives. In real machines, changes to many of these parameters are not easily achieved and it is often more appropriate to perform accelerated testing in a laboratory environment on rigs where the real contact conditions are simulated and “overloaded”, with more controlled parameter variation possibilities. Uetz et. al. ^[1] divided the simplification of a tribological test into six levels of simulation, as shown in figure 1.1. Test complexity decreases when moving from field test level to the simple sample test. As the simplicity of the test increases the interpretation of the results becomes easier, the cost of each test reduces and the repeatability and statistical significance of the results improves. However the practical utilisation of the results and the interactive effects between the different parameters become less apparent. The considerable risk with the use of simplified accelerated tests is if the acceleration is introduced by overloading, which can stimulate a change in the wear or lubrication mechanism ^[2]. The consequence of this is to produce results of little significance for the considered application. Results from simplified and overloaded accelerated tests are only reliable if measures are taken to ensure that the simulated contact conditions are similar to, or are in a controlled relationship with, those of the real component.

Figure 1.1 : The six levels of simulated tribological testing ^[1]

Swanson ^[3] studied the usefulness of laboratory tests to evaluate the durability of agriculture equipment and found major limitations in their ability to simulate all of the wear mechanisms observed in the field trials. He found a good correlation between relative wear resistances of steels between the laboratory tests and the field trials but significant differences with heterogeneous materials due to the relative scale of the abradant size to the distribution of the hard phase in the materials. Tylczak et. al. ^[4] compared the results from different abrasive laboratory tests with the behaviour of ferrous based alloys in field trials for the mineral processing industry. They found comparable results where the laboratory test exhibited similar wear mechanisms to those in the field trials. However they stressed that the use of hardness as a method of predicting wear behaviour of materials should be used with caution, and only as a first good indication of resistance to pure abrasion, because of effects such as changes in the wear modes and work hardening. So, while laboratory wear tests can help eliminate poorly performing materials, Tylczak et. al. concluded that they will rarely be able to unambiguously identify the optimum material to use for a particular wear application.

Consequently, in order for the pump manufacture to be proactive they required a laboratory-scale wear test which would accurately simulate the wear conditions in the pumping element of their pumps whilst producing rapid and meaningful results that could be easily interpreted. The fundamental crux of the project lay within achieving a full understanding of the tribological system of the pumping element.

Therefore a primary objective of the thesis was to understand and simulate the wear behaviour in the pumping element of progressive cavity pumps in order to:-

- (a) establish the variables which effect the wear behaviour
- (b) obtain a better understanding as to the material properties required to improve the wear life of the pumping element
- (c) design and manufacture a laboratory wear test to rank rotor and stator materials according to their wear behaviour

A clear understanding of the theory and principles of operation of the progressive cavity pump was essential to determine the variables which may effect the wear behaviour in the pumping element. These fundamentals are described in Chapter 2. Most of this information was correlated from previous research projects conducted by the pump manufacturer and other published pump literature. Other useful sources of information were the web sites of other progressive cavity manufacturers and a German Ph.D. thesis by Wirth on “Hydraulics and tribological modelling of progressive cavity pumps”^[5]. From this it was concluded that the following factors may contribute to or have an effect on the wear behaviour:-

- i) the slurry velocities – rubbing, particle and fluid, which are directly related to the geometry of the pump and the operating speed
- ii) the slurry characteristics of the product, i.e. particle concentration, shape, size and hardness
- iii) the movement of the abrasive particles within the slurry whilst being pumped
- iv) the load applied at the interface between the rotor and the stator
- v) the presence and thickness of the lubricating film
- vi) the intrinsic material properties of the bulk, surface and near surface of the rotor and stator
- vii) the stresses subjected on the pumping element by the eccentric movement of the rotor
- viii) the differential pressure between the inlet and the outlet of the pumping element

A review of wear mechanisms by hard particles, presented in Chapter 3, led to the conclusion that, by definition, the wear experienced in the pumping element was that of low stress abrasion. Low stress abrasion occurs when the applied loads are small enough not to cause fracture to the abrasive particles. Mechanisms involved with this type of wear are two- and three-body abrasion, and parallel solid particle erosion where the impingement angle tends to zero. During the review it became apparent that a certain degree of confusion and variation exists regarding the terminology of wear mechanisms, and often different terms are used to describe fundamentally the same wear behaviour. Attempts have been made by ASTM and DIN to standardise the wear terminology ^[6,7].

An inadequacy in wear modelling became apparent after reviewing classical abrasive wear theories and wear studies by various authors, which altered the emphasis of the thesis. Two non-intrinsic material properties, used to describe the abrasive wear resistance of a surface, are the wear coefficient and the dimensional wear rate. These are two different entities although often confused and misused. The dimensional wear rate is determined experimentally and only relates to the wear system in which it was derived. Whereas the wear coefficient is an unitless quantity defined as the wear constant of a surface under given conditions and for engineering purposes is defined as the dimensional wear rate divided by the hardness of the wearing surface.

Thus, it became apparent that since a large hardness differential existed between the two contacting surfaces in the pumping element it was questionable as to whether classical abrasive wear theories could be used to model the wear resistance of the rotor coatings and stator materials. Based on Archard's adhesive wear equation, Rabinowicz's ^[8] model of abrasive wear only considers the hardness of one of the two contacting surfaces in the system and most studies in deriving the dimensional wear rate assume the hardness value to remain constant throughout the wearing process.

The importance of the difference between these two wear rate entities highlighted the fact that wear is not an intrinsic material property and the slightest system variable change within the pumping element could have a direct effect on the wear life of the coated rotor and the stator. Since the majority of the variables within the system are beyond the control of the pump manufacturer, quantifying the wear life of these components is very difficult. Subsequently, an in depth study of the effects of these system variables was required using a specifically designed simulated in-service test rig. The design and validation of the rig is described in Chapter 5.

The results from the study are discussed in Chapter 6. A new wear model is proposed, which describes how the behaviour of the abrasive particles interact with the relative movement of the rotor and stator to initiate the wearing process. Comparisons are drawn between the new model and existing pump wear models and classical wear theories.

Rather than design a completely new laboratory wear test it was decided that it would be prudent to review existing standardised equipment to determine whether suitable test procedures already existed. An appraisal of the studies relating to laboratory hard particle wear testing is discussed in Chapter 4, from which it was concluded that the suitability of three wear test procedures should be evaluated, which were:-

- (i) the wet rubber wheel abrasion test
- (ii) the micro-scale abrasion test
- (iii) the slurry jet erosion test

Before test work could commence various modifications had to be made to existing available equipment. A dry rubber wheel abrasion tester had to be modified to accommodate a wet slurry feed which entailed discussions with numerous organisations in order to determine the optimum configuration. The variations in slurry jet erosion apparatuses were found to be vast and there appeared to be no standardised method. Hence suitable equipment had to be specifically designed and made to modify the simulated in-service test rig to accommodate a slurry jet erosion test.

From a comparison of the contact conditions between the simulated wear test and the laboratory tests it became apparent how critical the relationship was in the selection of an appropriate tribometer. Chapters 6 and 7 describe the in-depth study of the wear morphology and wear rates (according to classical abrasion theory) between the two different test levels of tribological testing and the results from the three hard particle laboratory wear tests.

The outcome of the study has produced a new wear model that describes the particle behaviour in the pumping element of a progressive cavity pump in abrasive applications, and recommendations for two tribometers are proposed to assess the wear performance of rotor coatings and stator materials.

1.2 REFERENCES

1. **K. Holmberg**, “*Tribological bases for accelerated testing*”, Operational reliability & systematic maintenance, Eds. Holmberg, K. & Folkesson, A., Elsevier Applied Science, London, pp 31- 50
2. **K. Holmberg**, “*Tribological accelerated testing*”, Finnish Jour. of Trib., 9, 1990, No 3 – 4, pp 13 – 35
3. **P. A. Swanson**, “*Comparison of laboratory abrasion tests and filed tests of materials used in tillage equipment*”, Tribology: Wear test selection for design and application, ASTM STP 1199, A.W.Ruff & R.G.Bayer, Eds., ASTM, Philadelphia, 1993.
4. **J. H. Tylczak, J. A. Hawk & R. D. Wilson**, “*A comparison of laboratory abrasion and field wear results*”, Wear 225-229, 1999, pp 1059 – 1069
5. **W. Wirth**, “*Hydraulics and tribological modelling of progressive cavity pumps*”, Ph.D Diss., Erlangen, Germany, 1993
6. **ASTM**, “*Standard terminology relating to erosion and wear*”, G40, Annual book of ASTM standards
7. **DIN 50 320**, Dec 1979, “*Wear : Terms, systematic analysis of wear processes, classification of wear phenomena*”, pp 1 - 8
8. **E. Rabinowicz, L. A. Dunn & P. G. Russel**, “*A study of abrasive wear under three-body conditions*”, Wear 4, 1961, pp 345 – 355.

Fundamentals of progressive cavity pumps

2.1 OPERATING PRINCIPLES

A progressive cavity pump is a rotary positive displacement pump defined as, “a machine in which liquid is trapped in confined volumes and transported from an inlet port to an outlet port by a rotational movement of the pumping element or elements” ^[1]. Unlike centrifugal pumps a positive displacement pump does not develop pressure, it only produces a flow of fluid. The downstream process, or piping system produces the resistance to the flow and thus generates a pressure in the piping system and the discharge portion of the pump ^[2].

The principle of a progressive cavity pump was invented by Rene Moineau ^[3], a French mathematician, in 1930. His work was based on the geometric fact that the hypocycloid created when a rolling circle rotates within a fixed circle twice its size, is a straight line path and not a curved one, figure 2.1 ^[4]. Utilising this concept he designed a pump that did not require a complex valve arrangement.

The main components of a progressive cavity pump are the rotor and stator, which together constitute the pumping element. The rotor, a single start helical screw, rotates eccentrically within a static two start helical sleeve, the stator. The meshing of the two parts opens and closes a cavity which moves from one end of the pumping element to the other thus transporting a volume of liquid, figure 2.2. As one cavity diminishes, the opposing cavity is increasing at exactly the same rate so the sum of the two discharges is a constant. The result is a pulsationless positive displacement flow with no valves ^[5]. The entrapment and movement of an initial volume of liquid creates a vacuum on the suction side which induces the flow of liquid into the pump. In order to reduce the internal leakage of the pumped liquid, it is normal practice to manufacture the stator from a resilient rubber material and to proportion it so that an interference fit exists between the rotor and stator.

Figure 2.1 : Hypocycloid movement – Point A on the inner circle follows a straight line path as it rolls within a circle twice its size ^[4]

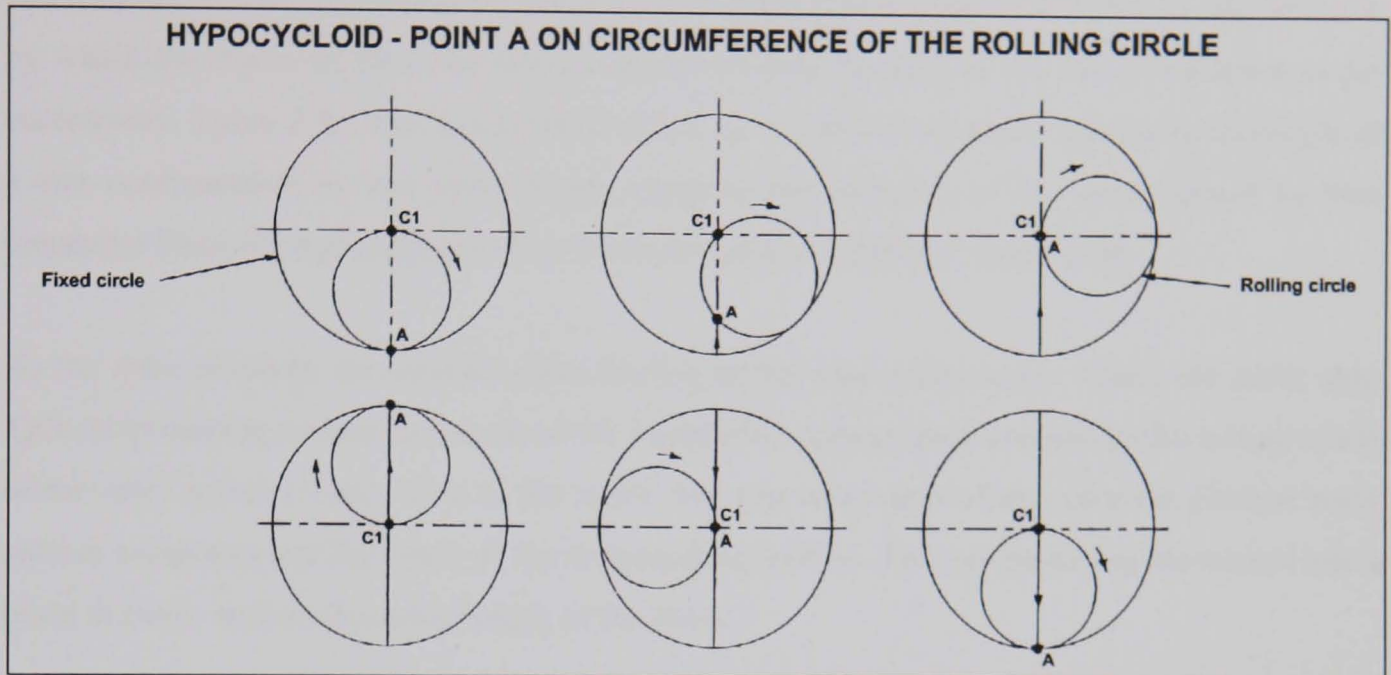
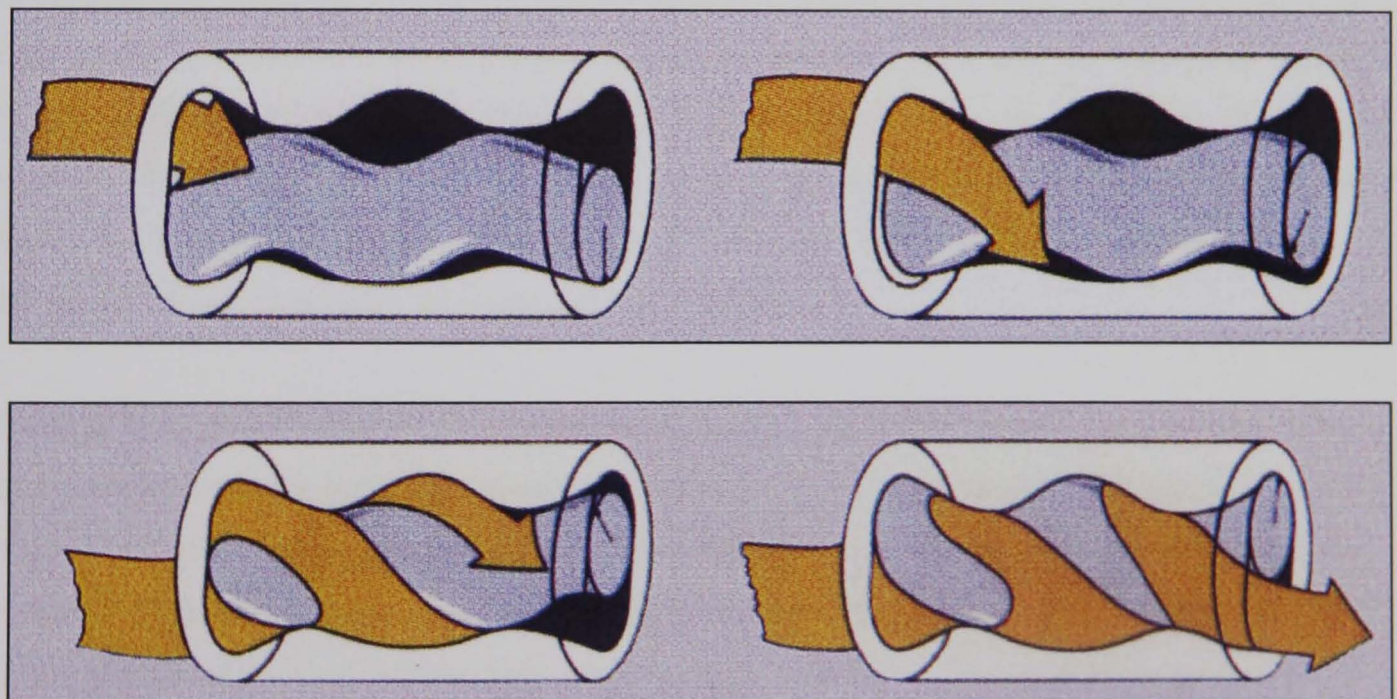


Figure 2.2 : The pumping element showing the capsulisms and movement of product ^[6]



The single start helical rotor has a constant circular cross section, which is at right angles to its axis, at any point along the length. The centre of each successive circular section lies along the helix, the axis of which constitutes the axis of the rotor. The radius of the helix, i.e. the distance by which the centre of the rotor section is off-set from the axis of the rotor, is known as the eccentricity, figure 2.3a. The double helix stator has a constant cross-section along its length of a slot configuration of two semi-circles, equal to the diameter of the rotor, joined by two tangential lines of lengths equal to four times the rotor eccentricity, figure 2.3b.

As the rotor revolves, the circular cross section of the rotor reciprocates within the stator slot. This reciprocating motion is a result of the straight line hypocycloid created by the rolling circle of the rotor and the fixed circle in the stator. For one revolution of the rotor the circular rotor section completes one full cycle of the reciprocating motion. This reciprocating movement takes place at every section along the length of the stator.

As the rotor turns eccentrically inside the resilient stator, a compressive force is created between the two components. This compression provides the seal between the suction and discharge end and enables the pumping element to operate against a discharge pressure. The compressive fit forms two continuous ribbons of contact, known as 'seal lines' that are 180° apart and extend the entire length of the pumping element ^[4,5,7,8]. During normal operation the lines of contact recreate themselves every revolution and move continuously at uniform velocity towards the outlet. The minimum stator length for securing a complete seal between the rotor and stator is that which can accommodate an internal twist of 360°.

The seal lines encapsulate the fluid cavities or 'capsulisms'. The reciprocating motion of the rotor section displaces the fluid capsulisms along the length of the stator from the inlet to the outlet. For one revolution of the rotor the capsulisms travel an axial distance equal to the stator pitch and displaces a fixed volume of liquid. Irrespective of the position of the rotor in the stator the magnitude of the fluid volume will always remain constant ^[9]. Therefore the capacity of the pump is proportional to the operating speed. An increase in rotor speed results in an increase in flow volume by the same proportion.

Figure 2.3a : Geometry of the rotor ^[4]

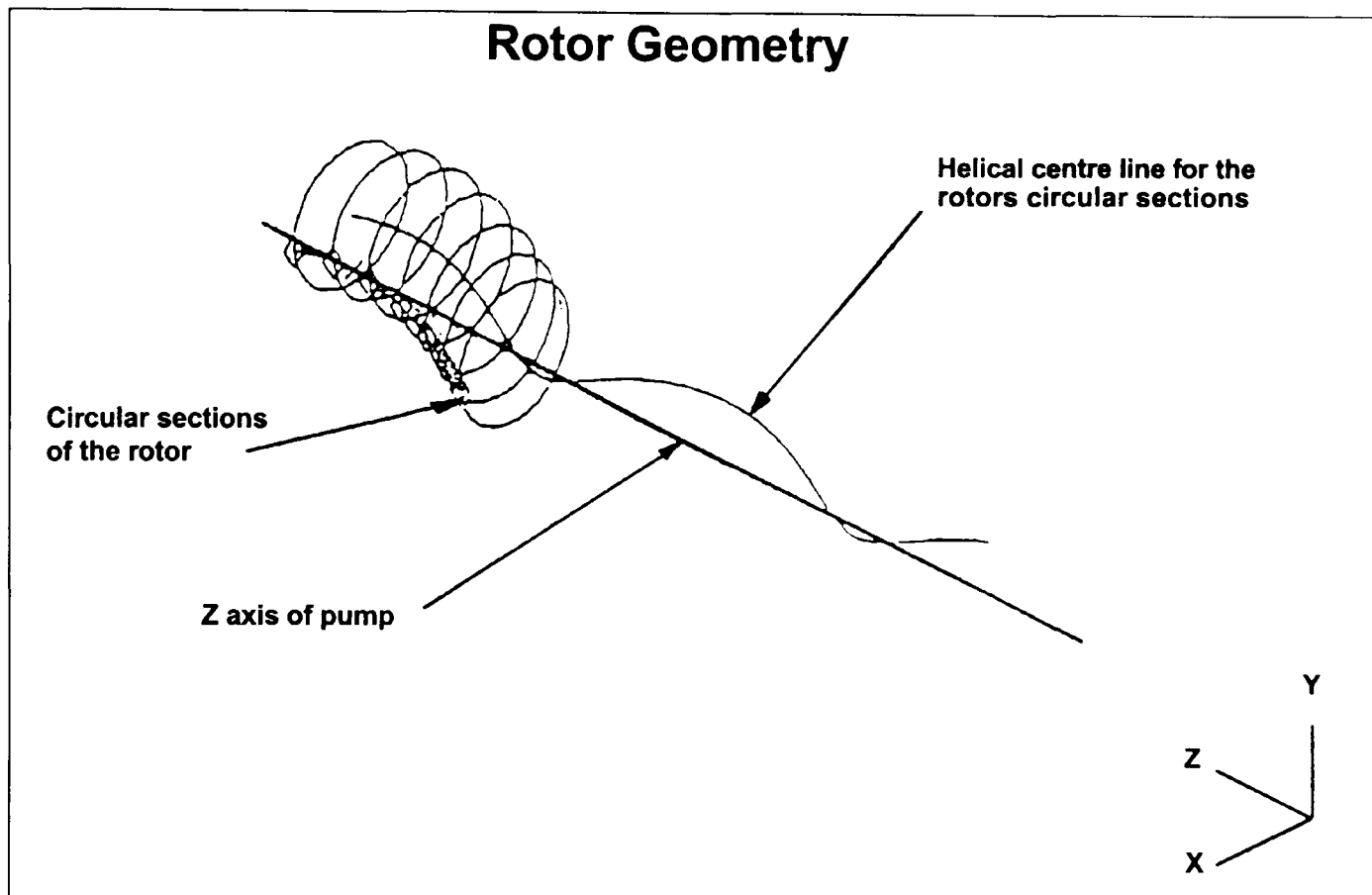
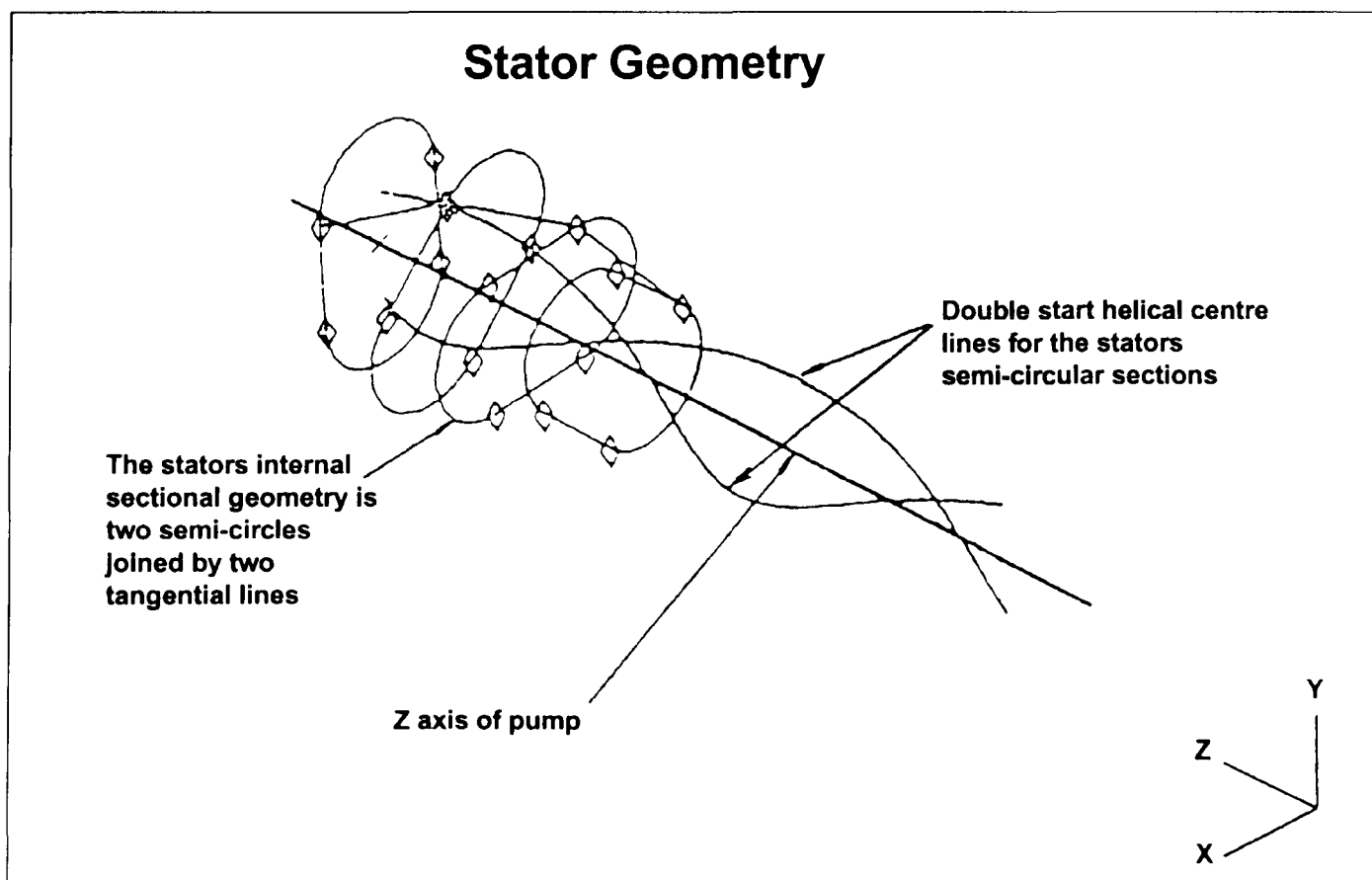
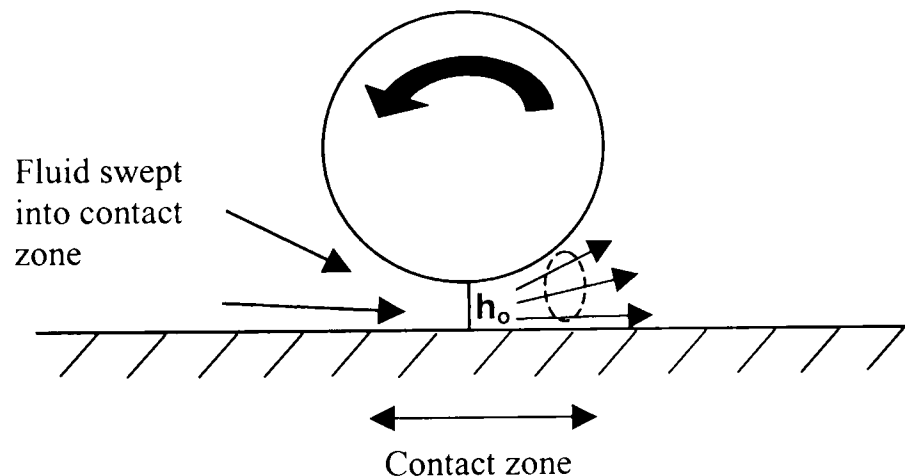


Figure 2.3b : Geometry of the stator ^[4]



For the pumping element to operate a lubricating film must be generated between the interface of the rotor and stator. This film is generated hydrodynamically by the relative movement of the two components with the pumping liquid acting as the lubricant. Without lubrication the frictional heat generated by the rubbing action of the two contacting surfaces would cause catastrophic failure to the stator. Arguments have been raised as to whether the lubrication conditions are strictly hydrodynamic ^[4]. In Belcher's ^[8] study of pressure distribution within the pumping element, he describes the presence of pressure spikes at every location around the stator slot as the rotor passes by. He relates the motion of the rotor along the stator slot to be similar to a converging-diverging wedge, figure 2.4, where the pressure in the fluid film, between the wedge and stationary surface, changes depending upon film thickness. As the fluid is swept into the converging gap by the relative motion of the rotor it reaches a minimum thickness, h_o , where it attempts to decrease in volume. However, since the fluid is incompressible a sudden increase in pressure is generated before the fluid passes beyond this point and the thickness of the film increases again. From Belcher's description it could be surmised that the conditions of lubrication are in fact elasto-hydrodynamic, although it cannot be excluded that the pressure spikes could have been a consequence of experimental error. Further investigation of this subject is, however, outside of the scope of this thesis.

Figure 2.4 : Converging-diverging wedge ^[8]



A progressive cavity pump can transport a diverse range of liquids, from those with the viscosity of water to pastes with the consistency of toothpaste, and from single phase liquids to multi-phase mixes of either liquid and solid, liquid and gas or all three phases. The flow through a progressive cavity pump is nearly axial, unlike all other types of rotary pumps where the flow is forced to travel circumferentially ^[9]. This, combined with low internal velocities, means that virtually no liquid agitation or churning occurs within the pump ^[2].

2.2 PUMPING ELEMENT GEOMETRY

The ratio of the rotor/stator geometry discussed in section 2.1 is known as a 1 in 2 (1:2), implying the single start helical rotor within the two start helical stator. (Note; other geometries are commercially available but for the purpose of this thesis only the 1:2, which is the most commonly used, will be considered). Figure 2.5, diagrammatically describes the diametric features of the pumping element. The length between two peaks on the rotor is called the rotor pitch. The stator pitch (P) is twice the length of the rotor pitch. The displacement of the pump in one revolution is equal to $4edP$, which is the flow area ($4ed$) multiplied by the stator pitch (P) and is sometimes known as the 'swept volume' ^[10]. The variables that are considered as the basis of the design of the pumping element geometry include stator pitch (P), eccentricity (e), major and minor diameters of both the rotor and stator, stator elastomer thickness, flow area, swept volume, fluid, particle and rubbing velocities. These velocities are all mathematically inter-related by the variables e, d and P.

2.3 STATOR LOADS

A consequence of the conventional design of a progressive cavity pump is that certain loads are imposed on the stator during normal operation of the pump, a summary of which is shown in figure 2.6 ^[4,8]. These loads need to be defined, as some or all may have a direct effect on the wear behaviour within the pumping element.

2.3.1 Drive shaft loads

The drive shaft transmits the power from the concentrically driven motor to the eccentric motion of the rotor. For the purpose of the thesis only the Flexishaft type of drive shaft shall be considered, which is a parallel shaft that 'flexes' during operation to accommodate the differences in rotational movement between the rotor and motor. Consequently, the Flexishaft exerts a side load and a bending moment onto the stator via the rotor, which is at a maximum at the inlet and tends towards zero at the outlet of the pumping element.

2.3.2 Rotor loads

The rotor imposes a variety of different loads onto the stator.

- (i) An out-of-balance load, which is a radial load reacted through the point of contact between the rotor and stator as a direct result of the eccentric mounting of the rotor relative to the axis of the pump.
- (ii) The running torque required to rotate the rotor exerts a rotational force on the stator at the point of contact between the rotor and stator.

Figure 2.5 : Diametric features of the pumping element ^[10]

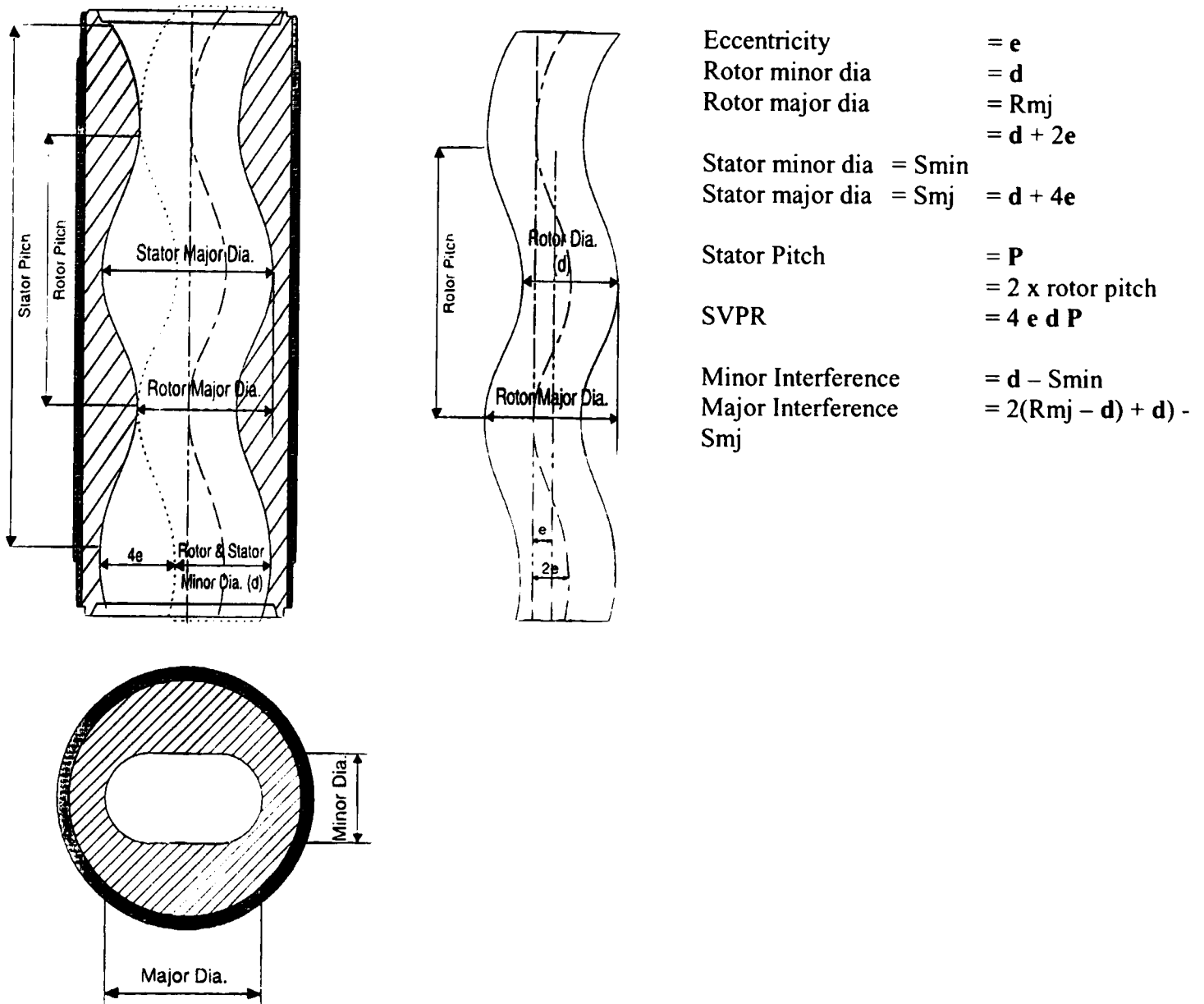
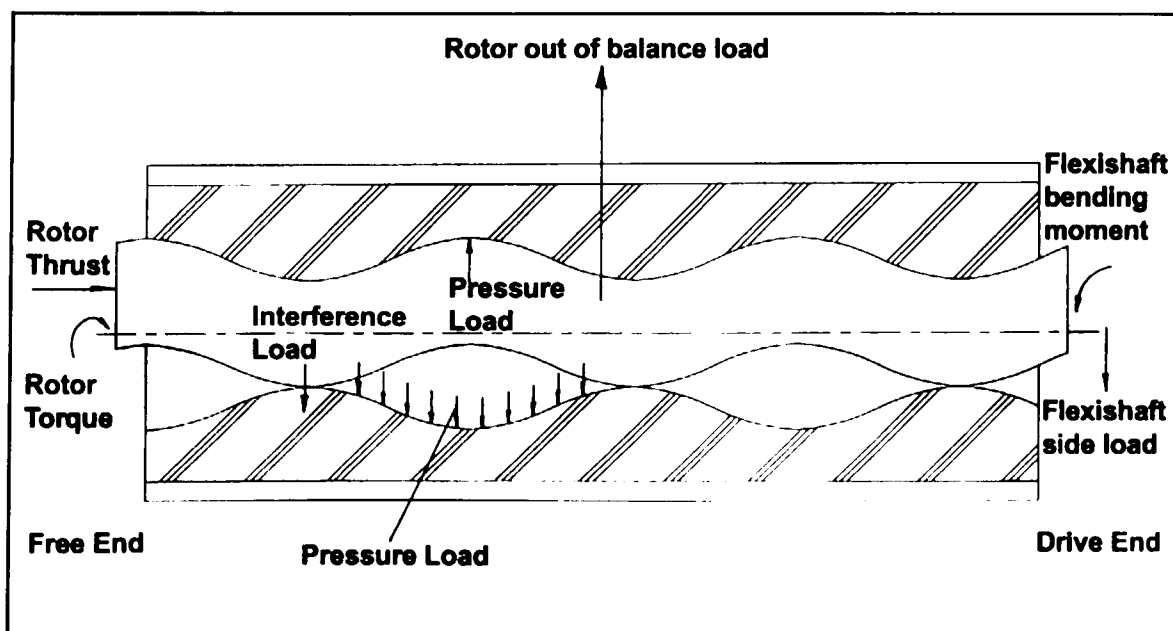


Figure 2.6 : Summary of stator loads ^[8]



- (iii) A rotor thrust force is created during operation due to the pressure differential across the pumping element that causes an end load on the rotor and a resultant longitudinal load on the stator at the point of contact between the two components.
- (iv) As described in section 2.1 the interference between the rotor and stator creates a compressive load on the resilient stator at the point of contact.
- (v) A pressure load exerted on the stator by (a) the pressure of the fluid within the capsulism acting directly on the resilient stator and (b) the pressure of the fluid acting on the rotor which in turn is reacted at the point of contact with the stator.

A further complication to the resultant contact load between the rotor and stator is the varying rubber thickness of the stator which governs the stiffness of the stator section. According to May ^[2] and Appleby ^[4] the hydraulic loading, caused by the differential pressure across the pump, is the principle cause of both the axial and radial loadings on the rotor and stator and is the major contributory load to the wear within the pumping element.

2.4 INTERFERENCE FIT BETWEEN THE ROTOR AND STATOR

As described in section 2.1 an interference fit exists between the rotor and the resilient stator. The resultant compressive force creates two continuous ribbons of contact which seal each individual capsulism. It should be emphasised that the interference, or seal lines, are dynamic in operation and are constantly changing as a capsulism moves from the inlet to the outlet of the pumping element.

Appleby ^[4] used the equation 2.1 to calculate the width of the seal line for his theoretical modelling of a progressive cavity pump.

$$\text{Seal Line Width (mm)} = 2\sqrt{\left\{(d/2)^2 - (d/2 - \partial)^2\right\}} \quad (2.1) \quad [4]$$

where ∂ represents the difference in rotor and stator minor diameters. Wetter and Wirth describe the interference fit as a displacement geometry defined by the shape of the rotor and stator ^[11], which can be derived as

$$\text{Interference 'w' (mm)} = \frac{d - S_{\min}}{2} \quad (2.2) \quad [11]$$

Both equations 2.1 and 2.2 are based on geometry and static, cold conditions and do not account for the material properties of the contacting surfaces, such as the elastic modulus and hardness of the resilient stator material or the effect of hydrodynamic forces.

Based on Belcher's ^[8] modelling, Appleby simplified the geometry of the seal lines into three types of contact, as shown in figures 2.7 & 2.8 ^[4].

(i) ***Capsulism seal line***

The capsulism seal line axially separates capsulisms on the same side of the rotor and forms the seal between the inlet and outlet pressures of the pumping element. In Appleby's ^[2] opinion, this type of contact does not contribute to the wear phenomena within the pumping element.

(ii) ***Side contact type 'a' (high contact velocity)***

This seal line separates the diametrically opposed capsulisms and accounts for one of the two continuous ribbons of contact. The contact velocity is at a maximum since the locus of the rolling circle and the rotation of the rotor are in the same direction.

(iii) ***Side contact type 'b' (low contact velocity)***

This seal line is the opposite ribbon of contact to type 'a' above. Since the rotation of the rotor is now in the opposite direction to the locus of the rolling circle the contact velocity is much less.

The contact or rubbing velocity is known to contribute significantly to the wear life of the pump and is directly related to the operating speed of the pump ^[10]. The rubbing velocity is a function of the rotational velocity and the traversing velocity between the rotor and stator as the rotor revolves and travels from the top of the stator slot down to the bottom and back up ^[10]. For one revolution of the rotor it reciprocates downwards creating a sliding velocity on one side and a rolling velocity on the other. The velocities then reverse as the rotor returns to the top of the stator slot. The maximum rubbing velocity occurs to the side contact type 'a', at point A, half way along the stator slot, as shown in figure 2.8.

Figure 2.7 : Fluid capsulism seal line geometry ^[4,8]

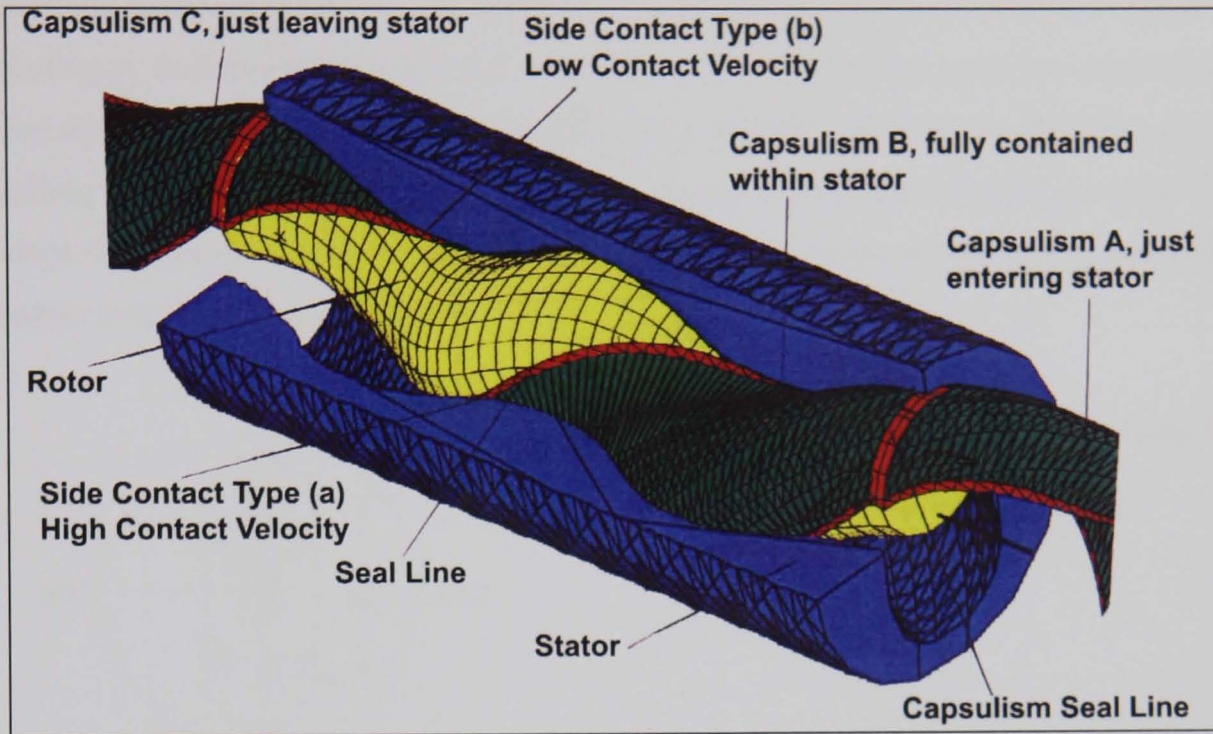
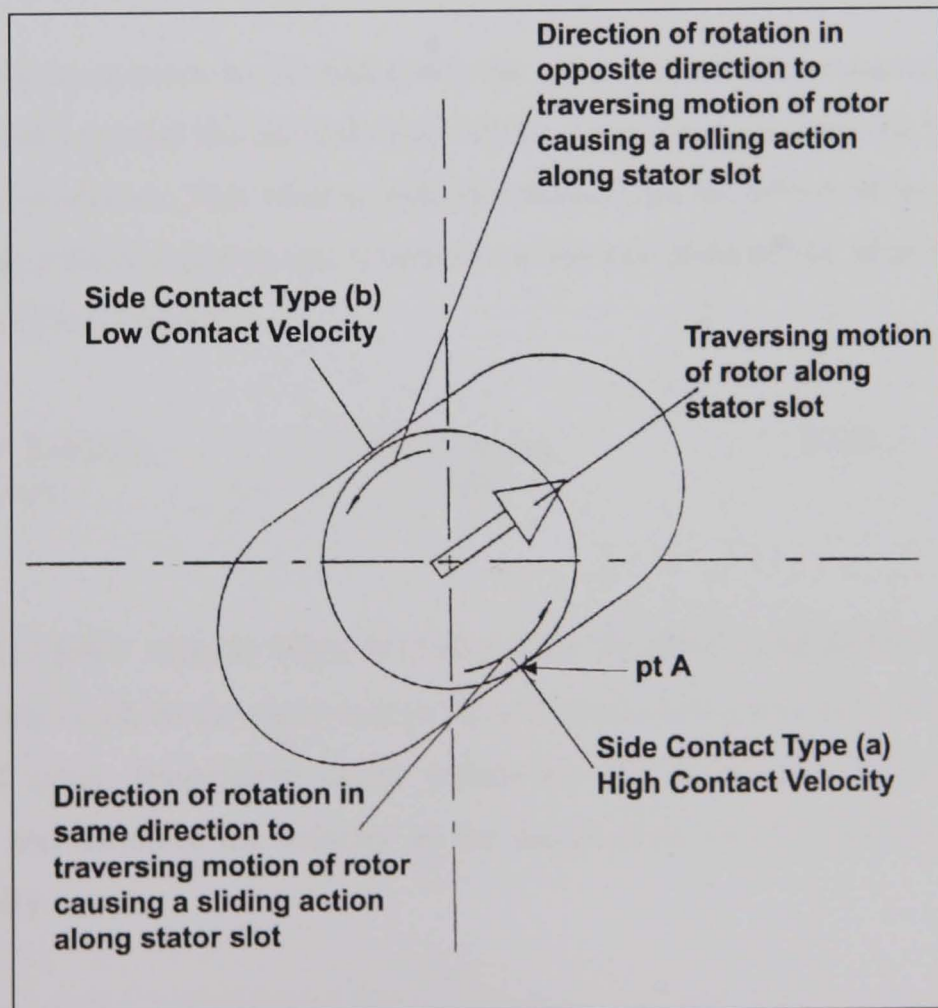
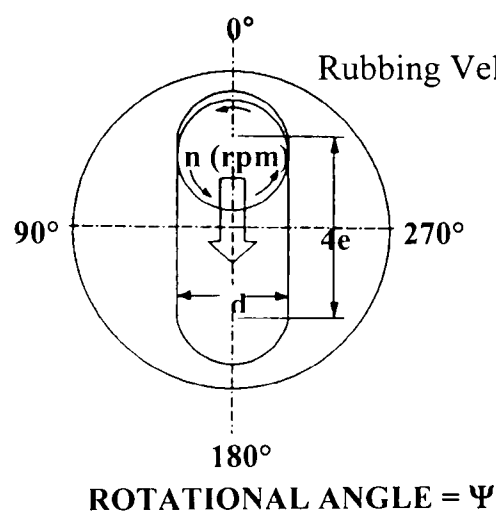


Figure 2.8 : Side contact (seal lines) between the rotor and stator ^[4]



Equation 2.3 shows that the rubbing velocity is a function of the rotor geometry and the rotational speed. According to Akincioglu^[12], rubbing velocity is directly related to the repeated scouring or friction erosion observed on rotors which is caused by particles trapped between the rotor and stator junction during the eccentric rotor motion. To minimise this type of wear, a low rubbing velocity is recommended by reducing the operational speed (n) of the pump^[10]. Typical values of rubbing velocities encountered in progressive cavity pumps when pumping abrasive slurries would be in the order of 0.5 - 2 m/s^[10].



Rubbing Velocity (m/s) = Rotational Velocity \pm Traversing Velocity

$$= \frac{\pi d n}{60} \pm \frac{4\pi e n \sin \Psi}{60} \quad (2.3) \quad [10]$$

An alternative equation to 2.3 calculates the peripheral rubbing velocity, which describes the linear distance around the circumference of the stator slot divided by the time the rotor takes to make one revolution. This velocity does not account for the effects of the change in the rolling and sliding velocities during one revolution as any one point on the rotor alternates between the two types of side contact.

$$\text{Peripheral Rubbing velocity (m/s)} = \frac{(\pi d + 8e) \times n}{6000} \quad (2.4) \quad [10]$$

2.5 SLURRY VELOCITIES WITHIN THE PUMPING ELEMENT

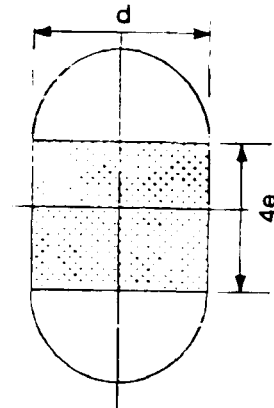
The velocity at which the slurry moves through the pumping element influences the wear of the rotor and stator. Progressive cavity pumps are generally used for pumping mixed phased products and therefore the velocity of the carrier fluid and the particles must be considered individually.

2.5.1 Fluid velocity

The fluid velocity is the speed at which the liquid travels through the pumping element^[3,13]. The magnitude of the fluid velocity is a function of the rotor-stator geometry spaces, i.e. d and e , and

the pump's rotational speed. The average fluid velocity (AFV) at which the product travels through the pump can be calculated by :-

$$\begin{aligned} \text{AFV (m/s)} &= \frac{\text{Flow Rate (m}^3\text{/sec)}}{\text{Flow Area (m}^2\text{)}} \\ &= \frac{Q \text{ (m}^3\text{/hr)}}{3600 \times 4ed \text{ (m}^2\text{)}} \end{aligned} \quad (2.5)^{[10]}$$



Regardless of the rotor position the flow area remains constant and is equal to $4ed$ ^[9,10]. High fluid velocities can cause erosive wear to the pumping element whilst insufficient velocity can lead to abrasive wear from abrasive solids settling within the capsulism ^[10].

2.5.2 Particle velocity

The particle velocity is the relative speed at which a particle, carried by a liquid, will travel through the pumping element. During one revolution a particle will travel a spiral distance equal to the length of the stator pitch plus the rotational path of the rotor. The velocity will be at a maximum when the particle is located at the extreme of the stator major diameter and at a minimum where the spiral path is shortest, i.e. the nearest point to the axis of the pump.

$$\text{Maximum Particle Velocity (m/s)} = \frac{n}{60} \times (\sqrt{\pi^2 (4e + d)^2 + P^2}) \quad (2.6)^{[10]}$$

The maximum particle velocity influences the viscous liquid handling and cavitation characteristics of the progressive cavity pump. The thicker the liquid, the slower the pump must run in order to avoid cavitation problems. Akincioglu found that high particle velocities caused impact wear when pumping round abrasive particles, but the effect was reduced as the particle size and sharpness increased ^[12]. From practical experience, typical fluid and particle velocities to minimise wear whilst pumping abrasive slurries would be in the order of 1- 4 m/s ^[10].

2.6 INFLUENCE OF OPERATING PARAMETERS

2.6.1 Discharge Pressure

When a progressive cavity pump operates against a discharge pressure the subsequent force created by the system tries to force the moving liquid back through the pumping element. This results in the product slipping back across the seal line. As the discharge pressure rises the slip

flow increases until a pressure is reached where the flow rate of the product being forced back through the pump is equal to the flow moving forward. The value of the maximum pressure depends upon the number of stages, where one stage is equal to just over one stator pitch length. For a single stage the maximum discharge pressure which a progressive cavity pump can realistically generate is 6 bar. By doubling the length of the pumping element to two stator pitches, the slip is effectively halved, so twice the pressure can be achieved^[5,14], i.e. 12 bar, although at the expense of a longer and therefore more costly pump. Therefore, to conclude, pressure capability must be a function of the number of times the progressing seals are repeated^[5,9].

Slip can be defined as ‘the difference in flow rates between 0 bar and the pressure at which the pump is operating’^[10] and according to Gray^[7] is the greatest single contributor to wear in the progressive cavity pump. The slip flow rate is a function of the area of the leak path, which may not be continuous along the length of the pumping element, the viscosity of the liquid and the differential pressure^[9,11,15]. Vetter and Wirth^[11] found that the total slip also depended upon the type of flow through the pump, i.e. whether laminar or turbulent and that when the interference fit, w , was greater than zero, a progressive cavity pump was practically leak free, regardless of the pressure differential across it. However, Gray’s findings disagreed and he found that slip was still present when $w > 0$.

Discharge pressure is independent of the rotor speed so the pump will generate the required pressure to transport a fixed volume regardless of the operating speed^[9]. Belcher’s^[8] studies, investigating the operating characteristics of progressive cavity pumps, concluded that the moving capsulism was exposed to a gradual increase in pressure. Full exposure to the discharge pressure was attained when the capsulism had sufficient area exposed to the discharge pressure to enable complete leakage back into the capsulism, which was the point at which the seal line at the leading edge of the capsulism no longer existed. However later work, at the same University by Appleby^[4], concluded through theoretical and experimental modelling, that the pressure across the pumping element remained equal to the inlet pressure until the point at which the moving capsulism started to open at the delivery end. At this point, a sudden increase of pressure was then experienced as the capsulism pressure changed to equal that of the discharge pressure in the system as opposed to Belcher’s gradual increase. However Appleby’s hypothesis fails to model how increasing the number of stages of the pumping element enables the pump to be used against higher discharge pressures, whereas Belcher’s theory of gradual exposure could still be applied.

2.6.1 *Speed*

It has been shown in sections 2.4 and 2.5 that the operating speed is directly related to the velocities experienced within the pumping element and consequently effects the wear life of the pumping element. From experience it is known that increasing the operating speed of the pump reduces the wear life of the rotor and stator ^[14]. A rule of thumb, derived from empirical tests, states that the wear rate is proportional to the pump speed cubed ^[2,9,14].

Speed contributes to the effects of slip. May ^[2] and Drane ^[15] state that a pump operated at a high speed will have little slip but high wear, whereas low speed results in a large degree of slip but much less wear ^[15]. This directly conflicts with the opinions held by Gray ^[7] and Bourke ^[5].

One manufacturer has derived an ‘abrasivity’ grouping system, which is used in the selection of operating speeds to minimise wear ^[16]. As the ‘degree of abrasivity’ increases, the selected operating speed is decreased. The information given in Table 2.1 is based on historical knowledge and extensive experience and relates to the manufacturers ‘Product manual selection curves’, that have not been included. The purpose of including the abrasivity table is to demonstrate the diverse range of products that progressive cavity pumps can handle and how historically the abrasivity of such slurries has been categorised. This categorisation is based on the use of a nitrile rubber stator and an electro-deposited hard chromium plated rotor, with an interference fit based on the stator minor being 20% larger than the rotor minor.

2.7 ROTOR AND STATOR MATERIAL SELECTION

The correct materials selection for the rotor and stator are essential to optimise the wear life of the pumping element. However, in the commercial world, this optimisation must be balanced against cost and often the most wear resistant materials can not be economically justified.

2.7.1 *Rotor surfaces*

Traditionally rotors have been surface treated with a layer of electro-deposited hard chromium plate as a means of protection against corrosion, abrasion and erosion. The hard plate has provided a cost effective, reliable, all-purpose rotor coating with years of trouble free, field proven service. Its smooth surface is easily polished to a fine micro-finish to provide the low coefficient of friction with the resilient stator material that is necessary to minimise the start up frictional torque when the pumping element is unlubricated. Hard chromium plate is the industrial standard against which the performance of all coating alternatives are measured ^[17].

Table 2.1 : Slurry Abrasivity Grouping ^[16]

Degree of Abrasivity	Example of Slurries
NONE	Clean, clear fluids Drinking water Bottled beer Wines & spirits Fuel & lubricating oils (clean) Cosmetic creams Shampoo
LIGHT	5 % v/v solids River & sea water containing up to 2% sand Chalk slurry up to 30%w/w fine particles Sewage sludge (no grit) Mine water (no solids) Biscuit creams Cake mixes Latex Paper stocks Abattoir effluent (less bone) Used engine oils
MEDIUM	10 % v/v solids Clay & chemical grouts up to 55% solids Drainage water (5% cement dust) Bentonite clay slurries China clay 60% w/w (10 microns) Cement & water 20 % w/w Graphite and water 60% w/w solids (fine grain) Toothpaste Paint slurries
HEAVY	15 % v/v solids Gypsum plaster mix 30% w/w solids Vitreous slip (S.G. 1.85 – 2.20) Tile slip 30% w/w (S.G. 1.3) Cement slurry grout (55% sand / 30% cement / 15% water) Mine water with 15% silica sand (20 mesh) Titanium di-oxide 60% w/w fine solids Cutting oils containing metallic swarf Stone slurry (granite, marble and slate particles) 25 – 30 % w/w

Continual development has led to a second generation of coatings that have extended pump performances even under extremely abrasive and/or corrosive service conditions. Alternatives that are now available on the market are plasma sprayed ceramic coatings, HVOF carbide type coating and solid silicon carbide rotors. The ceramic coatings provide a single phase surface with superior corrosion resistance to hard chromium plate, a very smooth micro-finish ^[17] and excellent abrasion resistance to fine abrasive slurries, of particle sizes $<50\mu\text{m}$ ^[2], where high particle impact loads are not present.

Tungsten carbide, combined with various binder metals, are the main HVOF coatings that have been developed, to enable progressive cavity pumps to be used in heavy abrasive applications, where hard chromium plate does not provide acceptable wear resistance. Such applications are slurries containing hard particles of diameters greater than 1mm, that tend to be either round or fragmented and of high solid concentrations. These tungsten carbide coatings provide excellent resistance to two- and three-body abrasion and have good corrosion resistance. The ductile metallic matrix provides the toughness necessary to withstand the impact loads from larger particles ^[17].

2.7.2 *Stator materials*

The stator material must be sufficiently resilient to enable the creation of the seal lines. The exception is highly viscous products where solid stators are necessary to ensure the generation of the hydrodynamic film. According to Bourke ^[5] the most abrasion resistant rotor / stator combination utilises an elastomeric material of 50 – 70 IRHD (International Rubber Hardness Degrees), which enables the abrasive particles to embed rather than abrade the stator material.

Another selection criteria for stator materials is their resistance to swelling. Natural and nitrile rubbers are commonly used as they do not swell significantly in water. Natural rubber is more wear resistant than nitrile but does swell in the presence of oils and fats, making nitrile the most predominant stator material available on the market to date. It is relatively cheap compared to alternative polymers and easy to mould. For abrasion resistance, polyurethane has been shown to out perform the rubbers but is more expensive and difficult to manufacture, involving different moulding technologies to rubber ^[18].

2.8 SLURRY CHARACTERISTICS

The slurry characteristics represent the customers' product and therefore are a fixed variable. Unlike most tribological systems that are designed to eliminate or minimise the particles or

debris that cause the wear, the pumping element must be designed to cope with the abrasives present in the fluid.

From empirical rules and historical experience, one manufacturer^[2,12,16] has made the following rules and assumptions.

- (i) Increasing the solids concentration in the fluid increases the wear on the pump simply due to more particles being available to cause wear to the rotor and stator.
- (ii) Higher viscosity fluids reduce the wear rate (subject to other factors remaining constant) as less slip occurs with thicker products.
- (iii) The harder the particles, relative to rotor hardness, the more damage they will cause to the pump
- (iv) Sharp and angular particles will cause more abrasive wear than rounded ones.
- (v) Larger particles will cause more damage than smaller ones. In May's^[2] opinion particle size affects pump wear significantly due to slip and the relationship between particle size and slip film thickness is described in section 2.7, thus indirectly agreeing with Gray^[7] that slip is the most significant contributor to wear.

2.9 REFERENCES

1. **BS EN ISO 14847:1999**, "*Rotary positive displacement pumps – technical requirements*",
2. **G.H. May**, "*Least whole life cost : Section 2 : Design of progressive cavity pumps related to wear rates*", Mono Pumps Ltd. technical literature : LWLC/MKTG, Issue 1, November 1995, pp 1 - 6.
3. **R.J.L. Moineau**, "*A new capsulism*", Ph.D.diss., Faculty of Science, University of Paris
4. **D. Appleby**, 1994, "*Experimental and theoretical study of a progressive cavity pump*", Ph.D.diss., Cranfield Institute of Technology.
5. **J.D. Bourke**, "*Pumping abrasive slurries with progressive cavity pumps*", Robins & Myers Inc., Presented by Moyno Products, Springfield, Ohio, n.d.
6. **Mono Pumps (Australia) PTY LTD.**, "*Mono Pumps water transfer : Agricultural products*", Mono Pumps Sales Literature ART04/03, March 1999.
7. **E.D. Gray**, "*Competitive parts analysis : rotors & stators*", Online, available: <http://www.moyno.com/mip/comppart.pdf> [accessed 10/05/00].
8. **I.R. Belcher**, 1991, "*An Investigation into the operating characteristics of the progressive cavity pump*". Vol.1, Ph.D.diss., Cranfield Institute of Technology.

9. **I.J. Karassik, J.P. Messina, P. Cooper, C.C. Heald**, "*Pump Handbook*", 3RD Ed., McGraw-Hill, 2001, ISBN 0-07-034032-3, pp3.3, pp 3.99 – 3.121.
10. **J. Drane**, "*Technical Notes 16 : Pump Element Geometry*", Confidential, Mono Pumps Ltd., 1999.
11. **G. Wetter & W. Wirth**, "*Understand progressive cavity pumps characteristics and avoid abrasive wear*", Proc. Of 12th Int. Pump Users Sym., pp 47 – 59, 1995
12. **S. Akincioglu**, "*Abrasive wear*", Mono Pumps internal memo, 16/04/82
13. **J. Drane**, "*Fluid velocity through a Mono pump*", Technical Note No.3, Mono Pumps Ltd., Confidential, not dated.
14. **J. Drane**, Mono internal e-mail dated 08/12/99 to R.Garlick, confidential.
15. **J. Drane**, "*Accuracy of pump performance*", Technical Note No.9, Mono Pumps Ltd., Confidential, not dated
16. **J. Drane**, "*Abrasion and solids in suspension*", Training Manual TM11, Mono Pumps Ltd., Confidential, not dated.
17. **K. Mirza**, '*Moyno Ultra-shield rotor coating technology*', Online, available: <http://www.moyno.com/moyno/main.html> [accessed 18/04/01].
18. **M. Johnson**, "*Abrasion resistance of stator materials*", Technical Note No. 21, Mono Pumps Ltd., Confidential, not dated.

Wear by hard particles

3.1 INTRODUCTION

Wear is not an intrinsic material property ^[1] and the rate and type of wear depends, not only on the composition and microstructure of the contacting surfaces, but also on the surrounding conditions. Hence the wear that occurs under the tribological action must be described by the 'system-related' wear characteristics. A tribological system can be divided into four elements: body, counterbody, interfacial medium and surrounding medium. These elements, together with their tribologically relevant properties and interactions between them, form the structure of a tribological system ^[2]. In the pumping element the rotor represents the body, the stator is the counterbody and the slurry is both the interfacial and surrounding medium. The material loss, which occurs through the action of the operating variables of the tribological system, tends to occur by several mechanisms.

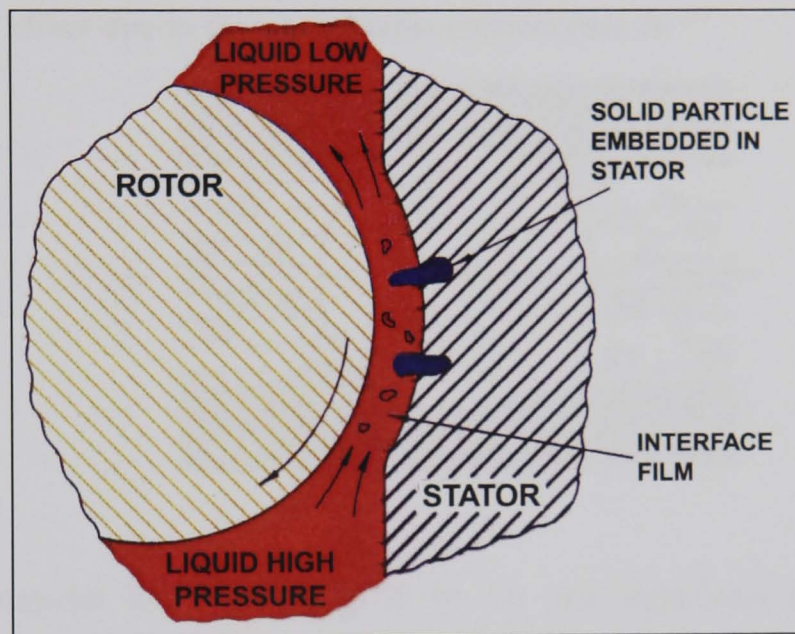
Progressive cavity pumps are operated within slurry handling processes such as the transportation of minerals and other solids through long distances pipelines. A slurry can be described as a mixture of solid particles in a liquid of such a consistency that it readily flows. From previous studies on wear in progressive cavity pumps ^[3-8] the modes of wear discussed relate to the wear mechanisms of abrasion by hard particles and solid particle erosion, although the terminology used is extremely varied. The studies by May, and Vetter and Wirth ^[3-6] established that as the rotor orbits in the stator it encounters intermittent sliding contact along the seal line. Based on the hardness values of the rotor and stator, and the characteristics of the slurry, the abrasive particles would either:

- (i) be rejected back into the capsulism
- (ii) embed into the stator wall
- (iii) be transferred through to the next capsulism via the lubricating film.

In addition, since most applications involve a differential pressure between the rotor/stator capsulisms, slip will undoubtedly occur. The thickness of the slip film will depend on the liquid viscosity and the discharge pressure and will have a direct influence on the behaviour of the abrasive particles. According to May ^[3,4] a relationship exists between particle grain size and slip film thickness. If a particle diameter is greater than that of the film thickness then the particle would embed in the stator wall and scour the rotor each time the rotor passes over it, causing two-body abrasion. However if the particles were smaller than the film thickness they

would be able to pass through the interference gap with the slip film. Three-body wear would then occur by the action of the particles rubbing between the two components as the rotor rotates. These mechanisms are schematically shown in figure 3.1. Wirth's ^[6] studies disagree with May's ^[3] and he found that the behaviour of a particle to be embedded, rejected or transferred was independent of its size.

Figure 3.1 : Wear mechanisms within the pumping element ^[3]

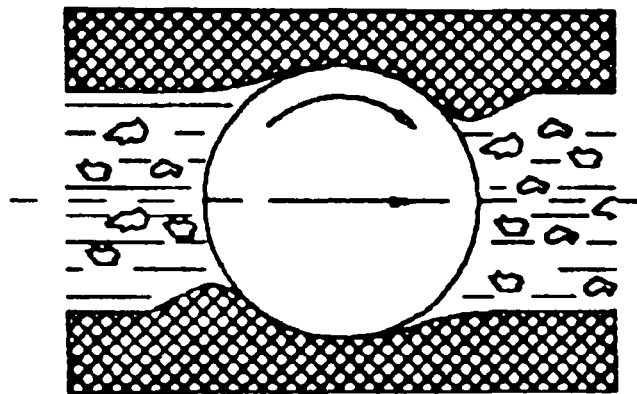


May found that particle embedding caused 'scouring' or two-body abrasion to the rotor surface as the component rolled and slid over the embedded particles. In Wirth's ^[6] opinion sliding wear was the predominant wear mechanism and that, as the embedding of particles into the stator wall increased, the amount of sliding wear to the stator decreased. This agreed with the studies of May, Wirth and Bourke ^[3,6,7] who all observed that the temporary embedding of particles in a resilient stator material protected the stator surface from wear. The resultant grooves created in the rotor surface were then found to cause counter-damage to the stator by cutting into the relatively soft rubber walls. Bourke ^[7] recommended that to minimise wear in the pumping element a rubber stator material should be used with a hardness range of 50 –70 IRHD which would allow sufficient deformation to partially accommodate large particles. Whilst Akincioglu^[8] recommended using a higher interference fit between the rotor and stator, combined with a hard natural rubber for the stator, to minimise the effects of scouring on pump performance.

May ^[3] described action (iii) as 'three-body' abrasion which he found generated significantly less wear, either to the rotor or stator, than action (ii). Three-body abrasion occurs when loose

abrasive particles are free to move relative to one another and possibly rotate whilst sliding between two surfaces ^[1] of either metallic or non-metallic type. Wirth and Vetter ^[5] found that the process of wear was influenced by the ‘fulling’ effect that the stator encounters, due to the interference fit, which leads to a localise elastic deformation of the rubber, as shown in figure 3.2. The local changes in the geometry of the cavity of the stator affect the entry of the particle into the sealing zone.

Fig 3.2 ‘Fulling’ effect due to the rotor/stator interference fit ^[6]



May ^[3] ranks material loss by erosion to be far less significant than the two abrasion mechanisms but does not define which component suffers the erosive damage or the mode of erosion. Wirth ^[6] uses the term ‘beam’ wear to describe erosive wear across the seal lines due to slip.

It is highly probable, that in some slurry handling applications, the synergistic effect of corrosive wear will occur. However both erosion-corrosion and abrasion-corrosion mechanisms are beyond the scope of this thesis and in order to ensure that these mechanisms are eliminated from the experimental studies a corrosion resistant stainless steel was used for the rotors substrate material.

3.2 WEAR BY ABRASIVE SLURRIES

The relative movement of the transportation of slurries can cause both abrasive and erosive wear. Erosion by hard particles refers to a series of particles striking and rebounding from a surface, whilst abrasion results from the sliding of abrasive particles across a surface under the action of an externally applied force. The clearest distinction lies in the source of the force. In erosion, the force exerted by the particles on the material is due to their deceleration, whilst the abrasive force is externally applied and approximately constant. The modes by which both

mechanisms remove material are dependent on the nature of the wearing surface; whether it is ductile or brittle.

3.2.1 Abrasion by plastic deformation

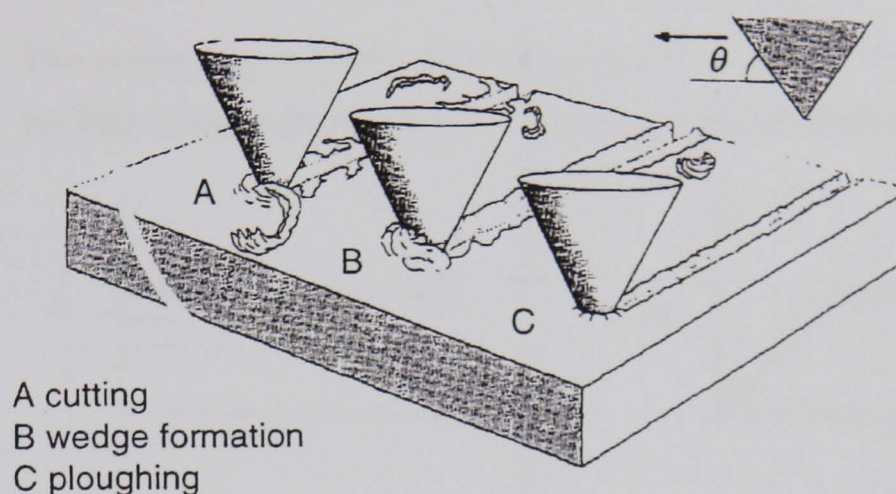
The mechanisms by which material is removed plastically by abrasive wear are very complex and it is generally the case that all of the material loss does not occur by a single mode. The mechanisms are generally divided into two types commonly termed as ‘two-body’ and ‘three-body’ wear ^[1], with each mechanism having several modes of material removal. Two-body abrasion occurs when a rough surface or fixed abrasive particles slide across a contacting surface, whereas three-body abrasion involves loose particles which are free to move relative to one another and possibly rotate whilst sliding between two surfaces. It can be seen from the descriptions that the terms are derived from the number of components involved in the wear system. However, more current opinions ^[9] suggest that this system analysis approach to describing the behaviour of abrasive wear is inadequate and two alternative terms are suggested that relate to the behaviour of the abrasive particles as opposed to the number of components involved in the system. The terms are defined as:-

- (i) Grooving wear – “an abrasive wear process in which effectively the same region of the abrasive particle or asperity is in contact with the wearing surface throughout the process. Wear surfaces produced by grooving abrasion are characterised by grooves parallel to the direction of sliding”
- (i) Rolling wear – “an abrasive wear process in which the region of the abrasive particle in contact with the wearing surface is continually changing. Wear surfaces produced by rolling abrasion are characterised by a heavily deformed, multiple indented appearance with little or no directionality”

The modes of three-body abrasive wear can occur under gouging, high-stress or low-stress conditions ^[10]. Gouging relates to rocks and other coarse abrasive particles that cut into the surface and remove relatively large fragments of material. Three-body abrasion under high stress conditions results in the abrasive particles themselves being crushed, as in ball mill grinding. Whilst, as the name suggests, low stress three-body wear involves sufficiently small enough loads as not to cause fracture to the abrasive particles. Low stress abrasion, whether by fixed or free particles, would describe the abrasive wear in the pumping element as the loads involved are insufficient to crush the abrasive particles except in particular applications such as pumping carbon where the solids are extremely brittle and fragile.

The different viable modes of material removal for the formation of a groove by two-body abrasion are ploughing, wedge formation and cutting, figure 3.3.

Figure 3.3 : The three modes of material removal by plastic deformation ^[11]



Ploughing occurs under light loads and does not directly result in material removal. As the abrasive tip forms a groove in the wearing surface the displaced material builds up at the front and to the sides of the groove. Any subsequent work to the ploughed surface would then result in the removal of the displaced material by micro-fatigue. Cutting and wedge formation directly result in material removal from the wearing surface, with cutting being the most severe mode of wear for ductile materials. During the cutting process, a microchip is formed by material flowing up the front face of the abrasive particle, leaving behind a groove with very little displaced material to the sides. Wedge formation is an intermediate behaviour between ploughing and cutting. In this situation the total amount of material displaced from the groove is greater than the material displaced to the sides ^[12].

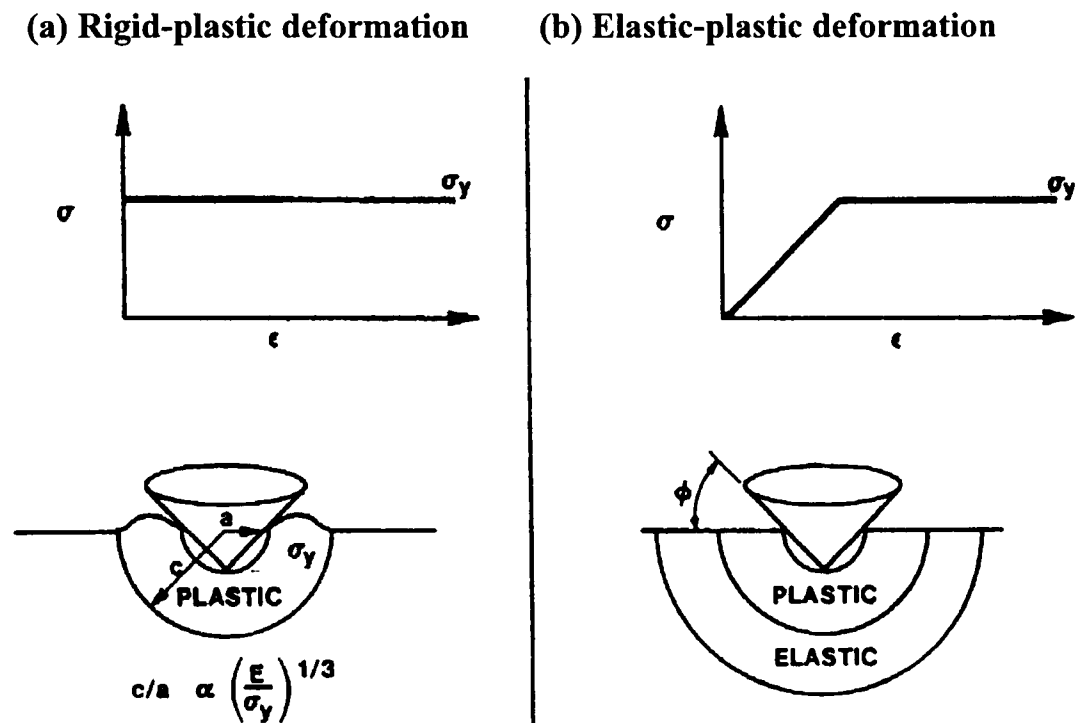
Hutchings ^[1] suggests that the controlling factors which determine the dominating mode are

- (i) the critical attack angle of the particle, θ
- (ii) the ratio of shear strength at the interface and the shear yield stress of the wearing surface, f .

To prevent the effects of hysteresis, the pumping element must be hydrodynamically lubricated and therefore the ratio 'f' can be assumed to be zero. For f values of less than 0.5, only the modes of cutting and ploughing are said to be possible ^[1].

Moore & Swanson ^[13] modelled two extremes of indentation behaviour to describe how the volume of displaced material from the groove is accommodated depending upon the angle of contact of the abrasive particle and the intrinsic properties of the wearing surface, figure 3.4.

Figure 3.4 : Two extremities of indentation behaviour ^[13]



For wear debris to be created, i.e. by cutting or by wedge formation, the angle at which the particle attacks the surface must be greater than a critical value, θ_c . In the pumping element there would be a whole distribution of attack angles, but only those particles with attack angles greater than the critical value would result in material removal. The actual value of this critical attack angle is influenced by the characteristics of the abrasive particles, the angle at which they embed into the stator, the material properties of the stator and the rotor and the thickness of the slip film. According to Hutchings ^[1] angular particles tend to present higher attack angles, which lead to a greater proportion of particles that cut and thus produce higher wear rates compared with more rounded particles.

The ratio of the intrinsic material properties of elastic modulus to hardness, E/H , strongly influences the value of the critical attack angle. For most metals, θ_c typically lies between 30° and 90° , with high values of E/H leading to high values of θ_c ^[1]. As the attack angle increases the mechanism of plastic deformation changes from ploughing to wedge formation to cutting.

Rabinowicz ^[14] proposed a simple model to describe two-body abrasion in elastic-plastic behaving materials. A single cone, under an applied load, slides across a surface, resulting in the formation of a groove. The model suggests that the volumetric wear rate per unit length of sliding distance (dV/dl) is directly proportional to the load carried by the particle, W , and will vary inversely with the indentation pressure, P , required to cause plastic flow.

$$\frac{dV}{dl} = k \frac{W}{3P} \quad (3.1) \quad [14]$$

where k is the constant of proportionality, the value of which depended on the angle of the cone and the mode of material removal. k is more commonly termed as the dimensional wear rate, with typical units of $\text{mm}^3\text{N}^{-1}\text{m}^{-1}$, and is a function of the changing variables within the tribosystem. Since the volume of removed material will change with sliding distance, equation 3.1 is only true for a given moment of time and therefore the changes must be measured experimentally in order to derive a k value for the overall conditions of the system. Rabinowicz found that a particle shape change from conical to spherical effected the relationship between the wear rate and hardness such that is inversely proportional to a power greater than one. Studies by Wirojampatump and Shipway ^[15] agreed that k was strongly dependent on particle characteristics as well as environment.

The dimensional wear rate is a term often incorrectly used for the 'wear coefficient', K , which is dimensionless. This is defined as the wear constant for a surface under given conditions and for engineering purposes can be defined as

$$K = \frac{k}{H} \quad (3.2)$$

where H is the hardness of the wearing surface. By dividing the experimental data, for a given system, by the hardness of the surface an engineering value for the wear resistance of that surface is achieved, but again, can only be relevant to that given tribological system. The dimensionless wear coefficient can also be defined in an equation identical to Archard's law of adhesive wear, which shows that the total volume removed per sliding distance, Q , is proportional to the applied load, W and inversely proportional to the hardness of the wearing surface, H , on the assumption that H is equates to three times the yield strength

$$Q = K \frac{W}{H} \quad (3.3) \quad [1]$$

The only difference between equation 3.1 and Archard's equation for adhesive wear ^[1] is the coefficient for adhesive wear is a non-dimensional probability, per contact, of forming a wear particle, while in the abrasive wear system, it represents the cotangent of the average angle of abrasants and is dimensional. The dimensionless equation 3.3 has generally been accepted as the 'wear equation' to model two- and three-body abrasion, although it makes several assumptions:-

- (i) the hardness of the wearing surface remains constant
- (ii) there is no hardness differential between contacting surfaces
- (iii) the applied load is carried equally between the particles in the contact zone
- (iv) the wear mechanism remains constant

This classical approach to two-body wear has also been applied to the study of three-body abrasion and material removal rates by three-body abrasion were found to be much less than those by the two-body mechanism as the material removal process is less efficient. Studies by Rabinowicz et al.^[14] found that three-body wear rates were up to 10 times less than two-body wear rates as the average loose grain spent 90% of its time rolling and only 10% of its time abrading the sliding surfaces between which it was situated. Misra and Finnie ^[10] observed that the mechanism of material removal by three-body abrasion appeared to involve repeated plastic deformation. As the surface roughened, protruding material was displaced by the abrading particles and 'lips' of material were separated occasionally from the surface. This observation would suggest that equation 3.3 was not suitable for modelling 'rolling' where individual non-directional indents are produced as opposed to directional grooving, the length of which directly relates to the sliding distance. Studies of abrasive wear in hydrodynamically lubricated bearings by Williams and Hyncica ^[16,17] suggested that the low material removal rates of three-body abrasion was related to the ratio of D/h , where D is the particle major axis and h is the separation of the surfaces. Their two-dimensional model of particle motion showed that an abrasive particle moving between two surfaces undergoes a transition from grooving to rolling when D/h reaches a critical value. Wirojampatump and Shipway^[15] related rolling behaviour to particle shape and found from rubber wheel abrasion tests that the tendency of rounded silica particles to roll was very low, as there were no angular corners to indent the mild steel test piece and induce rolling.

Relating the variables of load and hardness to the tribological system under review, the hardness would be that of the surface of the rotor and the normal load applied by the abrasive particles. The load which the abrasive particles could apply to the rotor surface would depend upon such

factors as stiffness of the rubber, the degree of interference fit between the rotor and stator, and the stator side loads. If the load remained constant as the rotor and stator wear, the contact pressure along the seal lines will decrease, with sliding distance, due to an increase in the contact area. However the effect of the wear would reduce the interference fit between the two components and consequently the contact pressure will decrease.

If the classical theory of abrasion was used to minimise wear in the tribological system of the pumping element, whether by sliding or abrasion, the loading on the particles must be minimised and the hardness of rotor surface should be maximised. May^[4] suggested a model to predict the wear life of the pumping element, based on the classical approach, where:-

$$\text{Wear rate} \propto \frac{KWS}{H} \quad (3.4) \quad [3]$$

where W is the load at seal line between rotor and stator, S is the speed of rotation of the rotor and H is the hardness of rotor surface and defines K to relate to the fluid characteristics. The expression is based on empirical data and predicts the wear life of the rotor to be proportional to the sliding distance, since sliding distance is a function of the rotational speed of the rotor. As with classical approach, neither of these equations consider the influence of the hardness of the counterbody or that of the abrasive particles. According to Gray^[18] it is slip and not the passage of the abrasive particle passing through the pumping element that is the primary cause of the wear. Therefore the classical abrasion theory would no longer satisfy the conditions, as it does not account for the consequence of pressure differentials, which generate high fluid velocities within the pumping element. This introduces the possible presence of material removal by solid particle erosion.

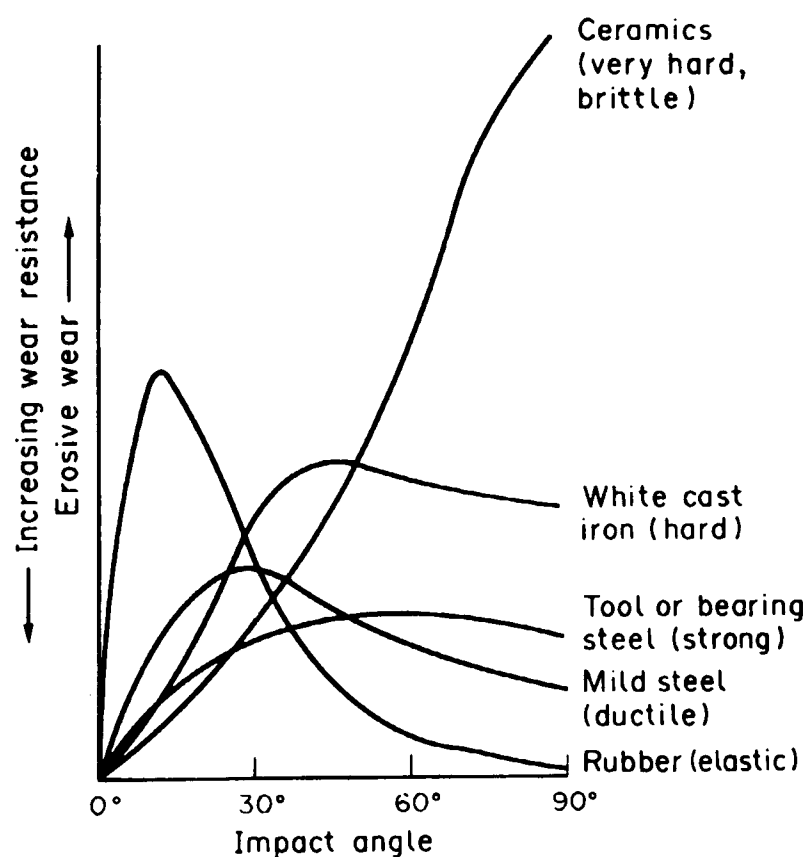
3.2.2 *Solid particle erosion*

Erosion by hard particles is caused when a stream of hard particles impinging on a surface at an angle θ , varying from a low glancing angle to 90° , with enough energy to cause permanent indentation.^[1,19,20] The stream of particles can either be dry or entrained in a gas or liquid medium and can occur at any significant velocity greater than 1 ms^{-1} ^[20]. In the tribological system of the pumping element, particle and fluid velocities are in the order of $1 - 4 \text{ ms}^{-1}$ and therefore, by definition, solid particle erosion may contribute to the wear in the system. When the hard particles are entrained in a liquid medium, the term 'slurry erosion' is commonly used to describe this wear phenomenon ^[21,22,23].

The amount of erosive wear depends upon the number and mass of the individual particles striking the surface and on their impact velocity. The erosion rate, E , is commonly given in terms of mass or volume of material removed per unit mass of erodent impacted compared to abrasion rates which are given as the volume of material removed per sliding distance ^[1].

The response of engineering materials to the impingement of hard particles varies greatly depending upon the type of material, the condition of the material, the environment and parameters associated with the erosion process, such as impact velocity, impact angle, and particle type and size ^[19]. Classical erosion theory holds that the response of a material to erosion depends on whether it is ductile or brittle and the impingement angle of the impacting particle strongly influences the severity of the erosion, (see figure 3.5). For ductile materials maximum erosion rates occur at low angles of incidence, whilst for brittle materials, such as ceramics, the maximum is at or near 90°. As with abrasion, erosive material removal mechanisms differ for the two types of materials and in practice can occur by a combination of the mechanisms, but are modelled separately for simplicity.

Figure 3.5 : Effect of impingement angle on erosive wear of brittle and ductile materials^[24]



On ductile surfaces, impacting particles cause localised plastic strain that eventually exceeds the strain-to-failure of the deformed material. When solid particles impact a metal, at a sufficient velocity, plastic impact craters are formed and material is displaced. The geometry of the crater

or indentation will depend on the particle impact velocity, the angle of impact and the shape and orientation of the particle. The material displaced, by the indentation of each particle, can either:-

- (i) be accommodated by elastic deformation of material away from the indentation
- (ii) form a rim of plastically deformed material around the indentation
- (iii) be removed in some way as wear debris

Of the three options, only (iii) will result in loss of material mass.

The models of erosive wear by plastic deformation are based on the angle of attack, with the simplest model assuming particle impingement at normal incidence to give a dimensionless rate of erosion of:-

$$E = \frac{\text{mass of material removed}}{\text{mass of erosive particles striking the surface}} = \frac{K\rho U^2}{2H} \quad (3.5) \quad [1]$$

where ρ is the density of the material being eroded, H the hardness of the eroded surface, U the impact velocity and K is a dimensionless factor that accounts for the fraction of material displaced from the indentation that is removed as wear debris. The model assumes that the surface deforms plastically when a constant indentation pressure (hardness), H , is applied. Therefore the only force assumed to be acting is that exerted by the contact surface which decelerates the particle due to the plastic flow pressure, H , acting over the contact area.

Equation 3.5 can be extended to accommodate particles impinging at low oblique angles. These models assume that the material is removed by a cutting action only when a rigid angular particle strikes a perfectly plastic material at a shallow angle. The volume of material removed is taken to be that swept out by the motion of the particle and therefore the model predicts zero erosion for attack angles of normal incidence. Equation 3.6 assumes the forces on the particle act at its extreme tip whereas equation 3.7 is a more realistic model, in which the point of action of the forces on the particle are allowed to move during impact.

$$E = \frac{(K\rho U^2) f(\theta)}{H} \quad (3.6) \quad [1]$$

$$E = \frac{(K_1\rho U^n) f_1(\theta)}{H} \quad (3.7) \quad [1]$$

Both models predict a strong dependency on the impact velocity which is a function of the impact angle θ . The velocity component n , for equation 3.7, lies between 2.0 and 2.5, and therefore predicts a higher dependency than equation 3.6 ^[1].

When the particles strike a ductile surface at high impact angles, debris becomes detached only after repeated deformation; and thus the equations 3.6 and 3.7 are no longer valid since these assume material removal by a cutting action only. The extreme case of erosion rate at normal incidence by spherical particles, in which cutting plays no role, can be expressed as:-

$$E = \frac{K_2 \rho \sigma^{1/2} U^3}{\epsilon_c^2 H^{3/2}} \quad (3.8) \quad [1]$$

where σ is the density of the spherical particles, and ϵ_c is the critical plastic strain at which detachment of wear debris occurs. There are a few noticeable differences between the models of shallow and high oblique impact angles. The first is the stronger dependency on velocity at higher impact angles, which is no longer a function of the angle. The second is the inclusion of the material property of strain and the stronger dependency on surface hardness and the final one is the introduction of the particle characteristic of density. Using this model, erosion of ductile surfaces is a consequence of repeated deformation of the surface, so the potential exists for work hardening of the surface. Therefore it is the hardness of the eroded surface that should be used to predict steady-state erosion and not the original surface hardness.

Regardless of the angles at which the particles strike the surface, all the models show that the erosion of ductile surfaces is strongly sensitive to the particle impact velocity and the dependence is often expressed in the form:-

$$E \propto U^n \quad (3.9) \quad [1]$$

Values between 2.3 and 3.0 are commonly reported for n ^[1].

The plastic deformation models for both abrasion and erosion by hard particles predict the wear rates to be inversely proportional to the hardness of the wearing surface, although the dependency is slightly less for erosion. Hardness is the only intrinsic material property included in the wear equation 3.3, whereas all the erosion models predict a dependency on material density as well as hardness.

3.2.3 Wear by brittle fracture

Abrasion and erosion by brittle fracture should be considered as possible wear mechanisms for causing damage to the plasma sprayed ceramic rotor coatings. Brittle materials have an additional mode of wear, known as micro-fracture, which occurs when the forces applied by the particle exceeds the fracture toughness of the contacting surfaces ^[12]. Figure 3.6, diagrammatically illustrates the behaviour of a brittle material, during the abrasion process, when a point load is applied then progressively unloaded from its surface ^[1]. Initially an elastic-plastic stress field is generated and at the point of contact very high compressive stresses occur which are relieved locally by plastic flow. The zone of deformed material is indicated by the letter 'D'. As the load of the indenter increases to a critical value, the tensile stresses across the vertical plane initiate a 'median vent crack', indicated by the letter 'M'. Increasing the load further would propagate the median vent crack deeper into the material (c), whilst reducing the load would close the crack (d). Continuing to unload (e & f) results in the formation and growth of lateral vent cracks, labelled L, which tend to curve upwards and terminate at the free surface when the load is completely removed. These lateral cracks are a direct result of the residual elastic stresses due to the deformed material relaxing around the region of contact. Ultimately it is the lateral cracking that leads to material removal but only if the loading of the particles exceeds a critical value which depends on the fracture toughness, K_c , and hardness, H , of the material and whether the angularity of the particle is sufficient to produce point loading. The ratio H/K_c can be used as a 'Brittleness Index' and materials with a low index would require a high critical load to initiate lateral cracking and wear by brittle fracture.

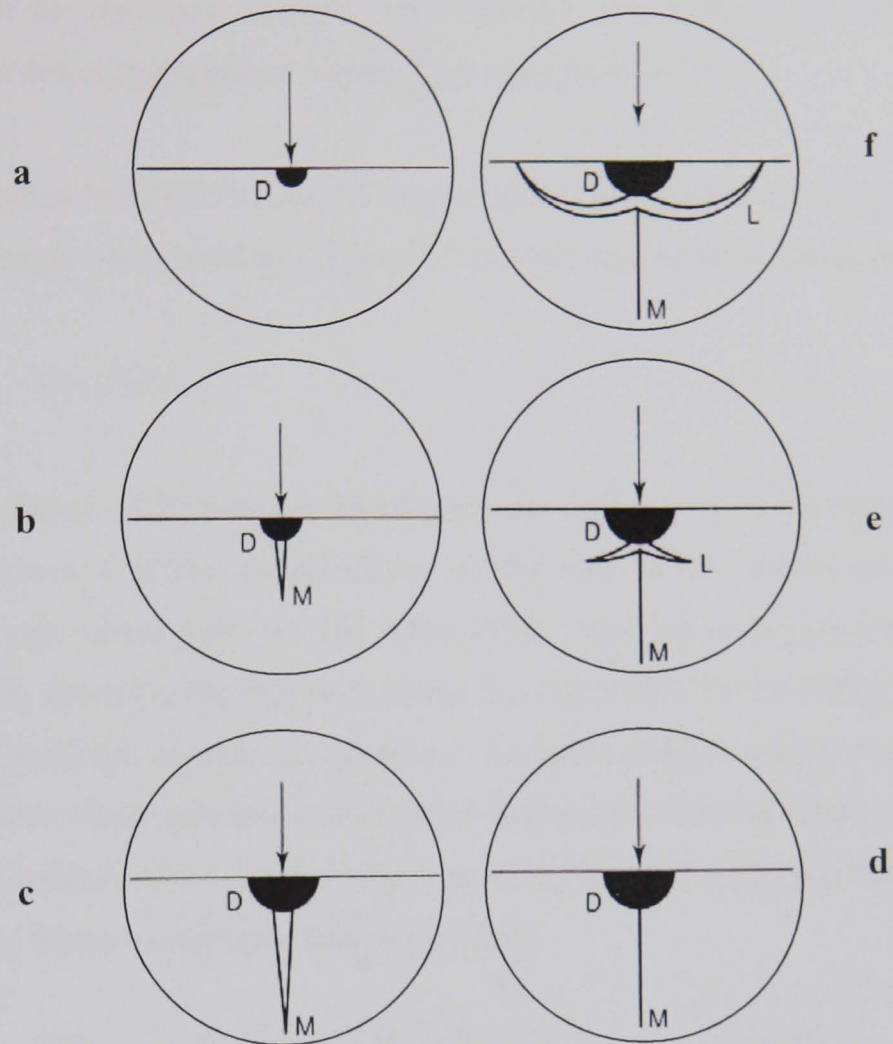
Hutchings ^[1] suggests three possible models to describe the volume wear rate per unit sliding distance, Q , in brittle materials, where N is the number of particles in contact with the surface, w is the normal load and α_3 , α_4 and α_5 are geometric constants.

$$Q = \alpha_3 N \frac{(E/H) w^{9/8}}{K_c^{1/2} H^{5/8}} \quad (3.10) \quad [1]$$

$$Q = \alpha_4 N \frac{w^{5/4}}{K_c^{3/4} H^{1/2}} \quad (3.11) \quad [1]$$

$$Q = \alpha_5 N \frac{w^{5/4} d^{1/2}}{A^{1/4} K_c^{3/4} H^{1/2}} \quad (3.12) \quad [1]$$

Figure 3.6: Schematic representation of material removal by brittle fracture ^[1]



These models demonstrate that the strongest influence on abrasive wear by brittle fracture is the number of particles that contact the wearing surface. All the equations show that the intrinsic material properties of fracture toughness and hardness play a significant role and predict an inverse correlation between the wear rate and some fractional power of these material properties. Comparison of the models described for abrasion by plastic deformation and by brittle fracture highlights several important features:

- (i) The wear rates by brittle fracture will increase more rapidly than linearly, which is the case assumed by the models of wear by plastic deformation.
- (ii) Material removal by brittle fracture will occur only when a critical load on each particle has been exceeded, whereas wear of ductile surfaces increases linearly with load.
- (iii) The models predict the wear rates by brittle fracture to be significantly higher than those by plastic deformation ^[1]

- (iv) Brittle fracture equation 3.12 predicts the wear rate increases proportionally with the size of the abrasives whereas quite different relationships have been associated with plastic deformation and are much more difficult to model.

Models for erosion by brittle fracture are based upon the erosion rate falling monotonically with impingement angle away from 90°, figure 3.7, and have led to expressions in the form of

$$E \propto r^m U^n \quad (3.13) \quad [1]$$

where r is the radius of the particle. This expression differs to the proportionality expression for ductile surfaces as it shows a dependence on the size of the particle as well as the impact velocity. For soft, round particles, the value of the exponent m is typically 1 whilst n ranges from 2.6 to 3.0, similar to the exponent values for expression 3.9 for plastic deformation [1]. For angular, hard particles, material is assumed to be removed by a similar mechanism to abrasion of brittle surfaces where subsurface lateral cracking results in micro-fracture of the surface. This has led to two models, which both predict a weak dependence on particle density and a stronger dependence on fracture toughness than on hardness.

$$E/\rho \propto r^{0.7} U^{2.4} (\sigma^{0.2} H^{0.1} / K_c^{1.3}) \quad (3.14) \quad [1]$$

$$E/\rho \propto r^{0.7} U^{3.2} (\sigma^{0.76} K_c^{1.3} H^{0.25}) \quad (3.15) \quad [1]$$

These models assume that the material being eroded is homogeneous and isotropic and fail to satisfactorily predict erosion of heterogeneous materials such as cemented carbides, composite materials with a ceramic or polymeric phase and two-phase ceramics such as reaction-bonded silicon carbide.

The models for abrasion and erosion of brittle surfaces both predict a dependency on the material properties of hardness and fracture toughness and certain characteristics of the particles. In erosion, the wear rate depends upon the radius and the density of the particles, whereas the abrasion models predict wear rates to increase as the number of particles present in the system increases, regardless of size.

3.2.4 Factors influencing wear

Since a tribological system consists of four components, all aspects relating to each component, plus the system variables, must be considered as potential factors that influence the wear in the system.

(i) Abrasive wear

Such factors would be abrasive particle characteristics – size, shape and hardness, the applied load, the mechanical and physical properties of the contacting surfaces and the lubrication conditions within the system. According to Moore and Swanson ^[13] the size and shape of the abrasive particles, the applied load and the mechanical properties of the wearing surface all influence the geometry of the groove formed in sliding abrasion and therefore determine the volume of material displaced from the groove per particle. With respect to the tribological system of the pumping element, Vetter and Wirth ^[5,6] list particle hardness, size and concentration as the factors most influencing the wear in the system, which agrees with numerous studies conducted not only on progressive cavity pumps ^[3,8] but on abrasive wear in general ^[10, 15, 16, 25-33].

Numerous studies ^[16, 25-31] have been conducted into the effects of particle shape and size on abrasive wear rates. The majority conclude that the rate of abrasive wear was very sensitive to the characteristics of the abrasive particles under dry and wet abrasive tests. Particle size and shape have a significant influence on the behaviour of the particles between the contacting surfaces. Their shape will determine whether a particle rolls or slides during three-body abrasion and size determines the transition of wear modes from three-body to two-body abrasion and therefore the severity of the wear.

It is a familiar observation that the wear process in both two- and three-body abrasion and erosion of ductile surfaces becomes less efficient as the eroding or abrading particle sizes decrease below about 100 microns. Studies by Jiang et al. ^[26] and Sin et al. ^[27] concluded that the size effect was related to particle shape. Ideally sharp particles complied with the classical abrasion model of plastic deformation with no size effect, whilst a size effect was observed with rounded geometry tips to a tip radius as small as 0.5 microns. Rabinowicz et. al. ^[14] observed that the value of the abrasive particle diameter at which full abrasion would occur, i.e. the critical size, was of the same magnitude as the average loose wear particles of the sliding materials, obtained in the absence of abrasive particles. However a paper by Misra & Finnie ^[25], published in 1981, which summarised the different theories presented on the size effect

phenomenon, concluded that the only explanation, which could not be discounted, related to the flow stresses in the surface layers of the contacting materials. Shallow surface layers exhibit a higher flow stress than that of the bulk material when they are being eroded or abraded. This explanation was first proposed by Kramer & Demer^[25] in 1961. They suggested their hard layer model in which the surface layer of about 50 – 100 microns work hardens more than the bulk material. Thus when small particles abrade the surface they only influence the hard layer, consequently encountering much harder material than larger particles which can penetrate the hard layer and plastically deform the softer material below the hard layer and abrade more. After some critical particle size, the influence of the hard layer will be minimal and thus there will be no increase in wear rate for a further increase in particle size.

Another published review by Misra & Finnie^[10] on abrasive wear surmised that the shape of the abrasive particle had a significant effect on the wear resistance of a metal. As might be expected angular particles were found to produce more wear, than rounded ones, as they tend to produce more chips, whereas spherical particles lead to more plastic deformation. Studies by Howarth^[32], focused on the abrasion behaviour of carbon steel surfaces, found that finer particles, particularly crushed quartz, presented a greater multiplicity of cutting edges for an equal volume of abrasives and therefore would cause more rapid wear than larger particles. In his opinion the angularity of a grain was a more potent factor than hardness, on the abrasivity of the media. This agreed with studies by Avery^[33] who found that angular particles of crushed quartz caused more wear than rounded quartz sand. Although softer than Ottawa sand, angular particles of crushed feldspar were found to be more abradent than the rounded Ottawa sand. Angular particles tend to present higher attack angles than round ones and therefore leading to higher wear rates^[1].

Two-body and three-body abrasion and erosive wear tests conducted by Stachowiak^[31] and Hamblin^[30] demonstrated that there was a linear relationship between particle angularity and abrasion / erosion resistance. Using two different techniques to determine the 'spike parameter', or angularity, of different particles they found that the number of 'active' peaks of a grit particle was an important factor. This agreed with Rabinowicz^[14] who found that a particle shape change from conical to spherical effected the relationship between k and hardness to one of inverse proportional to a power greater than one. Studies by Wirojampatump and Shipway^[15] agreed that k was strongly dependent on particle characteristics as well as environment.

Three-body abrasive studies by Rabinowicz et al.^[14] and Deuis et. al. ^[38] found that a wet environment promoted higher wear rates compared to dry test conditions. However a comparative study of the wet and dry abrasion resistance of mild steel by Wirojanupatump & Shipway ^[15] found that wear rates were considerably less under wet conditions, which agreed with the findings of Haworth ^[32]. Wirojanupatump & Shipway found that environment influenced the predominant wear mechanism which was three-body under dry conditions but altered mainly to the two-body mechanism in a wet environment.

The relationship between the hardnesses of the contacting surfaces and the hardness of the particles, and how these influence particle motion and wear in the system is discussed in section 3.4.

(ii) Solid particle erosion

The variables affecting pure erosion (i.e. with no corrosion synergistic reactions or in the absence of corrosion) can be broadly separated into three types. These are impingement variables that describe the particle flow, such as velocity and impact angle, particle variables relating to the abrasive particle characteristics, and material variables. This, thus reiterates the fact that a surface's ability to resist wear is strongly dependent on all the variables within the tribological system and not just the contact material properties such as hardness and toughness.

As discussed in section 3.2 and illustrated in figure 3.7, the rate of erosion is a strong function of the impingement angle of the particle. The most severe condition for brittle surfaces is impingement of particle at right angles to the surface whereas for elastic materials, such as rubber, erosion is high at low angles but tends to zero towards 90°. Maximum erosion of ductile surfaces occurs at low impingement angles typically between 15° and 30°^[19,20]. The reason for this intermediate range is related to the material removal mechanisms. As with abrasion, the most efficient removal rate of ductile surfaces is thought to occur by a cutting and ploughing action. At very low impingement angles, <15°, there is insufficient force to press the particles against the surface, thus resulting in little indentation. Whilst at high impact angles the tangential motion needed to cause the groove is very low. Thus at intermediate angles the erosion rate is highest. At angles close to 90° a fatigue mechanism is thought to be predominate for ductile materials ^[34]. Table 3.1 summarises the three basic types of material and their response to different particle impingement angles.

Table 3.1: Effects of impact angle on material response to solid particle erosion ^[21]

Type of material	Angle of impingement		
	< 20°	45°	90°
Elastic	Surface deformed	No observable effect	No effect
Ductile	“Cutting” wear maximum	Mixed regime	Deformation wear maximum
Brittle	Very little erosion	Intermediate erosion	Maximum erosion

When comparing the wet and dry erosive behaviour of HVOF sprayed coatings, Hawthorne et al. ^[21] found that the trend described above was less defined under wet erosive conditions. None of the ten coatings that were evaluated exhibited a characteristic ductile response, although they were classed as ductile type coatings. Studies by Dorfman and Mohanty ^[37], on HVOF sprayed tungsten carbide type coatings, found that particles tended to ride along the surface when the impact angle is less than 45° and produce an abrasive type wear.

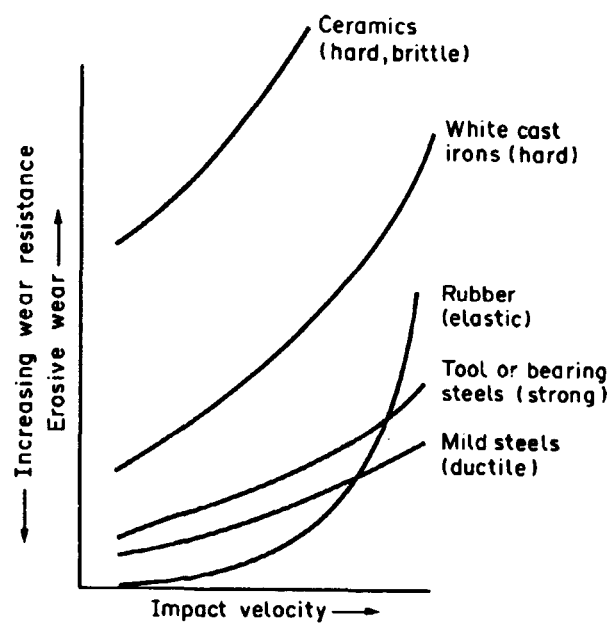
It has been shown in the modelling of solid particle erosion that the erosion rate is proportional to the impact velocity of the erodent regardless of the whether the target surface is ductile or brittle. For both types of materials, the erosion rate increases with increasing impact velocity. However the effect of the increasing velocity will depend upon the target material, as depicted in figure 3.7. For conventional materials of construction the impact velocity for which the collision remains purely elastic rarely exceeds 10ms⁻¹ ^[24]. Erosion slurry tests have found that the actual erodent-target impact velocities are much less than the impingement velocity due to both particle rebound shielding effects in concentrated slurries and to fluid dynamic effects ^[21].

Moore and Wood ^[36] studied the erosion of pipe materials in slurry flow streams. They concluded that particle energy, E_k , dominated the rate of erosive wear, regardless of the type of material, and could be derived by

$$E_k = \frac{1}{2} mv^2 = \frac{\pi \rho d^3 v^2}{12} \quad (3.16) \quad [36]$$

where m is the particle mass, ρ is the density and d is the diameter of the erodent particles and v is the impact velocity. This approach could be adapted to model the behaviour of the particles flowing through the pumping element, as the technique does not require the impingement angles to be quantified.

Figure 3.7 : Effect of impact velocity on erosive wear ^[24]



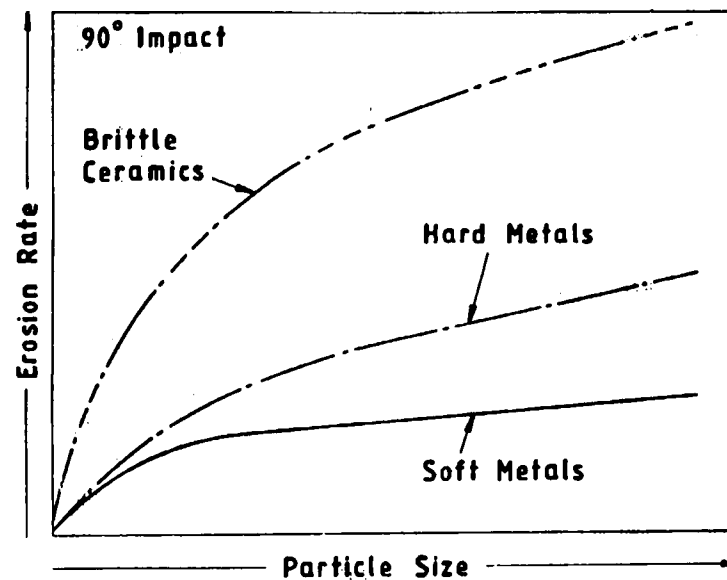
The equations for the maximum particle velocity and average fluid velocities are given in section 2.5. However these do not describe the behaviour of the particles inside the capsulisms with regards to impingement angles and impact velocities on the rotor or stator walls, or the velocity of the fluid across the seal lines when pumping against a pressure. Thus, actual particle and fluid velocities within the pumping element could potentially be much larger and contribute significantly to the wear mechanisms and the rate of wear.

As with abrasion, sharper particles create more erosive wear than rounded ones. The shape influences the pattern of plastic deformation around each indentation and the proportion of the material displaced from each indentation that forms the rim or lip. Rounded particles lead to less localised plastic deformation, and more impacts are required to remove each fragment of debris ^[1]. Increasing the impact angle has a similar effect. The degree of angularity of angular particles is also important, with erosion rates found to increase by a factor of 2 to 3 with angularity. The same applies with the fragmentation of spherical particles, which results in the formation of fresh angular cutting edges.

As described in section 3.2.3 the impact of hard angular particles on a brittle surface results in the formation of lateral cracking whereas spherical or blunt particles at low impact angles will only generate Hertzian cone cracks and therefore no material removal. Impact by angular particles, at low angles, will tend to cause plastic deformation of material and the extent of cracking is generally reduced ^[20].

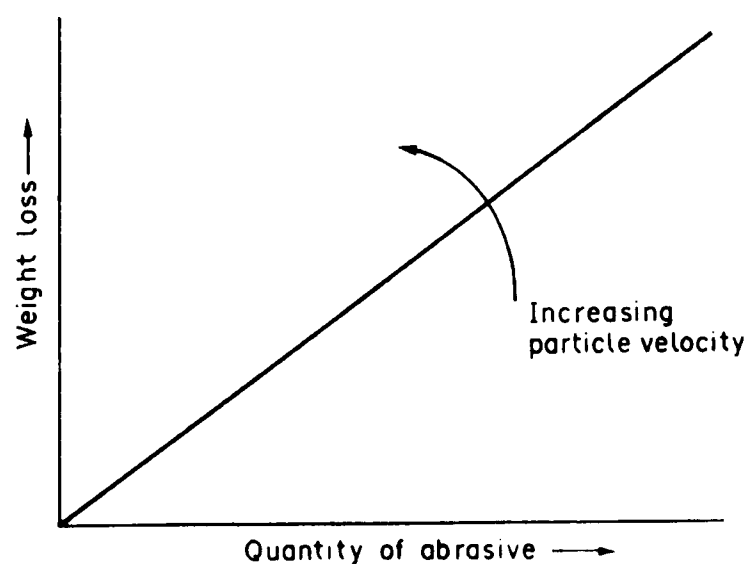
Classical theory predicts that the erosion rate of ductile material is independent of particle size above a critical value of about 100 – 200microns, but decreases rapidly below this value, as shown in figure 3.8 ^[1,20,24]. This size effect is similar to that observed for abrasion. For brittle surfaces, the erosive rate is proportional to the size of the particle as expressed in equation 3.13.

Figure 3.8 : Effect of particle size on the erosion rate at 90° ^[24]



Equation 3.5 predicts a linear relationship between the material weight loss and the concentration of particles in the system, figure 3.9. However studies by Turenne et al. ^[38] found that the erosion rate decreased according to a power law of the sand concentration in the slurry.

Figure 3.9 : Effect of particle concentration on weight loss ^[24]



Figures 3.10 and 3.11 summarise the material properties requirements for abrasion and erosion resistance under different conditions. For low impact angles and low velocities the main selection criteria to prevent a surface from eroding is high hardness. As the velocity increases the material requires adequate toughness as well as hardness. These are the same material requirements as those required to resist low stress abrasion by hard particles. For resistance to erosion a rubber component, such as the stator, whose function is to create a seal with a moving part, must be tough enough to resist penetration but retain resilience for the seal. Lansdown^[24] recommends a hardness of 50-90 IRHD and states that in order to maintain high resilience the hardness of the rubber should be achieved by cross-linking rather than by fillers.

Figure 3.10 : Guide to selection of material type for abrasion^[24]

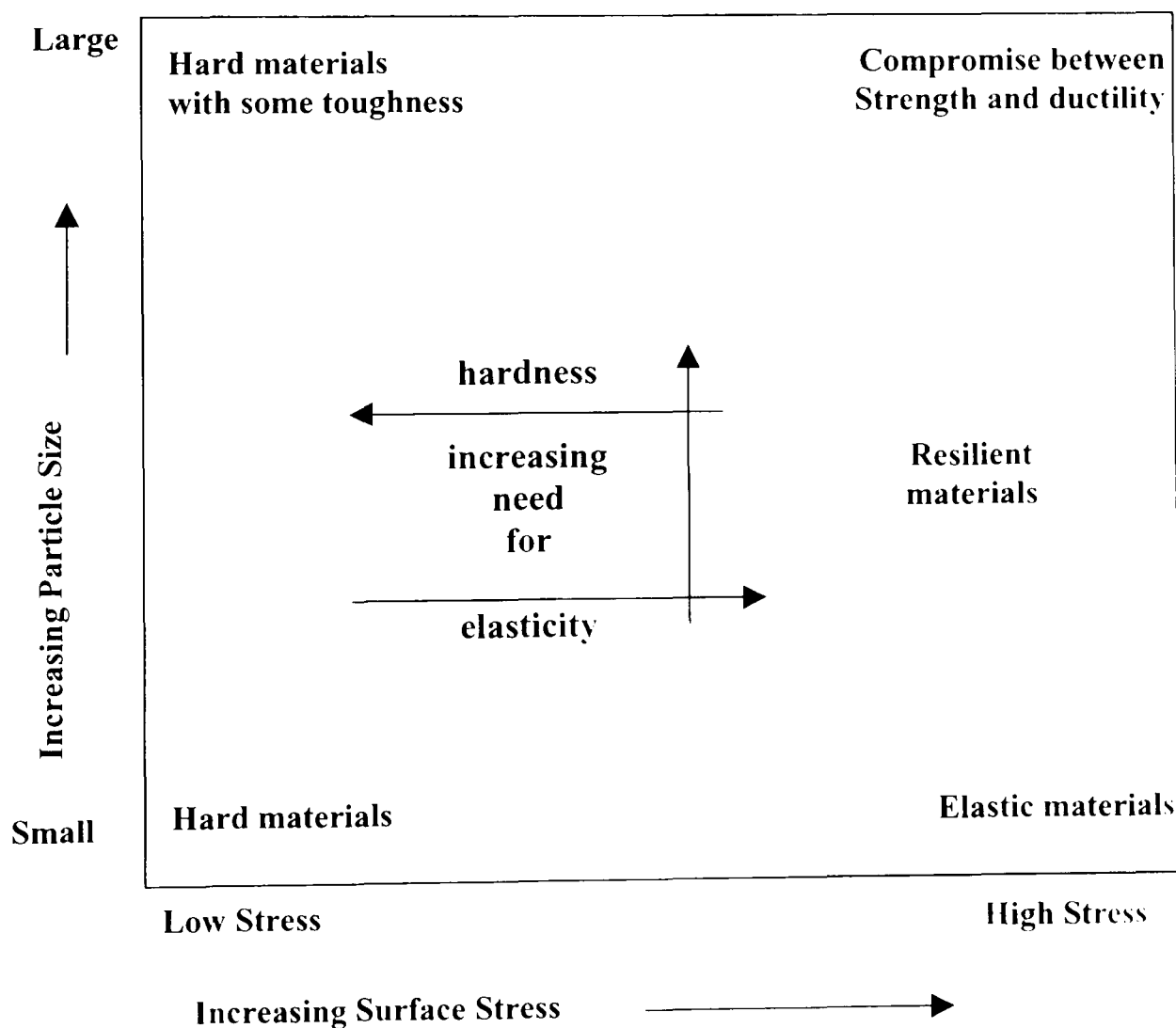
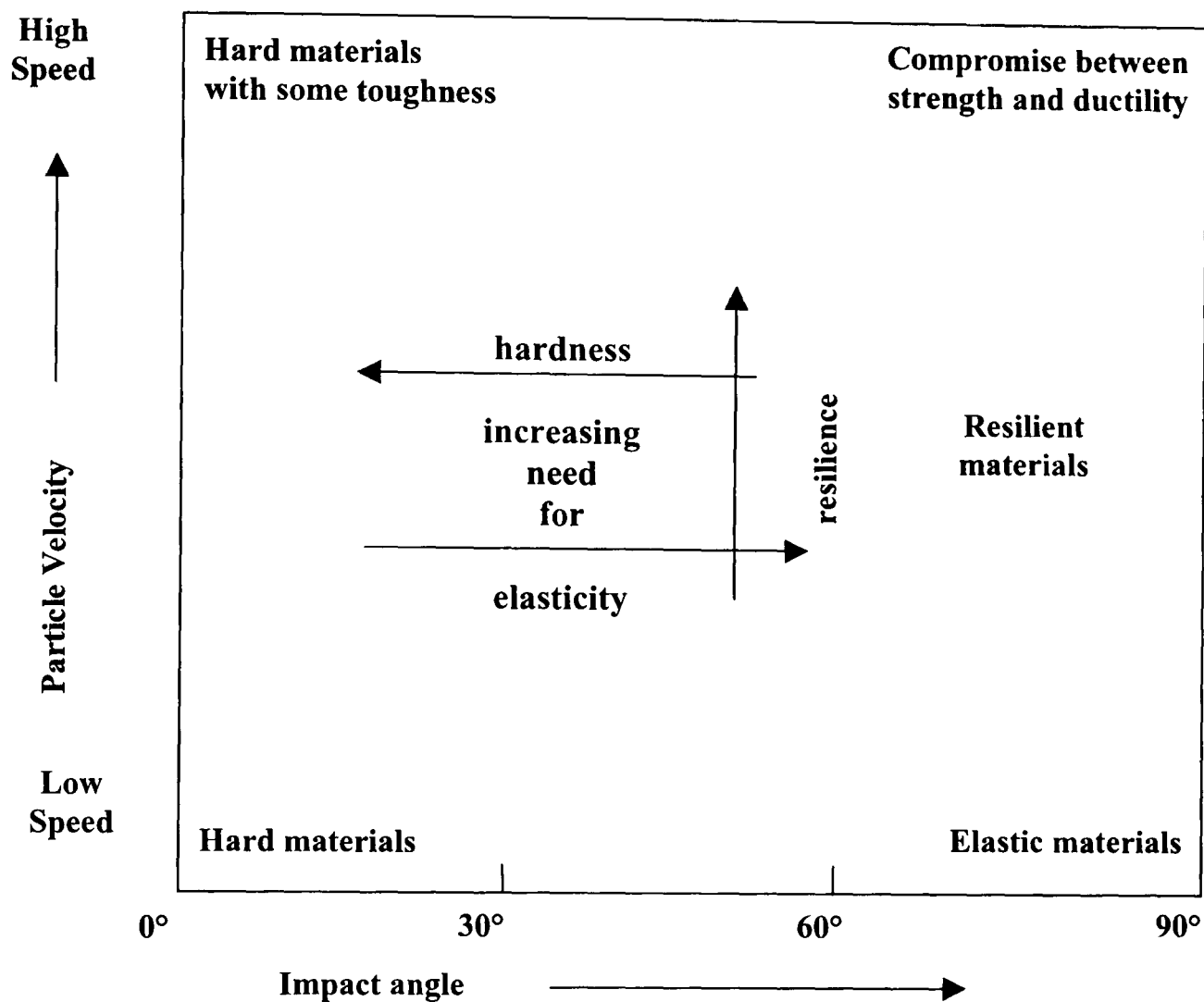


Figure 3.11 : Guide to selection of material type for solid particle erosion ^[24]

3.3 RUBBER ABRASION AND WEAR

It is important to clarify the terminology to be used in this section. The term 'abrasion', with respect to rubber, relates to all the mechanisms of wear, unlike when used to describe the tribological behaviour of other materials, where 'abrasion' is a specific wear mechanism which removes material by the scoring of hard sharp particles. The 'abrasion resistance' of rubber can be defined as 'the resistance of a rubber compound to wearing away, when in contact with a moving abrasive surface ^[39]. Standard tests, for published wear data on dry abrasion, comprise of a piece of rubber compound slid against an abrasive surface under specified load and speed. These standards include ISO 4649, ASTM D 2228, D1630, BS903:Pt. A9, DIN 53516.

A comprehensive review on rubber abrasion, by Zhang ^[40], divides rubber abrasion into the three categories of dry, oily and wet abrasion, with a fourth category, abrasive-erosion, added to in a later review ^[41]. Dry abrasion is subsequently sub-divided depending, upon the contact type; single point, line or multiple, and wet abrasion is sub-divided into two- or three-body. In the

original review, the concept of wet abrasion, according to Zhang, had been neglected as an independent form of wear, due to the close analogy of the process with abrasive-erosion.

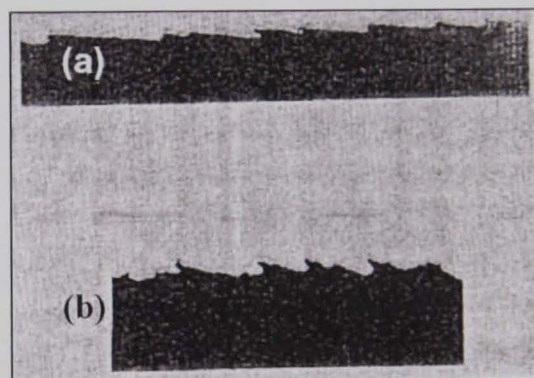
As with wear mechanisms of metals, rubber abrasion is a complex process composed of a number of distinguishable mechanisms. It is thought that the main cause of abrasion is tearing or fatigue under the action of high local stresses caused by friction^[39], a process described by Zhang, as a 'stick-slip' phenomenon^[41]. Friction must exist in the tribological system for rubber abrasion to occur, as the two are interrelated. The frictional coefficient of a rubber depends on many factors, including the geometric shape, composition and the surface finish of both contacting surfaces. It has been found to increase with sliding speed and decrease with temperature, but be independent of the applied load^[41]. However sliding of rubber with high frictional forces does not necessarily entail abrasion. Rather, abrasion of rubber results from mechanical failure due to excessively high local frictional stresses, which are most likely to occur on rough tracks. Therefore, to predict rates of abrasion details of the local stresses, along with strength properties of the rubber, are required. In the opinion of Muhr and Roberts^[39] contributions of friction arising from energy losses associated with bulk deformation, and from viscous dissipation in any lubricant film, will not cause large local strains and therefore will not contribute to abrasion. Thus in their view the overall average level of friction is of no direct significance for abrasion.

3.3.1 *Dry abrasion*

When an elastomer is abraded without a change in direction, sets of parallel ridges are often found on the surface of the sample and at right angles to the direction of the motion. These ridges are called 'abrasion patterns' and are characteristic to the wearing process of a low modulus elastomer sliding with high friction against a counterface^[39,42,43]. A cross-section of these ridges (figure 3.12) shows an asymmetric saw tooth profile, the steep sides of which face the direction of attack. During the sliding motion of the abradant, the "teeth" are bent backwards, exposing their underside to the action of the abradant. At the same time, part of their surface is protected, from the abrading action, at the rear, resulting in an undercutting effect. The teeth wear progressively thinner until the crests are torn away, producing large pieces of debris which leave behind blunt edges. In the meantime the ridges continue to grow out from the bulk material and the abrasion pattern becomes self perpetuating. In the absence of any serious chemical decomposition, the abrasion process initiates with micro-tearing of small rubber particles, just a few microns in size, which leave behind pits in the surface, the size of which depend upon the frictional stress. With continued rubbing, larger pieces of rubber (in the

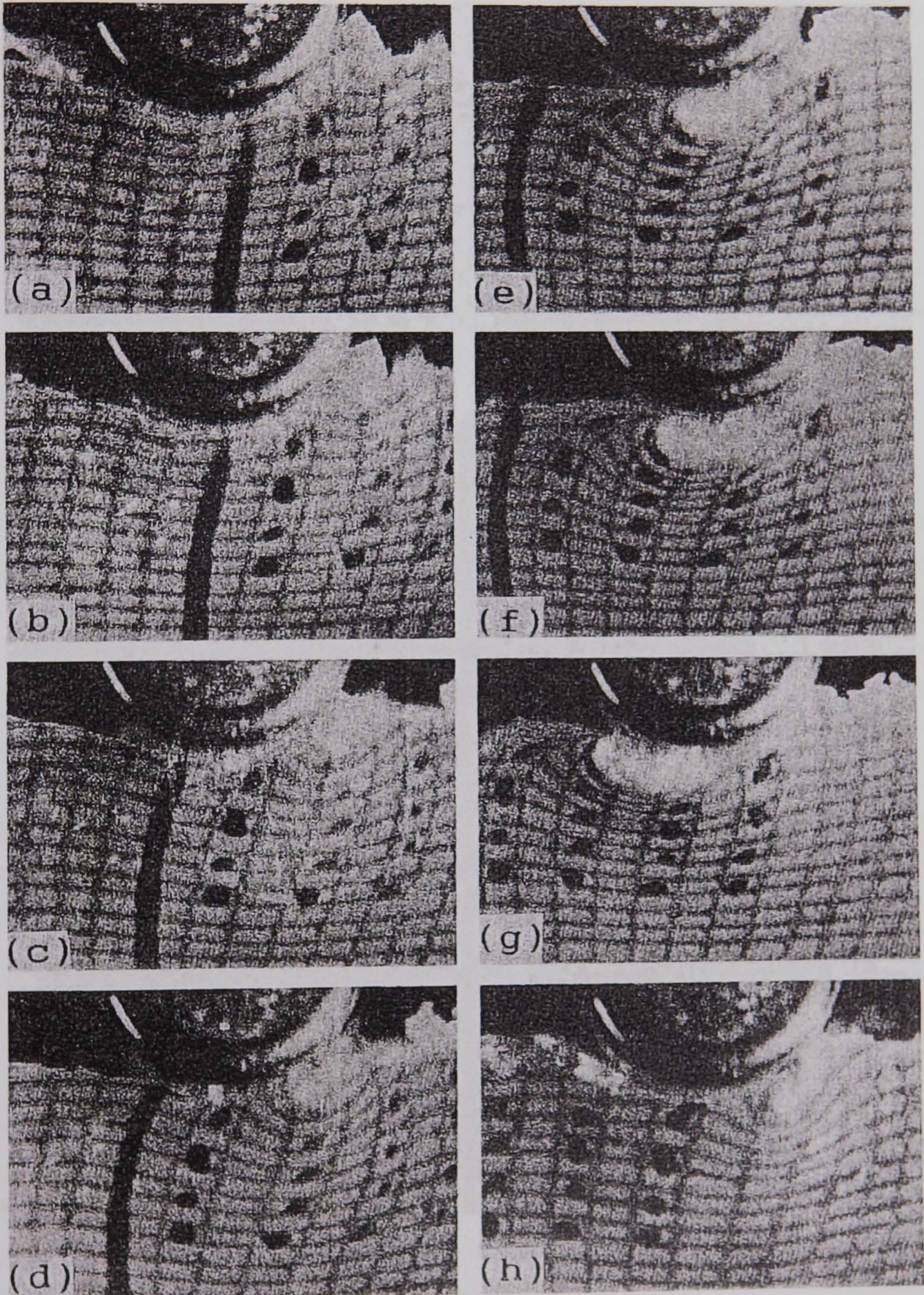
order of 0.1mm) are removed, which coalesce to form fine ridges that progressively thicken. Although more weight loss is attributed to the larger pieces, it is thought that the detachment of the smaller particles initiates the abrasion process^[39]. According to Fukahori and Yamazaki^[44] the stick-slip oscillation is the driving force which propagates the cracks whilst the micro-vibration, generated by the natural frequency of the rubber during the slip phase of the stick-slip, initiates the cracks. On sharp tracks the abrasion pattern is replaced with score lines parallel to the direction of motion if the modulus of elastomer is sufficiently high or if friction is reduced by the presence of lubricant^[39]. An abrasion pattern will only be generated if the sliding direction remains unchanged. When there are periodic changes in the travel direction of the abrasive particles, the formation of the pattern is prevented and 'intrinsic abrasion' is then said to occur.

Figure 3.12 :Cross-sections through abrasion pattern on (a) unfilled NR and (b) a worn tyre tread^[39]. (No scale given in original reference paper)



Uchiyama and Ishino^[45] studied the mechanisms of pattern abrasion by observing the deformation of a rubber wheel whilst rubbing against a steel cylinder. Printed on the side of the wheel was a fine grid, with radial lines at every degree. During the experiment photographs were taken using a 16mm movie camera, some results of which are shown in figure 3.13. At figure 3.13 (a) one ridge of the rubbing surface is just about to enter the contact area, to the right of the photograph. The ridge becomes increasingly deformed as it passes through the contact zone (figures 3.13 (b) through to (g)) with the largest strain appearing at the lower front part of the ridge, as shown in figure 3.13 (g). With the repeated cycles of compression and tension, cracks continue to propagate on the lower front part of the ridge, until finally the ridge springs back, figure 3.13 (h), and is released from the frictional force. The process then repeats with a new contact on the right-hand side of the next ridge.

Figure 3.13 : Deformation of a rubber specimen when a 6mm diameter cylinder slid on the ridge of the rubber surface from left to right ($W = 17.6\text{N}$; $N = 315$ rev). Photographs were taken every 0.1s ^[45]



Studies ^[39,45] have found that the evolution of the abrasion pattern, and hence the abrasion rate, is proportional to the sliding distance between the rubber and the counterface, and a power relationship exists between the linear wear rate and the spacing of the abrasion pattern. The movement of the abrasion pattern, which results from crack propagation at the root of the tongue and the subsequent cutting off when it has reached its largest size, is proportional to the applied load. It is thought that hardness has little effect on the abrasion resistance of rubber. In the stick-slip process the magnitude of the elastic restoring force, which tries to pull the surface back into its unstrained state once adhesion or 'stick' has occurred, is very important which not only depends on stiffness but also on resilience. With increasing deformation through the length of the contact the restoring force eventually exceeds the local friction force and the rubber surface slips at the rear of the contact zone with consequent abrasion. For a highly hysteretic rubber, abrasion does not happen, because, at the rear of the contact zone, the rubber is so slow to recover that no slip occurs.

3.3.2 Abrasion of rubber under wet conditions

Wear of rubber under wet, abrasive conditions can be divided into two types; wet abrasion and abrasive-erosion. The distinction between wet abrasion and abrasive-erosion is that the leading feature of the former is the abrasive fluid flowing between the interacting solid surfaces under load contact, whilst abrasive-erosion is initiated by a fluid medium containing particles flowing in a direction approximately parallel to the surface, at a certain speed ^[41]. Note that these are similar to the metallic wear definitions of abrasion and glancing angle slurry erosion.

(i) Wet abrasion

The definition of 'wet abrasion' or 'hydro-abrasive' wear describes the wear process of the operating surface of a body induced by a fluid medium containing abrasive particles between the interacting solid surfaces in relative motion ^[40]. As with abrasion of metallic surfaces, the movement of the abrasive particles in the contact area can produce the conditions of either two-body or three-body abrasion.

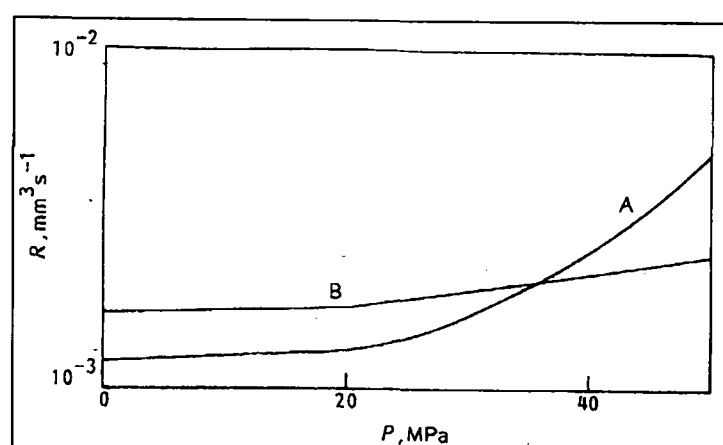
The contact conditions of wet two-body abrasion are the same as those for dry abrasion with the addition of the presence of a lubricant. Lubricated tests with a blade abrader have demonstrated that wear rates are dramatically reduced by at least a factor of ten due to the presence of a lubricant, whilst the frictional force decrease is significantly less at approximately only 10% ^[41,46]. In addition to a reduction in the wear rate the morphology of the worn surface changes to one of much finer pattern spacing.

From wet abrasion experiments on nitrile rubber in oil-well drillings, Zhang ^[46] compared the wear morphology generated by both two- and three-body wet abrasion. For both conditions he observed a series of parallel traces, or grooves, interspersed with a micro-layered surface texture, which he describes as small, closely spaced flaps. The distinction between the two was the frequency and appearance of the traces. Under three-body conditions the traces were described as ‘tearing’ with irregular edges, thought to be due to particle rotating as well as sliding through the contact zone. The traces, under two-body abrasion, were far less frequent with smoother edges, which Zhang described as ‘scratching’ traces. The morphology of the micro-layered texture was similar for two-body abrasion and under low loads in three-body abrasion, with the flaps lying almost at right angles to the traces. Increasing the normal load to above a critical value, changed the angle of the micro-layered flaps to that lying parallel with the direction of motion. This phenomenon was attributed to the fact that the flowability of sands in liquids is much worse under heavy contact loads. It was observed that the fineness of the micro-layered surface texture was an indication of the abrasion level of the worn surfaces. Zhang concluded that the mechanism of three-body wet abrasion appeared to involve two simultaneous processes of directional micro-tearing by the coarser particles and directionless micro-layering or micro-polishing by the fine particles, with the latter being the dominant material removal process. From this same study Zhang found that the wear characteristics of nitrile rubber were influenced by numerous other factors such as normal load, rotating speed, sliding distance, grit content and grit size in fluid medium. He found that the increase in grit content in the drilling mud was the primary factor in accelerating the wet abrasion rate of the rubber.

In Zhang’s earlier review of rubber abrasion ^[40] he provides several examples of studies by various authors on wet abrasion, which were directed at specific industrial applications. The Russian, Kanilina, designed a simulated ‘in-service’ wear rig to study the service conditions of a screw liner pair in a Dynadrill. A Dynadrill is a downhole drilling motor with a very similar tribological system as the progressive cavity pump. It comprises of a multi-lobed rotor and stator, which is operated in reverse to the pump, to convert hydraulic power into the high torsional drive required to rotate a drilling bit. The simulated wear rig comprised of a steel cylinder rotating inside a rubber-lined cylinder, immersed in water containing abrasives, and in drilling mud, to determine the effects of dynamic load and frequency, concentration of abrasives and thickness of the rubber-lined layer, had on the wear characteristics of the screw-liner pair. At a frequency of $\nu = 2\text{Hz}$ and magnitude $S = \pm 118 \text{ Ncm}^{-2}$ of dynamic stress, a plot of the rubber wear rates in an abrasive liquid containing 3 v.v.% of abrasives against dynamic load

was derived, figure 3.14. The wear rate of the rubber was found to increase with increasing dynamic load per unit area, in particular for $p \geq 20$ kPa. The wear mechanism of rubber under the action of dynamic load was predominantly due to a process of micro-cutting and micro-scratching. Furthermore it was proven that the lifetime of rubber was related to its tensile strength and tear strength.

Figure 3.14 : Wear rates, R , (mm^3s^{-1}), plotted against average dynamic load per unit area, P (kPa): 'A', in water containing abrasives; 'B' in drilling mud ^[46]



Studies by another Russian, Puchugen, referenced in [40], on the effect of various abrasive-containing liquids on the wear resistance of the rubber seal in the piston of a drilling pump found that the wear resistance of the rubber for all the test media was inversely proportional to the load per unit area, which agreed with Kanilina. The wear mechanism was found to be dependent on the load per unit area, as it was postulated that under conditions of high contact loads hardly any abrasive particles were able to enter the contact zone.

(ii) Abrasive-erosion

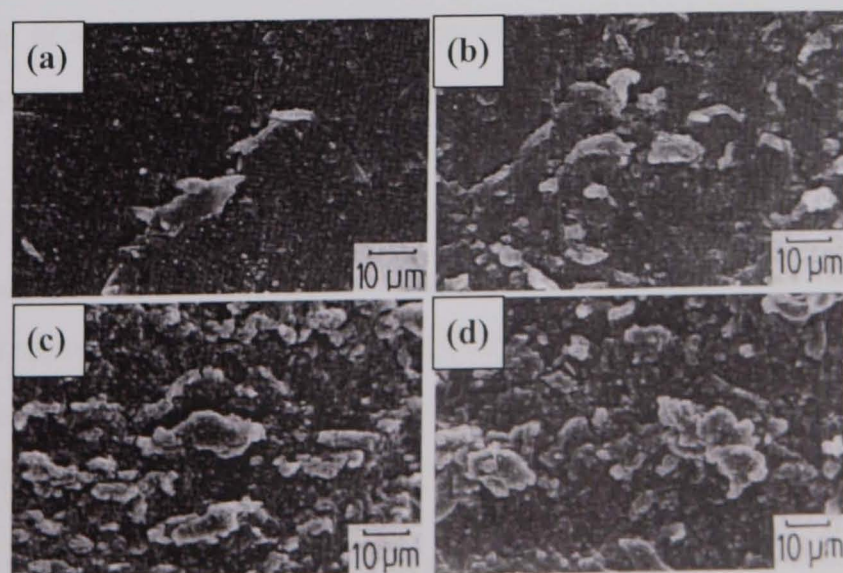
The mechanism of abrasive-erosion is dependent upon the type polymer. Arnold and Hutchings^[47] studied the erosive wear of unfilled elastomers and found that material was removed by fatigue-crack propagation, although the mechanism depended upon the particle attack angle. At high impact angles, the frictional forces from the particle impacts generate tensile stresses in the surface, that cause the growth and intersection of fine cracks on the surface, resulting in material loss. Whereas at glancing angles, the mechanism of material removal was found to be very similar in nature to that of abrasion by a sharp blade or a smooth indenter.

Research on the mechanism of rubber erosion has mostly been confined to the study of the physical process of the wear. The East China Petroleum Institute have studied the surface chemical effects in abrasive wear of polymers, and found the mechanical fracture of macromolecular chains and oxidative degradation to be the main chemical effects on the erosion on nitrile rubber ^[41].

3.3.3 Erosion of rubber

The mechanism of material removal of low angle erosion of rubber is thought to be different to the ploughing and cutting action observed with metals. Studies by Arnold and Hutchings ^[47] on low velocity erosion of rubber at low impingement angles of 30° found that the wear features produced, of very well-defined transverse ridges, were similar to the patterns produced by abrasion, with both processes accelerated by environmental degradation of the rubber. Consequently it is difficult to distinguish between the two mechanisms. At glancing impact angles the transverse wear features of tears and cracks, which form perpendicular to the erosion direction, could possibly suggest a fatigue type mechanism, as opposed to the cyclic stick-slip mechanism of abrasion. Although similar in features, an elastomer with good abrasion resistance exhibits poor erosion resistance, and vice versa. High erosion resistance is achieved with unfilled elastomers with low modulus and high rebound resilience, whilst filled elastomers with high modulus provide good resistance to abrasion. At higher impact velocities, Arnold and Hutchings observed that the ridges were still present but were much more broken up and less well-aligned. They published a series of SEM images, shown in figure 3.15, to demonstrate the progressive damage during the incubation period of an eroded rubber surface, at an impingement angle of 30° with 200 micron silica sand.

Figure 3.15 : SEM images of the surface of rubber samples at various stages during erosion at an impact angle of 30° and an impact velocity of 100ms^{-1} (erosion direction from the top): (a) after 0.1g; (b) after 0.5g; (c) after 5g; (d) after 200g (steady state)



3.4 HARDNESS RELATIONSHIPS BETWEEN CONTACT SURFACES AND ABRASIVE PARTICLES

An important aspect which classical abrasion theories do not consider is how the hardness relationships between the particles, the wearing surface and the counterbody surface interact and influence the behaviour of the abrasive particles. Archard's wear equation, and Rabinowicz's model, has been used by many to determine experimental wear rates of materials, from the gradient of the plot of volume loss against the product of sliding distance and load, and assume the hardness to remain constant. However where, for example, it has been used in three-body abrasion laboratory tests, such as the rubber wheel abrasion test, it can be argued that under these types of contact conditions Rabinowicz model no longer applies.

In a three-body abrasive tribological system there are three possible combinations of hardness ratios:

- (i) that between the wearing surface, H_s , and the abrasive particles, H_a
(H_s/H_a)
- (ii) that between the wearing surface, H_s , and the counterface, H_c
(H_s/H_c)
- (iii) that between counterface, H_c , and the abrasive particles, H_a
(H_c/H_a)

The effect on the wear rate of the hardness ratio of H_s/H_a , (or H_a/H_s , as it sometimes expressed), under two-body abrasion conditions has been well documented ^[10,48], which includes the famous scale created by the Austrian mineralogist Mohs ^[1]. Based on the observation that the abrading material must be harder than the material being abraded, Mohs graded ten minerals depending upon their ability to scratch one another. He assigned integer hardness numbers to the minerals and produced a scale where each mineral would only scratch those below it on the scale. With the exception of diamond, the ratio of indentation, i.e. H_a/H_s , between neighbouring minerals is nearly constant at about 1.6. The studies have demonstrated that for a surface to be resistant to two-body abrasive wear its hardness must be greater than that of the abradant, by ~20%.

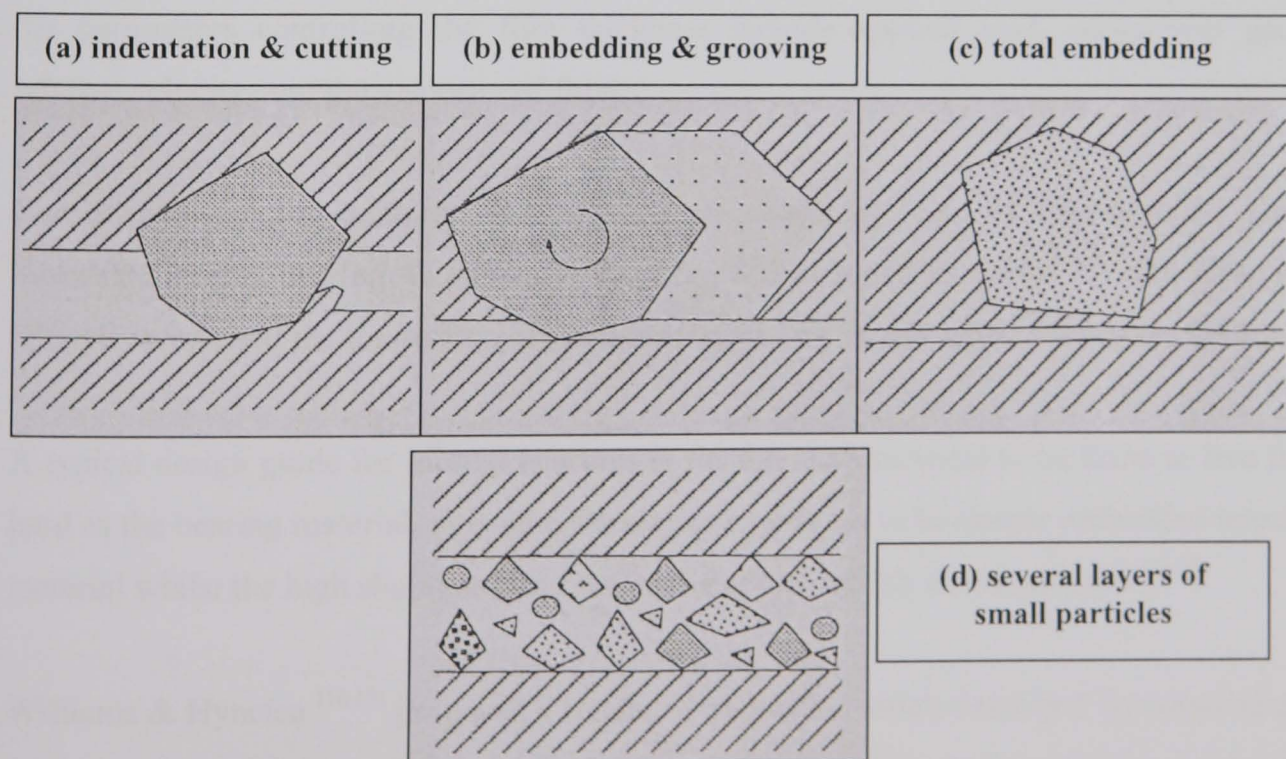
However only a few investigators have discussed the problem of any of these three critical hardness ratios in three-body abrasion. Xuan et al. ^[48] studies on the interdependence between three hardness ratios found that, under three-body abrasion conditions, a critical value for H_a/H_s did not exist and the wear rate tended to continuously increase for low values of H_s/H_a or a high H_s/H_c values. Bozzi and De Mello ^[29] demonstrated that this transition ratio from mild to severe

wear was only valid when the wear was dominated by plastic deformation mechanisms. Their studies looked at three-body abrasive wear of thermally sprayed tungsten carbide-cobalt coatings and the results indicated that the abrasion resistance and predominant wear mechanisms were strongly dependent on the hardness of the abrasive particles.

Axen et al. ^[49] examined the effect of counterbody hardness in abrasion with free particles. They studied the effect of the hardness differential, H_s/H_c , between metallic contacting surfaces from pure lead to quenched tool steel. Using a dimple grinder test they found that the wear rate of either part was higher when the counterbody was softer, regardless of whether the wearing surface was the stationary plate or the rotating grinding wheel.

According to Axen et al. in tribological systems involving abrasion with loose particles there are two extreme of particles behaviour which either remove material due to rolling or become pressed or embedded on one surface and groove the other, and thus simulate two body abrasion. Between these two extremes many types of interactions between the abrasive and the solid surfaces are possible, depending the hardness ratio of counterbody to abrasive particles, (H_c/H_a) . The possible interactions which could describe the contact conditions in the pumping element are schematically illustrated in figure 3.16.

Figure 3.16 : schematic overview of possible interactions between hard abrasives and two solid surfaces in sliding contact ^[49] .



From their studies on the effect of hardness differential between metallic contacting surfaces, under three-body abrasion, Axen et al. concluded that a particle will always partially penetrate the softer surface. How and to what extent will be determined by the hardness of both surfaces and the load. If the surfaces are of different hardnesses, a preferential indentation of the abrasives into the softer surface will take place, figure 3.16 (a). This can lead to the situation where the abrasive is held by the softer surface, and the wear mechanism changes to that of two-body abrasion with the harder surface suffering material removal by grooving wear. It is believed that it is the ability of the softer material to hold the abrasive that is the decisive factor on the wear rate. Abrasives that are deeply and firmly embedded in the softer surface result in a continuous cutting action and consequently the harder counterbody has a high wear rate. However situations where the particles are only temporarily embedded are also possible, i.e. they are torn out and re-embedded in some other part of the contact surface. The abrasive can also be deeply embedded but plough forward through the softer material, figure 3.16 (b), which would result in a more three-body abrasion and thus a lower wear rate. Or the fact that the abrasives are not firmly fixed but are moving around can result in continuous exposure of fresh cutting tips and therefore would contribute to a higher wear rate. All these types of particle/surface interactions describe the behaviour observed by May and others, in the limited data available, on the contact conditions of the pumping element. The another scenarios, postulated by Axen et al., that agrees with the observations of May is when the gap between the sliding surfaces is wider than the size of the individual particles so that no two-body abrasive cutting is possible, figure 3.18(d). In this case the load must be carried by the hydrodynamic pressure in the fluid film and the parameters controlling the film thickness include applied load, component geometry, relative velocity, and the viscosity of fluid.

Comparisons of the pumping element contact conditions can be drawn with studies on lubricated journal bearing. In particular those by Williams and Hyncica^[16,17] and Xuan et al.^[48] who all recognised the limitations of Archard's approach for three-body abrasive conditions.

A typical design guide for journal bearings is for the shaft material to be three to five times as hard as the bearing material, to enable the abrasive particles to be deeply embedded into the soft material whilst the high shaft hardness resists the cutting action of the particles^[16,48].

Williams & Hyncica^[16,17] proposed a model of abrasivity which described the abrasive particle motion under conditions of three-body abrasion, and within this model, considered the influence of a hardness differential between the two contacting surfaces. Loss of material will depend, not

only on the hardness of the wearing surface but also on those of the counterbody and the particles. The traditional approach to the situation is to improve the wear resistance of the more important or expensive part, at the expense of the counterface. However, when the embedded particles in the soft counterface act as very aggressive asperities this can be a false economy. Williams and Hyncica showed that an abrasive particle moving between two surfaces undergoes a transition from grooving to rolling wear at a critical value of D/h , where D is the particle major axis and h is the minimum thickness of the hydrodynamic lubrication film.

Their model of abrasive activity considered the mechanics of a single particle, figure 3.17, where D is the longest diagonal of the cross section, β , the angle that describes its shape, which must be $45^\circ < \beta < 90^\circ$ and h , the local lubrication film thickness. The surfaces of the body and counterbody, A and B, are assumed to be of the same hardness with the lower surface B moving from left to right. When D is small, D/h is < 1 , and the particle passes through the gap making only occasional impacts on the solid surfaces and therefore very little damage to either. The indentation force, R , is related to the size of the indentation and the hardness, H , of the solid surfaces, and is expected to be equal to the product of hardness and the projected area, and to act in a direction perpendicular to the indenting face. When the two surfaces A and B are of equal hardness, a similar indentation is assumed to be occurring at the opposite corner of the particle and thus the two forces R , form a couple which tends to rotate the particle. Increasing the particle sizes raises the D/h ratio to a critical value, where the particle rotates through contact with the two surfaces, but as yet is not sufficiently large enough to become lodged. This results in a certain amount of pitting damage but no grooving type wear, figure 3.18 (a) to (c). However beyond this critical value, the forces acting on the particle become collinear and the impetus for further rotation disappears resulting in grooving wear to both surfaces, figure 3.18 (d). The angle of rotation of the particle, θ_1 , is independent to the hardnesses of the contacting surfaces.

When a hardness differential, H , existed between the two surfaces, Williams and Hyncica observed more wear tended to occur to the harder surface due to the particle sticking to the softer one, figure 3.19, which agreed with the conclusions of Axen et al. ^[49]. For this to occur, there must be no relative movement along the interface PQ and the line of action of the forces acting on the particle must actually intersect PQ. The limiting value of the angle of rotation of the particle, θ_2 , now becomes dependent on the value of H . The ratio of H is given as that of the harder surface to the softer, so that grooving wear to the harder surface due to sticking of the particles to the softer surface will be enhanced when H is greater than unity.

Figure 3.17 : A single abrasive particle is described by the parameters D and B . The lower surface B is moving from left to right ^[16]

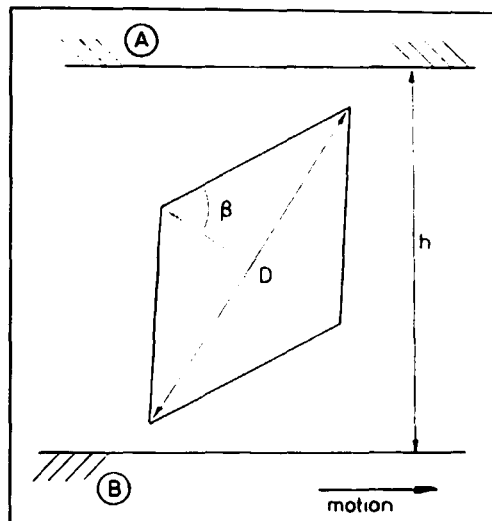


Figure 3.18 : (a) to (c): when $D/h > 1$ the particle rotates until a position of equilibrium is reached at a particular inclination resulting in the formation of a groove in both surfaces (d) ^[16]

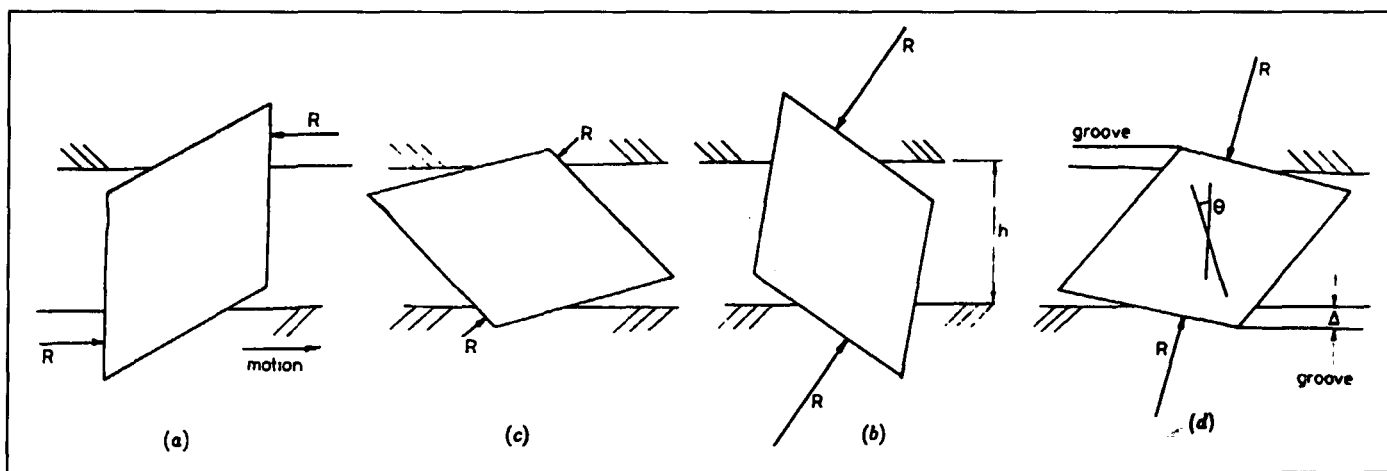
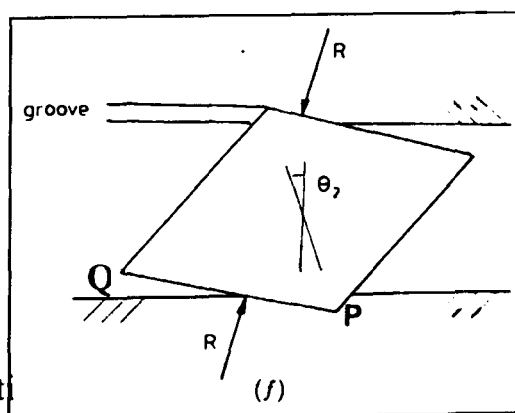


Figure 3.19: When a differential hardness exists between the two surfaces the groove tends to occur in the harder surface ^[3]



Applying this model to part (f), it is important to note that h will not remain constant throughout the contact area, so consequently the value of D/h will change. The pumping element lubrication conditions are discussed in section 2.1. According to

Belcher^[50], the film is generated hydrodynamically and therefore can be equated to that of a converging wedge where a minimum film thickness, h_o , is reached at the centre of the contact. However if in fact the lubrication conditions were created elasto-hydrodynamically then the minimum film thickness would be at the exit of the contact. Whether the critical value of D/h is greater than D/h_o will depend primarily on the abrasive particle size and will determine the point at which the transition from rolling to grooving behaviour occurs. Since wear is a dynamic process the contact conditions will not remain constant, once the process starts, due to the changes incurred in surface topography. For example if a particle were to pass in the wake of a groove created by a previous particle it might contribute less to the volume loss than if it were ploughing into a fresh surface^[16]. This would suggest an initially high wear incubation period followed by a lower steady state rate.

3.5 REFERENCES

1. **I. M. Hutchings**, "*Wear by hard particles*", Chapter 6, Tribology : Friction & wear of engineering materials, Edward Arnold, 1992, pp 141 – 166 & 171 - 186
2. **DIN 50 320**, Dec 1979, "*Wear : Terms, systematic analysis of wear processes, classification of wear phenomena*", pp 1 - 8
3. **G.H. May**, "*Least whole life cost : Section 2 : Design of progressive cavity pumps related to wear rates*", Mono Pumps Ltd. technical literature : LWLC/MKTG, Issue 1, November 1995, pp1 – 6.
4. **G. M. May**, "*Development of wear resistant rotors, Part 1 : Lab test rig*", Mono Pumps Ltd. Internal Report to L.T Mathewson, 15/12/88, Confidential.
5. **G. Vetter & W. Wirth**, "*Understand progressive cavity pumps characteristics and avoid abrasive wear*", Proc of 12th Int. Pump Users Sym., 1995, pp 47 – 59.
6. **W. Wirth**, 1993, "*The hydraulic and tribological modelling of a progressive cavity pump*", Ph.D.diss., University of Erlangen, Germany
7. **J.D. Bourke**, "*Pumping abrasive products with progressive cavity pumps*", Online available : <http://www.moyno.com/moyno/main.html> [accessed 18/07/01]
8. **S. Akincioglu**, "*Abrasive wear*" Mono Pumps Ltd. Internal memo, 16/04/82, Confidential.
9. **D. N. Allsopp, R. I. Trezona & I. M. Hutchings**, "*Transition between two-body and three-body abrasion : influence of test conditions in the micro-scale abrasive wear test*", Wear 225 – 259, 1999, pp 205 – 214.
10. **A. Misra & I. Finnie**, "A review of abrasive wear of metals", Journal of Eng. Mat. & Tech., Vol. 104, April 1982, pp 94 – 101.

11. **J. Williams**, "*Wear by hard particles*", Programme for Industry, University of Cambridge, 21/09/2001
12. **J. H. Tylczak**, "*Abrasive wear*", Friction, Lubrication & wear technology, ASM Handbook, Vol. 18, 1992, ISBN 0-87170-380-7, pp 184 – 190
13. **M. A. Moore & P. A. Swanson**, "*The effect of particle shape on abrasive wear: A comparison of theory & experimental*", Wear of Materials, 1983, pp 1 - 11
14. **E. Rabinowicz, L. A. Dunn & P. G. Russell**, "*A study of abrasive wear under three-body conditions*", Wear 4, 1961, pp 345 – 355.
15. **S. Wirojanpatump & P. H. Shipway**, "*A direct comparison of wet & dry abrasion behaviour of mild steel*", Wear 233-235 (1999) pp 655 – 665.
16. **J. A. Williams & A. M. Hyncica**, "*Abrasive wear in lubricated contacts*", J. Phys. D: Appl.Phys. 25, 1992, pp A81 – A90
17. **J.A. Williams & A.M Hyncica**, Mechanisms of abrasive wear in lubricated contacts, Wear 152, 1992, 57 - 74
18. **E.D. Gray**, "*Competitive parts analysis : rotors & stators*", Online, available: <http://www.moyno.com/mip/comppart.pdf> [accessed 10/05/00].
19. **B. Bhushan & B. K. Gupta**, "*Friction, wear & lubrication*", Handbook of Tribology, Chp. 4, 1997, pp 2.21 – 2.23
20. **T. H. Kosel**, "*Solid particle erosion*", Friction, Lubrication & wear technology, ASM Handbook, Vol. 18, 1992, ISBN 0-87170-380-7, pp 233 – 235
21. **H.M. Hawthorne, B. Arsenault, J. P. Immarigeon, J. G. Legoux and V. R. Parameswaran**, "*Comparison of slurry and dry erosion behaviour of some HVOF thermal spray coatings*", Wear, 225 – 229, 1999, pp 825 – 834.
22. **H.X. Zhao, M. Yamamoto & M. Matsumura**, "*Slurry erosion properties of ceramic coatings and functionally gradient materials*", Wear, 186 – 187, 1998, pp 473 - 479
23. **S. Ahmaniemi, J. Knuutila & T. Mantyla**, "*Wet abrasion and slurry erosion resistance of thermally sprayed oxide coatings*, VITT Symp. 180, 1998.
24. **A. R. Lansdown & A. L. Price**, "*Materials to resist wear : A guide to their selection and use*", Pergamon Press, 1986, ISBN 0-08-033442-3, pp 79 – 87.
25. **A. Misra & I. Finnie**, "*On the size effect in abrasive and erosive wear*", Wear 65, 1981, pp 359 - 373
26. **J. Jiang, F. Sheng & F. Ren**, "*Modelling of two-body abrasive wear under multiple contact conditions*", Wear 217, 1998, pp 34 – 45.
27. **H. Sin, S. Saka & N. P. Suh**, "*Abrasive wear mechanisms and the grit size effect*", Wear 55, 1979, pp 163 – 190.

28. **G. Huard et. al.**, *The effects of size & shape of abrasive particles on the measurement of wear rate using dry sand rubber wheel test*", *Wear of Materials*, Vol. 2, 1987, pp 689 – 699.
29. **C. A. Bozzi & J. D. B. De Mello**, *Wear resistance & wear mechanisms of WC-12%Co thermal sprayed coatings in three-body abrasion*", *Wear* 233 – 235, 1999, pp 575 – 587.
30. **M. G. Hamblin & G. W. Stachowiak**, *Description of abrasive particle shape & its relation to two-body abrasive wear*", *Tribology Transactions*, Vol. 39, 1996, 4, pp 803 – 810.
31. **G. W. Stachowiak**, *Particle angularity & its relationship to abrasive & erosive wear*", *Wear* 241, 2000, pp 214 – 219.
32. **R. D. Howarth, Jr.**, *The abrasion resistance of metals*", *Trans. Am. Soc. Met.*, 41, 1949, pp 819 – 869.
33. **H. S. Avery**, *Classification & precision of abrasion tests*", *Proc. Int. Conf. on Wear of Materials*, ASME, New York, 1977, pp 148 – 157.
34. **D. G. Teer & R. D. Arnell**, *Wear*", *Principles of Tribology*, Chp.5, Ed. J.HALLING, Macmillian, 1978, pp 100 & 108.
35. **M. R. Dorfman & M. Mohanty**, *Recent developments and applications of chromium plating alternatives using the HVOF thermal spray process*", 5th Int. Conf. of Adv. In Surf. Eng., not dated.
36. **A. J. Moore & R. J. K. Wood**, *Erosive wear mapping of pipe materials*", *Plastics Pipes VII*, Koningshof, September 1992, pp 1 – 10
37. **S. Turenne, M. Fiset & J. Masounave**, *The effect of sand concentration on the erosion of materials by a slurry jet*", *Wear* 133, 1989, pp 95 – 106.
38. **R. L. Deuis, C. Subramanian & J. M. Yellup**, *Three-body abrasive wear of composite coatings in dry and wet environments*", *Wear* 214, 1998, pp 112 – 130.
39. **A. H. Muhr, & A. D. Roberts**, "Rubber abrasion and wear", *Wear* 158, 1992, pp 213 – 228
40. **S. W. Zhang**, *Advances in studies on rubber abrasion*", *Tribology International*, Vol 22, Iss. 2, April 1989, pp 143 – 148
41. **S. W. Zhang**, *State-of-the-art of polymer tribology*", *Tribology International*, Vol.31, Iss. 1-3, 1998, pp 49 – 60
42. **M. F. Moore**, *Wear and abrasion*", *Principle and applications of tribology*, Int. series on Mat. Sci. & Tech., Vol. 14, Chpt. 9, 1975, pp
43. **Y. Fukahori & H. Yamazaki**, *Mechanism of rubber abrasion. Part I. Abrasion pattern formation in natural rubber vulcanizate*", *Wear* 171, 194, pp 195 – 202

44. **Y. Fukahori & H. Yamazaki**, "*Mechanism of rubber abrasion. Part II. General rule in abrasion pattern formation in rubber-like materials*", *Wear* 178, 194, pp 109 – 116
45. **Y. Uchiyama & Y. Ishino**, "*Pattern abrasion mechanism of rubber*", *Wear* 158, 1992, pp 141 – 155
46. **S. W. Zhang**, "*Wet abrasion of polymers*", *Wear* 158, 1992, 1 – 13
47. **J. C. Arnold & I. M. Hutchings**, "The mechanisms of erosion of unfilled elastomers by solid particle impact", *Wear*, 138, 1990, pp 33 – 46
48. **J. L. Xuan, I. T. Hong & E. C. Fitch**, "*Hardness effect on three-body abrasive wear under fluid film lubrication*", *Journal of Tribology*, 1989, Vol. 111, pp 35 – 40
49. **N. Axen, S. Jacobson & S. Hogmark**, "Influence of hardness of the counterbody in three-body abrasive wear – an overlooked hardness effect", *Tribology International*, Vol. 27, No.4, 1994, pp 233 – 241
50. **I. R. Belcher**, 1991, "*An investigation into the operating characteristics of the progressing cavity pump*", Ph.D.diss., Cranfield Institute of Technology.

Missing pages are unavailable

Design and validation on the simulated 'in-service' wear test rig

5.1 INTRODUCTION

The problem with tests for wear behaviour and lifetime evaluation is that they are both time consuming and expensive if performed under normal running conditions. The objective of accelerated testing is to provide the same information in a short space of time and at a low cost. However a test is relevant to real component performance only if it is done in a controlled way without changes in the tribological contact conditions. The tribological behaviour of any moving mechanical contact in a machine is usually very complex, and the pumping element in a progressive cavity pump is no exception, with the helical rotor moving relative to the stationary double helical stator. The intermeshing between the two components creates a set of contact conditions which, when pumping an abrasive slurry, is the fundamental reason why the two components wear.

Normally, in accelerated testing, the real contact conditions are simulated under harsher conditions in a simplified mechanical device with controlled variation possibilities. However, due to the complexity and lack of understanding of the real contact conditions in the pumping element, it was felt that the actual contact conditions needed to be used in the accelerated test, by incorporating a pump into the design of the test apparatus. By overloading the system variables the various system parameters could be isolated and individually assessed in order to study and evaluate the wear behaviour in the pumping element of the pump. Based on six levels of tribological test simulation^[1], this type of test apparatus would be classified at level II as an 'in-service wear test rig' that simulated real contact conditions with controlled parameter variation.

5.2 DESIGN CRITERIA

The fundamental design of the apparatus was based on a set of progressive cavity pumps, on a closed loop, re-circulating a slurry from an agitated tank. The criteria for the wear test rig was to:

- (i) simulate contact conditions in the pumping element
- (ii) enable accelerated testing
- (iii) isolate individual system parameters
- (iv) transport a slurry of known particle characteristics and concentration
- (v) monitor and maintain constant system variables

- (vi) analyse and compare surface damage of the rotors and stators with respect to system parameter
- (vii) be a suitable size not to require lifting gear
- (viii) run automatically through 24 hour periods
- (ix) eliminate the synergistic effects of corrosive wear

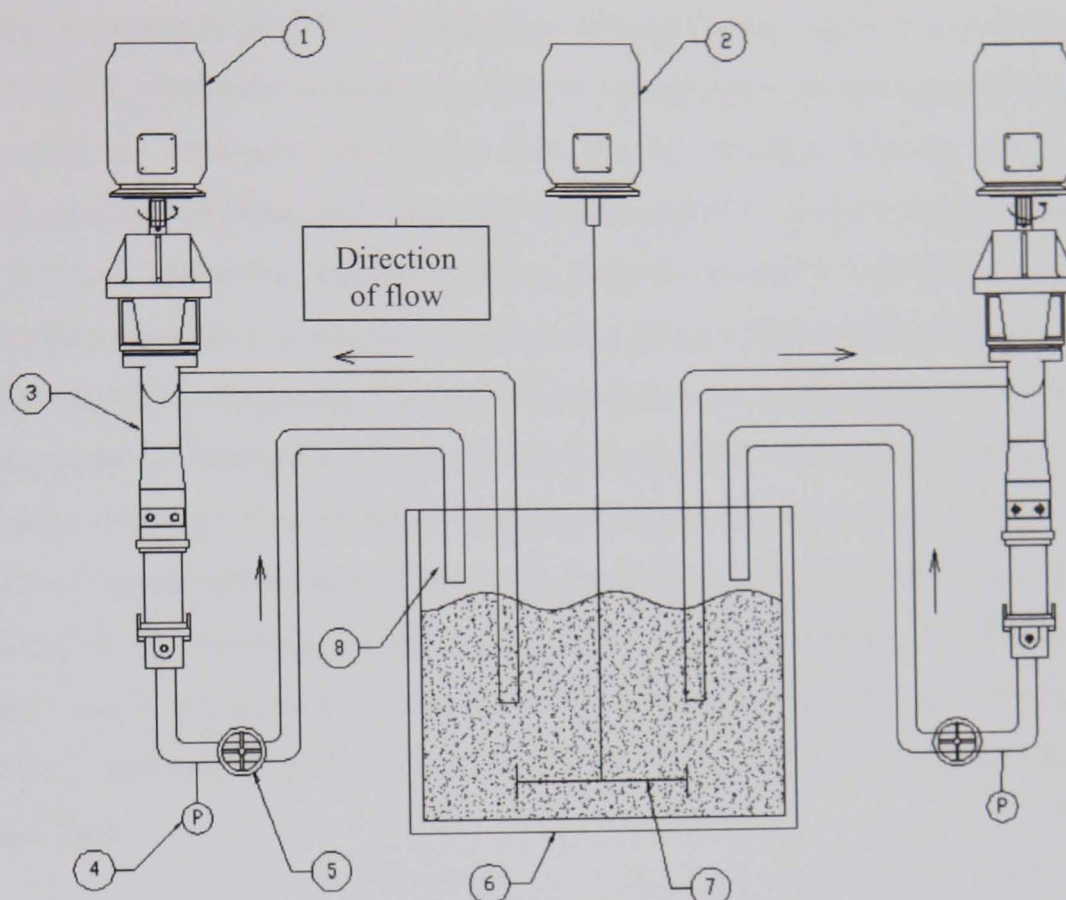
5.2.1 *Wear rig configuration*

Mono E031 pumps were selected based on their size, ease of assembly and relative light weight nature of the parts which would consistently require assembly/dis-assembly throughout the test programme. The basic configuration of the rig is shown in figure 5.1. Two single stage E031 pumps were used, which had nominal rotor dimensions of a minor diameter of 26 mm and an eccentricity of 5 mm and a stator pitch of 130 mm. These sizes produced geometric d/e and P/e ratios of 5 and 16, respectively. The two pumps were piped in a continuous loop to an agitated slurry tank.

Two Nord variable speed motors were used to transmit power to the pumps, which provided a speed range of 150 to 2000 rpm. The power was transmitted via a pulley and belt arrangement with a 1:1 ratio. Rubber lined ball valves were located horizontally in the pipework, 150 mm from the discharge end of the pump. Between the valves and the pump a bi-pass port, with a 6 mm diameter pipe, fed a pressure gauge through a pressure switch. When the valve was fully open the pump would operate under 'purely' abrasive conditions against a discharge pressure of 0 bar. Gradually closing the valve would increase the pressure differential across the pumping element up to 6 bar and induce erosive/slip conditions into the tribological system.

A 1 m diameter x 0.8 m deep tank was fabricated from mild steel plate with a cross member, of 100 mm rolled steel angle, across the top to add strength to the tank and support the agitator motor. Four strips of 50 mm rolled steel angle were welded down the sides of the tank to aid the agitation of the slurry. The Rushton turbine design was selected for the agitator blade, which consisted of a 300 mm diameter mild steel plate with six 50 mm x 75 mm blades welded, equi-spaced, around the circumference of the plate. The Rushton turbine blade was welded to a 50mm diameter shaft and mounted vertically so that the blade sat horizontally 100 mm from the bottom of the tank. A variable speed motor, secured to the centre of the cross member, was used to rotate the agitator.

Figure 5.1 Schematic of the simulated in-service test rig



- Key :
- | | |
|---------------------------|---------------------------------|
| 1 Pump Motor | 5 Loading valve (Back Pressure) |
| 2 Agitator Motor | 6 Slurry tank (Baffled) |
| 3 Progressive cavity pump | 7 Agitator (Rushton Turbine) |
| 4 Pressure gauge | 8 Flow rate (by time volume) |

5.2.2 Design problems

Originally the pumps were mounted horizontally on a purpose built framework. However initial trials revealed that settling of the abrasive was occurring in the pumping element that consequently had a direct effect of the wear behaviour. The pumps were then remounted vertically, which entailed significant changes to the framework and the mechanical seal arrangements. The pumps were mounted so that the inlet port was at the top providing a gravity feed to the pumping element, located at the bottom of the framework. This arrangement removed the settling out of the abrasive particles. However it did introduce a 'tapering effect' on the wear on the rotors where the wear bands increased in width towards the delivery end, but it was concluded that this effect was preferable to the settling.

It was found that the rotation speed of agitation was critical and had to be a compromise between maintaining the abrasive particles in suspension without introducing air in to the inlet pipe. Air in the system could potentially introduce cavitation erosion into the tribological system and created problems with the automatic settings on the pressure switches. For the rig to safely operate unattended, pressure switches were required to automatically switch off the pump if the pressure deviated above or below the settings. A fall in pressure would be caused by a valve wearing out whilst a sudden increase in pressure would detect a pump failure such as the rotor jamming in the stator. However air in the system was found to send pressure spike signals to the pressure switches and consequently automatically stop the pump, unnecessarily. However a reduction in the agitator speed resulted in a high percentage of abrasives settling underneath the Rushton blade and more than twice the calculated amount of sand was required to obtain the desired concentration levels. Consequently a 50 mm strip of mild steel was welded underneath the rushton blade which successfully swept the bottom of the tank. The resultant agitator speed for the standard test conditions was 126 rpm with a concentration limit of 0.5%. Higher levels could not be achieved due to settling effects.

In real applications the pumps are used to transport a slurry from A to B and therefore each particle only passes through the pumping element once. Since the simulated rig was a closed loop, which recirculated the slurry, it was essential to eliminate the effects of attrition. Therefore the abrasive was renewed at the start of every test. In practice this meant emptying, and cleaning the tank and pipe-work every 20 hours.

One of the design criteria for the test was to ensure that the possible synergistic effects of corrosive wear were not introduced, since the study was focused on mechanical wear of aqueous-based slurries. Therefore an austenitic stainless steel, grade AISI 316L, was selected for the rotor material and the slurry pH level was monitored to ensure a neutral environment. It was decided not to use an anti-corrodant in the slurry as it was important that the contact conditions were based on the lubricative ability of water.

5.3 TEST CONDITIONS

5.3.1 Contact conditions

The contact conditions relate to the interference fit between the rotor and stator. For the E031 pump, in an abrasive application, the major and minor interference would be 0.49 mm and 1.20 mm

respectively. The minor is quoted as a diametric interference, whereas the major is the radial interference at either end of the stator slot. From this data the standard contact conditions for the test programme were selected as: diametric 1.0 mm on the minor and a radial 0.45 mm on the major.

Forty rotors and stators were needed for the test programme, each requiring the majors and minors to be measured in order to calculate the interference fit. The rotors are measured using bar micrometers, with an average of three readings taken along the length of the scroll. A Mitutoyo CHN1008 co-ordinate measuring machine was used to measure the profile of the stators. For every stator, two profiles were taken 25 mm from each end. Each profile was then converted into a .dwg file using AutoCAD software and manipulated to determine the minor and major dimensions. Examples of the profiles and the AutoCAD drawings are given in Appendix A. It became apparent that an inherent problem existed relating to the manufacturing tolerances of the rotors and stators. The rotors could be machined to an accuracy of 0.01 mm. However, the moulding tolerances for the stators were typically 0.5 – 1.0 mm, which was normal for the techniques used. This created a fundamental problem in maintaining the repeatable interference fit necessary for the contact conditions to remain constant. Consequently, to resolve the issue, rotors had to be specifically made to suit individual stators. Batches of stators were moulded and measured as previously described. A spreadsheet was then used to calculate the machining sizes for a rotor to be paired with each individual stator to produce the required interference fit. For the coated rotors, the machining sizes are different to the finished size, as it depends on the deposition process. With electroplating, more plate is deposited on the peaks than on the troughs of the scroll due to the throwing power of the electrodes, whereas thermal spray techniques tend to deposit more material in the troughs than on the peaks. The stators were moulded using a four-stage core which meant that one mould produces four individual single stage stators. It was discovered that the core was slightly tapered at one end which meant only three of the four stators from each mould could be used.

5.3.2 Acceleration of service conditions

Tribological accelerated testing of components can be performed by increasing system variables such as load, speed, contact pressure and temperature. Since operational speed is known to have a power relationship of ~ 3 , with the wear rate of the pumping element components, this system variable was selected to accelerate the wear. The normal operating speed of the selected pump size, in an equivalent abrasive application, would be 200 rpm giving a rubbing velocity of 0.48ms^{-1} ^[2].

Design and validation on the simulated 'in-service' wear test rig

The selected speed for the standard test conditions was 500 rpm, which equated to a rubbing velocity of 1.2 ms^{-1} .

In addition to increasing a system variable to achieve accelerated test data, a soft stainless steel was selected for the rotor surface specifically to reduce the duration time of each test and ensure rapid generation of surface damage. In a real abrasive application this material would be used as a rotor substrate material but would be surface engineered by either a thermally sprayed coating or a electro-deposited hard chromium plate to provide a wear resistant surface. It was important that the choice of rotor material would not suffer from the effects of work hardening under the contact conditions and would enable the surface damage to be modelled by classical wear theories.

The load and contact pressure conditions in the system are fixed and are governed by the interference fit between the two components, as well as the stator temperature.

5.3.3 Standard test conditions

The standard test conditions selected for the simulated wear test programme are listed in table 5.1. Applying no differential pressure for the standard conditions meant that the influences of slip would be eliminated, and the tribological system could be assumed to be 'purely abrasive'.

Table 5.1: Standard test conditions for the simulated wear test programme

System Variable	Condition
Operating speed (rpm)	500
Discharge pressure (bar)	0
Minor diametric interference fit (mm)	1
Major radial interference fit (mm)	0.45
Abrasive medium	200mm silicon oxide
Abrasive concentration (%)	0.5
Abrasive carrier	Water
Rotor material	AISI 316L stainless steel
Stator material	Nitrile rubber; 68 IRHD

5.3.4 System parameters

A parameter can be defined as a measurable or quantifiable characteristic of a system, whilst a system variable is something that is not consistent or of a fixed pattern and therefore can be changed. The variables in the system relate to the system parameters. Every wear mechanism has its own distinct features, like a finger print, from which the mechanism can often be identified. By selecting and changing specific variables the direct effect of the individual system parameters on the

wear behaviour in the pumping element can be studied by analysing the wear finger prints that they create. A test programme was derived whereby each system variable was assessed by maintaining a standard set of operating conditions, in Table 5.1, whilst adjusting a specific system variable. Table 5.2 shows the relationship between the system variables and the system parameters and the variations included in the test programme.

Table 5.2 : Relationship between system variables and system parameters

System variable	Variation tested	System parameter
Discharge pressure (bar)	0, 2, 4, 6	Differential pressure
Diametric interference (mm)	0.2, 0.5, 1.0, 1.5	Contact pressure
Operating speed (rpm)	250, 500, 750, 1000, 1250, 1500	Rubbing, fluid & particle velocities
Abrasive media	120, 225, 450, 900 μ m SiO ₂ 4, 10, 16, 45, 80 μ m SiC	Abrasive particle characteristics
Rotor surface	AISI 316L stainless steel Electroplated hard chromium plate HVOF tungsten carbide Plasma sprayed chromium oxide	Material properties

(i) Differential pressure across the length of the pumping element

The differential pressure is the difference in pressure between the inlet and outlet sides of the pumping element. For the majority of pump applications, the suction end is flooded and the inlet pressure is 0 bar and the pump can be classed as operating under purely abrasive conditions. Increasing the discharge pressure generates 'slip' and the pump would then be operating under 'abrasive-erosive' conditions.

(ii) Contact pressure between the rotor and stator

The contact between the two intermeshing components consists of the type 'a' and 'b' seal ribbons which run the full length of the stator and are continually moving as the rotor revolves around the stator slot. Additionally the type 'c' contact has an intermittent contact of 180° of the rotor each time the rotor is at the two extremes of the slot. The width and depth of the two continual ribbons are controlled by the diametric minor interference whilst the type 'c' area depends on the major interference. Changing the minor interference fit has a direct effect on the load applied to the particles in the contact area. For the purpose of this study the major interference remained constant at 0.45 mm.

(iii) Rubbing, fluid & particle velocities

All three velocities are linked to the system variable of pump operational speed according to the equations 2.3, 2.5 and 2.6.

(iv) Abrasive particle characteristics

Silicon oxide makes up 60% of the earth's crust and thus progressive cavity pumps are frequently exposed to wear by quartz sand slurries. Four nominal particle sizes of silicon oxide were studied to determine whether the size effect, documented by Finnie & Misra ^[3], would be observed. For the comparison of particle characteristics silicon carbide slurries were also tested due to their high hardness, angular shape and availability in micron sizes. The properties of the two abrasives and the size range used are given in Table 5.3 below, whilst the shape of each abrasive is given in figure 5.2. For this set of wear tests tungsten carbide coated rotors were used to eliminate possible damage to the stators as a direct consequence of rotor wear.

Table 5.3: Characteristics of the abrasives used in the wear study

Type	Nominal size (μm)	Grade	Hardness (kgf/mm^3)	Shape
Silicon Oxide	120	E	1000 – 1200	Rounded to semi- rounded
	225	D		
	450	C		
	935	B		
Silicon Carbide	10	F800	2400 - 2500	Angular
	16	F600		
	24	F400		
	45	F320		
	80	F240		

(v) Material properties

The rotor coatings selected were those used commercially by the pump manufacturer and were discussed in more detail in section 2.7.

Figure 5.2 (i) : SEM images of showing the shape of silicon oxide particles of nominal sizes of (a) 935; (b) 450; (c) 225 & (d) 120 microns

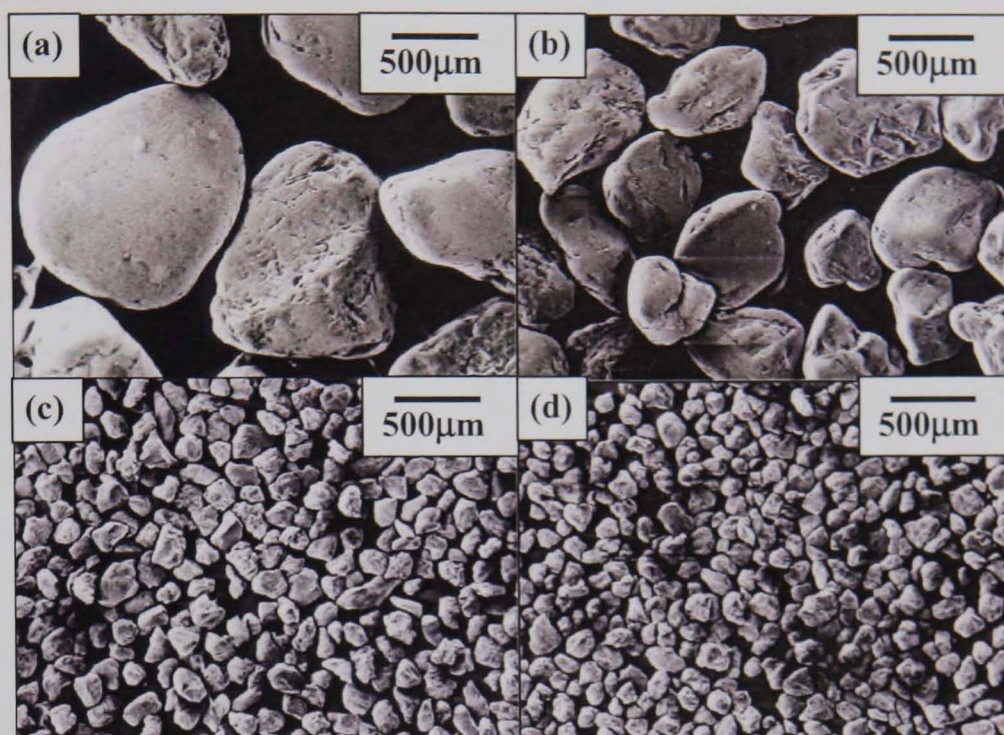
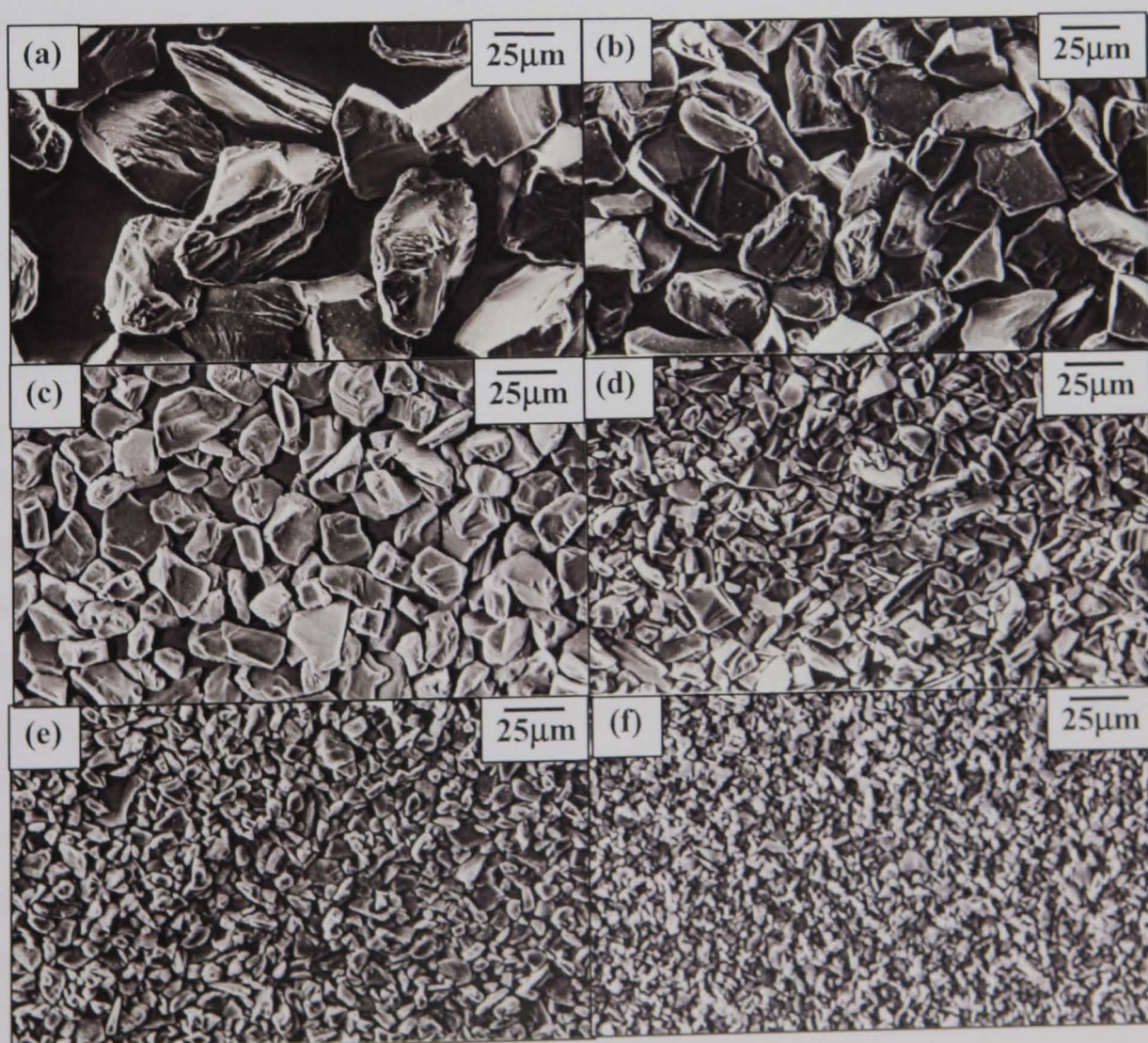


Figure 5.2 (ii) : SEM images of showing the shape of silicon carbide particles of nominal sizes of (a) 80; (b) 45; (c) 30 ; (d) 16; (e) 10 & (f) 4 microns



5.3.5 *Monitoring of system variables*

In addition to the system variables involved in the wear test programme, there were various others that required monitoring. There were three temperatures in the system which were all inter-related; the slurry temperature which is effected by the atmosphere temperature, which consequently effects the stator temperature. The stator temperature has a direct influence on the tribological system as a change in stator temperature effects the rubber's ability to deform and consequently changes the contact conditions. An increase would cause the rubber to expand more and increase the interference fit between the rotor and stator and therefore potentially alter the wear behaviour. Consequently, careful monitoring to maintain a constant slurry temperature was required, since the period of time spent testing the various system parameters spanned over the winter and summer months.

The other system variables monitored during each test were the flow rate, pH of water and abrasive particle concentration, in both the tank and the outlet pipe to ensure consistent agitation and no settling of particles in the system. The abrasive particle concentration was measured by taking a 500ml sample and weighing the dry particle content. Litmus paper was used to monitor the pH of the water. Due to the quantities of water required it was not practical or cost effective to use de-ionised water and mains water was used which had a constant pH level of 6. The most effective way to monitor the flow rate was simply to measure the time taken to fill a known volume, for which a 500ml measuring tube was used. Various designs of flow meters were tested but due to the abrasive nature of the slurry none proved to be as practical or as cost effective as the technique employed.

5.4 INTERPRETATION OF TEST RESULTS

Testing at this level of tribological simulation provides excellent information on the interaction effects between different parameters, but at the expense of difficulty in interpreting and quantifying the results. Using rotors and stators in the simulated tests ensured real contact conditions but created a serious problem with interpretation of results due to their weight and complex geometry. Previous attempts, by the pump manufacturer, to assess wear in rotors and stators, approached the problem from a purely engineering aspect and monitored the flow rate, whilst pumping an abrasive slurry, until such time that the rate became unacceptable, due to insufficient interference between the two components to maintain the capsulism seals. This technique was totally unsuitable for this study, as it provided no information as to the way in which the components were wearing. Analytical techniques were required that could either quantify the wear to each component or at best provide a

comparison to demonstrate how the severity, or the mechanism, changes with the system variable. Various analytical approaches were evaluated before satisfactory techniques were established. The initial stage of evaluation commenced with identifying what types of wear were occurring and their location on each of the components. This involved several 'dummy' runs at various discharge pressures and operating speeds, before the actual wear test programme began.

The order in which the analytical techniques were applied for both the rotors and stators was crucial to ensure that all relevant data was collected. This conundrum did create various delays in the progression of correlating the wear data. A prime example of this was the speed variable wear tests. These were conducted before it was realised that weight loss was the only way to quantify the wear rates, and since the rotors had not been weighed prior to the tests, these tests had to be repeated, which also entailed the process of making rotors to individually fit the stators.

5.4.1 Assessment of surface damage to rotors

From the dummy runs, it was identified that the main surface damage on the rotors consisted of bands of grooves. The grooves lay perpendicular to the axis of the rotor whilst the bands followed the helical scroll. The location of the bands and the morphology of the grooves varied depending upon the conditions of the test. The bands were located on the peaks of the scroll and/or to either side, i.e. down the leading and trailing flanks. The width of the bands did not remain constant along the length of the rotor but increased towards the delivery end. Likewise, the morphology and severity of the grooves varied depending upon the location of the bands. Other reoccurring features were a step at the tail and head end where the rotors protruded from the stator, and an isolated area of grooving, near to the tail, specific only to the wear tests involving a differential pressure.

Therefore the criteria for the rotor analytical techniques were to:

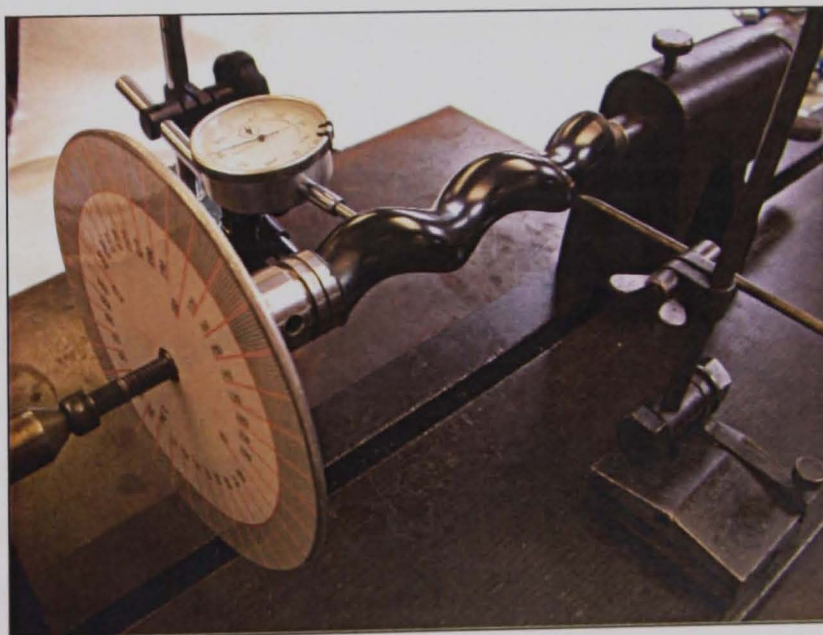
- (i) measure the location of the individual grooved bands
- (ii) quantify the surface topography of wear bands
- (iii) identify the different wear mechanisms on the rotors
- (iv) measure the 'step' at the head and tail end of the rotors
- (v) quantify a comparable 'wear rate'

Design and validation on the simulated 'in-service' wear test rig

Before any analytical studies were conducted the rotors were photographed using a 35mm Olympus camera to provide a permanent record of the wear features, prior to any sectioning of the rotors. This also provided 2D images of the wear features, which were then easier to study.

Originally, the low magnification photographs of the rotors were to be used to measure the location and width of the wear bands. However it became apparent that the required measurement needed to be with respect to the rotational position of the rotor inside the stator slot, and not the longitudinal position provided by the photographs. Measuring the degrees of rotation of the rotor would enable the position of the bands to be related to the contact areas between the rotor and stator, enabling the data to contribute to a model that would eventually describe the wearing process. A fixture was built that held each rotor between centres, figure 5.3, with a 360° scale secured at the head end. The rotational angle of 0° was taken as the highest point of the scroll at the head end, determined by a dial test indicator. Each rotor was rotated 360° from the 0° position enabling a fixed marker, located on the central axis of the rotor, to identify the angle, δ , at which the wear bands start and finish around the circumference of the scroll in three defined locations; 20 mm from the step at the tail and head end, and at the centre of the scroll.

Figure 5.3 : Fixture configuration for measuring width of helical wear bands



Several problems were encountered with analysing the morphology of the grooves, relating to their size, the lack of an original surface to act as a reference point and the geometry of the rotors. The scale of the grooves, which was macro as opposed to micro, combined with the curved geometry of the scroll, meant that a conventional stylus profilometer had insufficient depth range to provide

quantitative information on the topography of the worn surfaces. Subsequently laser profilometry equipment was employed, courtesy of the National Tribology Centre in Risley, UK. Profiles were measured across the wear bands at the same three locations used in measuring the width of the bands. Twelve rotors were incorporated in this measurement programme, which were the ones tested on discharge pressure, interference and operational speed. From the profiles, depth and width dimensions were taken and the data manipulated in an excel spreadsheet. Unfortunately several problems were encountered with interpreting and utilising the data. The first was the poor repeatability of the profiles and the second was the widening band and increased severity of the grooves as the band progressed along the length of the stator. This meant that there was no consistency in the collected data. This topographic approach was also used as a technique to quantify the volumetric material loss. It was postulated that a good approximation of the wear rate of the rotors could be determined by taking a summation of the widths and depths of the grooves, over a defined distance, the volume of material removed could be estimated and Archard's equation used to derive an approximation of the dimensional wear rates. However the widening tapering effect observed on the wear bands, and the absence of an original surface introduced a high error potential.

Scanning electron microscopy was used to identify the wear mechanisms which may have created the different wear features on the rotors. This entailed sectioning and mounting specific regions of the rotors.

It was observed that a characteristic step wore at the highest point of the scroll at both ends of the rotor where it protruded from the stator and that the step at the head end appeared deeper than that worn at the tail end. It was postulated that by measuring the difference in the depth of these two steps the data could be used to quantify a comparable 'wear rate' for the different variable conditions. Replicas were taken of all the steps from the rotors tested on the variables of discharge pressure, interference fit and operating speed. 1 mm thick slices were cut from each replica at the highest point of the scroll and a shadow-graph was used to trace the profile of the step and measure the depth. This data was then manipulated in an excel spreadsheet.

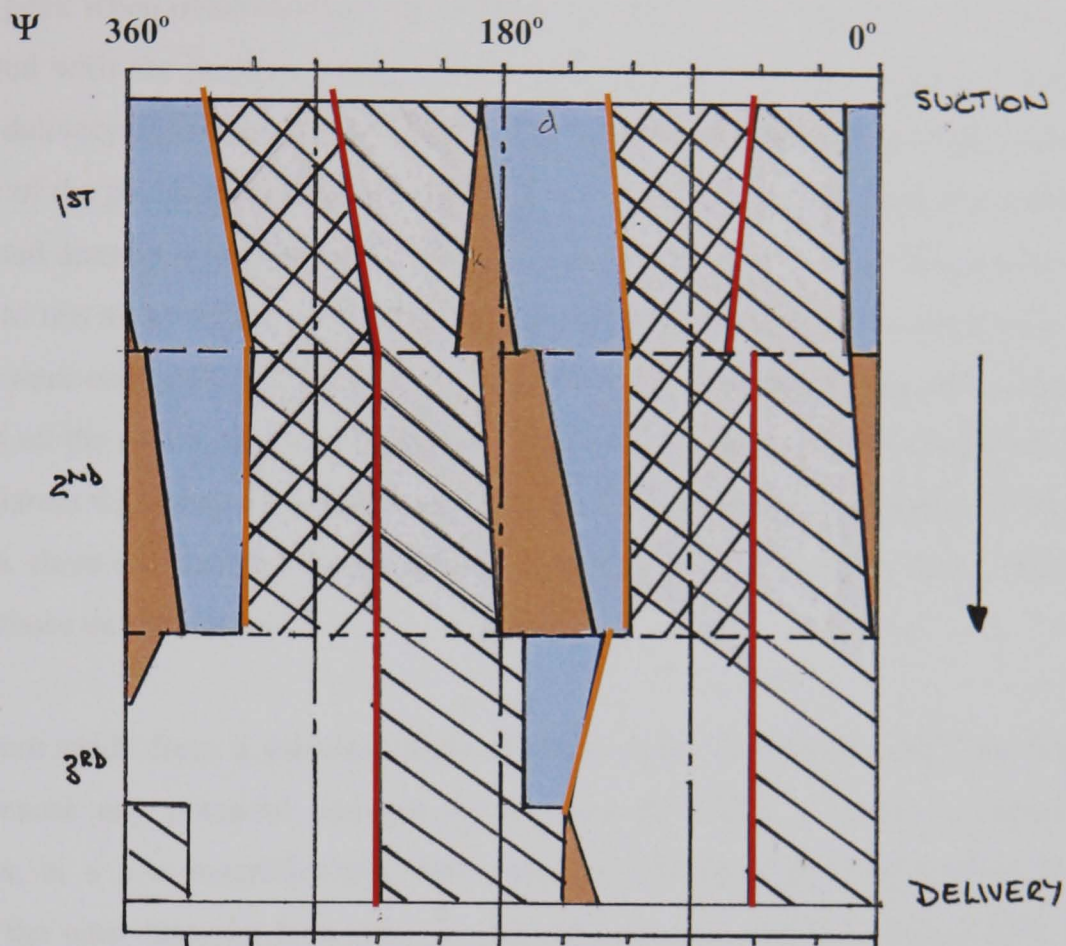
By evaluating the different techniques it became apparent that not all the same wear data was necessarily required from each set of rotors. It was concluded that from the interference and the rotor material sets it was sufficient to measure the change in position of the wear bands and record

any observational difference in the appearance of the wear bands. For the set of rotors tested at different pressures, the data required was the appearance, location and width of the additional wear band on the leading edge plus the location and change of appearance of the isolated worn area near to the tail end of the rotor. Only the wear rate for the variable of speed was quantified by repeating the set of tests and using weight loss measurements to determine the relationship between the dimensional wear rate and rubbing velocity. The data from the step depths and the groove profiling was analysed for the three sets of tests on pressure differential, interference and speed. All the data was then analysed in conjunction with the wear data collected from the corresponding worn stators. The weight loss approach identified a fundamental difference in the accuracy of analytical techniques used at different levels of tribological testing. Testing on a laboratory scale, the relatively small flat samples, meant that even very small amounts of weight loss could be measured using scales with a range from 0 to 300g, with an accuracy of 0.0001g. However the heavier weight of a real component, such as a rotor which weighs around 800g, restricts the accuracy of the scales that will weigh up to 1kg. For the wear study the most suitable scales available had an accuracy of 0.05g. This was found to be sufficient for the stainless steel uncoated rotors, but not for the coated rotors which either, did not suffer sufficient weight loss to provide meaningful data, even after extended periods of test durations or wore unevenly resulting in combined substrate and coating material loss. Consequently empirical data supplied by the pump manufacturer had to be used as a qualitative measurement of the wear life of the rotor coatings. The data provided uses hard chromium plate as the reference material, with a wear life of 1, and ranks the other two coatings accordingly, depending upon the nature of the abrasive media.

5.4.2 Assessment of surface damage to stators

The first problem with the assessment of wear damage to the stators was that the wear is located inside and therefore difficult to analyse without physically sectioning the stator, which, depending upon where this occurs, could potentially destroy important wear features. Therefore the stators from the dummy runs were sectioned lengthways, and wear maps sketched to identify the various repeating wear features, an example of which is shown in figure 5.4. Each colour and pattern represents a different wear pattern. The main features were identified as two distinct double helical wear bands consisting of mainly pitted holes, which are shown on the map as thick red lines and are located either side of the peaks of the scroll. As the cause of the pits was unknown, and the description of a 'worn' band, as used with the rotors, was not appropriate, the bands were given letters to identify each wear regime. Type 'a' was the band that ran on the side of the peak visible

Figure 5.4 : Example of a stator wear map




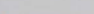


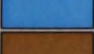
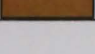
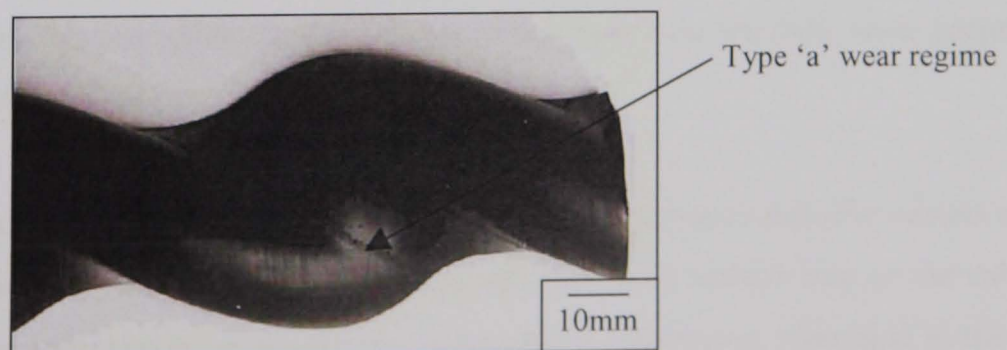
Key	Description
	Type 'a' wear regime, seen from suction end, double helical spiral thin band of fine pits located $\sim 60^\circ$ & 260°
	Type 'b' wear regime, seen from delivery end, double helical spiral thin band of fine pits located $\sim 135^\circ$ & 350°
	Grooves propagating clockwise from wear regime a, and matt
	Grooves propagating anti-clockwise from wear regime a, and shiny
	Matt, smooth
	Flow like grooving which waver & are matt in the centre, seen from delivery end

Figure 5.5 : Examples of the positive replicated features from within the stator



when looking down the suction, or inlet, end of the stator, whilst type 'b' was visible on the other side of the peak when observed from the delivery or outlet end. The other distinct feature, which was observed with the pressure variable wear tests, was a worn area of groove-like morphology near to the delivery end of the stator, which was related to the same type of feature observed on the rotors. One of the problems relating to the stator wear features was distinguishing between primary wear, that had directly occurred on the stator and secondary wear, which was a direct consequence of damage to the rotor surface, which are the hatched areas shown on the wear map. Although the wear maps were originally helpful, they proved to be both time consuming and difficult to relate to the features on the rotors, due to difference in geometry between the two components. Therefore it became apparent that what was needed was a technique to measure the location of the wear features to enable a three-dimensional computerised model to be built which could relate stator wear features to those on the rotors.

Replicas were made from a selected range of worn stators to examine the wear features without having to cause any potential damage, an example of which is shown in figure 5.5. Optical photographs, at a low magnification, were taken of the replicas in an attempt to measure the location of the wear features. However, as with the rotors, this proved unsuccessful. Consequently the following technique was developed to describe the position of the type 'a' and 'b' wear regimes in terms of their angular position in the stator slot, Ψ . On the end face of each stator lines were scribed to project the location of the type 'a' and 'b' wear regimes to the edge of the stator tube. The ends were then placed face down on a two-dimensional paper template of the cross section of the stator slot. The location of the scribed lines were marked on the template and a protractor used to determine the value of Ψ . This technique had a limited range of accuracy which meant that any subtle changing in the position of the wear regimes could not be accurately measured.

10 mm sections were then taken, 20 mm from both ends of the stators, and prepared for examination using a scanning electron microscope to explore how the two wear regimes were created and what system variables effected their morphology.

It proved to be very difficult to actually quantify the change in wear rates with the system variables. The weight loss approach could not be used, since the degree of weight loss to the rubber was insignificant to the overall weight of the stators, and particle embedding, identified in the type 'a'

and 'b' wear regimes, would have recorded as a weight gain if sufficiently accurate scales could have been used.

5.5 EVALUATION OF PARTICLE LOADING CONDITIONS

The loading conditions in the pumping element are very complex and problematic to quantify. There are many contributing factors, which have been discussed in section 2.3. However, by making various assumptions, a simplified model can be derived to enable good approximation to the load applied to an abrasive particle in the contact zone. Taking an arbitrary slice through any part of the pumping element produces a two-dimensional stator slot, containing the circular rotor, figure 2.8. The assumption is made that the predominant load at the points of contact, as the rotors revolves around the slot, is due to the interference fit between the rotor and stator and will depend upon the thickness and resilience of the rubber. The behaviour of the rubber in the curved regions of the slot is very complex. However, since particle embedding has been identified as occurring at the end of the straight sides of the slot, a further assumption can be made that only the minor, and not the major, interference fit contributes to the wearing process. These conditions can now be simply modelled as an applied load on a 26mm diameter steel bar over a 15mm thick rubber block. The thickness of the rubber block equates to the amount of rubber at the minor central position of the slot and the 100mm square eliminates effects from unsupported rubber. The diameter of the bar equates to the minor diameter of the rotor.

Three different approaches were investigated to derive the amount of load that would be required to deform the rubber stator by 0.5 mm, which equates to a 1.0 mm diametric minor interference fit. These approaches were:

- (i) computational analysis
- (ii) theoretical derivation
- (iii) experimental analysis

(i) *Computational analysis*

The simplified contact conditions were computationally modelled using 'COSMOSWorks, version 6' software, by Structural Research and Analysis Corporation. A block of rubber 15mm x 100mm x 100mm, and a 26mm diameter steel bar, of 300mm length, were modelled and the material properties set from the COSMOS library. An assembly was created with the bar in tangential contact with the large face of the rubber pad, then a 0.5mm deflection applied, to represent the

radial interference fit on the minor diameter. A stress analysis was run on the model, based on these conditions, which then produced the stress plot, shown in Appendix B (c), from which the maximum resultant stress is derived. Since stress is the ratio of force to the contact area, the applied load could be derived. The details of the calculations are given in Appendix B (a) and (b). The limitations of this approach are with the pre-set material properties provided by the COSMOS library, particularly for the rubber where intrinsic material properties are strongly dependent on the composition and temperature.

(ii) Theoretical derivation

The breakout torque is the amount of torque required to overcome the friction between the rotor and stator, on start up of the pump, when there is no lubrication between the two components. The breakout torque is a known quantity, derived experimentally by the pump manufacturers. By dividing the breakout torque by the coefficient of friction for rubber, an approximation to the load conditions at the contact interface could be derived. The details of the calculations are given in Appendix B (d). There are two potential errors incurred with this approach. Firstly, the applied load is presumed to be constant regardless of the location of the rotor in the stator slot, with the contact pressure being dependent on the width of the contact seal line. And secondly, the frictional coefficient of rubber, as with any material, is not an intrinsic material property and is strongly dependent on the system conditions, as discussed in section 3.3. The difference between a rubber coefficient of friction value of 0.1 and 0.2 would halve the value of the load derived, thus providing a large error potential.

(iii) Experimental analysis

To empirically determine a good approximation of the loading conditions a Lloyds EZ50 Tensile test machine was utilised. Using the simplified model, rubber blocks of three different thicknesses; 5, 10 and 15mm, to represent the different locations around the stator slot, were compressed with a 26mm diameter steel bar, to a load of 1.5kN and the degree of deformation recorded. A plot of load vs. deflection was produced for each test from which the load required for a 0.5mm deformation could be read. The stress calculations and an example of the plots are given in Appendix B (e) and (f), respectively. To confirm whether the elastic flow properties were eliminated using the 100mm square block, tests were performed with the rubber constrained within metal. The load values and the gradient of the curves were found to be the same as those produced with the unrestrained rubber.

Table 5.4 gives the contact loads and pressures for a 0.5mm deformation derived by each of the three approaches. With consideration of all the potential errors in each of the three approaches it was concluded that the experimental approach provided the best approximation of 272N for the load applied on a particle due to a diametric minor interference of 1.0mm. However, due to the hardness differential between the two contacting surfaces this does not represent the load applied to the wear surface to remove material, as predicted by Archard's equation. Rather, a combination of the load applied, by the rotor, to embed a particle into the stator, against the force of the rubber resisting the interference deformation and applying a resultant load to the abrasive particle, to subject the rotor to wear.

Table 5.4 : Resultant loads and contact pressures for a 0.5mm rubber deformation, derived from the three approaches

Approach	Applied load (N)	Contact Pressure (Nmm ⁻²)
Computational analysis	180	0.25
Theoretical derivation	466	0.14
Experimental analysis	272	0.38

5.6 EVALUATION OF THE LUBRICATION FILM THICKNESS

A progressive cavity pump can only operate under lubricated conditions to prevent frictional heat destroying the stator by hysteresis. The lubrication film between the rotor and stator is generated hydrodynamically and the lubrication media is that of the abrasive slurry. It has been shown that the relationship between the film thickness and the abrasive particle size in any tribosystem directly relates to the efficiency of a particle to remove material and the mechanism by which the material is removed. Rabinowicz ^[4] observed a significant reduction in the wear coefficient of metals at the transition from grooving to rolling wear due to the ability of a free rolling particle to remove material was far less efficient than that of a fixed particle. Studies by Williams and Hyncica ^[5] on hydrodynamically lubricated bearing surfaces showed that an abrasive particle moving between two surfaces undergoes a transition from grooving to rolling wear at a critical value of D/h , where D is the particle major axis and h is the minimum thickness of the hydrodynamic lubrication film. It was therefore postulated that by examining the morphology of wear scars generated using slurries containing different abrasive particle sizes, the lubrication conditions, plus a good estimate to the film thickness, could be determined.

Slurries containing a range of silicon carbide particle sizes from 80 to 10 microns were pumped through the simulated wear test rig, for periods of 4 hours, using the 'purely abrasive' standard operating conditions. The weight loss of the rotors were measured to determine the dimensional wear rate and the wear morphology of each rotor and stator examined, using a scanning electron microscope. Unfortunately, due to the weight of the rotors, the significantly small amount of weight loss could not be measured and, consequently, the changes in the dimensional wear rate could not be used to determine whether a change in particle behaviour had contributed to a volumetric material loss. Examination of the rotors identified a reduction in the width of the grooves in the wear bands, that corresponded to the decrease in particle size. Grooving type wear was observed on all of the rotors, irrespective of the size of the particles in the slurries. However the severity of the wear was significantly reduced with the smallest size particle slurry of 10 microns and the grooves were of a similar magnitude to the original machined surface finish. The SEM images and effect of particle size on stator wear are discussed in detail in section 6.1.3. It is sufficient for this discussion, on lubrication, to observe that particle embedding into the rubber stator occurred regardless of particle size.

The results for the evaluation of the thickness of the hydrodynamic lubrication within the pumping element were found to be inconclusive using the two approaches discussed. These findings suggest that the wear process in the pumping element does not conform to the model proposed by Williams and Hyncica.

5.7 REFERENCES

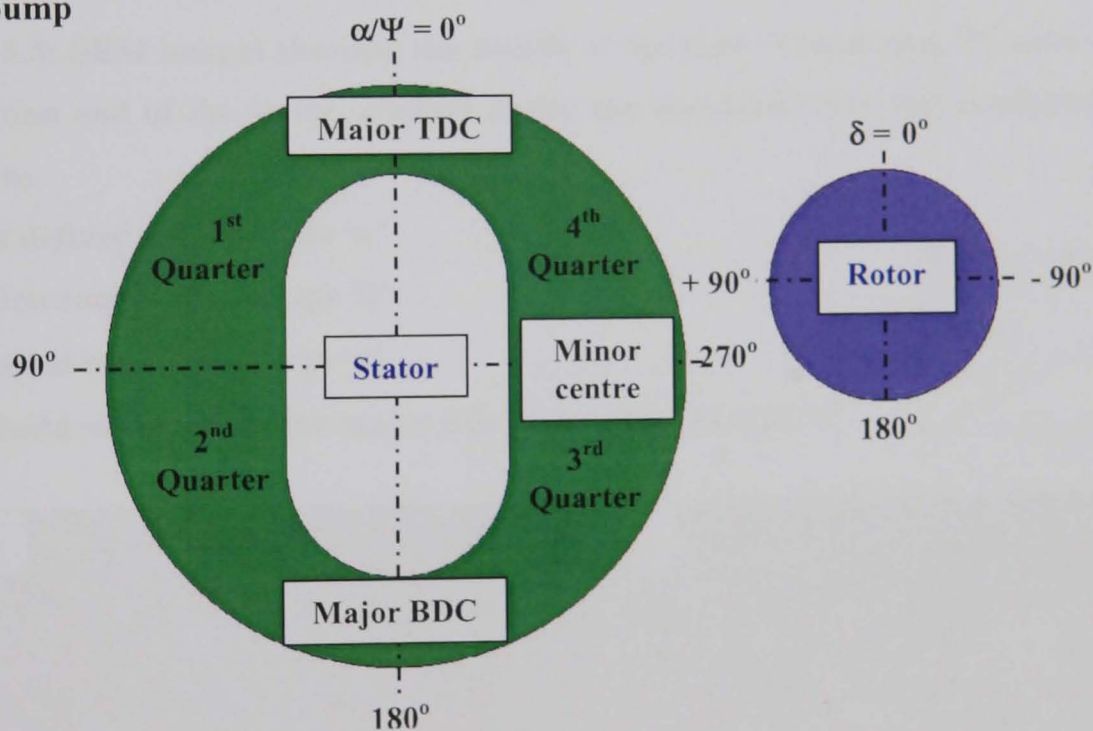
1. **K. Holmberg**, "*Tribological bases for accelerated testing*", Operational reliability & systematic maintenance, Eds. Holmberg, K. & Folkesson, A., Elsevier Applied Science, London, pp 31- 50
2. **Mono Pumps Ltd.**, "*Selection curves for E031 pump*", Mono Pumps Intranet, Pump selection manual, Vol.1, Section 3, p120, Confidential
3. **A. Misra & I. Finnie**, "*On the size effect in abrasive and erosive wear*", Wear 65, 1981, pp 359 - 373
4. **E. Rabinowicz, L. A. Dunn & P. G. Russel**, "*A study of abrasive wear under three-body conditions*", Wear 4, 1961, pp 345 – 355.
5. **J. A. Williams & A. M. Hyncica**, "*Abrasive wear in lubricated contacts*", J. Phys. D: Appl.Phys. 25, 1992, pp A81 – A90

Modelling the tribological system of the pumping element

6.1 THE WEAR SYSTEM IN THE PUMPING ELEMENT

The following discussions on the rotor and stator wear features are based on those generated by the standard wear test conditions of pure abrasion, defined in section 5.3. A two-dimensional model of the pumping element, divided into four quarters, is used to aid in the descriptions of the wear features, as shown in figure 6.1. The location of the wear features on the stator are described as values of Ψ . The angular motion, in an anticlockwise direction, of the rotor, around the slot, is defined as α , and the angular positions of the contact of the rotor with the stator are described as positive or negative values of δ .

Figure 6.1 : Two-dimensional model of the pumping element, viewed from the suction end of the pump



6.1.1 Characteristic wear features in the stator

The main wear features, observed in the stator, were two pairs of helical wear 'bands', identified as type 'a' and 'b'. Figure 6.2 schematically shows the location of these wear bands, with type 'a' shown as a pair of red lines, and type 'b' as yellow lines. The SEM images in figure 6.3 show in detail the specific features of bands. Both wear regimes are located in the same section of the slot, in each of the four quarters. Taking the top of the stator slot as $\Psi = 0^\circ$ and rotating in an anti-clockwise manner, their cross sectional location translate to; type 'a' at $\Psi = 65^\circ$ and 245° , and type 'b' at $\Psi = 115^\circ$ and 295° . From a longitudinal view they lie either side of the minor peaks.

Figure 6.2 : Schematic showing the location of the main wear features identified on the stator, under the standard wear test conditions of 'pure' abrasion

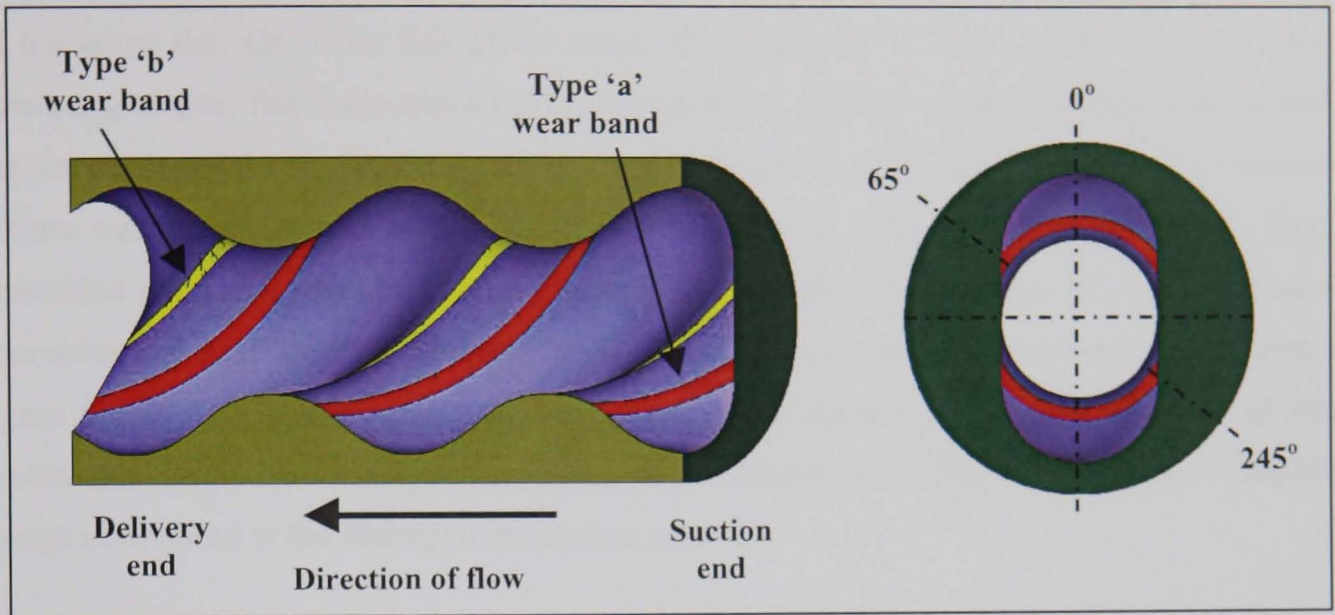
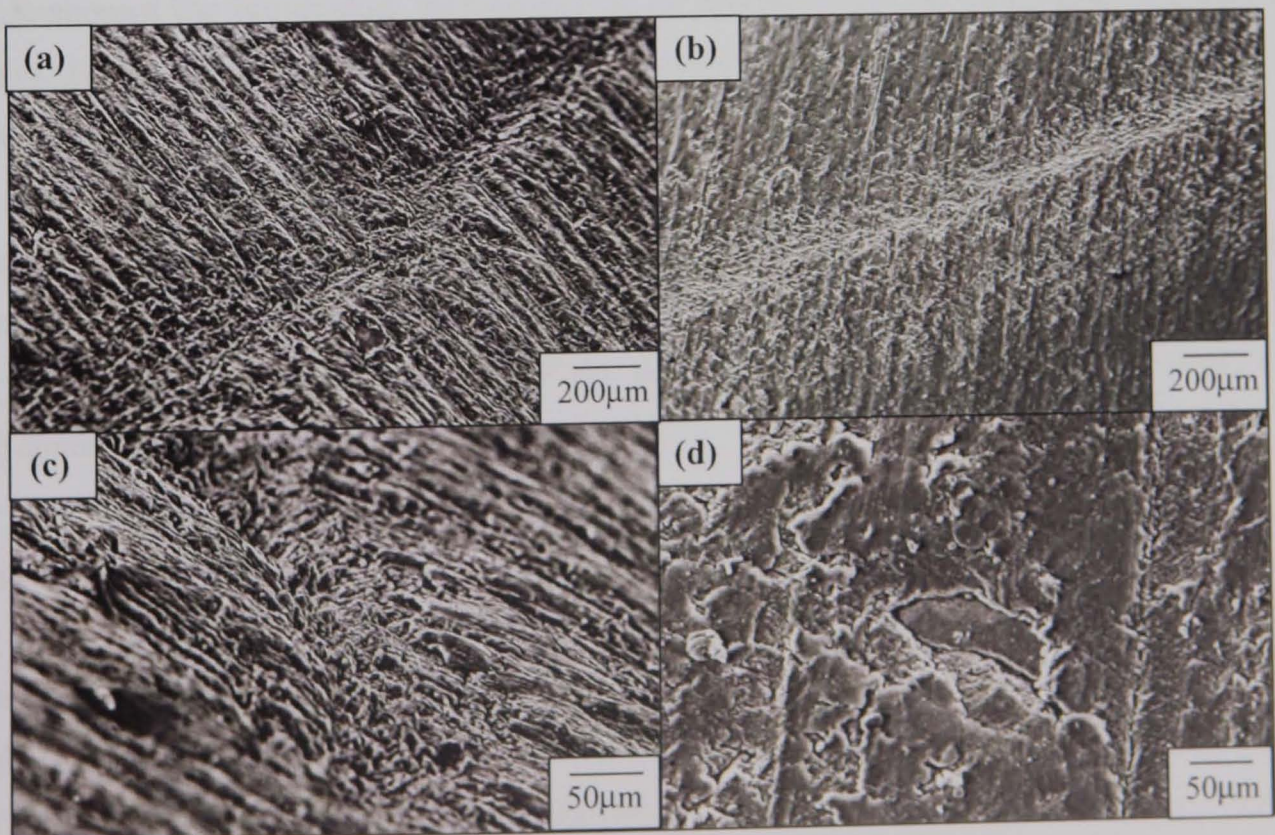
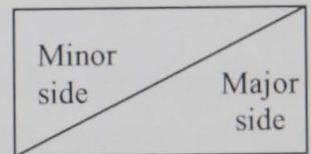


Figure 6.3: SEM images showing the details of the type 'a' and type 'b' wear regimes, at the suction end of the stator, created under the standard wear test conditions of 'pure' abrasion;

- (a) well defined ridge of type 'a'
- (b) coalescence of pits in type 'b'
- (c) detail of the ridge of type 'a'
- (d) embedded particle in the major side of the ridge of type 'a'

Key for (a) and (b) :



Of the two features, type 'a' is more prominent than type 'b'. The main feature of the type 'a' wear regime was a well defined ridge, shown in figures 6.3 (a) and (c), with the steep side of the ridge facing the major end of the slot, so that the shallow side sloped towards the minor centre of the stator slot. On either side of the ridge, the rubber had a micro-layered surface texture consisting of pits, flaps/cuts and a rippled morphology, similar to a dry abrasion pattern, with the steep sides of the ripples facing the major end of the slot. The severity of the micro-layered texture was greater on the major side of the ridge, where silicon oxide particles were found embedded into the rubber. The angle of embedding was observed to be normal to the surface of the rubber and there were no signs of low angle impingement or dragging of particles, as seen in figure 6.3(d). The type 'b' wear regime, figure 6.3(b), shared similar features, although less severe and the well-defined band consisted of a coalescence of pits which formed a shallow trough as opposed to the definite ridge seen in type 'a'.

The micro-scratches that can be seen in the SEM images, which ran nearly perpendicular to the two wear regimes, were found to be a direct consequence of two-body abrasive type wear to the rotor surface and which subsequently cut into the rubber. Evidence for this argument was found by repeating the wear tests with tungsten carbide coated rotors which resisted the abrasive action of the sand. The resultant wear features observed on the stator were purely of the type 'a' and 'b' wear regimes as described, with no evidence of micro-scratching.

It was difficult to distinguish from the morphology of the worn surface textures, the wear mechanisms active in the system. The studies by Arnold and Hutchings, discussed in section 3.3.3, showed the progressive morphology of an eroded surface at low impact velocity and angles. Similarities are drawn with these features, and likewise with those created by wet abrasive-erosion and pattern abrasion.

The location of both wear regimes was found to be very significant as they remained fixed throughout the wear test programme, regardless of which system variable was changed. With the rotor sitting at either end of the stator slot the wear regimes were located at the edge of the line contact created between the two components.

Appleby^[1] defines rubber frequency as "the speed of deformation just at the point of contact as the rotor moves over the stator" and states that the frequency for compressing and releasing the rubber will not be equal to the speed of the pump. For most of the time, the majority of the rubber is stationary and therefore the properties, locally, could change drastically to the rest of the rubber as the rotor compresses and releases the rubber as it slides and rotates by. Appleby found that the rubber frequency was extremely high during contact between the two components

and subsequently the local hardness of the rubber must also be extremely high. The speed of deformation will produce a change in Elastic modulus, and consequently, according to Appleby, its ability to embed particles.

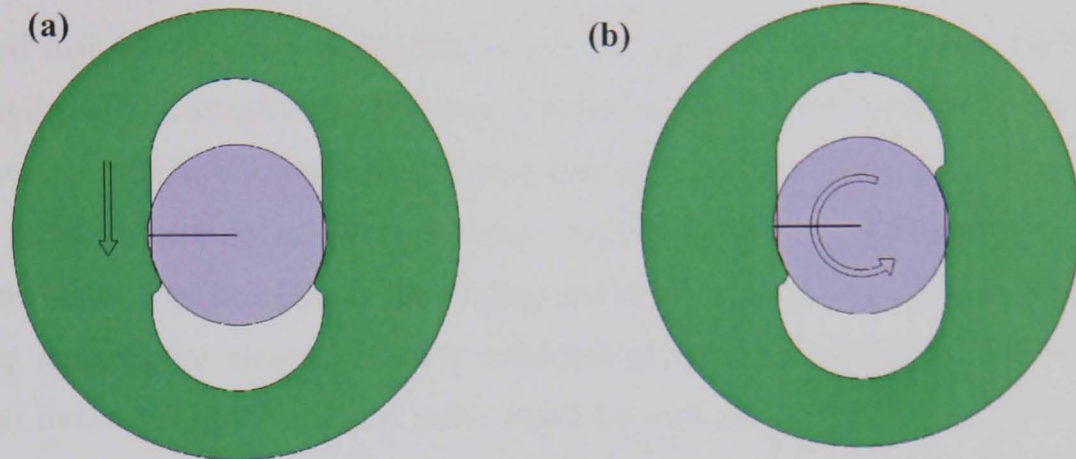
It is proposed that the characteristic wear features in the stator are created by a 'sweep and wave' effect. Wirth ^[2] found that the process of wear was influenced by the 'fulling' affect that the stator encounters, due to the interference fit, which leads to a localised elastic deformation of the rubber. And any local changes in the geometry of the cavity of the stator would effect the entering of the particle into the sealing zone. In theory the rubber that the rotor pushes against due to the interference fit, must be accommodated elsewhere in the stator bulk, since rubber deforms elastically not plastically. It is postulated that the displaced rubber creates a wave that proceeds the rotor, which Wirth described as 'fulling'. According to Wirth a wave will exist on both sides of the slot, at opposite sides of the rotor, but he did not quantify whether the waves were of equal size, or remained at a constant size, during the oscillating movement of the rotor in the stator slot.

Consider the rotor in sliding motion only, in the two-dimensional model of the pumping element. As the rotor accelerates along the slot, the rubber at the front of the rotor is in compression, whilst that at the back is in tension, thus creating a wave either side of the rotor, figure 6.4 (a). In the pumping element the sliding velocity is not constant, reaching a maximum at the minor centre where the wave size will be greatest. For rotational movement only the compression /tension effect would occur at opposite corners, as described by Wirth ^[2], and shown in figure 6.4 (b). However, in reality the rotor is both sliding and rotating, so the combined effect would create a primary and secondary wave, the positions of which would depend upon the relative difference between the two velocities. The rotational velocity of the rotor is always constant and greater than the sliding velocity, although the difference reduces as the rotor accelerates towards the minor centre of the slot. Consequently there will always be a larger primary wave proceeding in front of the rotor, on the high contact load side, with a smaller secondary wave, on the opposite side, in the rotors wake. The magnitude of these waves will be dependent on the position of the rotor in the stator slot, as shown in figures 6.4 (c) to (h).

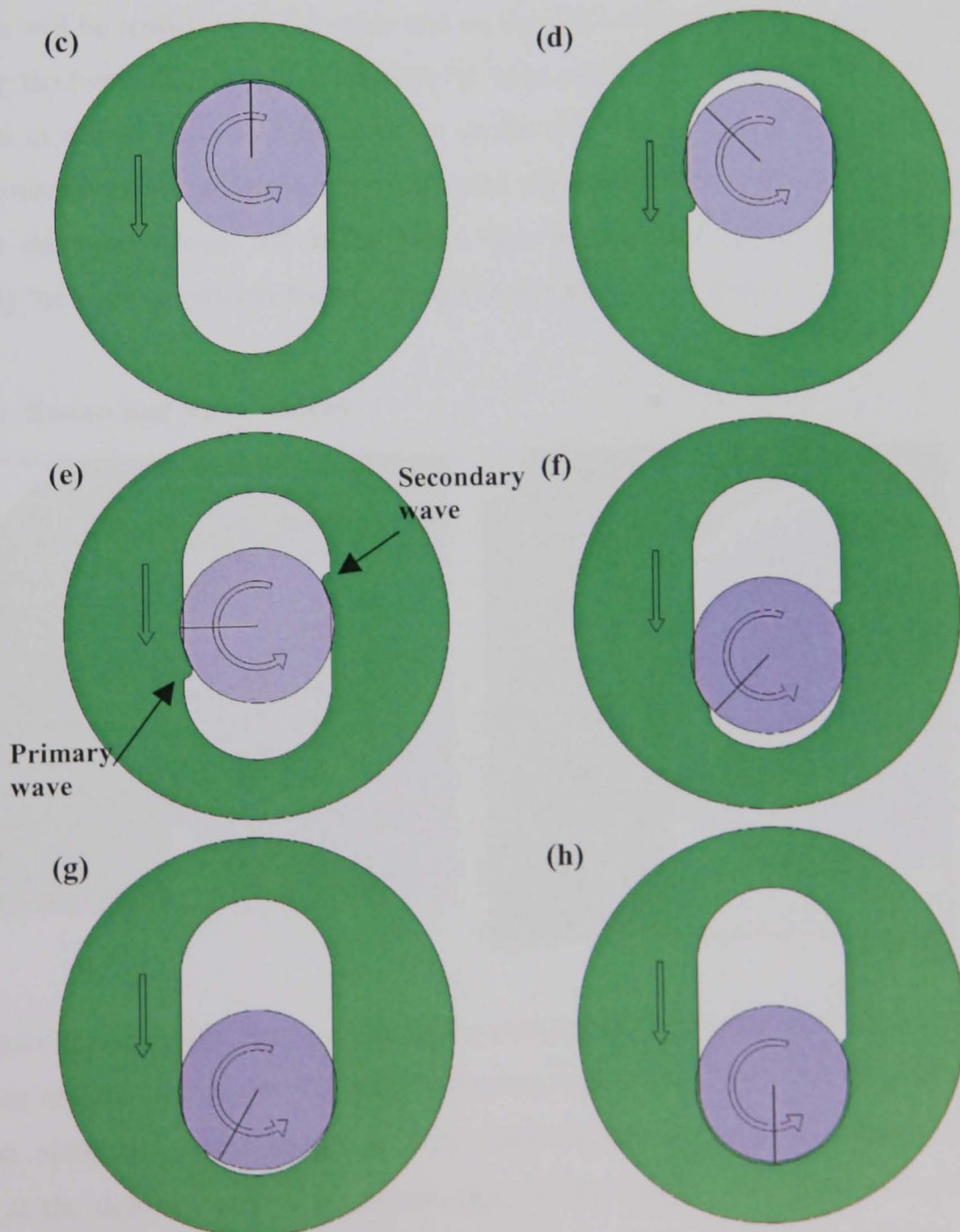
When the rotor approaches either end of the slot, there will be a transitional period where the point contact, in a two-dimensional aspect, converges to a line contact. The seal it creates will start to grow from each of the two point contacts as the rotor leaves the straight section of the slot and decelerates to a purely rotational velocity, completing the full 180° seal at the stator position of $\Psi = 0^\circ$ and 180° . Once this contact has been made, and the seal created, there will be a short period of time where the rotor is rotating, maintaining a 180° contact with the rubber, but

Figure 6.4: Schematic of the proposed wave effect due to the interference fit between the rotor and stator

(a) Wave effect due to sliding velocity (V_s) only; Wave effect due to rotational velocity (V_r) only;



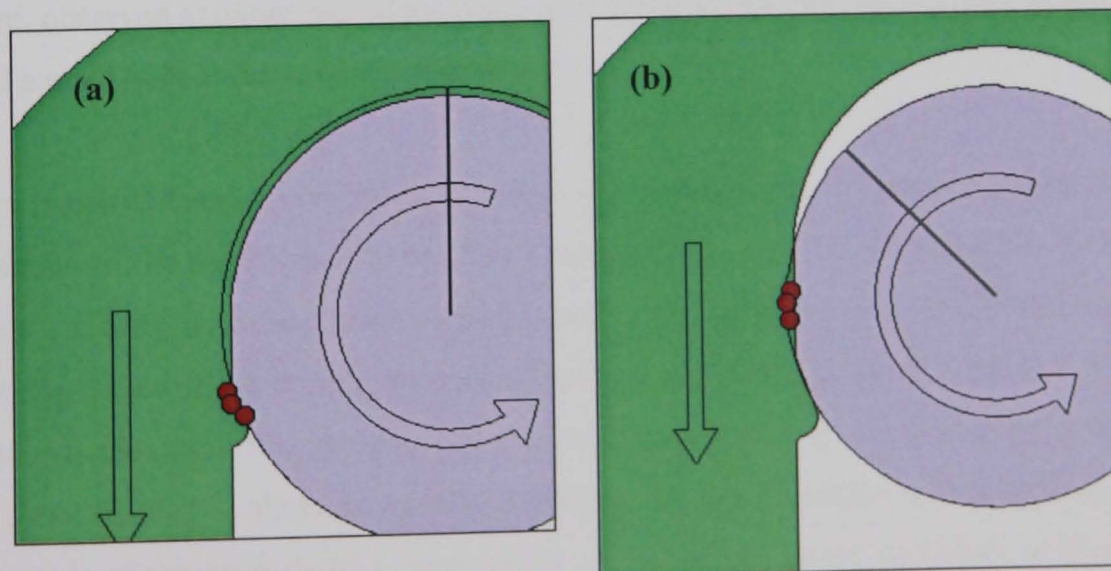
Combined effect when $V_r > V_s$ at $\Psi =$ (c) 0° ; (d) 45° ; (e) 90° ; (f) 135° ; (g) 150° ; (h) 180°



not sliding. This period relates to an angular rotation of 30° of the rotor, at either end of the slot, resulting in a total of 60° of rotation, per revolution, where the velocity contribution to the contact conditions would be purely rotational.

It is postulated that, as the rotor decelerates to zero sliding velocity, the particles left in the converging region will be swept round the curved section of the slot and expelled at the edge of the flank. Here they will be hindered from entering the capsulism by the creation of the primary wave, which starts to form during the time delay when the rotor is purely rotating with 180° contact with the stator. The particles hit the sloping side of the wave, embedding into the rubber, and removing material by abrasive-erosion mechanisms, as schematically shown in figure 6.5(a). As the rotor starts to accelerate away from the end of the slot, the wave is pushed forward, leaving in its wake the particles, which, are either pushed into the stator, by the action of the rotor sliding over them, or fall into the void of the capsulism, as shown in figure 6.5(b). This process will be replicated at the other end on the slot and be repeated on every revolution thus creating the two helical bands of the type 'a' wear regime. Over a period of time a ridge is formed from continual impact of the particles on the wave wall, causing material removal by abrasive-erosion in the same location, for each rotor revolution. Once the rotor pushes the wave forward the damaged rubber left in its wake then relaxes back to its original shape and consequently the wearing process forms a trough which grows to a ridge.

Figure 6.5 : 'Sweep and wave' theory



It is postulated that a similar process, due to the movement of the secondary wave, creates the type 'b' wear regime. The main difference in the two regimes was their severity with respect to the location along the stator length. It was observed that the type 'b' regime was more prominent at the delivery end of the stator, than at the suction end, and under certain test conditions was only observed from the middle section onwards. Likewise, the type 'a' wear

regime was less pronounced at the delivery end of the stator, with a similar severity as the type 'b' regime. These observations imply that the Flexishaft side loads contribute significantly to the contact pressure, and thus the severity of the two wear regimes. As discussed in section 2.3.1, the drive mechanism of the Flexishaft produces uneven side loads conditions on the rotor. At the suction end, all the side load is applied to one side of the rotor, whilst at the delivery end the side loads tend towards zero enabling the rotor to free float in the slot. Consequently, the applied load, on both of contact points between the rotor and stator, at the delivery end, becomes balanced.

6.1.2 *Characteristic rotor wear features*

The diagram in figure 6.6 schematically shows the location of the four distinct helical wear bands observed on the rotor under the purely abrasive conditions of the standard test variables. These comprised of:

- (i) a grooved band on the leading side of the scroll, **band I**
- (ii) a grooved band on the trailing side of the scroll, **band II**
- (iii) a smooth thin band on the peaks of the scroll, separating bands I and II, **band III**
- (iv) an unworn band lying in the troughs of the scroll, **band IV**

The combined widths of the bands I, II and III was found to equate to the angular length of a worn step, observed at either end of the rotor. The depth of the step was greatest at its centre and provided a good indication as to the degree of wear.

The worn bands of I and II consisted of a series of grooves which lay parallel to one another and perpendicular to the direction of flow. The severity of the grooves were greater on the trailing side, with a clearly definable edge with the start of the unworn band, IV, in the troughs. The clarity of the edges of the leading side wear band I with bands III and IV was less pronounced. SEM analysis identified that the material removal mechanism for the formation of the grooves was by classical ductile abrasion modes of cutting, wedge formation and ploughing. However the magnitude of the grooves was observed to occur on two levels, as shown in figure 6.7 (a). Macro-grooves were observed, of an order twice the size of the abrading particles, which were found to contain micro-scratching of widths $\sim 1/10^{\text{th}}$ of the abradant. The troughs and the peaks of the macro-grooves appeared smooth and rounded, as opposed to sharp and angular, implying they were formed by the action of multiple passes of the abradants. The morphology of the sides of the macro-grooves was observed to be different, as shown in figure 6.7 (b) and (c). One side was relatively smooth and directional, consisting of micro scratches lying parallel with the

Figure 6.6 : Schematic showing the location of the main wear features on the rotor, under the standard wear test conditions of 'pure' abrasion, with optical inserts of actual wear morphology

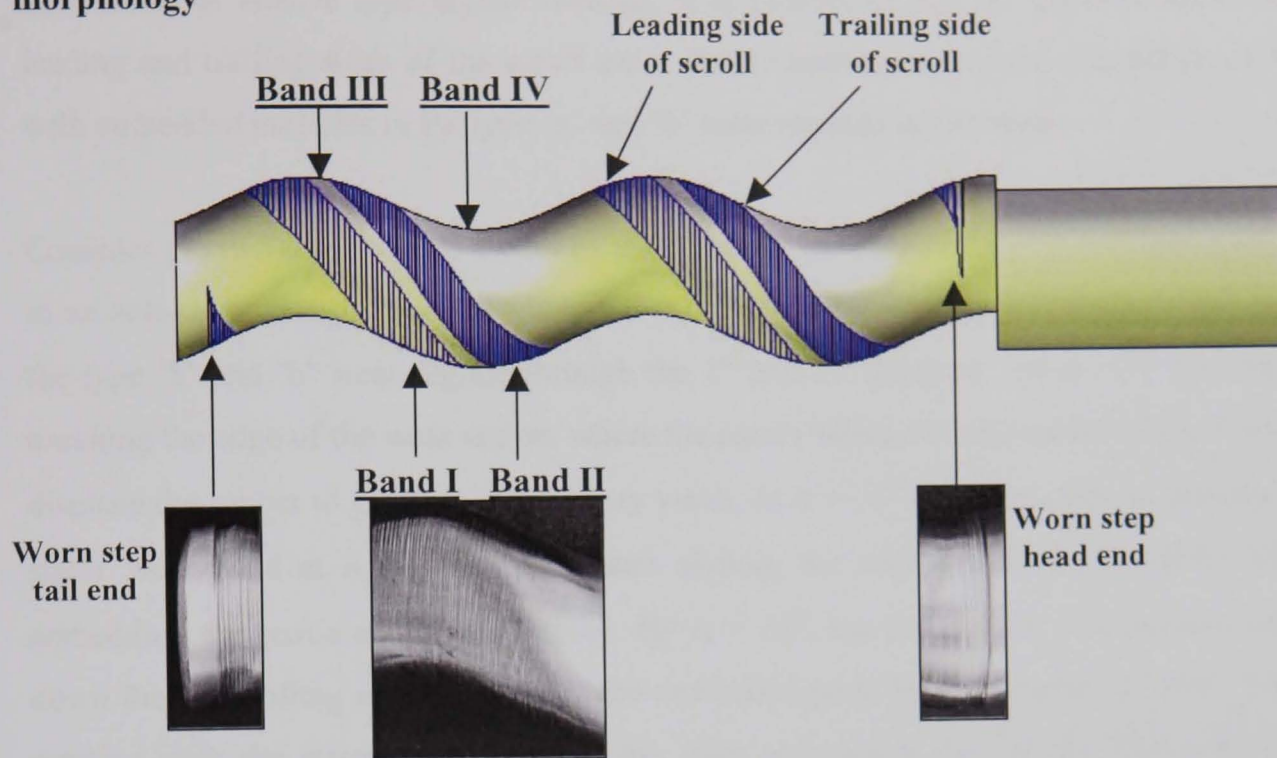
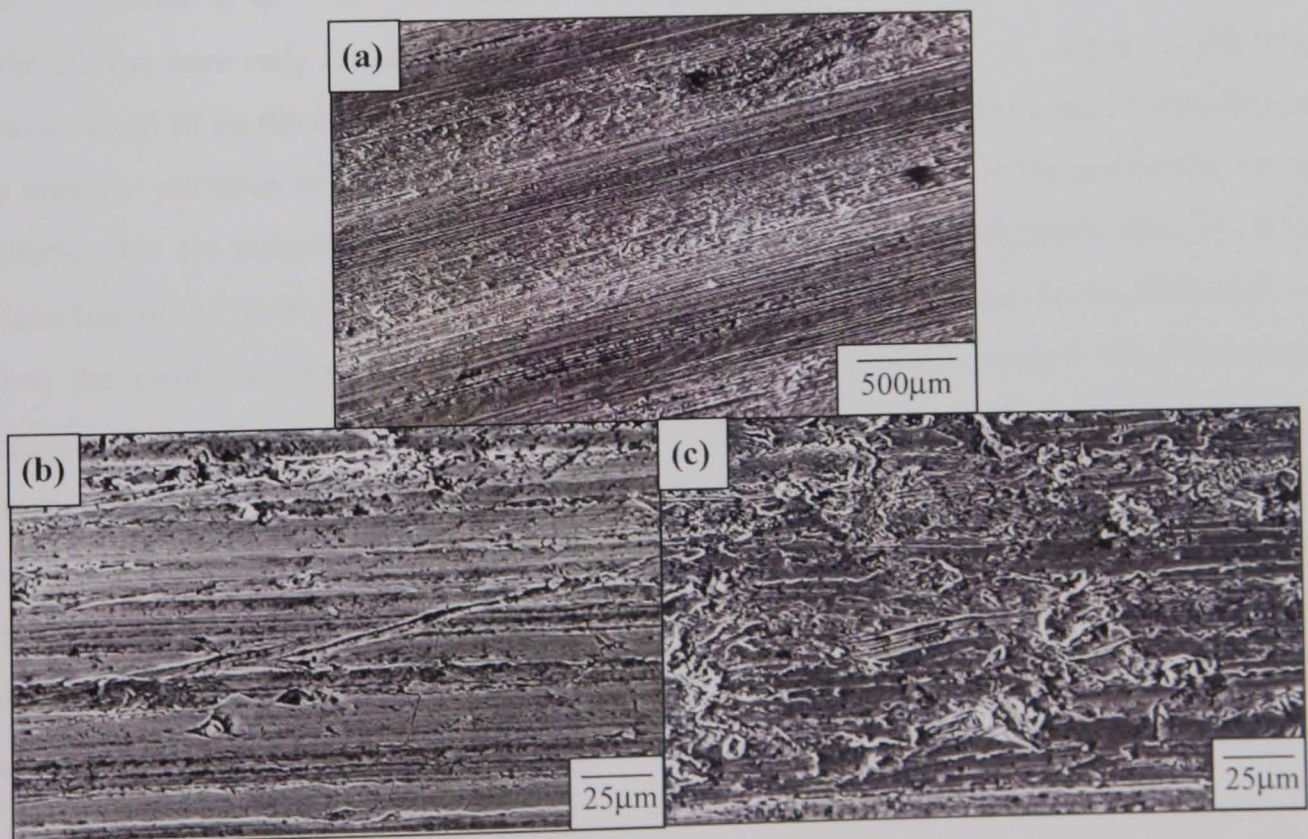


Figure 6.7 : SEM images of the stainless steel rotor tested under standard wear test conditions of pure abrasion showing (a) macro-grooves; and detail of the macro-grooves on the (b) smooth side and (c) rough side



macro grooves and of an average width of 10 microns. The morphology of the other side was much rougher and less directional, with intermittent ploughing and wedge formation, plus indications of erosive type impact damage. It is postulated that the grooves observed on the leading and trailing sides of the scroll are a direct consequence of the interaction of the rotor with embedded particles in the type 'a' and 'b' wear regimes in the stator.

Consider the two-dimensional model of the pumping element and half a revolution of the rotor in an anti-clockwise direction. Figures 6.8 (a) to (f) transcribe the interaction of the rotor with the type 'a' and 'b' wear regime through the 1st and 2nd quarters. At $\alpha = 0^\circ$ the rotor is just touching the edge of the wear region, where the purely rotational movement of the rotor starts to displace the rubber to generate the primary wave. At $\alpha = 25^\circ$ the rotor starts to interact with the stator wear band at $\delta = 80^\circ$. Yet to start sliding, the rotor pushes hard against the wave, embedding the particles into the rubber. By $\alpha = 30^\circ$, the rotor starts to accelerate and rotate down the slot, rolling and sliding over the embedded particles of the type 'a' wear. Interaction remains with the stator wear band, as the rotor accelerates through the first quarter, to the position at $\alpha = 87^\circ$. The angular position of the rotor is now $\delta = 3^\circ$. This contact between the rotor and the stator wear features, from $\delta = 86^\circ$ to 3° , translates to the worn band I on the leading sides of the rotor scroll, whose angular width can be quantified as 83° . From $\alpha = 87^\circ$ through to the 2nd quarter at $\alpha = 93^\circ$, the contact interface is exposed to maximum sliding velocity, although the rotor only rotates by 6° , from $\delta = 3^\circ$ to -3° . This defines the angular width of the smooth band III on the scroll peaks as 6° . The smooth appearance of this band implies there are no abrasive particles in the contact zone, during this portion of the rotor movement, or, any particles that are present, are smaller than the thickness of the hydrodynamic film, i.e. $d < h$. Interaction of the rotor with embedded particles resumes in the 2nd quarter at $\alpha = 93^\circ$ and $\delta = -3^\circ$, when the rotor encounters the type 'b' stator wear regime. The contact between the two components continues to $\delta = -80^\circ$, as the rotor decelerates to $\alpha = 155^\circ$, defining the angular width of the worn band on the trailing sides, III, of the rotor as 83° , on the assumption that the widths of type 'a' and 'b' are equal. For 3rd and 4th quarters, the interaction would be replicated, with rotor contact with the type 'a' wear regime in 3rd quarter occurring on the leading side between $\delta = 86$ to 3° , and interaction in 4th quarter between type 'b' and the trailing side, II, of the rotor at $\delta = -3^\circ$ to -80° .

Consequently, there is a region of the rotor's circumference which never makes contact with the stator. This is equates to the band of unworn material, band IV, observed in the trough of the scroll, at $\delta = -80$ to $+80^\circ$ (through 180°), and defines the angular width of the steps, worn at either end of the rotor.

Figure 6.8 (a) to (f) : Interaction of the rotor with the type 'a' stator wear regime in the 1st quarter and type 'b' wear regime in the 2nd quarter

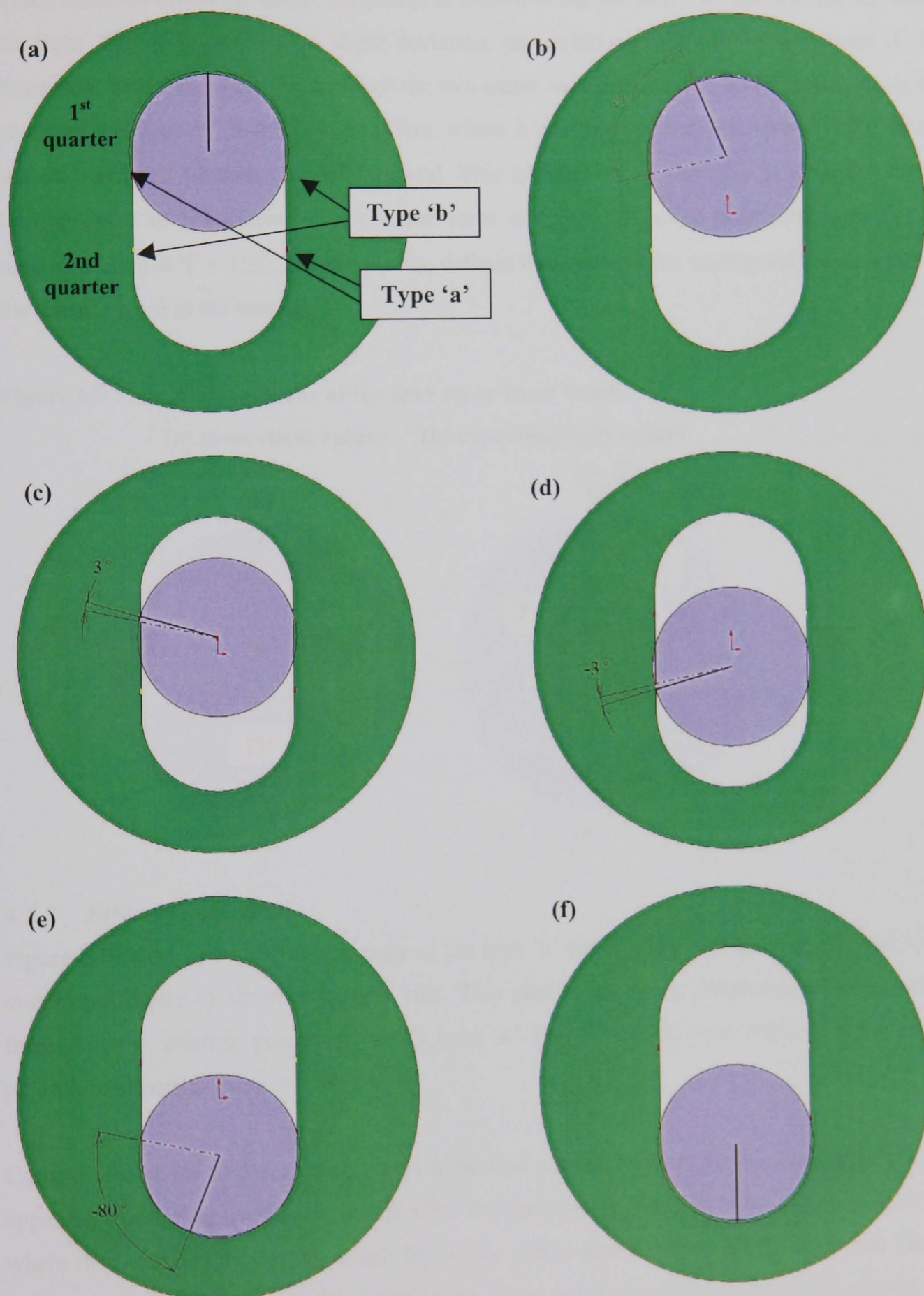
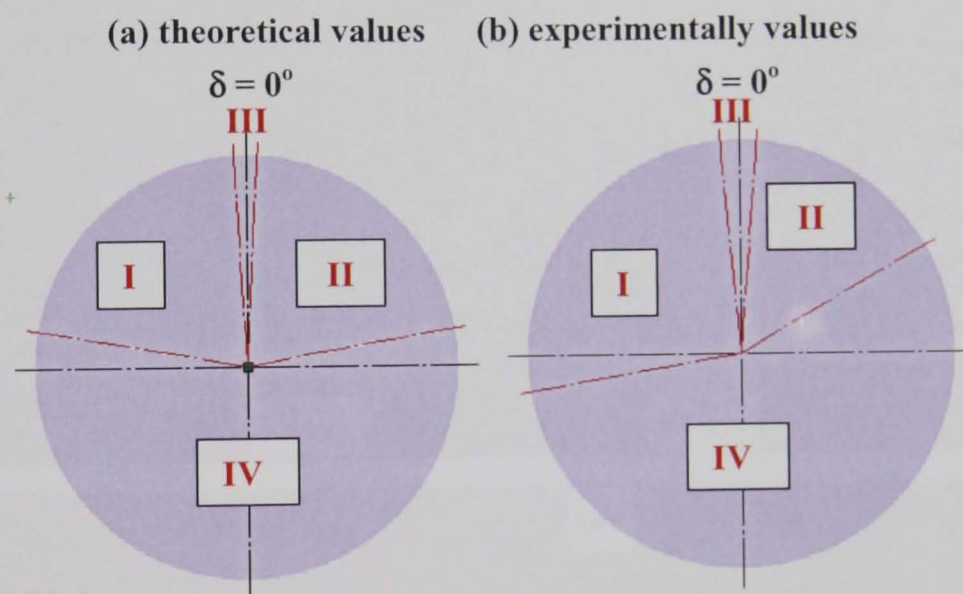


Figure 6.9 compares the theoretical angular positions of the four wear bands, derived from the model in figure 6.8, with those measured experimentally. The leading side of the scroll, i.e. that which faces the discharge end of the pump, is located to the left of $\delta = 0^\circ$, and the trailing side to the right. The diagrams show a slight deviation, particularly on the trailing side band II. The theoretical model assumes the width of the two stator wear bands to be equal. However, it was observed that type 'b' had a tapered effect, where it was thinner and less severe at the suction end and widened towards the delivery end. This translates to a variation in δ values for the starting point of the contact between the rotor and type 'b' wear band, although the end remained fixed at $\Psi = 155^\circ$, equating to the defined line between the trailing side wear band and the unworn band in the troughs.

Figure 6.9 : Angular positions of the four rotor wear bands



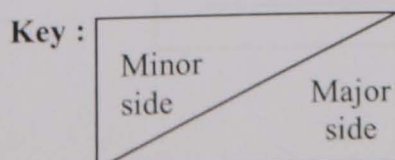
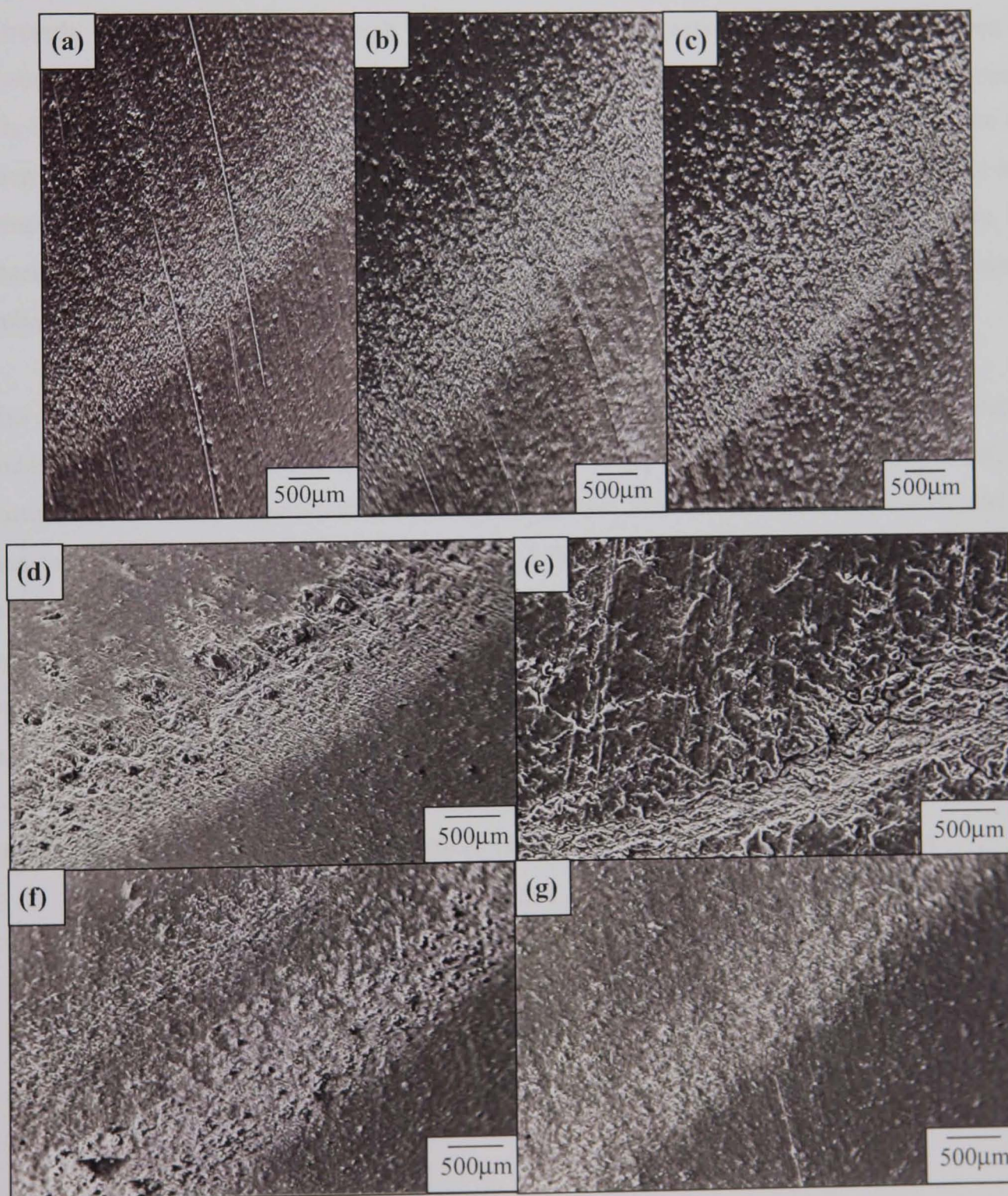
6.1.3 Effect of particle size

Figure 6.10 shows how the morphology of the type 'a' stator wear regimes was affected by the system parameter of abrasive particle size. This part of the study demonstrated an important feature in the wearing process; that the type 'a' and 'b' stator wear regimes were created regardless of particle size.

Comparison of the different wear scars identified certain features in the wear regimes, that appeared to be independent of particle size. All the wear regimes demonstrated a distinct line where the wear regime started, which lay on the major side of the regimes. From this line the 'damage' propagated towards the minor centre of the stator slot, initially relatively densely then reducing in frequency. The 'damage' consisted of a micro-layered surface texture, of small cuts or flaps in the rubber, ridges, and pits and holes that had coalesced to form larger holes or troughs. The open side of the flaps and cuts, and the steep sides of the ridges, all faced the same

direction, towards the major side of the stator slot. Particles were found embedded amongst the damage regions. However no signs of drag or shallow angles of impingement of the particles were observed. The particles appeared to have been pressed directly into the rubber from an impingement angle of 90° . All this evidence supports the 'sweep and wave' theory for the creation of the two stator wear regimes.

Figure 6.10 : SEM images of type 'a' wear regime, generated under standard wear conditions, using particle sizes of (a) 16; (b) 24; (c) 45; (d) 120; (e) 225; (f) 450 and (g) 900 microns

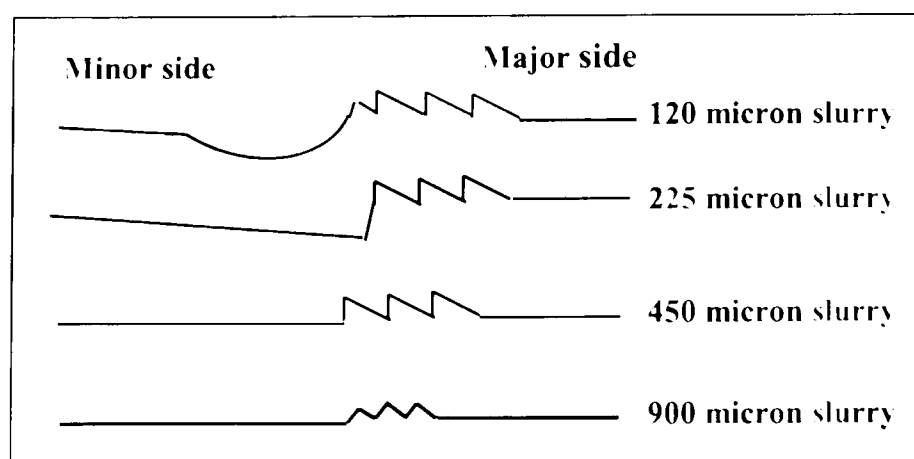


The width of the wear regimes and the amount of particles embedded in the rubber were found to be dependent on particle size. Also, it was observed that the size of the abrasive particles has a profound effect on the severity of the type 'a' and 'b' stator wear regimes, with a nominal distribution relationship.

The most severe damage was caused by the 120 micron silicon oxide particles, followed by the 225 micron particles. Both of these created a ridge, as the feature for the finite start of the damage. The ridge from the 225 micron particles has been described in section 6.1.1. The ridge from the 120 micron particles was more severe, creating undercutting in the rubber, resulting in a trough, the straight side of which faced the major side, with the sloping side leading out towards the minor centre of the slot. The schematic diagram in figure 6.11 shows the demise in this feature as the particle size increased further to 450 and finally disappeared with the 900 micron particles. A higher percentage of 125 and 225 micron particles were observed to have remained embedded in the damaged areas than for the larger sizes. No ridge feature was observed with the smaller particles sizes of 45 microns and less, and the percentage of embedded particles was significantly lower.

The creation of a ridge, and its severity dependency on particle size, is a significant feature in understanding which system parameters effect the wearing process in the pumping element. It is postulated that the phenomenon relates to the relative size of the rotor and stator, and the maximum particle size that can be swept around the gap, created by the closing capsulism, as the 180° line contact is made between the two components. For the pump size in the simulated wear rig, that maximum particle sizes appeared to be ~200 microns. Any stator wear observed from slurries containing particles larger than the maximum size, would result from smaller particles within the grade, due to the particle size distribution in any one grade of grit.

Figure 6.11: Schematic of the reduction in ridge size with increasing particle size



Further evidence to support the phenomenon of a critical size range was provided by comparing the dimensional wear rates and SEM analysis of the worn rotors. Comparing the dimensional wear rates against particle size for the silicon oxide slurries, graph 6.1, showed high material removal rates for the two smaller silicon oxide particles, then a significant fall in the rate for the larger particle sizes, providing a strong indication that a change must have happened in the contact conditions. From the SEM analysis, this can be related to the reduction in particles contributing to the wearing process.

Comparison of the macro-grooves created by the different size silicon oxide slurries, revealed differences in their morphology, figure 6.12. From the slurries containing particles smaller than 225 microns, the morphology on the sides of the macro-grooves were observed to be different. One side was relatively smooth and directional, consisting of micro-scratches lying parallel with the macro-grooves and of an average width of 10 microns. Whilst the morphology of the other side was much rougher and less directional, with intermittent ploughing and wedge formation, plus indications of erosive type impact damage. However, for the larger particle slurries of greater than 450 microns both sides of the macro-grooves were found to be smooth, with micro scratches lying parallel along the grooves. This would imply that only fixed particles contributed to the wear process with the larger particle size slurries, whilst both fixed and free motion particles were present in the contact zone when pumping the smaller size particle slurries. It was observed that the width of the macro-grooving was independent of particle size, with similar widths measured for all four particle sizes. However, the depths appeared to be a function of particle size, which was reflected in the volume of removed material and the subsequent results in graph 6.1. These observations would suggest that the micro-scratching reflects the behaviour of individual particles within the contact zone, whereas the formation of the macro-grooves is controlled by the whole wearing process of the sweep and wave concept, and how the particles congregate in the rubber.

Therefore, it is proposed that there are three conditions of wear, whose limits can be defined as $d < x_1$; $x_1 < d < x_2$; $d > x_2$, where d is the nominal particle diameter and x_1 and x_2 are critical particle sizes. It is postulated that, for every size of pump, there is a critical particle size range, that will cause maximum wear to the pumping element components, whose upper and lower limits can be described by x_1 and x_2 . For the size of pump under evaluation, it is surmised that the limits for the critical particle sizes are $x_1 = 100$ microns and $x_2 = 250$ microns. When conditions are outside of the critical particle range the severity of wear will reduce with decreasing x_1 values and increasing x_2 values.

Graph 6.1 : Dimensional wear rates of 316L stainless steel rotors vs. nominal silicon oxide particle size

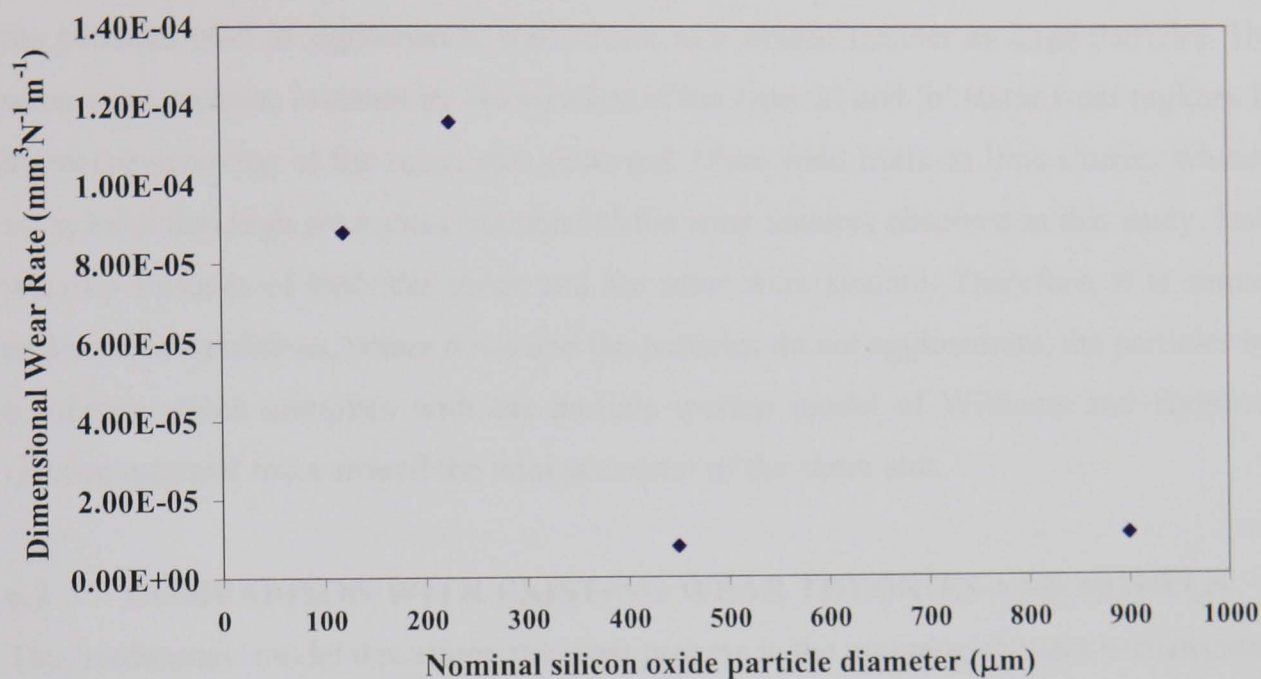
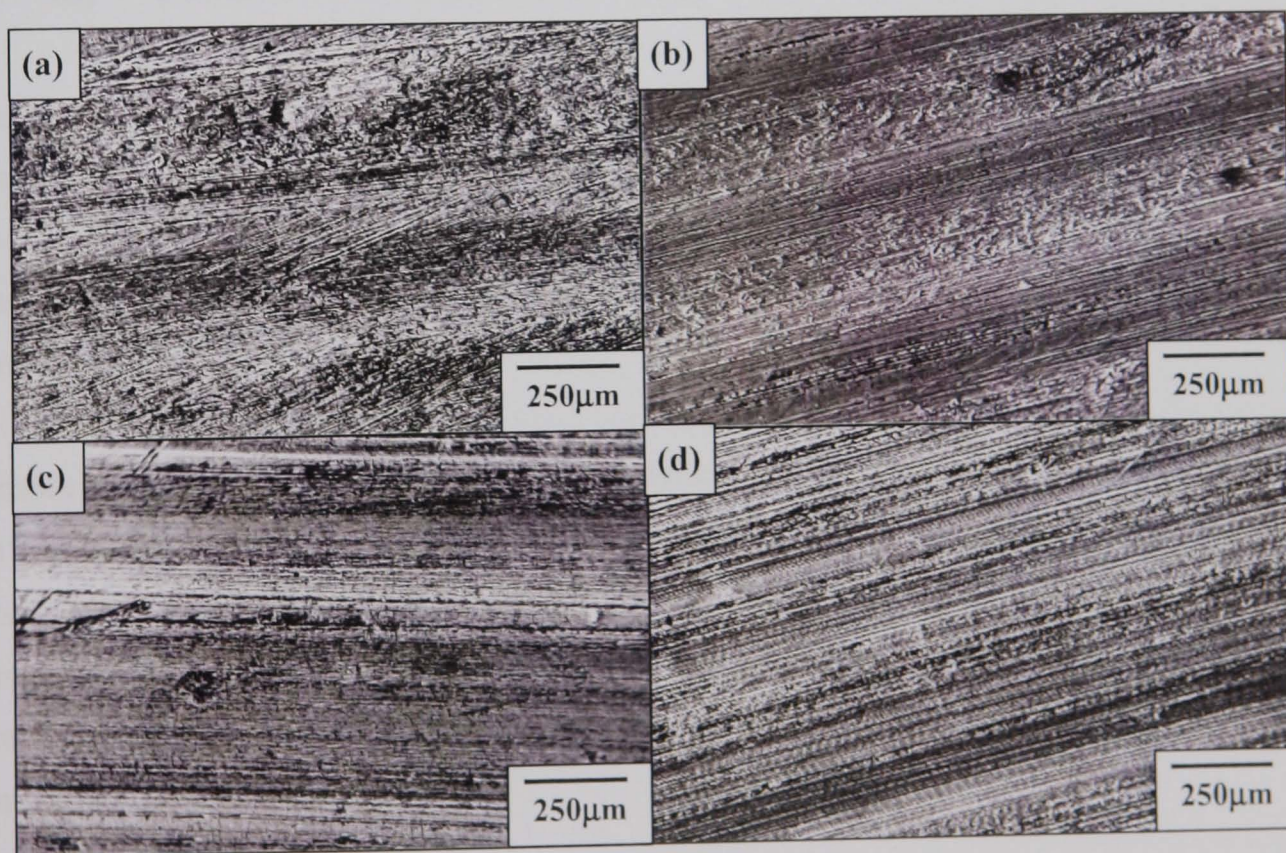


Figure 6.12 : SEM images of the stainless steel rotors tested under abrasive conditions with an aqueous silica sand slurry containing a mean particle size of (a) 900; (b) 450; (c) 225 and (d) 120 microns



Another condition, which cannot be ignored, is when the particle size is less than the thickness of the hydrodynamic film, h , where the conditions can be described as $d < h < x_1, x_2$. Field trials on high concentration slurries containing 0.5 micron of titanium dioxide demonstrated that the particles tend to agglomerate and behave in a similar manner as large particles. Hence the same wear process, initiated by the creation of the type 'a' and 'b' stator wear regimes followed by macro-grooving of the rotor, was observed. Other field trials on lime slurries where $d < h < x_1, x_2$ exhibited high wear rates but none of the wear features observed in this study. Instead, the wearing surfaces of both the stator and the rotor were smooth. Therefore, it is surmised that under these conditions, where $d < h$ and the particles do not agglomerate, the particles behave in a manner which complies with the particle motion model of Williams and Hyncica^[3] and remove material from around the total perimeter of the stator slot.

6.2 COMPARISON WITH EXISTING WEAR THEORIES AND MODELS

The 'traditional' model describing the wear process in the pumping element was discussed in section 3.1, where May^[4], Bourke^[5], Wirth^[2] agreed that an abrasive approaching the seal line contact would behave in one of three ways:

- (i) be rejected back into the capsulism
- (ii) embed into the stator wall
- (iii) be transferred through to the next capsulism via the lubricating film

In May's opinion the selected behaviour was dependent on the relative size relationship between the particle and the thickness of the hydrodynamic film, whereas Wirth's studies concluded the behaviour to be independent of particle size. However, this approach to modelling the wear process makes several assumptions, which, from the results of this study, have been proved to be unfounded.

The model assumes the thickness of the hydrodynamic film to remain constant throughout, when in fact this is not the case, since the film thickness is directly proportional to velocity and inversely proportional to pressure. The velocity of the rotor is known to vary per revolution and it has been experimentally demonstrated that the contact pressure changes with rubber thickness. Hence, the thickness of the hydrodynamic film can be assumed to be greatest when the rotor is at the centre of the slot.

May^[4] made the assumption that the material removal, during the wearing process on the rotor, occurred by the cutting mode of two-body abrasion, and based his wear equation on Archard's wear law. The results from this study have clearly demonstrated that the characteristics of the stator plays an integral part in the wearing process. Using the classical abrasion approach for

quantifying the wear means that the contribution of the stator properties are not considered, since the model, based on ductile wear, is too simplistic to describe wear in a system where the load applied to the particle is due to a resilient counterface.

A further assumption of the model was that the seal line ribbons or contact zones equate to the wear bands, since the wearing process was said to occur in the contact region which is hydrodynamically lubricated. The results from this study have provided the evidence to prove that this is not the case. It is known that the contact between the rotor and stator is dynamic, i.e. the seal line ribbons, types 'a' and 'b', are constantly moving, up and down the sides of the stator slot, and this motion generates the hydrodynamic film necessary to lubricate the seal lines. If the seal line ribbons equated to the wear bands, then wear would be expected along the full length of the stator slot. However, the major wear features to the stator have been identified to lie on two pairs of distinct helical paths which are fixed and do not move. All this evidence suggests that there is a fundamental difference in the contact conditions, at the type 'a' and 'b' wear regimes, and the sealing conditions around the remainder of the stator slot.

It is important to state that these features occur under the conditions of abrasive slurry applications. Where the pumps are used for pumping clean liquids, an inevitable reduction in the interference fit between the two components will ultimately occur as a result of the dynamic contact of the seal lines. This will be a more uniform reduction on wear, removing the rubber away from the straight sides of the stator slot, which equates to flattening of the peaks from a three-dimensional aspect.

Williams and Hyncica's two-dimensional model of particle motion ^[3] and Axen et al.'s ^[6] studies of loose particle behaviour, both consider how hardness differentials of the contacting surfaces and particle size, effect the mechanisms of wear. Initially, it was thought that these models bore relevance to the wearing process in the pumping element. However, as with the traditional pump model, they assume that the process would occur anywhere around the stator slot, and therefore do not assist in determining the probability of a particle being swept and embedded into the wall of rubber, at specific locations.

Although Wirth's studies ^[2], on the wear in progressive cavity pumps, were focused on rotor wear, he did recognise the fact that the wear process does not occur all the way round the stator slot. From his studies on the wear of a CrNi steel rotor a maximum wear was observed at $\delta = 45^\circ$ and -45° , which equates to the middle of the leading and trailing wear bands, I and II. He observed the abrasion on the negative angle to be less, and postulated that, at $\delta = 45^\circ$, the

rotating movement of the rotor pushes a heel of elastomer and was therefore subjected to an increased contact pressure, and subsequent higher wear. The experimental rotor wear observations and the postulated 'sweep and wave' theory agree with his studies. However, Wirth failed to relate these to the wear features in the stator, and in doing so his wear theory fell short. He concluded that the location of the rotor wear was related to the differences in lengths of contact between the rotor and stator, for each revolution of the rotor. Plotting the trajectories for the eight individual angular positions of the rotor, Wirth found that there were considerable differences in the contact lengths for each point on the rotor with the stator. The longest contact length or path of interaction, S , per revolution was dependent on the initial stress from the interference fit and the angular position of the rotor. In calculating the paths of interaction, it became apparent to Wirth that the angular positions with the maximum paths of wear were not at the position of $\delta = 0^\circ$, but were shifted by a certain angle, the value of which depended on the amount of interference. He thus concluded that the wear on the rotor would, theoretically, occur between $\delta = 90^\circ$ and -90° , which agrees with the findings from this study. However, experimentally, he observed that material abrasion occurred outside of this range, which he concluded must occur by a different wear mechanism such as fatigue. Such a material removal mechanism was not identified in this study, and the anomalies from the theoretical δ values were found to relate to variations in the width of the type 'a' and 'b' stator wear bands and not to a change in wear mechanism.

6.3 INFLUENCE OF SYSTEM PARAMETERS

Table 6.1 provides a summary of how the identified wear features on the rotor and stator were found to be effected by the system variables. Details of the relationships between the wear and the system parameters are discussed in the following section of this chapter.

6.3.1 *Velocities within the pumping element*

As discussed in section 2.4 and 2.5, the three pump velocities of rubbing, fluid and particle can be controlled by the system variable of operating speed, with rubbing velocity, said to have the greatest influence on the wear life of the rotor and stator ^[7].

Table 6.1 : The effect of system variables on the wear features on the rotor and stator

Description	Effect of variable on severity of wear				
	Pressure	Speed	Interference	Abrasive size	Rotor coating
Type 'a' stator wear regime	↑	↓	↓	45μm < ↑	↑
Type 'b' stator wear regime	↓	↓	↓	↑ > 450μm	↑
Worn step at either end of the rotor scroll.	↑	=	↓	45μm < ↑ ↑ > 450μm	↑
Wear band on the leading edge of rotor scroll	↓	↓	↓	↓ < 225 μm => 450 μm	↑
Wear band on the trailing edge of rotor scroll	-	↓	↓	↓ < 225 μm => 450 μm	↑
Wear band on the peaks of rotor scroll	↓	↓	↓	=	↑
Abrupt change in the grooved wear band in the trough of the stator, at tail end	↓	n/a	n/a	n/a	n/a
Abrupt change in the grooved wear band on the trailing edge of the rotor scroll, at tail end	↓	n/a	n/a	n/a	n/a

(i) Effect on stator wear features

Increasing the operational speed was found to have a direct effect on the severity and morphology of the type 'a' and 'b' stator wear regimes. The SEM images, in figure 6.13, compare the type 'a' wear regime generated at 250 and 1500 rpm. At 250 rpm, the morphology of the wear regime was a thin band, ~ 200 microns wide, consisting of pits and embedded particles. To the minor side of the band was another band of intermittent cuts and flaps in the rubber, the open edges of which faced in the major direction. At 1500 rpm, the morphology of the wear regime was found to have significantly changed. The line of pits had been replaced with a wide shallow trough, ~ 1000 microns in width, with a fine micro-layered texture, propagating towards the minor centre of the slot. No particles were found embedded in the worn region. The finer texture of the 1500 rpm wear suggests that more particles were actively present in the contact zone. This evidence supports the 'sweep and wave' theory, as an increase in rotational speed would have a direct effect on the number of particles and velocity at which, the particles are swept around the converging gap as the rotor approaches the end of the stator slot.

Fig 6.13 : SEM images of the type ‘a’ stator wear regime generated under standard wear test conditions at operating speeds of (a) 250 rpm and (b) 1500 rpm

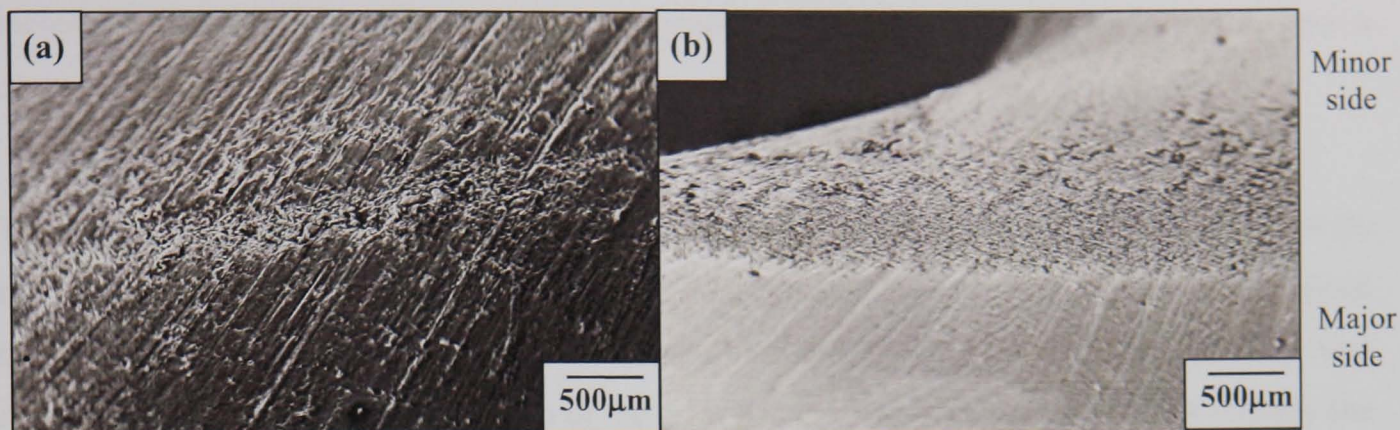
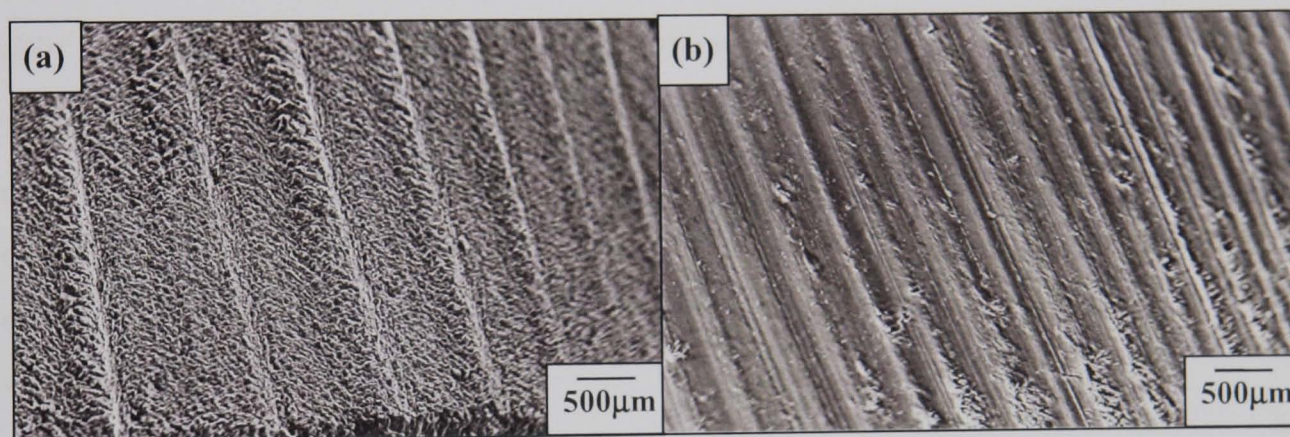


Fig 6.14 : SEM images of the wear tracks in rubber, as a direct result of macro-grooving to the rotors from wear testing under standard conditions, at operating speeds of (a) 250 rpm and (b) 1500 rpm



A significant difference was observed in the manner in which the grooves in the rotors removed the rubber, as shown in figure 6.14. At the high speeds the resultant damage was smooth sided grooves, implying that the rubber had been cut by a sharp edge. Whereas at the low speeds, the morphology of the grooves in the stator was textured, very similar to that observed when rubber is removed by the ‘stick-slip’ process. This would imply that at the lower speeds there is a possible change in the lubrication conditions, and the asperities on the surface are greater than the thickness of the lubricating film. The spacings between the grooves was observed to reduce with increasing speed, which reflects the increase in fineness with speed, observed with the type ‘a’ wear regime.

(ii) *Effect on rotor wear features*

Visual comparison on the wear features on the rotors, at increasing speeds, was found to be difficult to quantify. The severity of the grooved band II on the trailing side of the scroll, appeared to increase with speed, although at the high speeds greater than 1250 rpm, the band was devoid of grooves and was very smooth. Also instead of the line, that defined the edge of the grooved band on the trough side, there was a definite step in the metal where material had

been removed on the band II side. The profile of the scroll was observed to change with speed, becoming multi-faceted from the leading side, over the peak and down the trailing side. The increased severity of this effect resulted in a gradual change in the profile of the scroll from a curved geometry to angular.

These observations agree with Akincioglu ^[8] who stated that the rubbing velocity was directly related to the scouring wear on the rotors, which he concluded were caused by particles trapped between the rotor and stator, and thus to minimise the effect a low rubbing velocity was required. Measuring the angular width of the wear bands I and II demonstrated that initially the width was a function of speed, up to 600 rpm, where the bands reached a maximum width and became independent of speed.

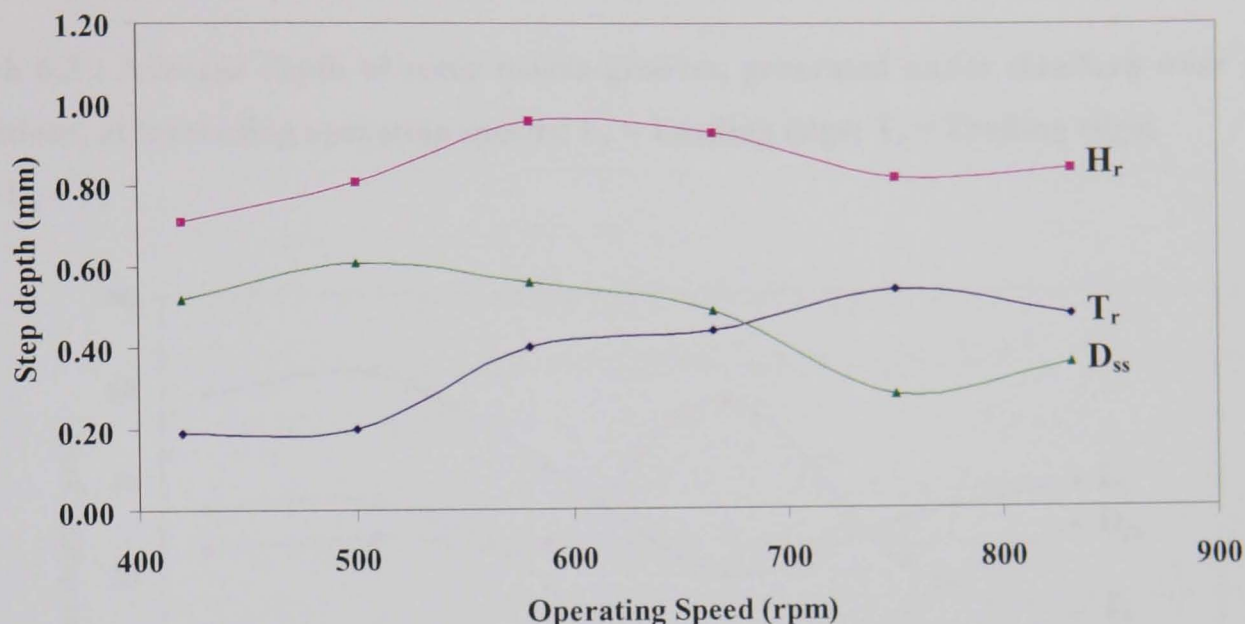
(iii) Relationship between wear rate and the system variable of speed

Three different approaches were used in an attempt to quantify a relationship between the wear rate of the rotors and the system variable of speed. One technique involved measuring the depth of the step worn at each end of the scroll, the second used laser profilometry to measure the depth of the macro-grooves, whilst the third used weight loss measurements to derive the dimensional wear rates of the rotors.

The results from the first approach are plotted in graph 6.2. The depth of the step at the suction end of the pumping element was found to always be greater than that at the delivery end. Initially, up to speeds of 580 rpm, a similar increase in step depth at both ends was observed. This trend continued, with increasing speed, at the tail of the scroll, but not at the head of the scroll where it was seen to reduce. These observations can be explained by the influence of the sideloads imposed by the Flexishaft, discussed in section 2.3.1. The sideloads are greatest at the suction end and tend towards zero at the delivery end, explaining why the step depth worn at the head of the rotor scroll was always greater than that at the tail end. The plot of the difference in the step depths, reveals a gradual reduction with increasing speed, suggesting that the influence of the Flexishaft sideloads is greater at lower speeds, and centrifugal forces introduced at the higher speeds help maintain a more balanced rotor. The consequence of this would be a positive influence on the contact conditions, due to a more uniform contact pressure along the full length of the pumping element. However, due to the complexity of the loads in the system, it was concluded that this approach was not conclusive in quantification of the wear rate of the rotors with respect to operational speed.

Graph 6.2 : Depth of the steps, at either end of the rotor scroll, generated under standard wear test conditions at increasing operating speeds; H_r = rotor head; T_r = rotor tail;

$$D_{ss} = H_r - T_r$$



Profile measurements were taken, on both the leading and the trailing sides of the rotor scroll, at three different locations along the length. The average macro-groove depth, at each speed, was derived from these measurements and plotted against the operating speed, graph 6.3. With the exception of the 665 rpm value, the results show a decrease in groove depth with increasing speed, which was greater on the leading side than on the trailing side. This could imply a reduction in the wear rate or, alternatively, that the worn surfaces became smoother with increasing speed. Taking depth measurements from the profile can be erroneous as the relationship between the top of the groove and the original rotor surface is unknown. The observations of the smoothing of the wear bands with speed provides evidence that the top of the grooves, particularly at the higher speeds, did not equate to the original surface. The data generated from using this approach was found to be ambiguous, and potentially erroneous, thus concluding that it was also an unreliable method of quantifying material removal rates.

The results from the third approach of mass loss, shown in graph 6.4, demonstrated a linear relationship of increasing rotor wear with speed, which could be expressed using equation 6.1, where Rv is the maximum rubbing velocity.

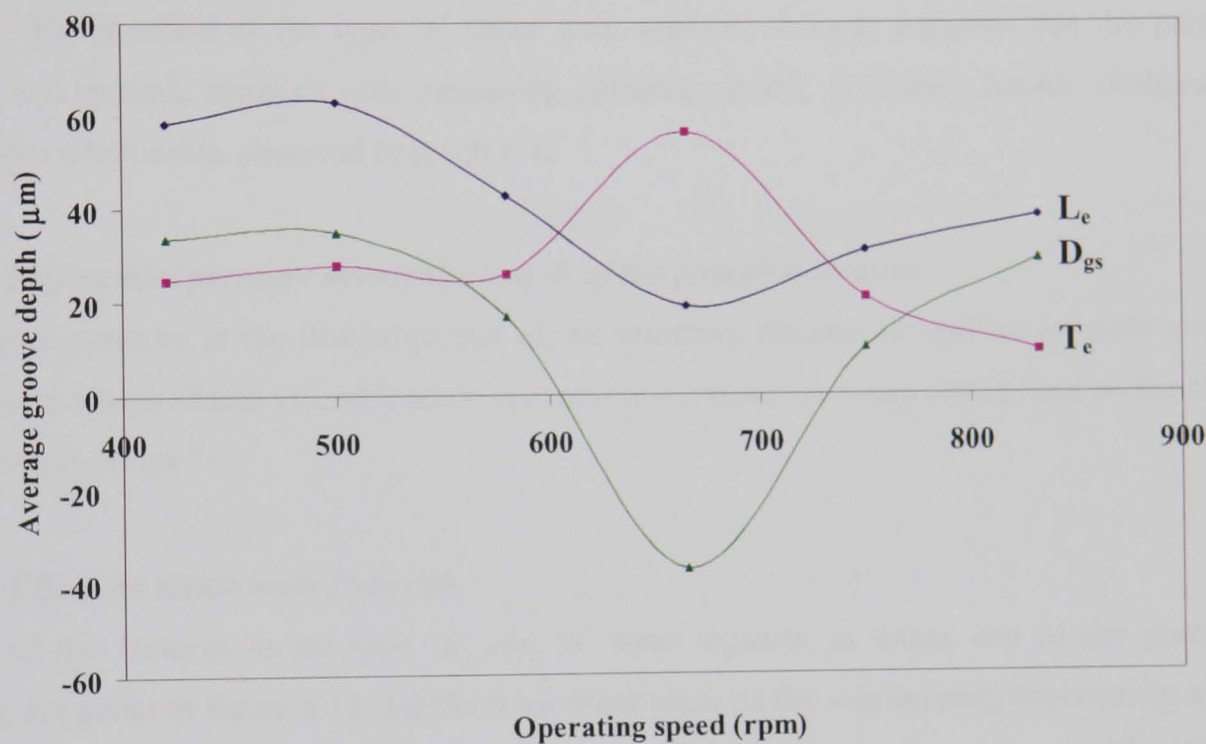
$$k \propto Rv^{0.35} \quad (6.1)$$

Drane and others ^[4,5,10,11] also describe a linear type relationship between the wear rate and pump speed, although they found the dependency to be much greater. However, their studies

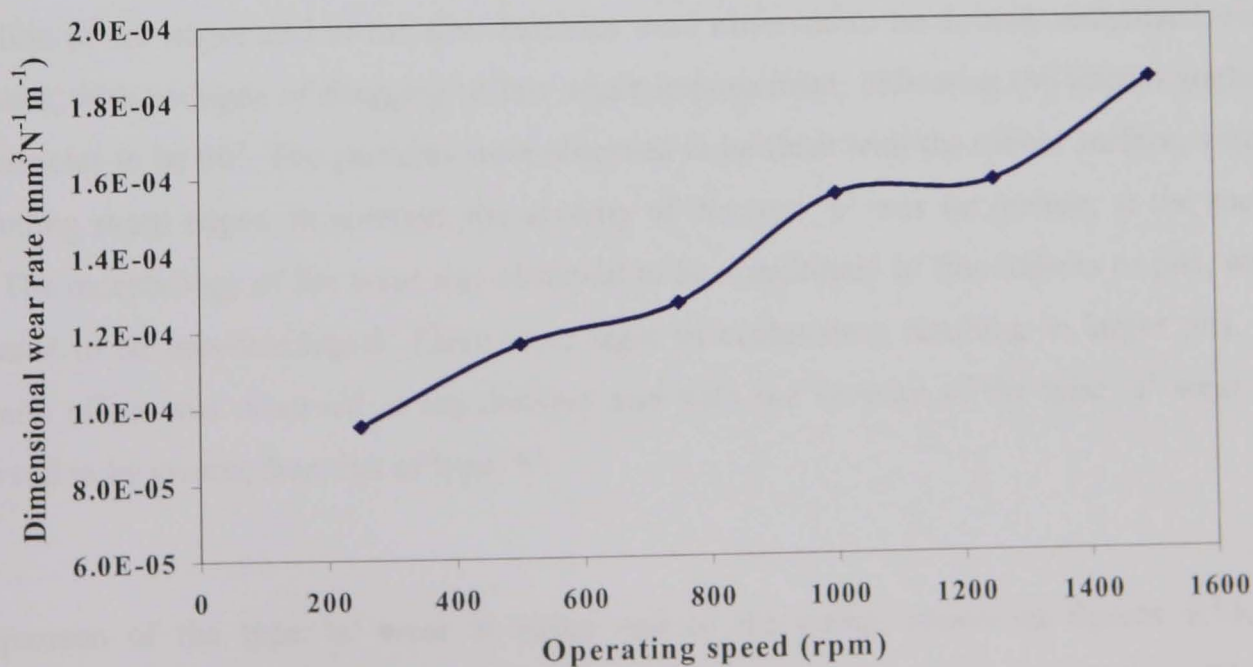
were based on the combined wear of the rotor and stator, whereas the experimental data for equation 6.1 purely relates to rotor wear, possibly explaining the difference in power values, which would suggest the wear rate of the stator is twice that of the rotor.

Graph 6.3 : Average depth of rotor macro-grooves, generated under standard wear test conditions, at increasing operating speeds; L_e = Leading edge; T_e = Trailing edge;

$$D_{gs} = L_e - T_e$$



Graph 6.4 : Dimensional wear rate of the rotor against rubbing velocity, for standard wear test conditions at increasing operating speeds



Classical ductile abrasion theory ^[12] states that the wear rate is independent of sliding velocity, but the results in graph 6.4 imply that the volume removed from the rotors, for a constant sliding distance, is a function of velocity, as May ^[3] expressed in his variant of Archard's equation. Both approaches assume a constant load and include a wear coefficient. Measuring the depth of the worn steps produced evidence to suggest that the load conditions in the contact zone do not remain constant with speed, a plausible explanation as to the deviation from classical abrasion theories. According to abrasion models by Moore & Stevenson ^[13] K , the dimensionless wear coefficient, accounts for changes in particle behaviour and the fraction of particles which cause 'cutting'. Examination of the type 'a' stator wear regimes strongly suggests that the particle density, and motion, changes with increasing operating speed, providing further evidence to support the relationship observed in graph 6.4.

6.3.2 *Differential pressure across the length of the pumping element*

Applying a pressure at the discharge end of the pumping element is said to generate a rotor thrust force, which causes an end load on the rotor and a resultant longitudinal load on the stator at the contact points ^[1].

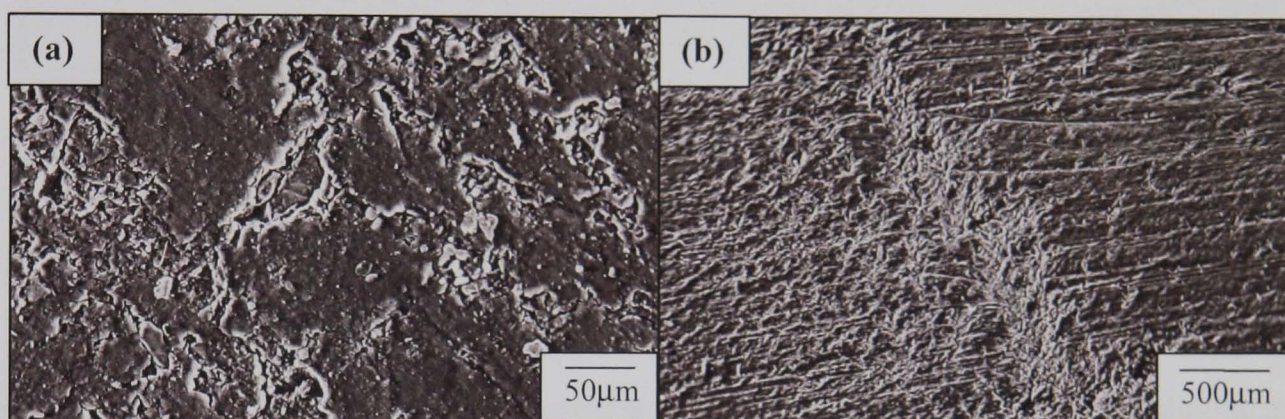
(i) *Effect on stator wear features*

Details of the features in the type 'a' and 'b' wear regimes, at either end of the pumping element, are given in figure 6.15, for the 6 bar wear tests. At the suction end, the severity of the type 'a' wear was found to be significantly less than that created under no pressure, although the width of the regimes were comparable. The characteristic ridge was absent from the wear feature, which consisted of a low density band of cuts and flaps, with the open edges facing the direction of the major end of the slot. Particles were observed to be directly embedded within the band, with no signs of dragging or low angle impingement, indicating the impact angles of the particles to be 90°. The particles were observed to be flush with the rubber surface, with no protruding sharp edges. In contrast, the severity of the type 'b' was far greater, at the suction end. The morphology of the wear was observed to be a multitude of fine indents or pits, which appeared to be non-directional. There were signs of coalescence resulting in larger pits. The opposite effect was observed at the delivery end with the severity of the type 'a' wear was observed to be greater than that of type 'b'.

Comparison of the type 'a' wear at either end of the pump, shown in figures 6.15, the characteristic ridge feature at the delivery end of the pump, as opposed to the suction end. This suggests that, applying a 6 bar differential pressure across the pumping element, reverses the severity of the wear, due to the change in the flow direction of the slurry. At the suction end, the

slip appeared to counteract the detrimental effect of the wave and significantly reduce the amount of rubber damage in the type 'a' wear regime, whilst increasing the intensity of the type 'b' wear, due to the reverse flow of the slurry which acts on the opposite side of the stator peak, i.e. those which face the delivery end. This evidence suggests that the effects of a differential pressure, i.e. the slip of the fluid, is experienced over the total length of the pumping element, and not, as Appleby suggested, just in the second half of the element.

Figure 6.15 : SEM images of the details of type 'a' wear regime, generated under standard wear test conditions, against a discharge pressure of 6 bar, at (a) the suction end and (b) the delivery end.

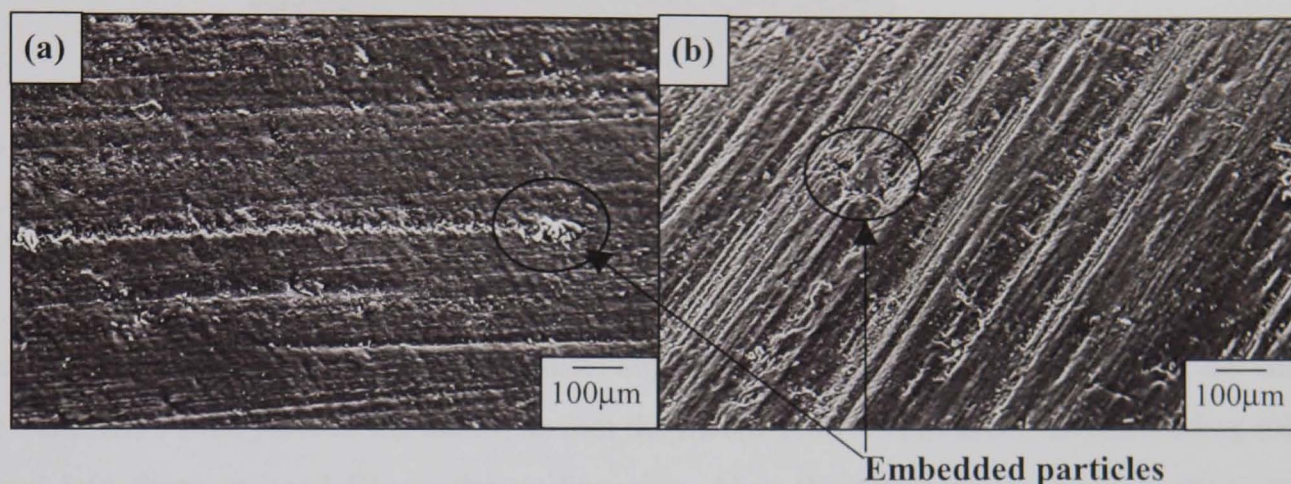


Between the two wear regimes, on the straight section of the stator slot at $\Psi = 75$ to 115° and 255 to 285° , grooves were observed in the rubber, the severity and frequency of which were much greater at the delivery end than at the suction end, as shown in the SEM images in figure 6.16. The direction of the grooves lay parallel to the straight sides of the two-dimensional stator slot. These grooves were not observed under purely abrasive conditions, and only when a differential pressure greater than 4 bar was applied to the system. These grooves imply an erosive type wear mechanism across the dynamic seal lines and confirm the phenomenon of slip.

The counteraction effect of reducing the primary wave effect could be explained by the difference in the pressure distribution and film thickness between the slippage and the hydrodynamic film. As slippage is a flow of fluid, as opposed to a hydrodynamically generated fluid film, its thickness is greater than the lubrication film, resulting in an increased gap between the rotor and stator. The resultant pressure, induced at the contact zone, will be dispersed evenly resulting in a more uniform deformation of the rubber than by a point or line contact. Evidence to suggest that the slip film is thicker than the hydrodynamic film, was found between type 'a'

and 'b' wear regimes, where particles, greater than 50 microns in size, had become embedded in the rubber, having been dragged through the contact seal lines, as shown in figure 6.16.

Figure 6.16 : SEM images of grooves down the straight section of the stator slot at (a) the suction end and (b) the deliver end, generated under standard wear conditions against a discharge pressure of 6 bar.



An additional wear feature in the stator, with a corresponding feature on the rotor, was observed, under pressure, which was not present under the purely abrasive wear conditions and increased in severity and size, with increasing discharge pressure. The feature was a specific region of flow-like grooves, in a 'eye' shape, which lay on the helix, as shown in figure 6.17. On the rotor, it was located between the trailing side wear band II and the unworn band, IV, in the troughs, equating to an angular position of $\delta = 238$ to 300° , at a distance of 41mm from the tail. The total linear length of the feature, after exposure to a differential pressure of 6 bar, was 17mm. Two corresponding areas were identified in the stator, which were located below the type 'b' wear regimes at $\Psi = 135$ to 145° and 315 to 325° . From the appearance and location of the wear feature, it is postulated that it was generated by erosion, caused by slippage, due to a pressure spike experienced across the seal lines at the rear of the moving capsulism, from initial exposure to the discharge pressure, as it opens up to the outlet end of the pumping element. This would agree with Appleby's hypothesis that, when pumping against a differential pressure, the pumping element is exposed to a sudden increase in pressure towards the delivery end and not a gradual increase across the total length. Thus evidence exists to support both Appleby's^[1] and Belcher's^[14] differential pressure theories.

Figure 6.17 : Optical images of the ‘eye’ shaped area of flow-like grooves, generated under standard wear conditions, against a discharge pressure of 6 bar, on the rotor



(ii) Effect on rotor wear features

It was observed that pumping against a discharge pressure greater than 4 bar closed the thin wear band III, on the peak of the scroll, so that the macro-grooves in band I, on the leading side merged into those in band III, on the trailing side. Also, the morphology of the leading side grooves changed from straight and parallel to wave-like, implying a change of wear mechanism from two-body abrasion to erosion. Similar flow-like channels were observed in the stator between the type ‘a’ and ‘b’ wear regimes along the straight sections of the slot, as shown in figure 6.16. It has been shown, in section 6.1.2, that the contact between the wear band III, on the peaks of the scroll, with the stator occurs during maximum rubbing velocity along the straight section of the stator slot, from $\Psi = 75$ to 115° (255 to 285°). The evidence suggests that the introduction of a pressure differential, greater than 4 bar, results in erosive wear across the dynamic side contact seal lines, which produces flow-like channels along the peaks of the rotor and the straight sections of the stator slot.

(iii) Relationship between wear rate and the system variable of discharge pressure

As with the study on the effects of operating speed, laser profilometry and step depth measurements were used in an attempt to describe the effect that differential pressure had on rotor wear.

Graph 6.5 plots the depth of the worn steps, at either end of the scroll, against increasing discharge pressure. A linear relationship of reducing wear with increasing discharge pressure was observed. These results correlate well with the stator wear morphology observations, as a reduction in the severity of the type ‘a’ wear regime, would be accompanied by less material loss from the rotor. However, these findings disagree with empirical data, where reduced

pumping element wear life with increasing differential pressure were found ^[5,15]. It was also observed that the difference between the step at either end of the rotor remained relatively constant, which would imply that the additional load applied to the components did not significantly counter-balance the eccentric loading effects of the Flexishaft side loads. Again, this disagrees with May ^[6,9] and Appleby ^[1] who stated differential pressure as the major load contributing factor to the wear within the pumping element.

Graph 6.6 plots the average depth of the macro-grooves against discharge pressure. These results show that a discharge pressure of 4 bar or greater was necessary to significantly contribute to the wearing process on the rotors and then only on the leading side of the scroll. Unlike the results from the speed wear tests, where increased abrasive type wear caused a flattening of the grooves, the wearing process had increased the depth of the macro-grooves. This would be probable, as it was the leading sides of the scroll that were exposed to the high velocities of the fluid being forced back through the pump. This supports the wear morphology observation of a change in the wear mechanism from abrasion to glancing angle solid particle erosion, where the slip of the fluid had taken the least line of resistance and opened up the macro-grooves to form channels.

6.3.3 Contact pressure between the rotor and stator

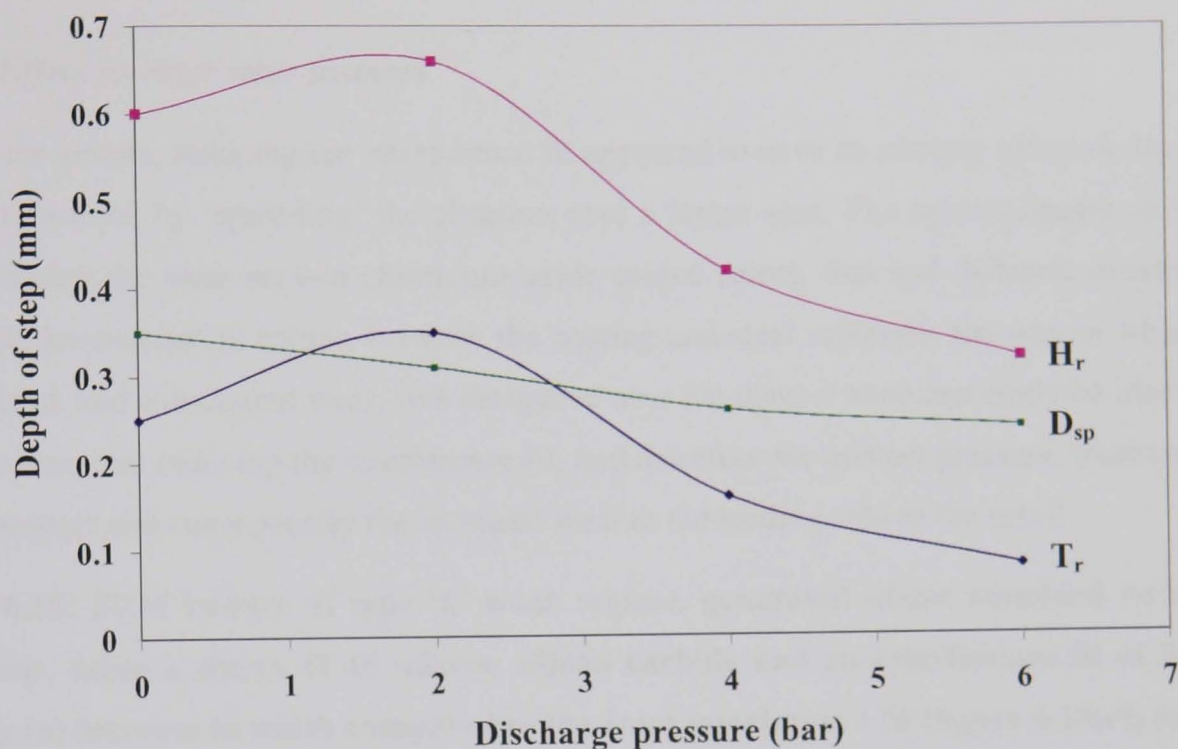
Changing the system variable of the interference fit between the two components directly effects the contact pressure between the rotor and stator. Experimentally, the minimum and maximum interference fits possible were 0.2mm and 1.5mm respectively. Interference fits less than this produced insufficient pressure at the seal lines to generate a flow through the pump, whilst the breakout torque became too high for the motors to overcome at interferences greater than 1.5mm. According to Wirth ^[2], the wear of the pumping element is largely caused by the contact between the rotor and stator, due to the pressure generated by the interference fit.

(i) Effect on stator wear features

Of the four system variables discussed in this section, it was found that reducing the interference fit had the greatest effect on the type 'a' and 'b' wear regimes. The SEM images in figure 6.18 compare the type 'a' wear regime, generated using a 45 micron silicon carbide

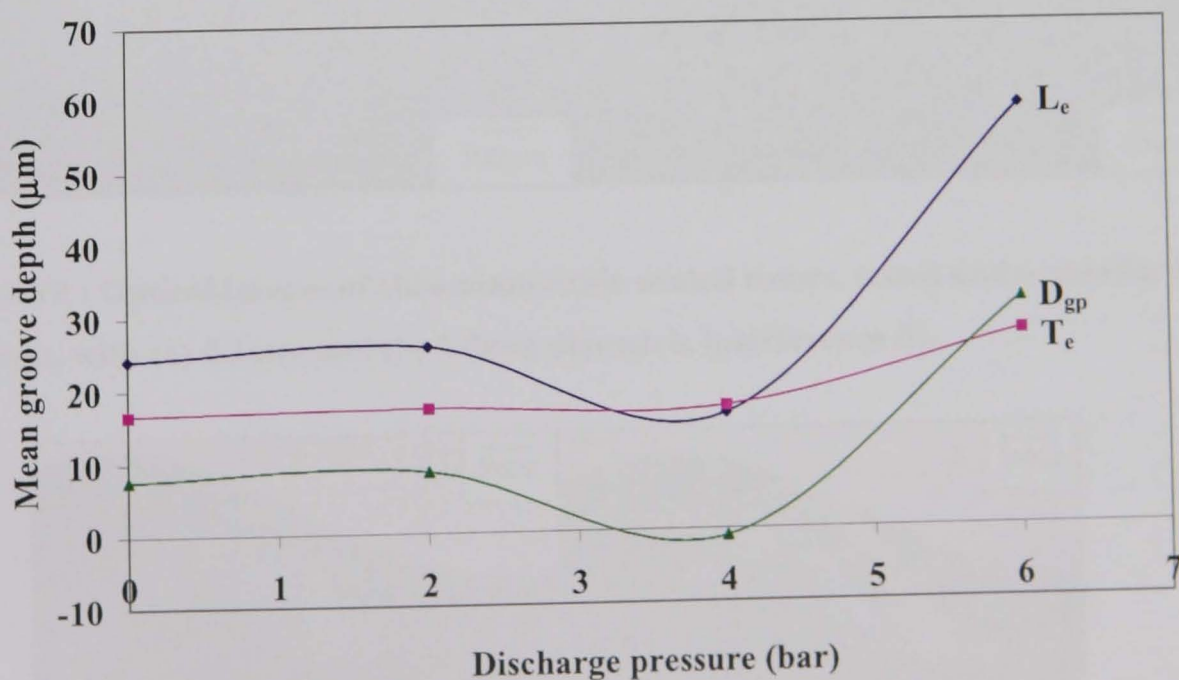
Graph 6.5 : Depth of the steps, at either end of the rotor scroll, generated under standard wear test conditions at increasing discharge pressure; H_r = rotor head; T_r = rotor tail;

$$D_{sp} = H_r - T_r$$



Graph 6.6 : Average depth of rotor macro-grooves, generated under standard wear test conditions, at increasing operating speeds; L_e = Leading edge; T_e = Trailing edge;

$$D_{gp} = L_e - T_e$$



45 micron silicon carbide slurry, with a 0.2mm and a 1.0mm diametric interference fit. The effect of the reduced pressure, at the contact area, significantly increased the width of the regime and the percentage of embedded particles.

(ii) *Effect on rotor wear features*

As with the stators, reducing the interference fit appeared to have an adverse effect on the wear rate of the rotors, by ‘spreading’ the abrasion over a larger area. The optical images in figure 6.19, compare the wear on two chromium oxide coated rotors, that had different interference fits. With the contrast in colour, between the coating and steel substrate, the way in which the contact load, and subsequent wear, was dissipated over the contact zone can easily be identified. It can be seen that reducing the interference fit, and therefore the contact pressure, increased the area of contact and consequently the localised wear to the leading side of the scroll.

Figure 6.18: SEM images of type ‘a’ wear regime, generated under standard wear test conditions, using a slurry of 45 micron silicon carbide and an interference fit of 0.2mm showing (a) increase in width compared to the 1mm interference fit (figure 6.10(c)) and (b) the high percentage of embedded particles

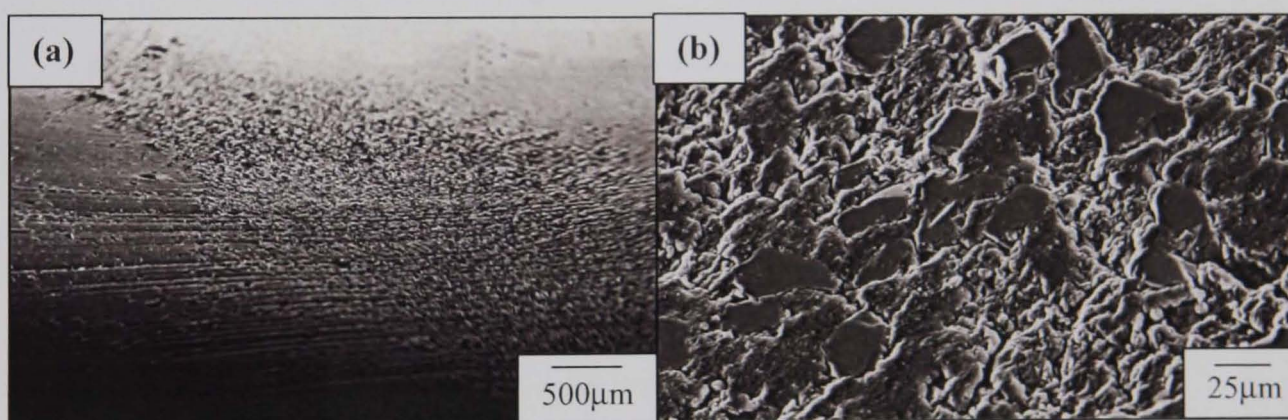
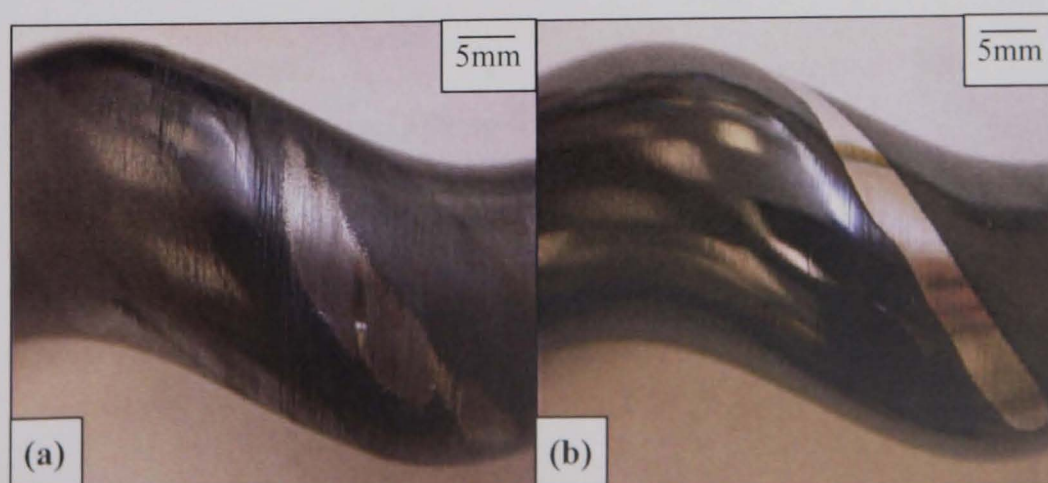


Figure 6.19 : Optical images of chromium oxide coated rotors, tested under standard conditions, with (a) 0.2mm and (b) 1.0mm diametric interference fit

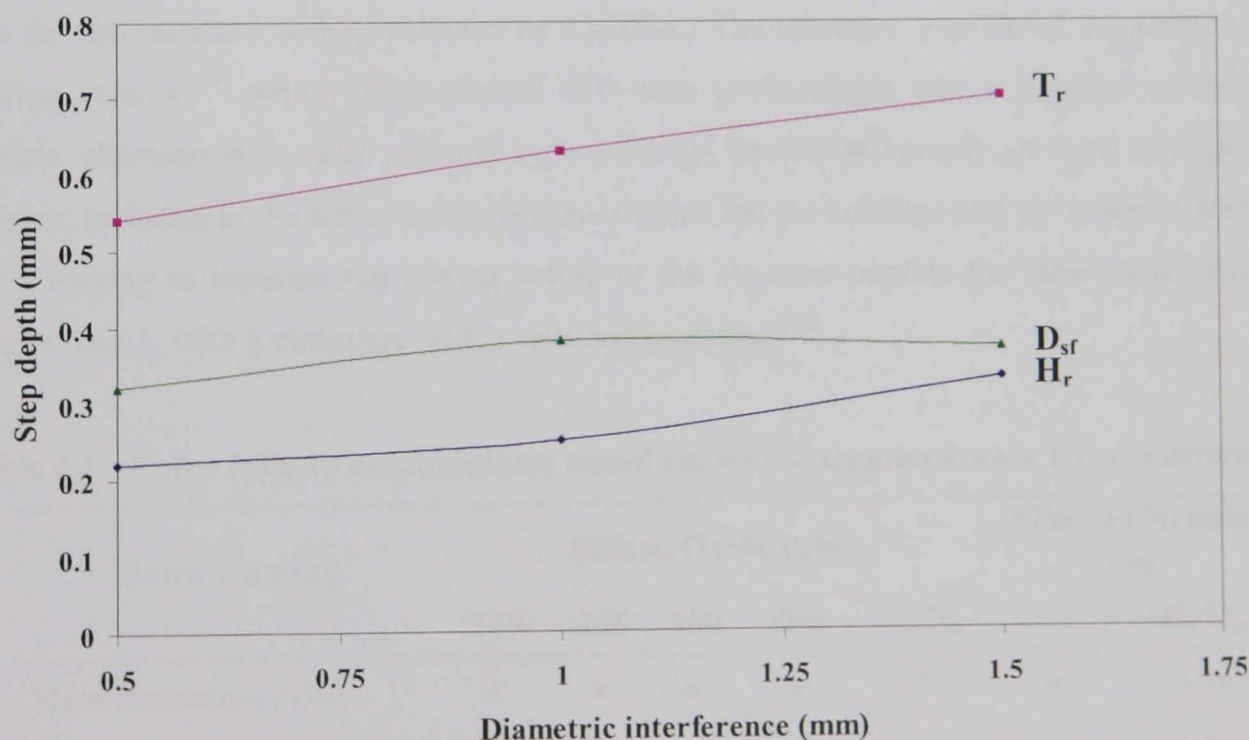


(iii) *Relationship between wear rate and the system variable of diametric minor interference*

The results from the laser profiling of the macro-grooves and the measurement of the worn steps are plotted against an increasing diametric interference, between the rotor and the stator, in graphs 6.7 and 6.8. A linear relationship was observed between the step depth and the interference fit, which increased with increasing interference. Thus, it can be concluded that of the three system variables of operating speed, discharge pressure and interference fit, only the latter demonstrated a significant detrimental effect to the wear rate of the rotor, which agrees with Wirth's studies [2]. The results from the profilometry approach were less conclusive. Increasing the interference fit appeared to have no effect on the size of the macro-grooves on the trailing sides, whilst on the leading sides, the results implied a reduction then an increase in wear. As discussed with the operating speed results, this approach was found to be unreliable for quantifying wear rates.

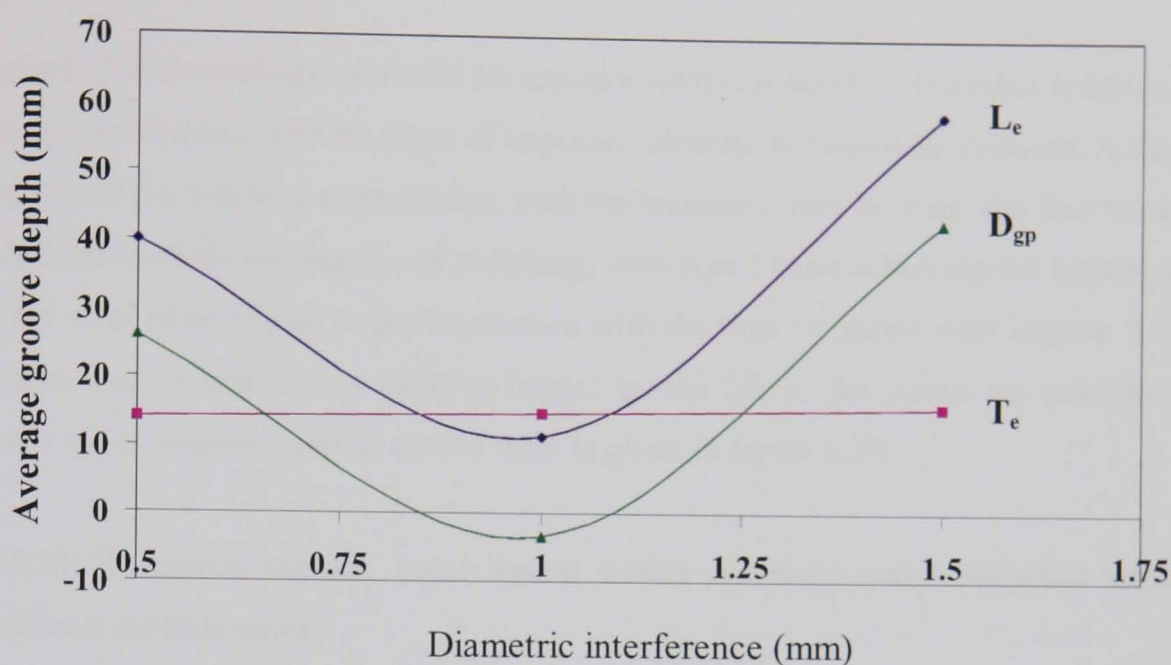
Graph 6.7 : Depth of the steps, at either end of the rotor scroll, generated under standard wear test conditions, with increasing interference fit; H_r = rotor head; T_r = rotor tail;

$$D_{sf} = H_r - T_r$$



Graph 6.8 : Average depth of rotor macro-grooves, generated under standard wear test conditions, at increasing interference fit; L_e = Leading edge; T_e = Trailing edge;

$$D_{gt} = L_e - T_e$$



6.3.5 Rotor surface properties

The rotor coating / slurry combinations tested are listed in table 6.2. The duration of the tests was for the standard sliding distance of 73,000m. The selection was based on previous rotor coating studies ^[15] which demonstrated that wear performance was a function of the slurry particle characteristics, and ceramic type coatings performed poorly in sand and grit type slurries. Included in the table are the hardness ratios for the coatings and the relevant abrasives. For a coating to resist the cutting action of the abrasive particle the ratio must be at least greater than 1, with a minimum of 1.2 commonly quoted ^[16].

Table 6.2 : Rotor / slurry combinations tested under the standard wear test conditions

Rotor Coating	Silicon Oxide (μm)					Silicon Carbide (μm)	
	120	225	450	900	H_s/H_a	45	H_s/H_a
Hard chromium plate	•	•	•	•	0.77	•	0.35
Tungsten carbide coating	•	•	•	•	1.14	•	0.51
Chromium oxide coating	•	x	x	x	1.18	•	0.53

Problems were encountered in quantifying the wear rate of the coatings. The high weight ratio of the rotor to the coatings, meant that the weight loss technique, employed on laboratory scale wear testing, was inadequate. In addition, the coatings did not wear evenly along the length of the scroll and once the substrate was exposed it wore at a greater rate than the coating, so any

weight loss measured could not be solely attributed to coating wear. Consequently the analysis of the wear tests was based on visual observations and the relative position of the wear features, with respect to their location of the rotor scroll and interaction with the type 'a' and 'b' stator wear regions.

The tungsten carbide coatings exhibited far superior wear resistance, to the other coatings, under all of the test conditions, with no signs of exposed substrate or two-body abrasion. A degree of polishing type wear had been experienced, with the boundary lines between the four wear bands clearly defined by different degrees of polishing, with type I band achieving the highest surface finish. This wear band relates to the interaction with the type 'a' stator wear regime. This type of polishing wear would have a positive impact on the life of the stator. An example of the surface of a worn tungsten carbide coated rotor is given in figure 6.20.

Figure 6.20: Tungsten carbide rotor tested under standard test conditions with a 45 micron silicon carbide slurry



With all of the silicon oxide slurries, the hard chromium plated exhibited good wear resistance. Regardless of particle size, light micro-scratching was observed on the plated rotors across the type I and II wear bands, replacing the macro grooves observed in the uncoated rotors. The overall appearance of the plate was more highly polished than the original surface finish. The micro scratching implied that the plate was not resistant to the cutting action of the embedded particles, and it is postulated that over a longer period of time, macro-grooving, and subsequent damage to the stator, would result. Changing the particle characteristics to hard and angular significantly reduced the wear resistance of the plate. A band of exposed substrate material was observed on the leading side of the scroll, as shown in figure 6.21, which transcribes to the interaction of the rotor with the type 'a' stator wear band. The edges of the plate were very well defined and micro-scratching was observed in the exposed steel, synonymous to the observations from the particle size analysis wear tests on the stainless steel rotors. On the trailing sides of the plated rotor, a band of macro grooves was observed, but no exposed

substrate. The reduction in wear resistance with particle hardness was reflected in the corresponding reduction in hardness ratio. However, it should be noted that using a slurry containing particles of silicon carbide effectively changed all three particle characteristics of size, hardness and shape. The particle shape would not only influence the way the particle interacts with the rubber, but the angular geometry of the silicon carbide would present more cutting edges to the rotor surface.

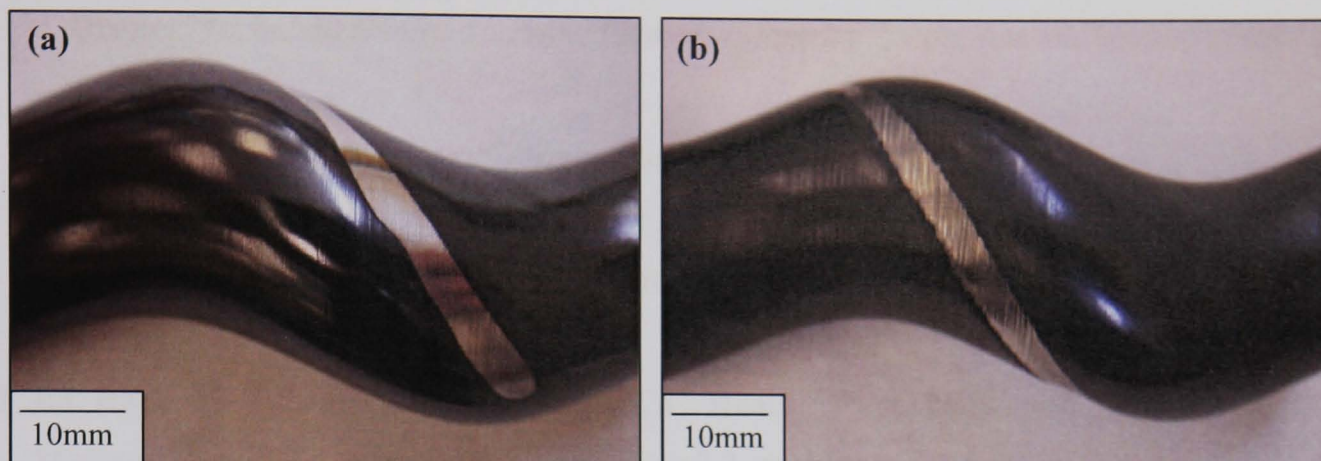
Figure 6.21 : Exposed substrate on the leading edge of a hard chromium plated rotor tested under standard test conditions with a 45 micron silicon carbide slurry



The chromium oxide coating was tested with the smallest silicon oxide particle and the largest silicon carbide particle. Both types of particles removed sufficient coating to expose a helical band of substrate material, although a significant difference was observed with the location of the bands.

The silicon carbide slurry produced the same type of wear as that observed on the hard chromium plated rotor, with a band of exposed substrate signifying high wear on the leading edge of the rotor scroll, as shown in figure 6.22 (a). However, changing the particles to silicon oxide, moved the area of high material removal to the trailing sides, as shown in figure 6.22 (b). Macro grooves were observed in the soft substrate, which ran into the chromium oxide coating at the edges of the band, producing a rough, feathered effect. This correlates well with the wear observed on the stainless steel rotors, where visually, the grooved type II wear band, on the trailing side appeared more severe than that on the leading side. The remainder of the coating, with both slurries, had gained a more highly polished finish than its original surface.

Figure 6.22: Exposed substrate on a chromium oxide rotor tested under standard test conditions with a (a) 45 micron silicon carbide slurry and (b) 120 micron silicon oxide slurry



Comparison of the relevant hardness ratios with the coatings wear performances clearly demonstrated that hardness, alone, could not be used to predict the wear resistance of a surface, particularly when dealing with coatings. Although the chromium oxide coating had similar hardness ratios as the tungsten carbide coating, their wear capabilities were very different, reflecting the nature of the coatings. Chromium oxide is a ceramic coating and consequently hard but brittle in nature. Although the tungsten carbide coating achieves it comparable hardness from hard ceramic particles, these are embedded in a ductile metallic matrix, which provides toughness to the coating. It is unclear, from this wear evaluation, the reasons why hard chromium plate performed better against the silicon oxide, than the chromium oxide coatings, but exhibited similar performance with the harder, angular silicon carbide.

6.4 REFERENCES

1. **D. Appleby**, 1994, "*Experimental and theoretical study of a progressive cavity pump*", Ph.D.diss., Cranfield Institute of Technology.
2. **W. Wirth**, 1993, "*The hydraulic and tribological modelling of a progressive cavity pump*", Ph.D.diss., University of Erlangen, Germany
3. **J. A. Williams & A. M. Hyncica**, "Abrasive wear in lubricated contacts", J. Phys. D: Appl.Phys. 25, 1992, pp A81 – A90
4. **G.H. May**, "*Least whole life cost : Section 2 : Design of progressive cavity pumps related to wear rates*", Mono Pumps Ltd. technical literature : LWLC/MKTG, Issue 1, November 1995, pp1 – 6.
5. **J.D. Bourke**, "*Pumping abrasive products with progressive cavity pumps*", Online available : <http://www.moyno.com/moyno/main.html> [accessed 18/07/01], n.d.

6. **N. Axen, S. Jacobson & S. Hogmark**, "Influence of hardness of the counterbody in three-body abrasive wear – an overlooked hardness effect", *Tribology International*, Vol. 27, No.4, 1994, pp 233 – 241
7. **J. Drane**, "*Technical Notes 16 : Pump Element Geometry*", Confidential, Mono Pumps Ltd., 1999.
8. **S. Akincioglu**, "*Abrasive wear*", Mono Pumps internal memo, 16 04'82
9. **G.H. May**, "*Least whole life cost : Section 2 : Design of progressive cavity pumps related to wear rates*", Mono Pumps Ltd. technical literature : LWLC/MKTG, Issue 1, November 1995, pp 1 - 6.
10. **I.J. Karassik, J.P. Messina, P. Cooper, C.C. Heald**, "*Pump Handbook*", 3RD Ed., McGraw-Hill, 2001, ISBN 0-07-034032-3. pp3.3, pp 3.99 – 3.121.
11. **J. Drane**, Mono internal e-mail dated 08/12/99 to R.Garlick.
12. **BS EN ISO 14847:1999**, "*Rotary positive displacement pumps – technical requirements*".
13. **M. A. Moore & P. A. Swanson**, "*The effect of particle shape on abrasive wear: A comparison of theory & experimental*", *Wear of Materials*, 1983.
14. **R. Belcher**, 1991, "*An investigation into the operating characteristics of the progressing cavity pump*", Ph.D.diss., Cranfield Institute of Technology.
15. Private communication with Mono Pumps Ltd.
16. **I. M. Hutchings**, "*Wear by hard particles*", Chapter 6, *Tribology : Friction & wear of engineering materials*, Edward Arnold, 1992, pp 136

Comparison of standard hard particle laboratory wear tests with the wear behaviour in a progressive cavity pump

7.1 INTRODUCTION

The impetus behind the wear study was to significantly reduce the assessment time of development rotor coatings and stator materials by designing a laboratory scale wear test that could simulate the contact conditions in the pumping element, of a progressive cavity pump. The requirements of the test were to:

- (i) duplicate the wear mechanisms generated in the pumping element
- (ii) demonstrate a reliable ability to rank rotor and stator materials relative to the results from the simulated in-service test rig
- (iii) produce test data that could be easily and accurately analysed
- (iv) accelerate the wear analysis duration of wear resistant coatings
- (v) assess the abrasivity of 'real' slurries

The wear study of the pumping element, discussed in Chapter 6, concluded that it was a two-stage process initiated by particles embedding into the stator walls, which subsequently caused grooving wear to the rotor. The severity of the wear was dependent primarily on the size of the abradant. Rolling wear was observed when the particle size was smaller than the thickness of the lubricating film. When a discharge pressure was applied, both the rotor and stator were also subjected to glancing angle solid particle erosion.

Rather than design a completely new test it was decided that it would prudent to evaluate existing laboratory wear tests. The justification was that a suitable test may already exist and using test data from a standardised procedure would be more readily acceptable and understood in the commercial market. Of the laboratory tests reviewed in Chapter 4 it was decided that the wet rubber wheel abrasion test and the micro-scale abrasion test were most likely to simulate the desired wear mechanisms as their contact conditions were similar to those in the pumping element. To assess a stator materials resistance to particle embedding, a slurry jet erosion test was included in the study. The ROS tribometer and the Miller abrasion test, described in section 4.2.3 and 4.2.5, respectively, were used by Wirth, in his studies of the wear in progressive cavity pump. Unfortunately neither apparatus were available for this study.

As with the rotor wear assessment, AISI 316L stainless steel was used as the test sample material to assess the wear mechanisms generated by the laboratory tests. As the purpose of the test would be to evaluate the wear resistance of rotor and stator materials, three rotor coatings plus nitrile rubber, were selected, based on their commercial use. The rotor coatings were:

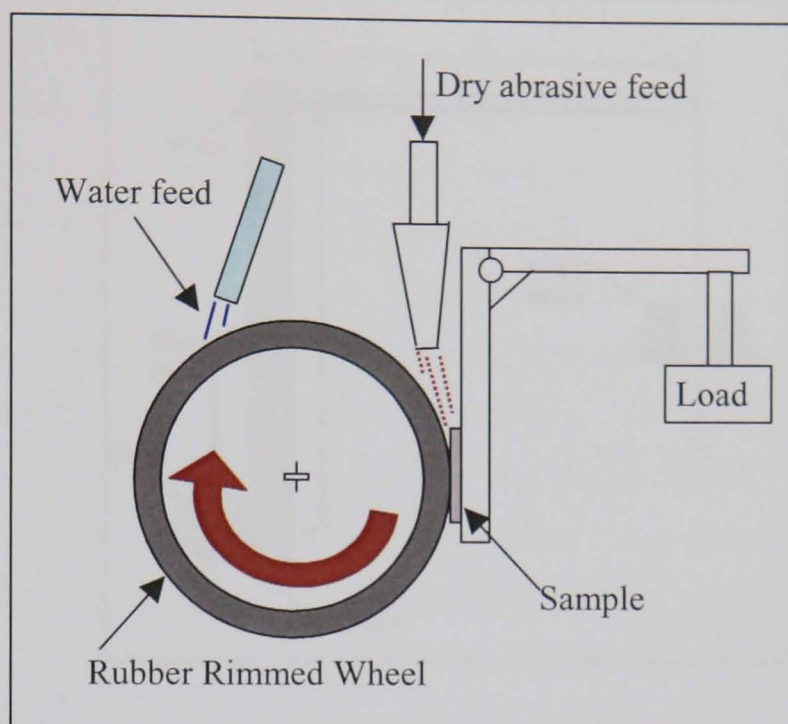
- (i) electro-deposited hard chromium plate
- (ii) HVOF tungsten carbide cobalt chrome
- (iii) plasma sprayed chromium oxide

Samples, 50mm x 25mm x 5mm in size, were coated to a thickness of 250 μ m on both sides, to allow sufficient coating thickness for both faces to be ground flat and polished or lapped to a surface finish equivalent to that applied to a coated rotor. Weight loss measurements were used for the wet rubber wheel abrasion test and the slurry jet erosion test to rank the performance of the coatings, whilst derivation of the dimensional wear coefficient was used for the micro-scale abrasion test. Justification for the selection of each test procedure and the details of the apparatus are discussed below.

7.1.1 Wet rubber wheel abrasion test

A wet slurry version of the standard rubber wheel abrasion test was selected as its tribological system consisted of the same four key elements as the pumping element. The body or rotor surface is represented by a flat test sample, 50mm x 25mm x 5mm in dimension. The counterbody is rubber with a curved geometry to replicate the conforming contact of the stator with the rotor. As with the pumping element both the interfacial and surrounding media was an abrasive slurry. The rubber wheel abrasion apparatus was a modified version of the standard ASTM G65 to incorporate a water feed for the slurry, the arrangement of which is shown in figure 7.1. A water feed pipe wets the wheel prior to the introduction of the dry abrasive and the rotational movement of the wheel draws the wet slurry through the contact zone. The flat test sample is mounted vertically and a dead load applied, via a counter lever, to press the surface against the wheel. The steel wheel, which has a chlorobutyl rubber rim, 0.025m wide and 0.228m in diameter, rotates at a velocity of 2.39ms⁻¹. The surface of the test samples were ground flat to a 17Ra finish. The stainless steel and chromium oxide coated test samples were weighed every 200 revolutions, up to a total of 1000 revolutions, giving a total sliding distance of 718m. Whereas the hard chromium plate and the tungsten carbide coated samples were weighed every 1000 revolutions, for a total of 10,000 revolutions, equating to a total sliding distance of 7,183m.

Figure 7.1 : Configuration of the wet rubber wheel abrasion apparatus



7.1.2 Micro-scale abrasion test using a hardened steel ball and a resilient rubber ball

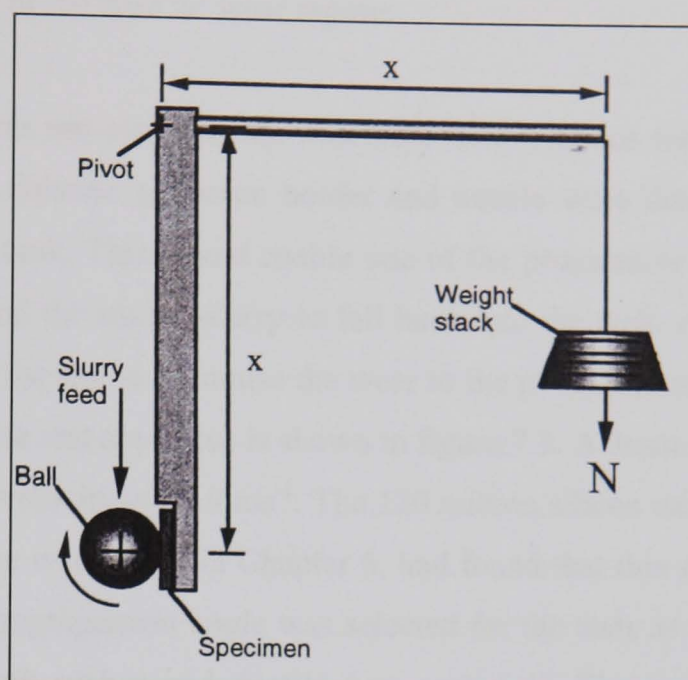
In the micro-scale abrasion test, a ball of a radius, R , equal to 12.7mm, rotated, at a sliding velocity of 0.08ms^{-1} , against a loaded flat specimen, and an aqueous slurry was drip fed into the top of the contact zone. A schematic of the apparatus is given in figure 7.2. The diameter, b , of the generated spherical wear scar was measured with a calibrated optical microscope and the volume of material removed, V , calculated using equation 7.1:

$$V = \pi b^4 / 64 R \quad (7.1) \quad [1]$$

The stainless steel wear craters were measured after 200 revolutions, and the coated samples were measured in stages at 300, 600 and 1000 revolutions. These equate to sliding distances of 24, 48 and 80 m.

Two concentrations of slurries were used, according to the procedure outlined by National Physical Laboratory, UK [1]. These are given as a 2% vol. concentration to produce 'two-body' abrasion and a 20% vol. concentration for 'three-body' abrasion. Distilled water was used as the abrasive carrier. Due to the fineness of the wear craters it was necessary to polish the test samples to a 9 micron finish.

Figure 7.2 : Configuration of the micro-scale abrasion apparatus



Three different material combinations for the ball and the flat specimen were used during the evaluation of the test to determine whether any replicated the tribological conditions of the pumping elements. These variations are given in table 7.1.

Table 7.1 : Ball / flat specimen material combinations for micro-scale abrasion test

Variation	Ball	Flat specimen
1	Highly polished hardened steel	316L grade stainless steel & coated samples
2	Buna N rubber, 70 IRHD	316L grade stainless steel
3	Highly polished hardened steel	Nitrile rubber, 68 IRHD

7.1.3 Slurry jet erosion test

A slurry jet erosion test was selected to try to simulate the type 'a' and 'b' stator wear regimes. In addition glancing angle erosion tests were conducted on stainless steel and coated samples, to assess the theory proposed by Schmid et al. ^[2], that if the predominant material removal mechanism of a ductile surface was cutting, regardless as to whether the wear mode was abrasion or erosion, an erosive type test could be used to evaluate the wear resistance of that surface. The potential versatility of this type of test would enable the assessment of the:

- (i) rotor surface/coating to resist cutting type wear
- (ii) toughness of rotor coatings as the applied test load is a direct result of particle impact, as opposed to an external force as with abrasion

**Comparison of standard hard particle laboratory wear tests
with the wear behaviour in a progressive cavity pump**

- (iii) resistance of stator material to low angle solid particle erosion, postulated as the cause of the type 'a' wear regime.

Suitable apparatus were not available and therefore modifications were made to the simulated in-service test rig. A suitable specimen holder and nozzle were designed to fix to the cross member of the slurry tank. This would enable one of the progressive cavity pumps to feed the slurry to the nozzle and the excess slurry to fall back into the tank. A tungsten carbide coated rotor was selected for the test to minimise the wear to the pump and maintain a consistent flow. The configuration of the test apparatus is shown in figure 7.3. A 3mm diameter nozzle was used to generate an impact velocity of 11.9 ms^{-1} . The 120 micron silicon oxide was selected for all of the erosion tests, as the wear study in Chapter 6, had found that this size of particle caused the severest wear. A 30° impingement angle was selected for the tests as this is known to generate high wear rates in both rubber and ductile type materials. The test samples were mounted 150mm from the nozzle, in a pivoted jig, to enable slurry impingement angles of 0° to 90° . The test samples were weighed at 2 minute intervals for a total duration of 20 minutes. The morphology of the wear scars were examined under a scanning electron microscope.

Figure 7.3a : Modification to the cross member of the simulated in-service test rig to accommodate a slurry jet erosion apparatus

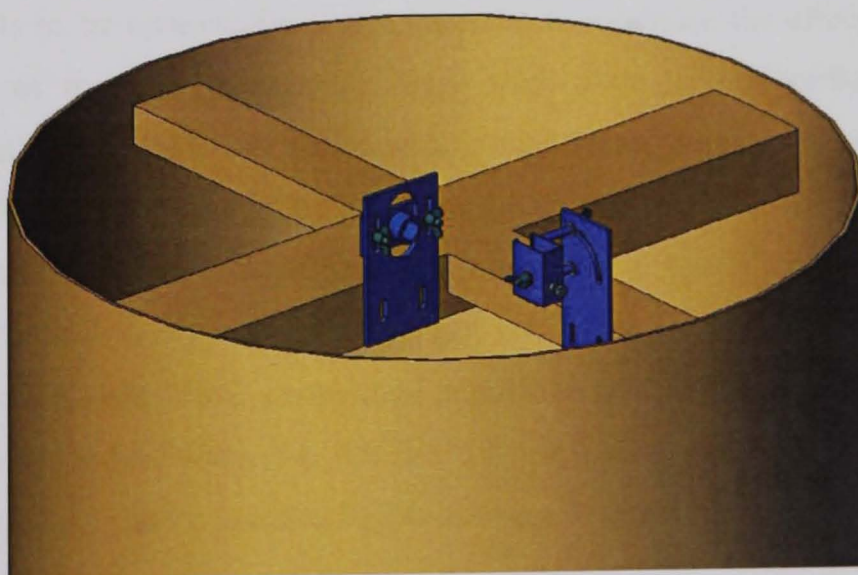
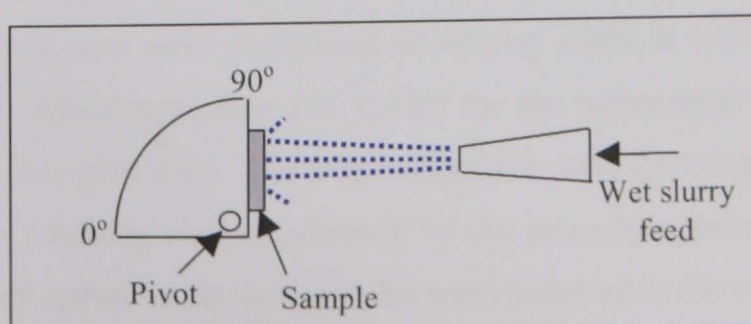


Figure 7.3b : Details of the configuration of the nozzle and specimen holder



7.2 EVALUATION OF LUBRICATION CONDITIONS OF THE ABRASION TESTS

As discussed in section 3.4, the relationship between the type and thickness of the lubrication film with the abrasive particle size, in any tribosystem, directly effects the material removal rates and mechanisms. Therefore suggesting that the lubrication conditions of the laboratory test should be comparable with those of the industrial tribological system. William and Hyncica's model of abrasivity activity was used in section 5.6 to estimate the lubrication film thickness of the pumping element although the results were inconclusive. This evaluation was repeated with the wet rubber wheel abrasion test and the micro-scale abrasion tests to assess their lubrication conditions and estimate the thickness of the lubrication film.

The methodology of the evaluation examined the wear morphology generated by slurries containing different sized particles, to identify the critical d/h ratio where the particle behaviour changed from grooving to rolling wear. At this value the thickness of the film will approximately be equal to the major diameter of the particle. To support this evidence the dimensional wear coefficient for each test was determined as a change in wear behaviour from two-body to three-body abrasion is known to produce a significant reduction in the material removal efficiency ^[3].

For the test results to be comparable it was essential to minimise the effects of the system's variants in each of the test procedures. These were principally identified as the particle characteristics, the applied loads and the material properties of the wearing surface. Section 3.2 and 3.4 discussed the influence of particle characteristics on wear mechanisms and rates in a tribosystem. To minimise the effects of particle hardness and shape, silicon carbide was selected for the abradant for both test procedures. The grit grade was C6, purchased from Washington Mills, Manchester, UK, which had a consistent angular shape. Six different grit sizes were used which had nominal particle sizes 80, 45, 30, 16, 10 and 4 microns. SEM images of the morphology of each size can be found in figure 5.2, section 5.3.4.

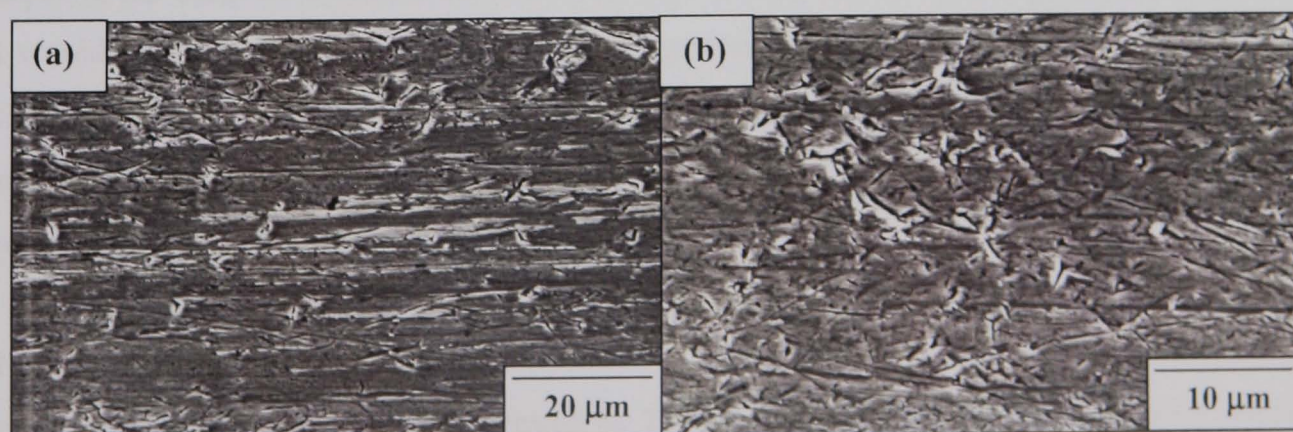
To determine the load required for comparable contact pressures in the contact zone initial wear tests on 316L stainless steel were performed, at varying loads. It was found that for a load of 130N on the rubber wheel apparatus and 0.35N for the micro-scale abrasion test, a contact pressure of 415kPa was generated. This was comparable with the estimated contact pressure at the seal lines in the pumping element, derived by the procedure described in section 5.5. For both of the laboratory apparatus the test samples were mounted in the vertical plane and pressed

against a rotating counterface under a dead load. This was thought to fairly represent the loading conditions within the pumping element where the interference fit between the rotor and stator was identified as the primary source of the applied load on the particles. Finally austenitic stainless steel, AISI grade 316L, was used as the wearing surface to minimise the test duration and enable the material removal rates to be derived using classic ductile abrasion models.

7.2.1 *Wet rubber wheel abrasion test*

The morphology of the wear scars, from the slurries containing the large particle sizes of 80 and 45 microns, were long, continual grooves which lay parallel to the direction of the flow. Reducing the particle size down to 24 microns produced both continual and intermittent grooves through out the length of the wear scar. The intermittent grooves were observed to finish in sharp points and, within these grooves, a high degree of sharp indentations were identified. In the entry region of the contact zone, the particles appeared to first become embed in the soft counterbody and generate grooving wear. Then subsequently rotate to an angle where they loose contact with the solid surface and roll through the contact zone. The wear morphology of the wear scars generated by slurries containing 45 and 24 micron particles are shown in figure 7.4. These observations suggest a change in particle behaviour due to the reduction in their size. Reducing the particle size further to 16 microns encountered practical problems with the apparatus due to poor flow characteristics and consequently reliable test data could not be produced.

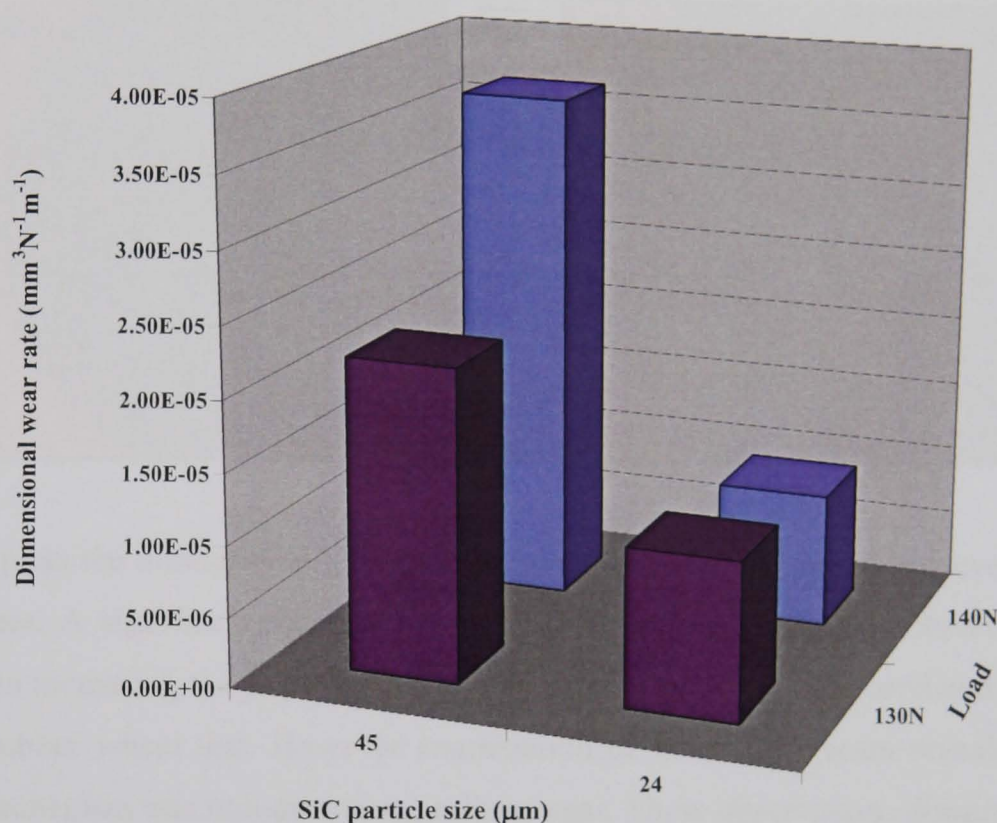
Figure 7.4 : SEM images of the wear scars of 316L stainless steel generated by the wet rubber wheel abrasion test with slurries containing silicon carbide of particle size of (a) 45 and (b) 24 microns under a load of 130N



Comparison of standard hard particle laboratory wear tests with the wear behaviour in a progressive cavity pump

Graph 7.1 shows the change in the dimensional wear rates determined for two slurries containing 45 and 25 micron particles, under two different loads. Comparison of these wear rates provides further evidence of a change in particle behaviour with size. The wear rates were observed to be dependent on load for the larger size particles, but independent for the smaller sizes.

Graph 7.1 : Comparison of 316L stainless steel dimensional wear rates against silicon carbide particle sizes for two different loads on the wet rubber wheel abrasion test



Applying Williams and Hyncica's model of abrasive activity would suggest a film lubrication thickness in the order of 20microns. However, this value is an order of magnitude greater than what would be expected for a hydrodynamically generated film. It is therefore postulated that the change in particle motion was more likely related to a change in the load distribution in the contact zone, with the load per particle being less for the smaller particles enabling them to generate a rolling action.

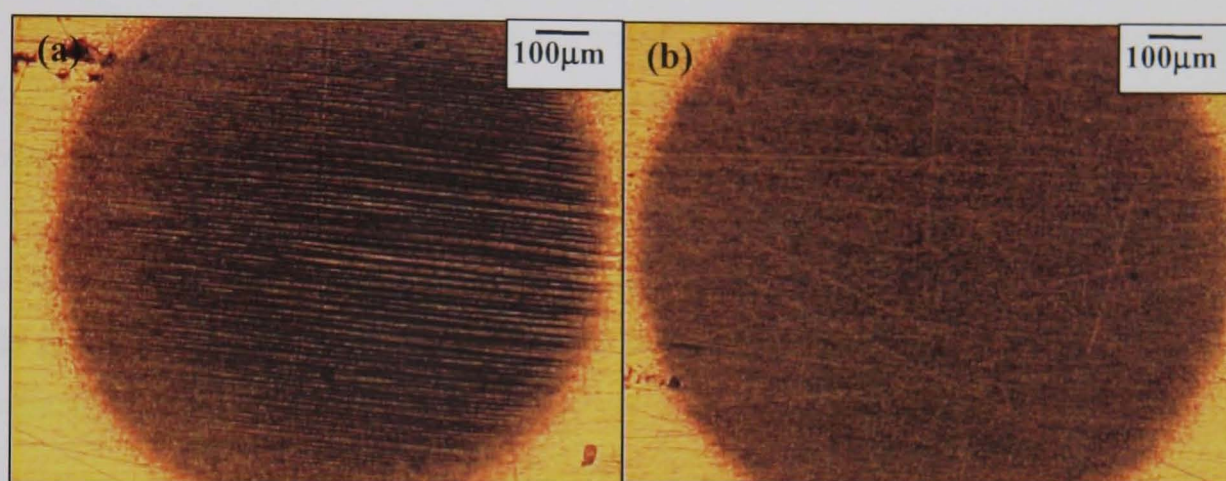
7.2.2 Micro-scale abrasion test

Optical images of the wear craters generated by 2 wt.% and 20 wt.% concentration of 4 micron silicon carbide slurries, with a hardened steel ball, are shown in figure 7.5. The expected wears modes of grooving wear from the 2% vol. concentration and rolling wear from the 20% vol.

**Comparison of standard hard particle laboratory wear tests
with the wear behaviour in a progressive cavity pump**

concentration demonstrated that particle behaviour was predominantly dependent on particle concentration and not particle size. This behaviour was observed for slurries containing particles up to a size of 30 microns. Beyond this particle size the wear craters exhibited a heavily pitted, non-directional rolling type wear, regardless of the particle concentration level.

Figure 7.5 : Optical images of the wear craters generated in 316L stainless steel by the micro-scale abrasion test using a hardened steel ball with slurries containing 4 micron silicon carbide of concentrations of (a) 2% and (b) 20%, under a load of 0.35N



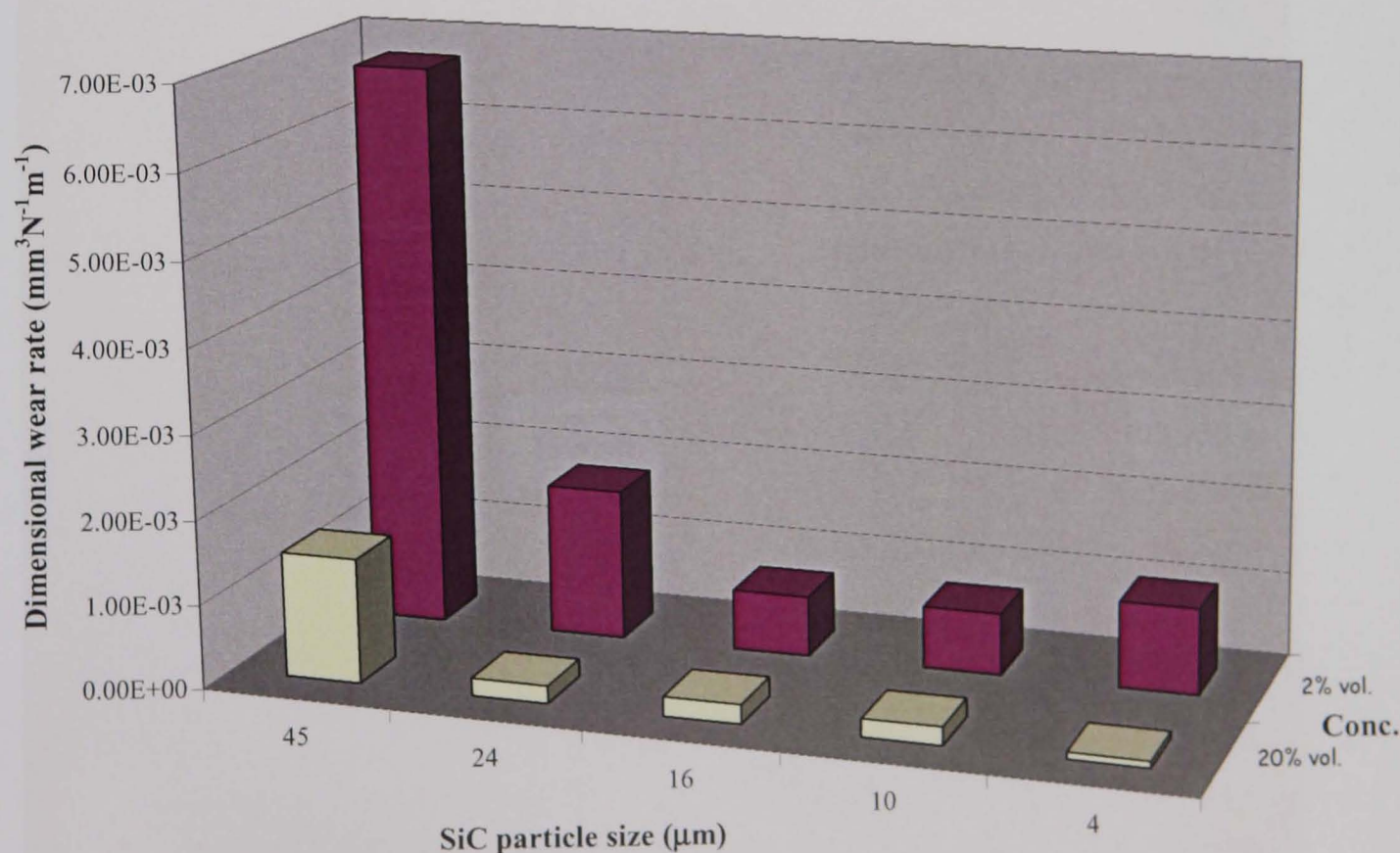
Graph 7.2 plots the dimensional wear rates for the two slurry concentration levels for all of the particle sizes. A significant increase in the dimensional wear rate was observed, for the 2% slurry, when increasing the particle size from 30 to 45 microns, which correlated with the results from the rubber wheel test. However examination of these wear scars revealed the material removal mechanism was non-directional rolling wear. These observations disagree with those of previous studies ^[3] which have demonstrated that rolling wear was a far less efficient material removal mechanism than grooving wear. Profiling all of the wear craters revealed that only the craters generated by slurries containing particles of 16 microns, or less, were of the necessary spherical geometry to comply with equation 7.1, to derive the volume of removed material. This would provide an explanation for the unusually high wear rates from the large particles sizes. All this evidence suggests that this tribosystem is not hydrodynamically lubricated and the load at the contact zone is supported by the particles regardless of their size.

In an attempt to change the lubrication conditions of the micro-scale abrasion test the hardened steel ball was replaced a 25.4mm diameter Buna N rubber ball, of 68-72 IRHD. Wear tests were completed for the same range of particle sizes, at concentrations of 20% and an applied load of 0.35N. After 200 revolutions optical examination of the wear craters revealed a relationship

**Comparison of standard hard particle laboratory wear tests
with the wear behaviour in a progressive cavity pump**

between wear morphology and particle size, as shown in figure 7.6(a) to (c). From the slurry containing the 45 micron particles the wear was predominantly superficial scratches, lying parallel to the direction of rotation of the ball, with rolling wear around the peripheral of the crater. Reducing the particle size to 24 microns reduced the amount of peripheral rolling wear giving the impression of a reduced contact area. But comparison of the diameters of just the scratched area of the craters revealed the contact area to be the similar. The scratches from the 24 micron slurry were less pronounced than those from the 45 micron slurry and were only evident in the second half of the crater. Some intermittent scratches were observed indicating a change in the motion of the particles. Similar observations were made for the wear crater from the 16 micron slurry. No visual wear features could be recorded from the wear craters created by slurries containing particles of 10 and 4 microns, as these produced only a circular area of superficial polishing wear.

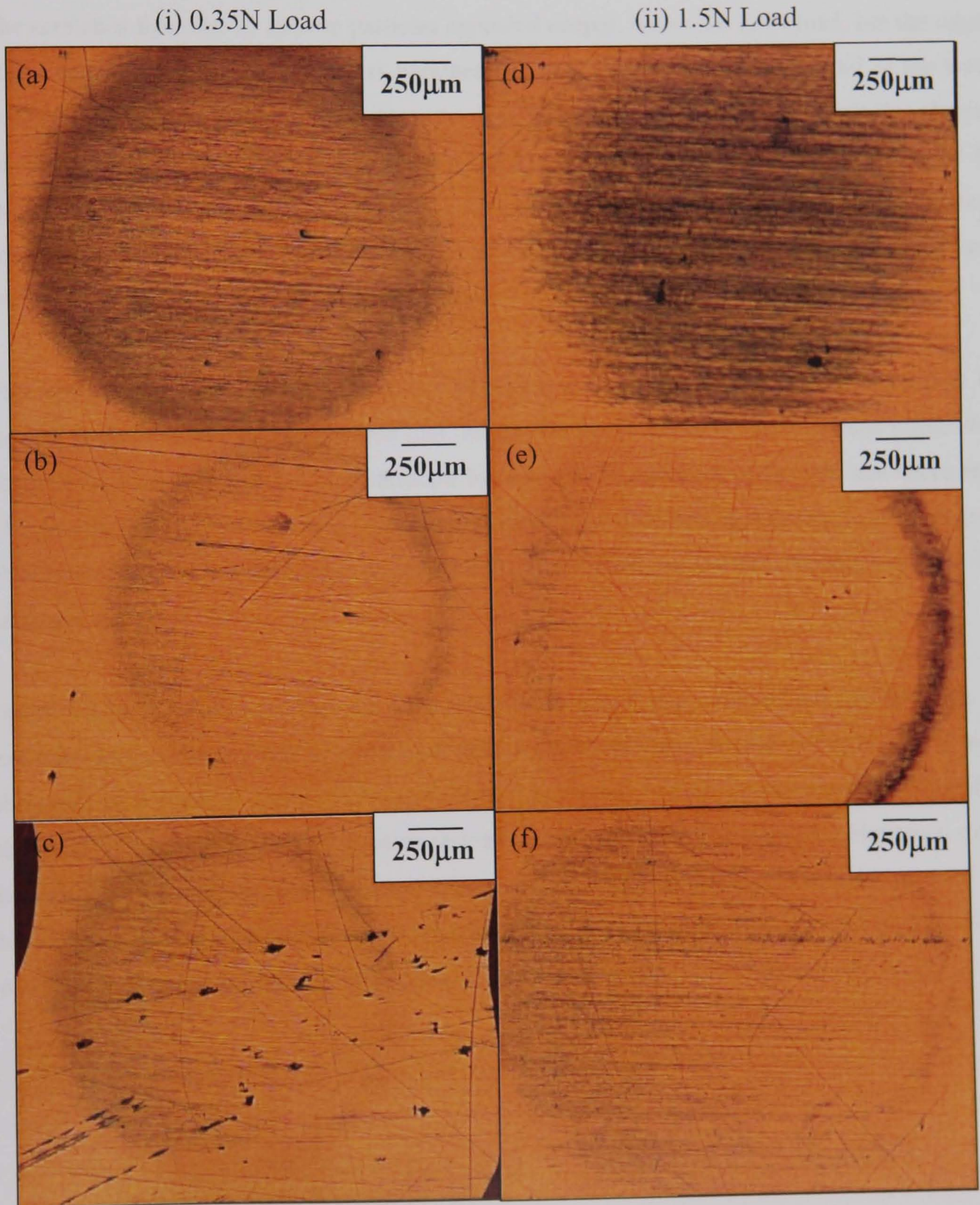
Graph 7.2 : Comparison of 316L stainless steel dimensional wear rates against silicon carbide particle sizes for two different slurry concentrations on the micro-scale abrasion test using a hardened steel ball



Comparison of standard hard particle laboratory wear tests
with the wear behaviour in a progressive cavity pump

Figure 7.6 : Optical & SEM images of the wear craters on 316L stainless steel generated by the micro-scale abrasion test using the rubber ball with slurries containing 20% silicon carbide of nominal particle sizes of

- (i) (a) 45; (b) 24 and (c) 16 microns under a load of 0.35N
(ii) (d) 45; (e) 24 and (f) 16 microns under a load of 1.5N



Comparison of standard hard particle laboratory wear tests with the wear behaviour in a progressive cavity pump

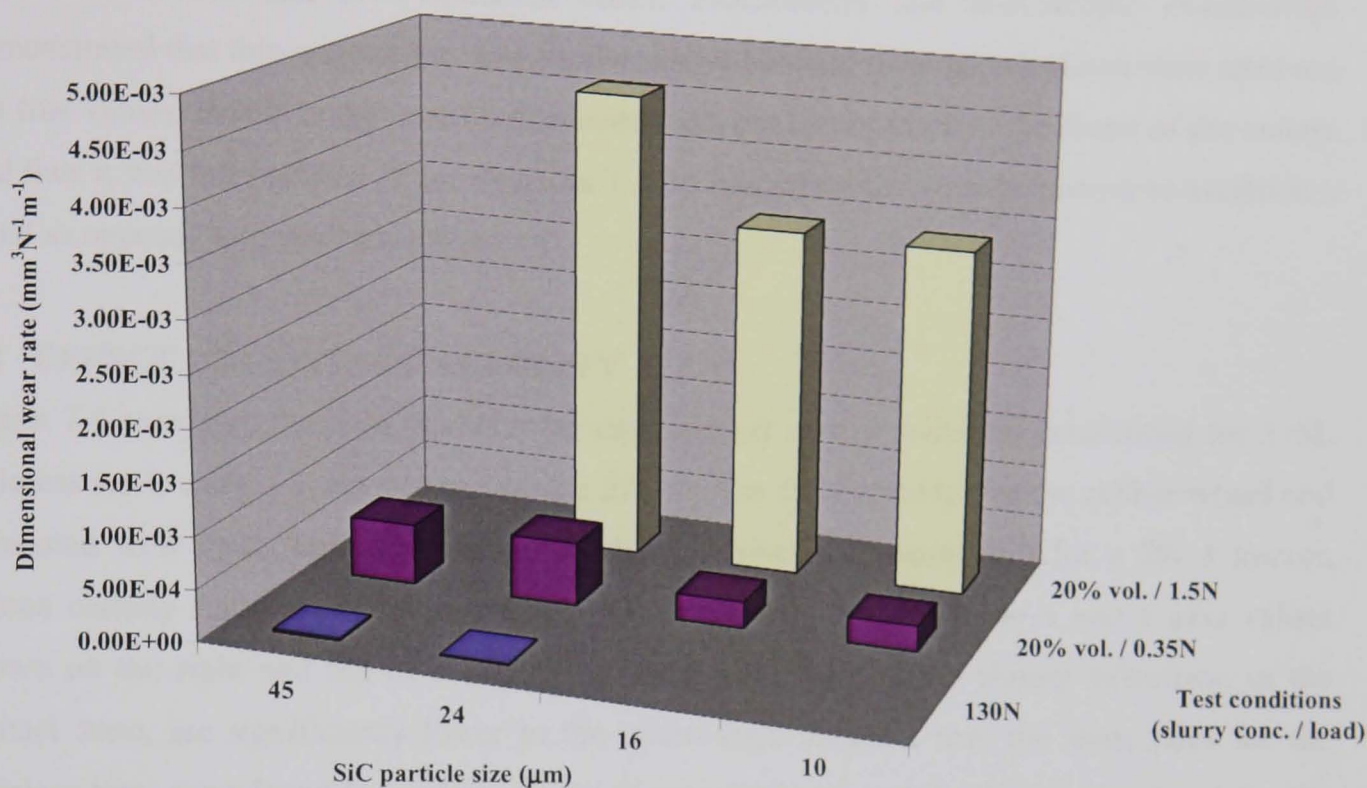
Examination of the wear craters in the SEM revealed that, although under an optical microscope different wear modes could be identified, these were actually superficial and there was no depth to the wear features. Therefore the tests were repeated under a load of 1.5N to determine whether spherical wear craters could be produced. Under the higher load very similar wear features were observed, as shown in figure 7.6 (d) to (f).

The scratches from the 45 micron particles appeared deeper, under the 1.5N load, but the edges of the sphere were less defined. Less peripheral rolling wear was observed on all of the wear craters. It was observed that increasing the load increased the contact area for the slurries containing particles of less than 30 microns, but had no effect on the larger particle size of 45 microns. For both loads a characteristic 'blue/brown' crest was observed at the exit of the wear craters, generated by particles of less than 24 microns, indicating the presence of frictional heat which would imply a break down in lubrication.

This apparent lack of change in particle behaviour with load disagrees with the findings of Adachi et al. ^[4] whose results showed that the motion of the abrasive particles was influenced not only by load and abrasive concentration but also by the materials of the ball and specimen. The results from the rubber ball tests support their latter findings as two-body abrasion was observed with a 20% slurry using a rubber ball, whilst three-body wear mechanisms with the hardened steel ball.

Graph 7.3 compares the dimensional wear rates for the two rubber counterbody test methods. A reduction in the dimensional wear rates under both load conditions, for the rubber ball tests, was observed for a particle size reduction of 24 to 15 microns, which was a similar relationship observed with the rubber wheel abrasion test, although at a smaller particle size. However, even though the wear rates suggest a change in particle behaviour with size, it was not supported by the morphology examination of the wear craters, where no transition in particle motion from two-body to three-body abrasion with particle size was observed.

Graph 7.3 : Comparison of 316L stainless steel dimensional wear rates against silicon carbide particle sizes for the two rubber counterface test methods



A further attempt was made to generate hydrodynamic lubrication conditions on the micro-scale abrasion tester wear tests by increasing the sliding velocity. A 2% 4 micron silicon carbide slurry was used, since it had already been demonstrated that this concentration and size produced two-body abrasion at 0.08 ms^{-1} . Using 316L stainless steel as the wearing surface and loads of 0.35N and 1.5 N with the hardened steel and rubber balls, respectively, and a sliding distance of 16m, wear craters were generated using relative sliding velocities from 0.11 to 0.21 ms^{-1} . Optical examination of the wear scars revealed no change in the particle motion for any of the test conditions and the morphology of the wear craters remained two-body, directional abrasion. However, a change in the appearance of the steel ball was apparent. Rather than the thin continual wear track, as previously seen, the ball's surface topography showed clear signs of three-body abrasion from rolling, non-directional particle motion.

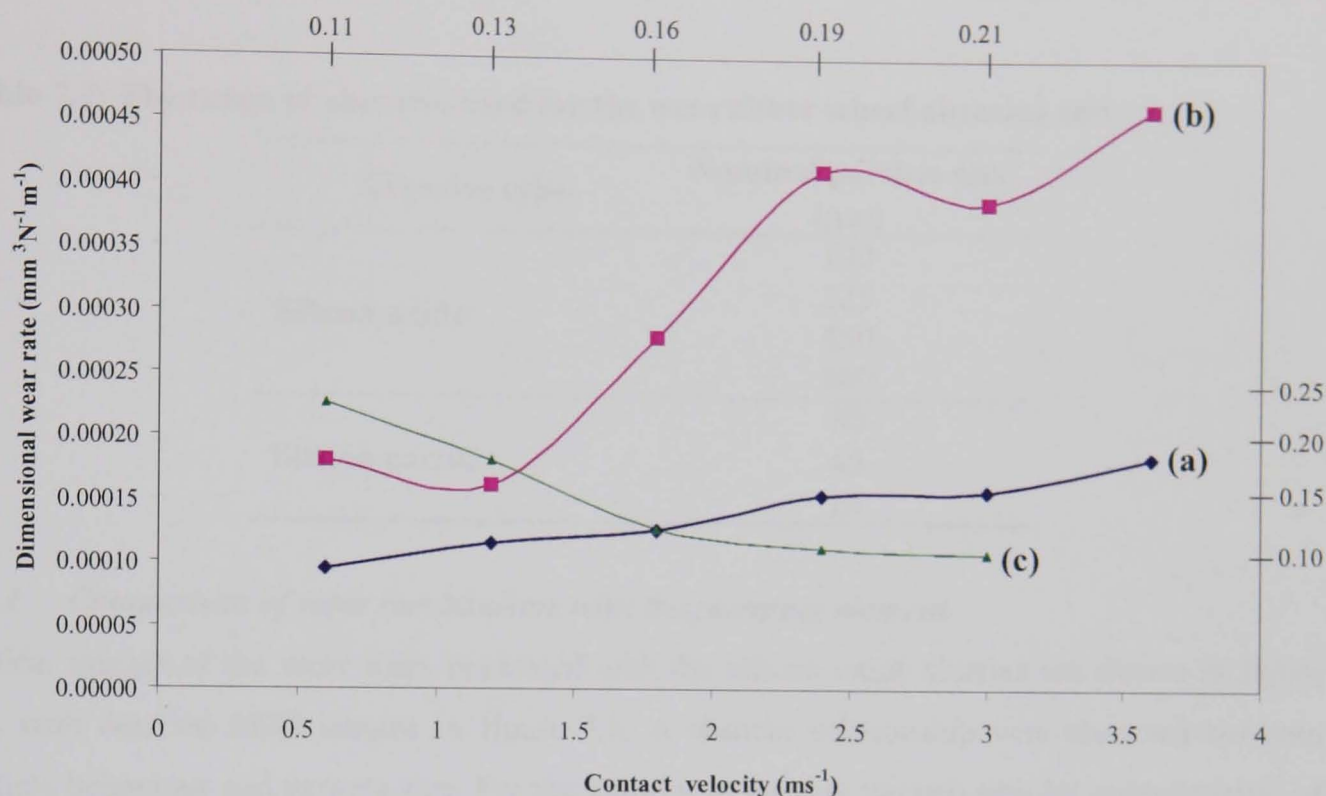
Two final wear tests, at different loads, were performed with the rubber ball counterface, to clarify whether the applied load was effecting the particle motion at the highest sliding velocity. Repeating the tests, under the reduced loads of 1.0N and 0.5N demonstrated that the particle motion still remained that of two-body abrasion, and hydrodynamic lubrication conditions could not be generated.

It should be noted that the derivation of the dimensional wear rates for the micro-scale abrasion test, for the rubber ball counterface, was on the assumption that the geometry of volumetric material loss was that of a spherical crater. Profilometry and microscopic examination demonstrated that this was not the case for the rubber ball and thus the calculated wear rates are not true values. However the profiles demonstrated a consistent trend in the shape of the craters and thus it was felt justified to use equation 7.1 for modelling the wear behaviour to establish a trend as opposed to quantitative data.

7.3 EFFECT OF CONTACT VELOCITY

Graph 7.4 compares the dimensional wear rates against contact velocity, determined for 316L stainless steel, using a slurry containing the 225 micron silicon oxide, for the rubber wheel and simulated wear tests. The same data from the micro-scale abrasion test, for a 2% 4 micron silicon carbide slurry, has been super imposed onto the graph, with the x and y axis values shown on the right and top of the graph. Even though the relative sliding velocities, in the contact zone, are significantly lower in the micro-scale abrasion test, the wear rates for the stainless steel were found to be three orders of magnitude greater than those calculated for the other two tests. Both the rubber wheel and the simulated wear tests demonstrated an increase in material removal rate with contact velocity, with the laboratory test showing a stronger dependency, whilst the wear rates measured on the micro-scale abrasion test decreased. It was observed with the shape of the wear crater generated on the micro-scale abrasion test changed with increasing sliding velocity, losing its roundness to become more oval. This would have introduced an error into the actual calculated values. Since k is as a function of the changing variables within a tribosystem, the results demonstrate that the contact conditions, in each test system, are dependent on the contact velocity. For the simulated test, it is possible that the load conditions change with operational speed, due to the contribution of centrifugal forces from the Flexishaft, although this would be difficult to quantify. However for the two laboratory tests the physically applied dead load remained constant, so the changes in k may indicate the occurrence of dynamic loading in the contact regime. Another contributing factor may be changes in the contact zone, as an increase rotational speed would effect the amount of particles fed into, and the time spent in, the contact zone.

Graph 7.4 : Effect of contact velocity on the dimensional wear rate for (a) Simulated wear test; (b) Rubber wheel abrasion test and (c) Micro-scale abrasion test



It is important to note the difference in the contributing factors to the contact velocity for each test method. For the laboratory tests the contact velocity equates to the sliding velocity of the wheel/ball, which remains constant for the duration of the test, with continual contact with the wearing test sample. For the rotors, in the simulated wear tests, the contact velocity is the sum of the constant rotational velocity plus the variable sliding velocity, generated by the oscillating movement of the rotor. At either end of the stator slot the sliding velocity is zero and accelerates to a maximum midway along the slot. Consequently, only one point on the rotor surface is exposed twice to the maximum contact velocity.

7.4 WET RUBBER WHEEL ABRASION RESULTS

The standard test procedure, ASTM G65, for the rubber wheel abrasion tests uses silicon oxide of a nominal particle size of 200 microns for the abrasive media. However, progressive cavity pumps are used for a diverse range of slurries, and therefore it is important that, for a laboratory wear test to assess rotor coatings, it is capable of simulating wear conditions over a range of particle sizes and shapes.

Wear tests were performed using silicon oxide and silicon carbide, over the range of particle sizes listed in table 7.2. The two types of abrasives were used to assess the test apparatus ability

**Comparison of standard hard particle laboratory wear tests
with the wear behaviour in a progressive cavity pump**

to replicate the wear conditions observed in the simulated tests with respect to the different particle characteristics. All the tests were performed under the wet conditions described in section 7.1.1 on stainless steel, AISI grade 316L.

Table 7.2: The range of abrasive used for the wet rubber wheel abrasion test

Abrasive type	Nominal particle size (μm)
Silicon oxide	120
	225
	450
	900
Silicon carbide	80
	45
	24

7.4.1 Comparison of wear mechanisms with the pumping element

Optical images of the wear scars generated with the silicon oxide slurries are shown in figure 7.7, with detailed SEM images in figure 7.8. A distinct relationship was observed between particle behaviour and particle size. For the slurries containing the two smaller size particles, of 120 and 225 microns, micro-scratching, due to two-body abrasion, was observed with a small degree of rolling wear at the entry and exit regions of the contact zone. However, for the larger size particles, of 450 and 900 microns, the wear morphology changed and a high degree of plastic deformation was observed creating a rippled effect, the severity of which increased with particle size. The rippling effect was not observed in the entry and exit regions of the scars. Here, rolling wear was observed similar to that created by the smaller size particles. Discontinuous scratches were identified amongst the ripples that were a few microns in width.

Graph 7.5 compares the dimensional wear rates, of the stainless steel, for each particle size, from the rubber wheel and simulated in-service wear tests. The wear rates, derived from the laboratory abrasion test, were found to be greater but of the same order of magnitude as those from the simulated wear test, with a similar relationship with particle size. A gradual reduction in wear rate was observed as the particle size increased to 450microns, although the gradient of the reduction was far steeper in the laboratory test than the simulated test. Further increasing of particle size saw the wear rate become independent of particle size regardless of the test method. However, although a similar wear/particle size relationship was observed with both test procedures, the morphology examination revealed different wear mechanisms to be responsible for the fall in the wear rates.

Figure 7.7 : Optical images of the stainless steel wear scars from the wet RWAT after a sliding distance of 7183m under a contact load of 100N, with an aqueous slurry containing a nominal particle size of (a) 120; (b) 225; (c) 450 and (d) 900 microns, (arrow indicates direction of rotation of wheel)

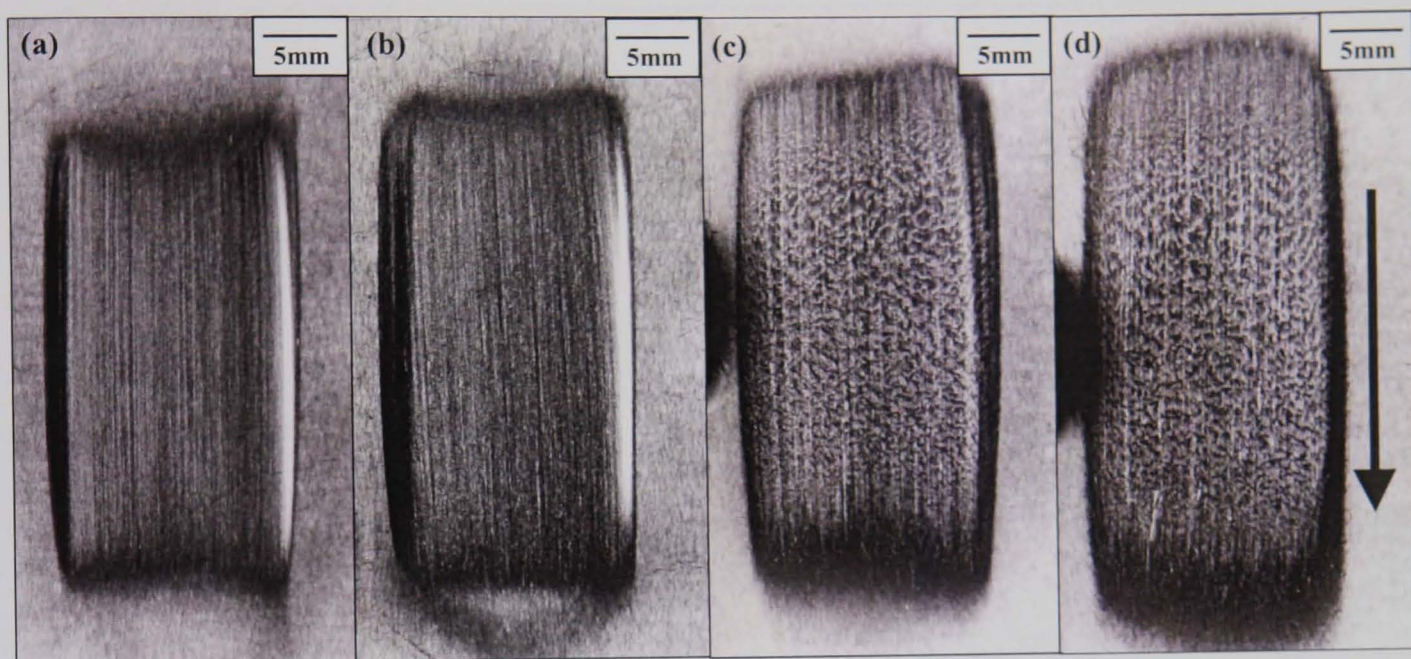
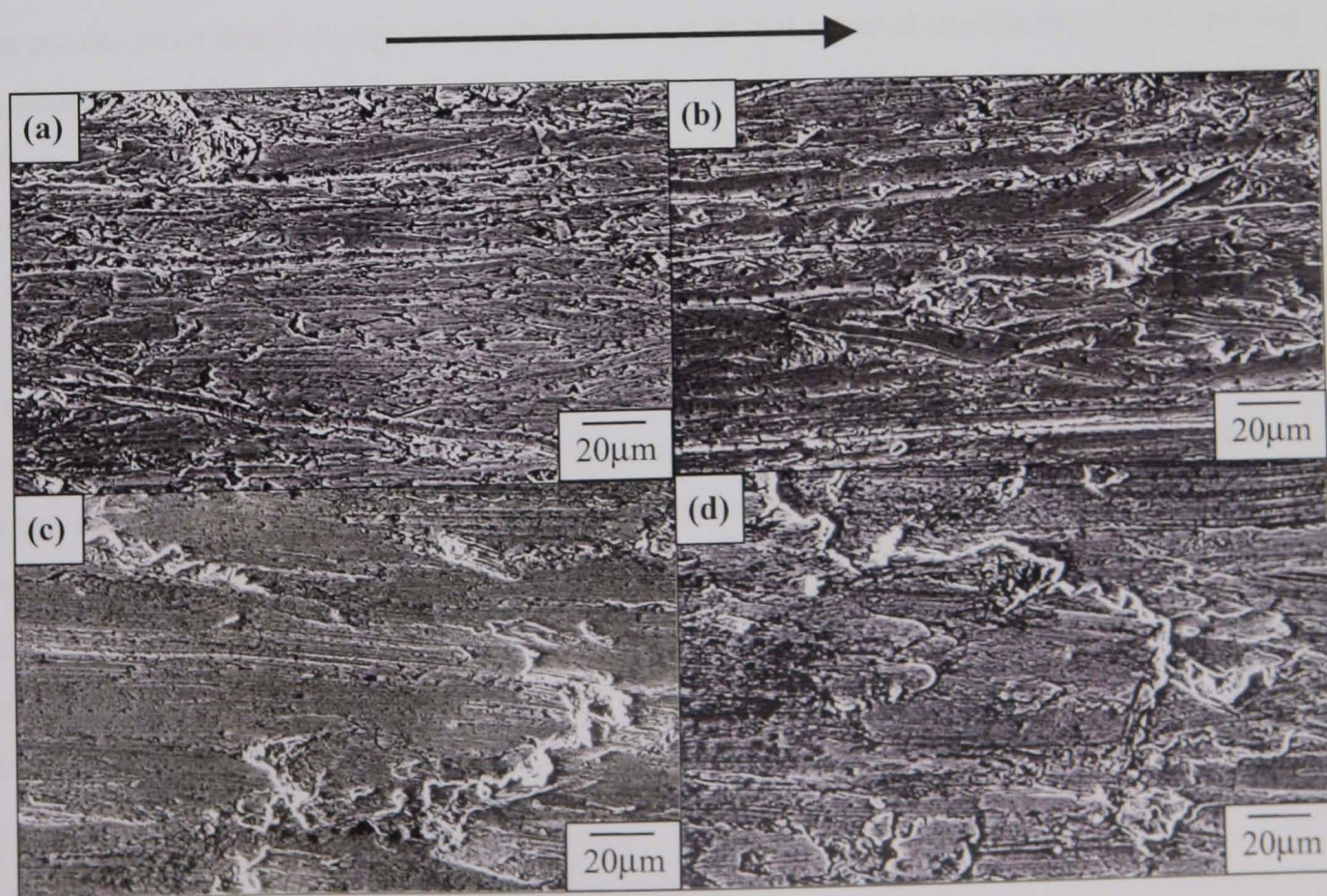
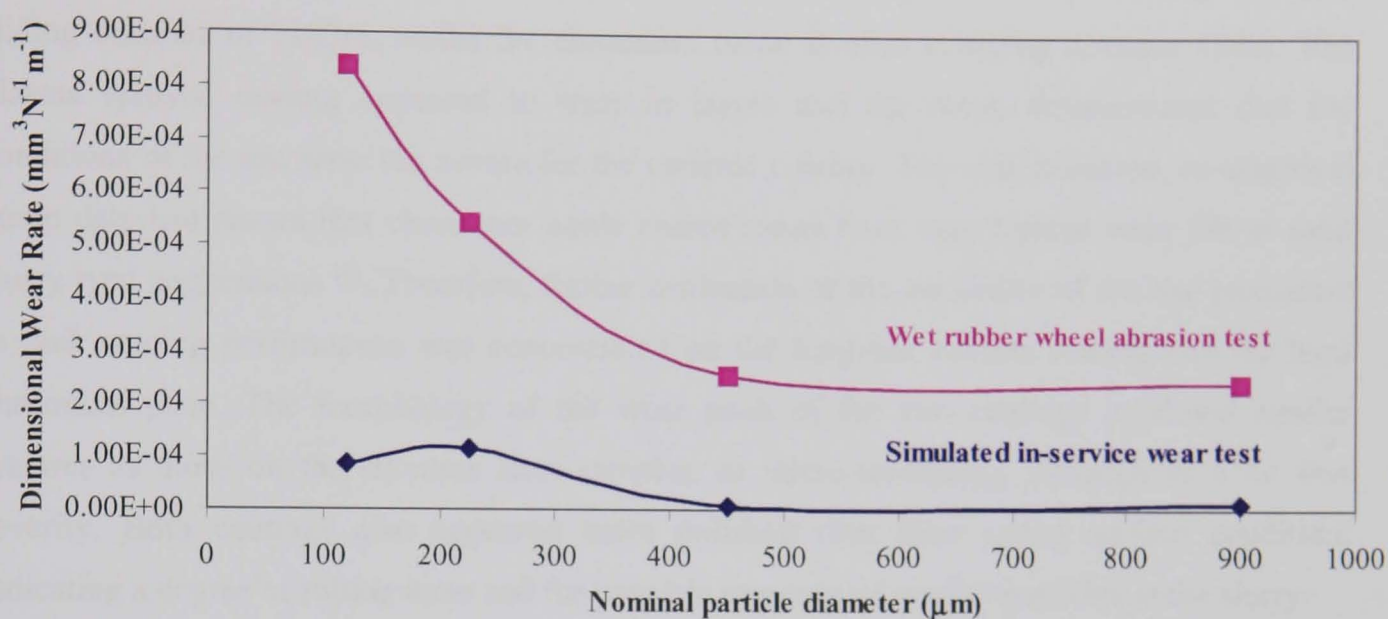


Figure 7.8: SEM images of the stainless steel wear scars from the wet RWAT after a sliding distance of 7183m under a contact load of 100N, with an aqueous silica sand slurry containing a nominal particle size of (a) 120; (b) 225; (c) 450 and (d) 900microns, (arrow indicates direction of rotation of wheel)



Graph 7.5 : Comparison of dimensional wear rates derived from the wet rubber wheel abrasion test and the simulated in-service wear test for silicon oxide slurries of various particle sizes



As discussed in section 6.1.2, material removal from a rotor occurred predominantly by two-body abrasion, regardless of the size of the silicon oxide particles, although the scale of the generated grooves depended upon on particle size. In general, ‘macro-grooves’ were observed, which contained either micro-scratches and /or indentations, and the severity of the macro-grooves was responsible for the changes in the dimensional wear rates. The laboratory abrasion test results show that a change in the predominant material removal mechanism, from grooving to smearing, was responsible for the wear rate becoming independent of particle size. This agrees with studies by Tucker and Miller ^[5], who observed that wear rates produced on the rubber wheel abrasion test were sensitive to variations in abrasive size. These differences in material removal mechanisms, with the larger size abrasants, highlight a fundamental difference in the tribological systems of the two tests. With the laboratory test, the abrasive particles are fed directly into the contact zone regardless of their size, whereas the particles in the slurry passing through the simulated test rig, are free to choose their own flow paths and are subjected to the effects of the turbulent flow patterns. Therefore, it is postulated that there is a critical particle size, which when exceeded, the larger particles, in the slurry, will not enter the contact zone, due to influencing factors, such as the thickness of the hydrodynamic film, rubber hardness and contact pressures, and consequently, the wear rate becomes independent of particle size. The critical particle size is estimated to be ~300 – 400 microns.

7.4.2 *Ranking of rotor coatings*

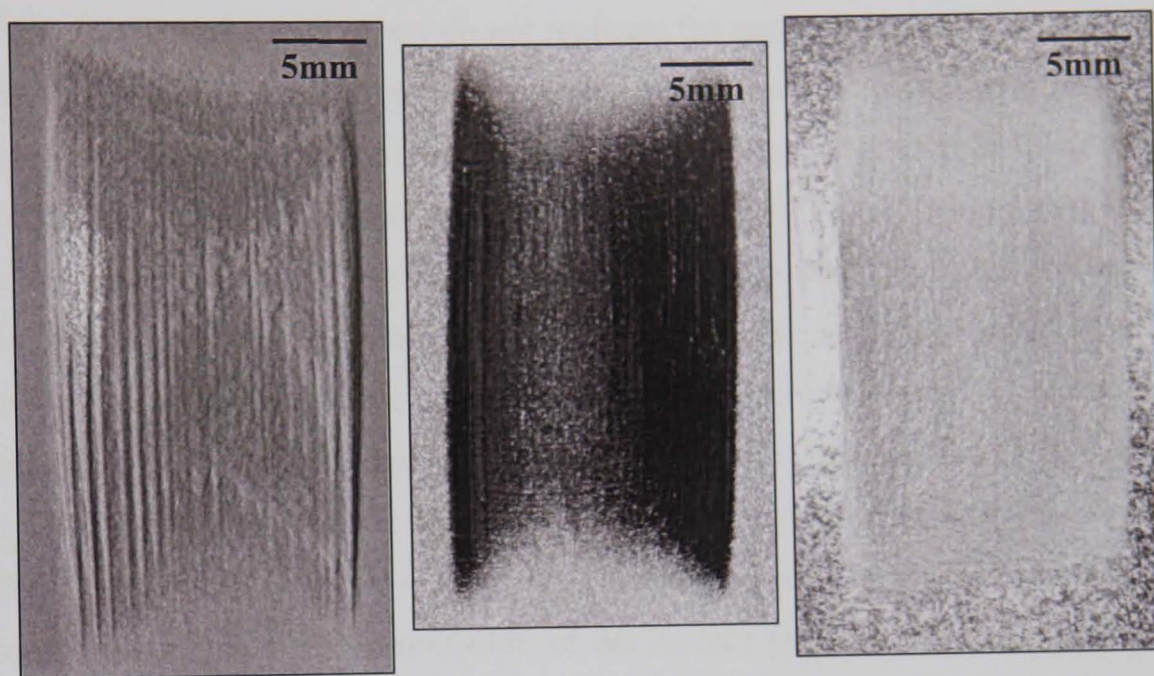
The initial wear performance of the three coatings was assessed using a slurry containing 225 micron particles of silicon oxide. Optical images of the wear scars generated are shown in figure 7.11. The wear scars for the hard chromium plate and the tungsten carbide coating are for a sliding distance of 7183m, whilst the chromium oxide is after a sliding distance 144m. The plasma sprayed coating appeared to wear in layers and the result demonstrated that the conditions of the test were too severe for the ceramic coating. This was expected, as empirical pump data had shown that chromium oxide coated rotors have very limited wear life in sand slurry type applications ^[6]. Therefore, further evaluation of the suitability of the test procedure to rank coating performance was concentrated on the tungsten carbide coating and the hard chromium plate. The morphology of the wear scars of the two coatings exhibited similar features as those on the stainless steel samples, of micro-scratching, although of a far less severity. Both coatings also appeared more polished than their initial surface condition, indicating a degree of rolling wear and the possible presence of smaller particles in the slurry.

Slurries containing the four different silicon oxide particle sizes were used to assess the relative ranking of the two coatings with respect to their performance on rotors, in the simulated wear test rig. In the laboratory test the coatings were tested for a total sliding distance of 7183m, with weight loss measurements taken every 718m. Under the standard test conditions no weight loss was measured for either coatings, on the simulated wear test. Therefore the operating speed and the sliding distance were doubled to increase the severity of the test conditions. The results are plotted on graph 7.6 and show a similar relationship, with particle size, for both test procedures, with the laboratory test producing higher material removal rates, agreeing with the stainless steel test results and confirming that the laboratory test procedure accelerates the wear process.

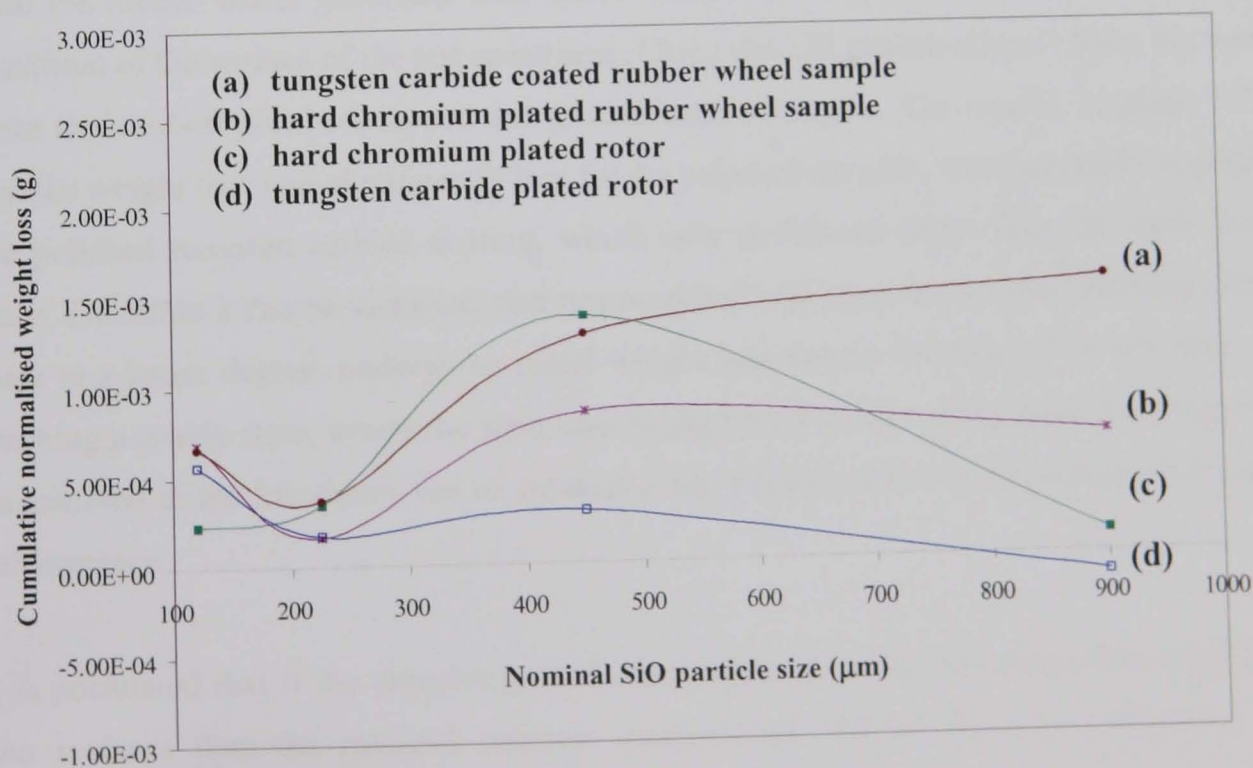
Although the relative changes in weight losses with particle size were very small, all four test combinations showed a definite trend. Weight loss was dependent on size, for the slurries containing the two smaller particle sizes, with a minimum weight loss from the 225 micron slurry, and became independent of size for particles greater than 450 microns, with the exception of the hard chromium plate on the simulated test. This relationship was the same as that observed with the stainless steel tests, although a maximum weight loss was observed at 225microns as opposed to a minimum.

Comparison of standard hard particle laboratory wear tests
with the wear behaviour in a progressive cavity pump

Fig 7.11 : Optical images of the wear scars generated from a slurry of 225 micron silicon oxide, under a load of 100N on surface of (a) chromium oxide coating; (b) hard chromium plate; (c) tungsten carbide coating



Graph 7.6 : Comparison of cumulative normalised weight loss against nominal particle size for rubber wheel and simulated wear tests.

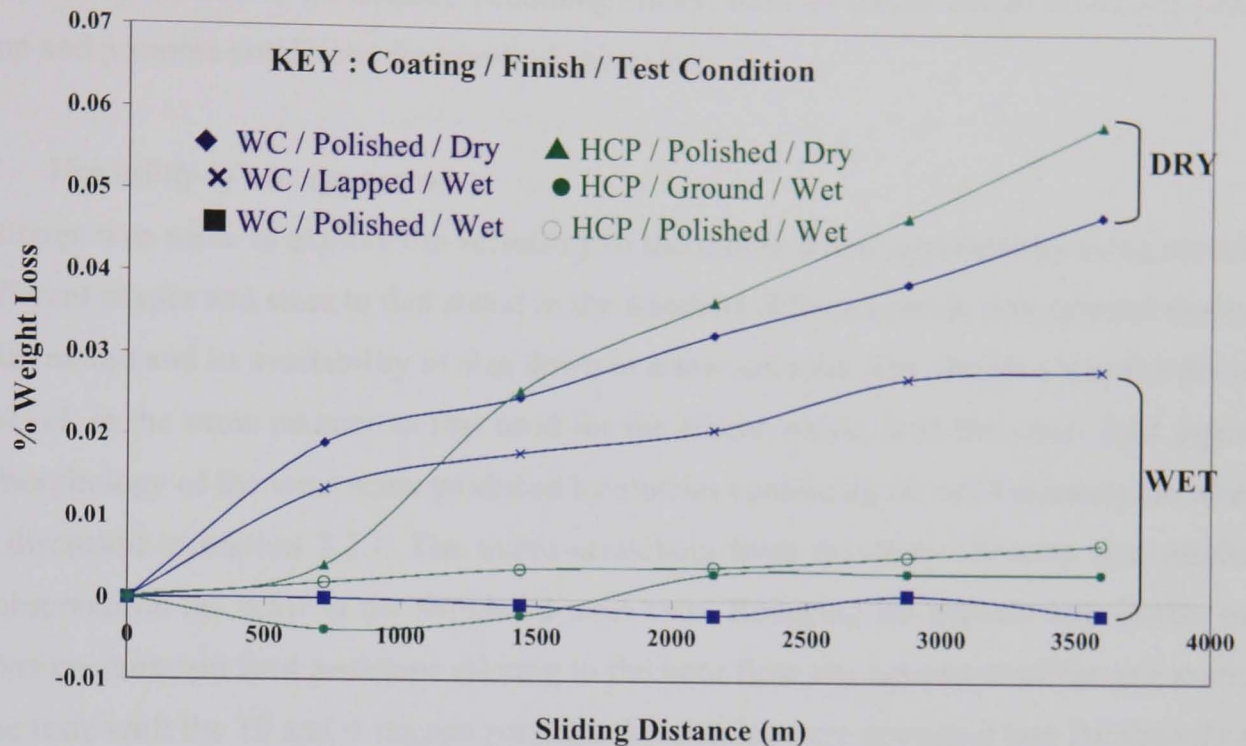


Comparison of standard hard particle laboratory wear tests with the wear behaviour in a progressive cavity pump

However, the relative rankings of the two coatings was found to be different. On the simulated test, the tungsten carbide performed better than the hard chromium plate, as expected from empirical data ^[6], whereas the coating suffered higher weight losses on the rubber wheel test, compared to the hard chromium plate. This would suggest that, under the contact conditions of the test, the rubber wheel abrasion test do not replicate the same wear performance ranking as that which would be expected in a progressive cavity pump. Examination of the worn rotors and rubber wheel wear scars suggested a feasible explanation relating to the surface finish of the test specimens. This is a critical parameter, and for a laboratory test, should normally replicate that of the real application. However, with the rotors the situation was slightly different. Because of the helical geometry of the rotors they can not be hard ground, so flexible diamond belts are used to attain a sufficiently smooth enough surface to produce a low coefficient of friction with the rubber under dry conditions. This is essential, so as to minimise the start up torque of the pump, as for the first ~10 seconds there is no lubrication between the rotor and stator. The surface finish of the coatings, used in the rubber wheel evaluation tests, were the same as that applied to the rotors. However examination of the surface finish of the worn coated rotors revealed that they had become highly polished during the wear tests, in addition to the grooving wear. With the tungsten carbide coating, in particular, this would be advantageous to the stator life, and reduce production costs on finishing of the coating. The same observation was made with the rubber wheel generated wear scars. Therefore the question is raised as to the initial condition of the surface of the test specimens. Using the 225 micron silicon oxide, the wear tests were repeated on polished, lapped and ground coated samples. The results, in graph 7.7, show that the weight loss was significantly less for the polished samples, and practically negligible for the polished tungsten carbide coating, which now performed better than the hard chromium plate. Therefore it can be surmised, that rotors coated with tungsten carbide, and hard chromium plate to a lesser degree, undergo an initial weight loss due to flatter of its aspirates, before reaching a steady state, where the wear was negligible. It is this steady state wear that needs to be assessed in the laboratory test to conduct a fair representation of a coatings long term wear performance.

It is postulated that if the abrasive particles are larger than the lubrication film separating the two surfaces then the material removal mechanisms will be the same, regardless of the lubrication conditions. Various studies have shown that wear rates on the rubber wheel test are far greater under dry conditions than wet ^[8,9]. Therefore, testing under dry conditions could potentially accelerate the assessment of rotor coatings by increasing the severity of the test whilst maintaining the same wear mechanisms.

Graph 7.7 : Cumulative weight loss vs. sliding distance for tungsten carbide coating and hard chromium plate under wet and dry test conditions



A 225 micron silicon oxide slurry was used to test the tungsten carbide coating and the hard chromium plate under dry conditions. The results, shown in graph 7.7, agree with the studies, that under dry conditions, the test is more severe than under wet conditions. Both coatings exhibited a continual increase in weight loss with sliding distance, compared to the wet conditions where the weight loss was negligible, with some weight gain recorded for both coatings due to pick up of the abrasives. The dry test results also show that the tungsten carbide coating performed better than the hard chromium plate, regardless of the surface finish of the coatings. Examination of the dry wear scars revealed similar appearances to the wet scars, of micro-scratches lying parallel to the rotation of the wheel and an increase in surface finish. Thus indicating a predominant wear mechanism of two-body abrasion with a degree of three-body abrasion from smaller particles. According to Eaves ^[10] a polishing type wear would be expected under dry abrasion as the loads involved cause fragmentation of the abrasive. These findings of accelerated wear with no change in the wear mechanism agree with Swanson and Klann ^[8] but not with the studies of Wirojanupatump and Shipway ^[9], who observed a change in wear mechanism from three-body to two-body when dry and wet testing on steels.

It was observed during the dry tests that a high degree of frictional heat was generated causing the sample, the wheel and the sample folder to become too hot to touch. This change in temperature would have a direct effect on the contact conditions, in particular the rubber wheel,

and could contribute to the increased wear rates observed with the dry tests. The surface properties of the rubber would change with temperature, with an increase in resilience and a slightly sticky texture to the surface becoming sticky, both of which would effect the particle motion and promote conditions for two-body abrasion.

7.4.3 Versatility of test apparatus

An attempt was made to explore the versatility of the rubber wheel apparatus by using abrasants of different shapes and sizes to that stated in the standard. Silicon carbide was selected due to its angular nature and its availability in size down to a few microns. The abrasive was fed dry onto the wheel, in the same manner as that used for the silicon oxide, with the water feed separate. The morphology of the wear scars produced by slurries containing 80 to 24 microns has already been discussed in section 7.2.1. The micro-scratching from two-body abrasion was similar to that observed on the rotor in the simulated wear tests. Reducing the particle size further to 16 microns encountered feed problems relating to the poor flow characteristics of the dry stock, so for the tests with the 10 and 4 micron particles the slurries were premixed and fed directly into the top of the contact zone. For these tests no weight loss was measured, although a superficial wear scar was visible, producing a highly polished surface finish.

These results demonstrate that the rubber wheel test could be used on a practical level for abrasive particles down to a size of ~25 microns, as in order to generate a measurable amount of weight loss the particle must be greater than the thickness of the lubricating film. Flow characteristics is also an important factor to enable the particles to be fed dry. Alternatively the apparatus could be modified to feed a slurry, for which an agitator would be required to ensure the particles remained in suspension.

An important observation during the abrasion tests was the ease of use, which would effect its versatility in testing the abrasivity of 'real' slurries. Relatively large quantities of the slurry would be required to perform a full assessment of the rotor coating, producing large amounts of waste. Disposal of the waste could potentially be an issue, with respect to health and safety legislations, particularly when the slurries contain chemicals such as weak acids or chlorides.

7.5 MICRO-SCALE ABRASION TEST RESULTS

7.5.1 *Comparison of wear mechanisms with the pumping element*

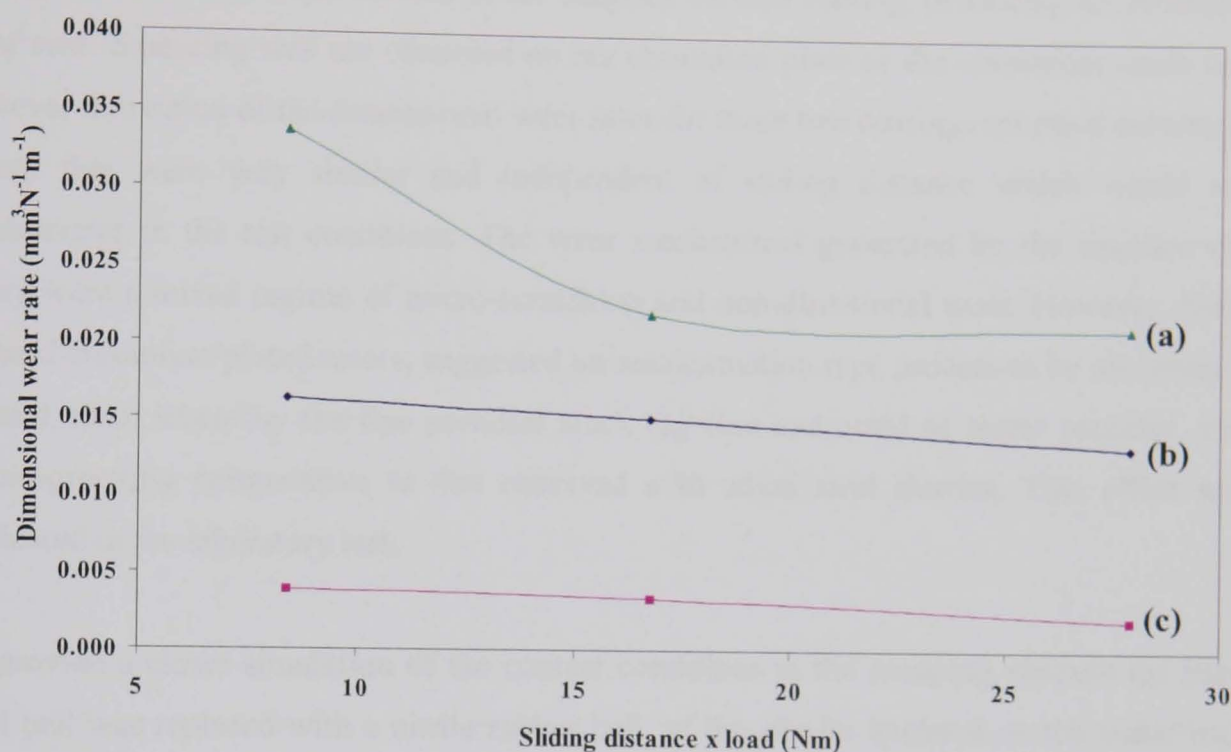
Using the standard test procedure prescribed by the National Physical Laboratory, the micro-abrasion test produced two- and three-body abrasive wear, depending upon the concentration of the slurry, as previously shown in figure 7.5. The nature of the two-body abrasion was comparable to the micro-scratching observed within the macro-grooves of the rotors. However, the morphology of the three-body abraded crater was different to that observed on the rotors, or rather the use of the terminology to describe the wear mode is different. The term 'three-body abrasion' or 'rolling' wear, with pumps, tends to be used to describe a 'polishing' effect which increases the surface finish of the rotor, whilst maintaining a smooth surface. This is opposed to the dimpled, non-directional morphology, generated by a 20% slurry concentration of 4 micron silicon carbide particles in the laboratory test.

7.5.2 *Ranking of rotor coatings*

Unlike the rubber wheel abrasion test, all three coatings were able to be tested and the dimensional wear rate values derived for each are shown in graph 7.8. The tungsten carbide coating exhibited the highest resistance to the abrasive slurry, with the ceramic coating being the least resistant. The wear scars, in the chromium oxide coating and the hard chromium plate, were clearly defined spherical craters of parallel scratches from two-body abrasion, with no sign of three-body abrasion around the edges. The shape of the wear crater in the tungsten carbide were less clear, with two-body abrasion through the centre and non-directional to either sides producing hazy edges. The amount of three-body abrasion reduced with sliding distance, improving the clarity of the crater and the degree of two-body abrasion.

These findings do not correlate with empirical pump data ^[6], which clearly show that chromium oxide performed better than hard chromium plate in fine particle abrasive slurry applications. It is postulated that the difference in ranking is related to the nature of the coatings and the behaviour of the fine particles in the pumps. Both, the micro-cracking in the hard chromium plate, and the heterogeneous structure of hard particles in a ductile metallic matrix of the tungsten carbide coating, would promote embedding of the abrasive particles within themselves, thus effectively improving the wear resistance of the surface. It is observed in field trials ^[6], that fine abrasive particles tend to produce a polishing type wear, as opposed to the two-body mechanism simulated in the micro-scale abrasion apparatus.

Graph 7.8 : Comparison of dimensional wear rates derived from the micro-scale abrasion test using a harden steel ball, a load of 0.35N and 2 wt.% 4 micron silicon carbide slurries on (a) chromium oxide coating; (b) hard chromium plate and (c) tungsten carbide coating



The abrasion resistance of all three coatings appeared to remain relatively constant with sliding distance, with the exception of the first reading of the chromium oxide coating. This data correlate well with the wet rubber wheel abrasion results.

7.5.3 Versatility of test apparatus

An attempt was made to assess the versatility of the apparatus by replacing the standard slurry particle size with a range of larger silicon carbide particle sizes and two slurries from field applications. The advantage of the micro-scale abrasion test over the rubber wheel apparatus is the relatively small quantities of slurry required for the test, and the cleanliness of the test procedure. The results from the larger silicon carbide particles have already been discussed in section 7.2.2 from which it was concluded that the apparatus had a maximum particle size limit of ~16 microns. Beyond this size, entrainment of the particles into the contact zone, was affected, resulting in derivation of the spherical crater shape and a predominant three-body particle behaviour, which was independent of particle concentration. This was also demonstrated using a slurry, from a quarry, containing 50 micron of silicon oxide. The wear scar produced was of a mixed wear regime of two-body abrasion, through the centre of the crater, with three-body around the peripheral making it difficult to quantify the edges of the

Comparison of standard hard particle laboratory wear tests with the wear behaviour in a progressive cavity pump

crater. Profilometry of the crater revealed a non-spherical crater. For a slurry containing 0.5 micron particles of titanium dioxide, it was discovered that the test apparatus also had a minimum size limit to the particle range. Attempts to use this fine slurry resulted in smearing of the titanium oxide onto the surface of the tungsten carbide coating, producing an unmeasurable wear scar. Smearing was not observed on the chromium plate or the chromium oxide coating, however derivation of the dimensional wear rates for these two coatings revealed extremely low values that were very similar and independent of sliding distance which would suggest inaccuracies in the test conditions. The wear mechanisms generated by the titanium dioxide slurry were a mixed regime of micro-scratching and non-directional wear. However, field data on hard chromium plated rotors, suggested an amalgamation type process to be occurring in the contact zone, where by the fine particles stuck together and acted as larger particles, creating macro-grooving comparative to that observed with silica sand slurries. This effect was not replicated in the laboratory test.

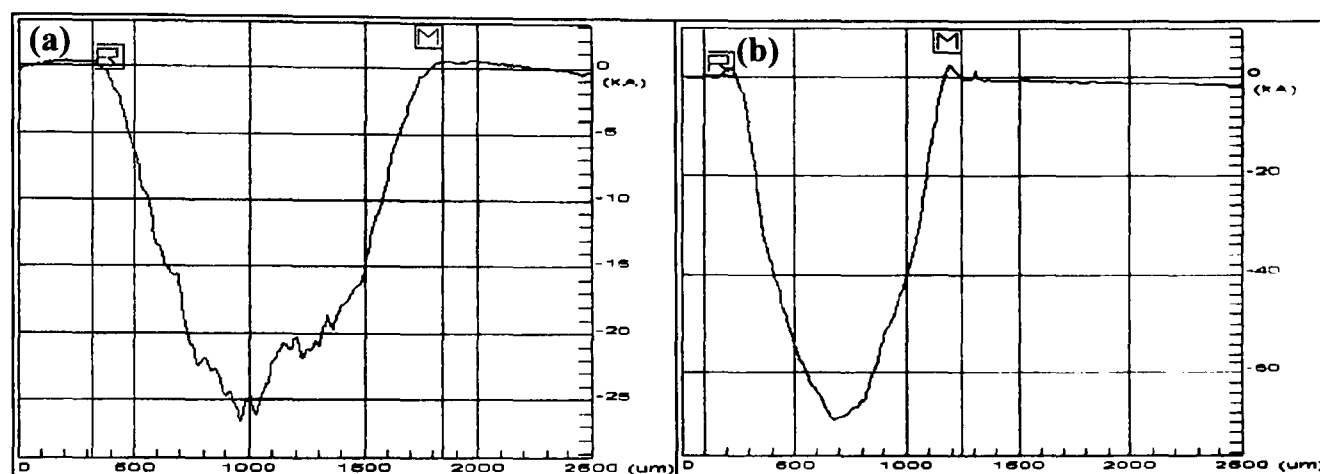
To provide a closer simulation of the contact conditions in the pumping element the hardened steel ball was replaced with a nitrile rubber ball, of the similar hardness as the stator material. Some of the results have already been discussed in section 7.2.2, with figure 7.6 showing optical images of wear scars generated by slurries concentrations of 20 wt.% of various silicon carbide particle sizes. It was observed that in order to generate two-body abrasion, the size of the particle in the slurry had to be larger than that used in the standard test procedure for the hardened steel ball. Under an applied load 0.35N, a particle size of 45 microns was necessary before sufficient two-body abrasion was generated to define a complete spherical shaped wear scar. A circular band of non directional three-body abrasion was found to enclose the wear scar. Increasing the applied load to 1.5N, removed the three-body wear band, and increased the intensity of the two-body scratches. However the edges of the spherical crater had become less defined. Consequently, the potential for erroneous results was prevalent under both loads if the geometric dimensions of the wear scar were to be used to determine the material loss.

The prescribed standard test procedure assumes the wear scar to replicate the 3-D spherical geometry of the ball counterbody, to enable the material loss to be calculated through a simple mathematical equation. Figure 7.12 compares the profiles of craters created by a hardened steel and a rubber ball, under the same test conditions. It can be seen, from these, how the crater, from the rubber ball, deviates from the spherical shape. Consequently, using equation 7.1 to derive the dimensional wear rates would produce rates approximately an order of magnitude

**Comparison of standard hard particle laboratory wear tests
with the wear behaviour in a progressive cavity pump**

greater, as the material loss would be greater than assumed. Subsequently the wear rates would be

Figure 7.12 : Profiles of wear scars on 316 stainless steel, generated using (a) a rubber ball and (b) a hardened steel ball, with a 20wt.% slurry of 45 micron silicon carbide, under an applied load of 0.35N



similar to those produced by a hardened steel ball, under the same test conditions. When the rubber counterface was tested against the hard coated specimens the main problem was providing adequate contact pressure to generate wear, whilst maintaining a consistent geometric crater. Increasing the load was found to cause further deviation from roundness of the wear scar, suggesting severe flattening of the rubber ball, without actually increase the depth of the wear. Consequently any appearance of a wear scar was purely superficial and unquantifiable.

Shipway ^[11] found, under loads less than 2N, counterface balls of nylon and polypropylene produced similar wear scars to those of a steel ball, with clearly definable spherical craters consisting of fine lines parallel to the sliding direction. The lack of crater depth in the wear scars from this study, and the deviation from roundness at low loads, suggests that there a limit exists on the requirement of the elastic properties of the counterball material. Therefore, to employ a rubber counterface on the micro-scale abrasion tester an alternative method, or mathematical equation, would be required to determine the volume of material loss. The change of the wear mechanism from three- to two-body abrasion with a 20 wt.% concentration agrees with the finding of Adachi & Hutchings ^[4] and Trezona and Hutchings ^[12] on the effects of soft elastomeric counterballs. Trezona and Hutchings observed that soft balls, on soft specimen surfaces, resulted in grooving wear due to embedding of the particles into the soft ball, rather than roughening of the ball surface, as they predicted.

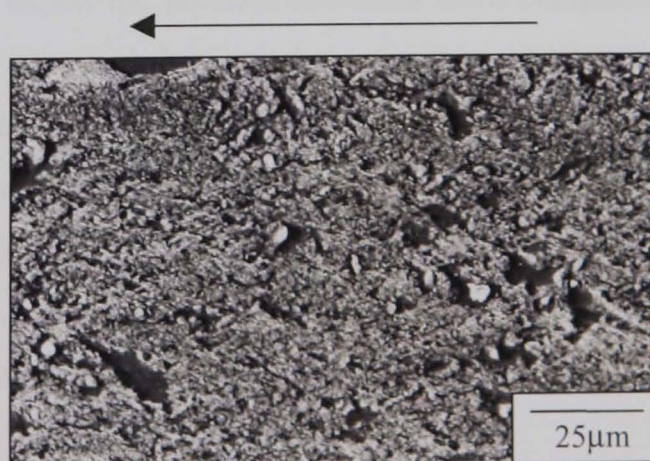
7.6 SLURRY JET EROSION TEST RESULTS

7.6.1 *Simulate of type 'a' stator wear regime*

The main focus of the slurry jet erosion test was to simulate the type of wear that had been observed in the stators. A nitrile rubber target, set for an impingement angle of 30° was eroded for 20 minutes, at a velocity of 11.9ms^{-1} . SEM images of the worn surface is shown in figure 7.13. The wear features are a combination of cuts, craters and embedded particles, similar to that observed in the stators. The direction of the cuts and craters lay parallel to the impinging slurry. For comparison, an abrasion test was also performed on the rubber, using the micro-scale abrasion apparatus with a hardened steel ball and a 2% 4 micron silicon carbide slurry. Although a spherical wear scar was visible after 200 revolutions, closer examination, under the SEM, revealed a very high percentage of embedded particles and only superficial polishing. It is postulated that further testing of this material combination would ultimately lead to a higher material loss to the steel ball than the rubber counterface.

These preliminary tests indicate that abrasion tests are not suitable for predicting the relative wear life of a stator material and that a slurry jet erosion type test would produce more useful data with respect to resistance to particle embedding, cutting and fatigue type material removal mechanisms.

Figure 7.13 : SEM images of nitrile rubber after 20 minutes erosion by a 0.3% slurry of 120 micron silicon oxide particles at an impact velocity of 11.9ms^{-1} and an impingement angle of 30° . (Arrow indicates direction of impact)

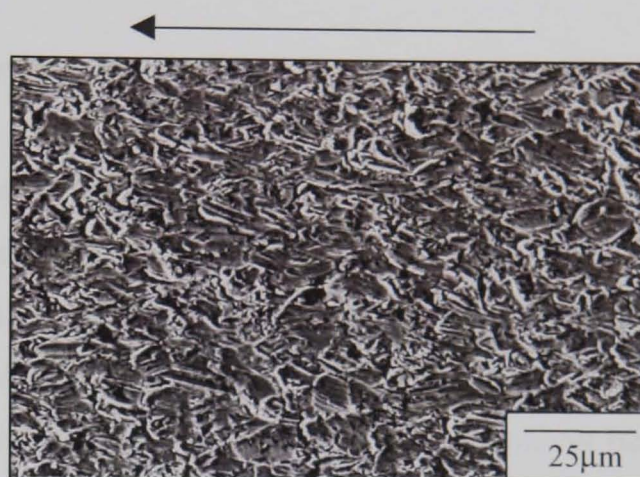


7.6.2 *Comparison of wear mechanisms with the pumping element*

The morphology of the eroded 316 stainless steel sample, eroded at an angle of 30° , for a duration of 20 minutes, is shown in figure 7.14. The wear features consisted of a very fine pattern of elongated craters, lying predominately parallel to the impinging slurry. The length to

width ratio of the craters was approximately 10:1, indicating that only the leading face of the particle was contacting the surface and was responsible for removing the metal by a cutting action, agreeing with classical ductile erosion models ^[13].

Figure 7.14 : Worn stainless steel surface after 20 minute exposure to a 0.3% slurry of 120 micron silicon oxide particles, at an impingement angle of 30° and an impact velocity of 11.9ms⁻¹. (Arrow indicates direction of impact)



A comparison of this eroded surface, with those generated on the rubber wheel abrasion apparatus and on rotors, tested with the same type of slurry, revealed several similarities. A cutting type action was the dominant material removal mode in all three test procedures and the magnitude of the scratches were similar, if compared with the micro-scratching on the rotors, and not the macro-grooving. However a difference lay with the length and depth of the scratches. For the erosion test the scratches were short, with tapered sides, reaching a maximum depth in the centre, whilst the abraded scratches were continual and of constant depth. The length and depth of the scratches are determined by the contact duration time between the particle and the wearing surface, which can be related to the particle loading conditions. Abrasion occurs due to an external force applied on a particle, so the length of the scratch equates to the duration of the applied load, producing a roughly constant depth. In contrast, particle loading in erosion results from their deceleration on impact producing the characteristics craters, with tapered sides.

These observation suggest that Schmid et al.'s ^[2] theory of substituting two-body abrasion tests with low impact erosion tests may be viable for ductile materials, but care should be exercised when comparing weight losses or wear rates of coated samples.

7.6.3 Ranking of rotor coatings

The erosion rates of the coatings were compared to those of the stainless steel and rubber samples. Several different techniques were explored to determine the erosion rates, since no standardised method had been identified. The techniques used were:-

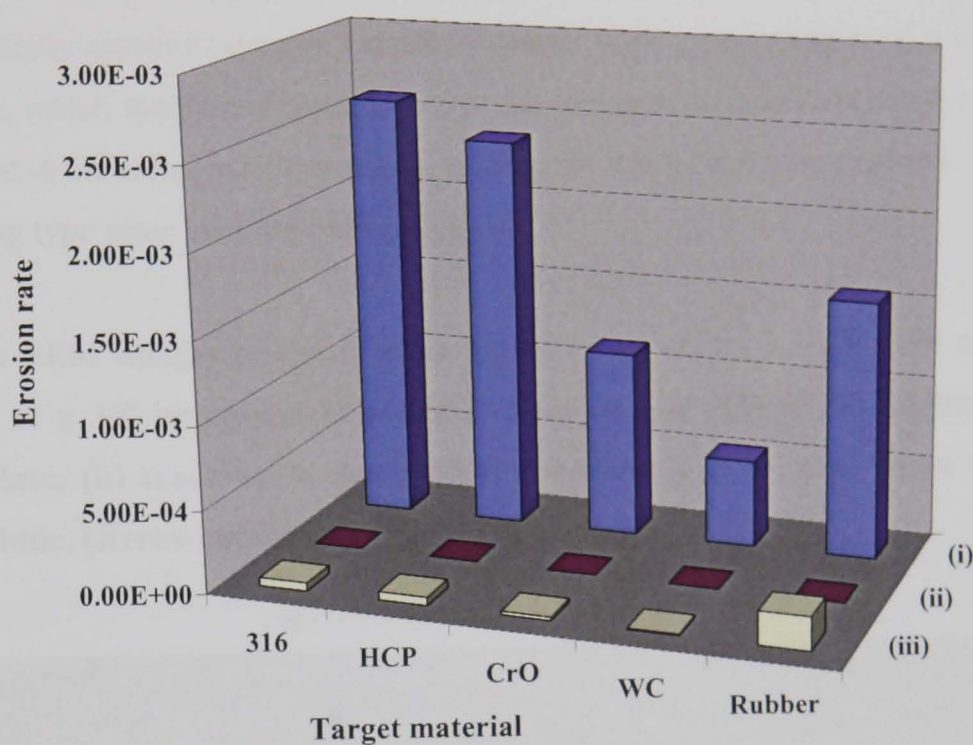
- (i) weight loss per unit time
- (ii) normalised weight loss per unit time
- (iii) the gradient of the plot of normalised weight loss against time

All three techniques describe the erosion rate as a function of time as opposed to the mass of erodent particles. This was deemed to be acceptable since the objective of the test was to achieve a relative ranking of materials, under identical system conditions. Graph 7.9(a) and (b) shows that the ranking and magnitude of erosion resistance varies depending upon the technique selected. Techniques (ii) and (iii), using normalised weight loss, produced similar relationships with the rubber exhibiting the highest erosion rate. Unlike technique (i), where the rubber had a lower wear rate than both stainless steel and the hard chromium plate. This was found to be a consequence of the relative weights of the test samples. Whereas the steel and coated samples were of similar weights, the rubber was an order of magnitude less, a factor that was not considered in technique (i). Consequently, using a normalised weight loss, the erosive rate of the rubber significantly increased to the least resistant of the five target materials, and the magnitude of the erosion rates reduced by an order of four and two, for techniques (ii) and (iii), respectively. For all three techniques the two thermal spray coatings exhibited the highest level of erosion resistance, with the tungsten carbide coating showing the lowest rate each time. The high erosion resistance of the chromium oxide was an unexpected result, considering the brittle nature of the ceramic coating. Also, unexpected, was the poor performance of the hard chromium plate, whose erosion rate was only comparable to that of the uncoated stainless steel. The ranking of the coatings does not correlate with that experienced in the pumps, where hard chromium plate performed significantly better than the ceramic oxide coating and stainless steel in the simulated wear tests. A possible explanation may relate to the difference in particle rebound behaviour, between each target material, causing a shielding effect around the area of impact.

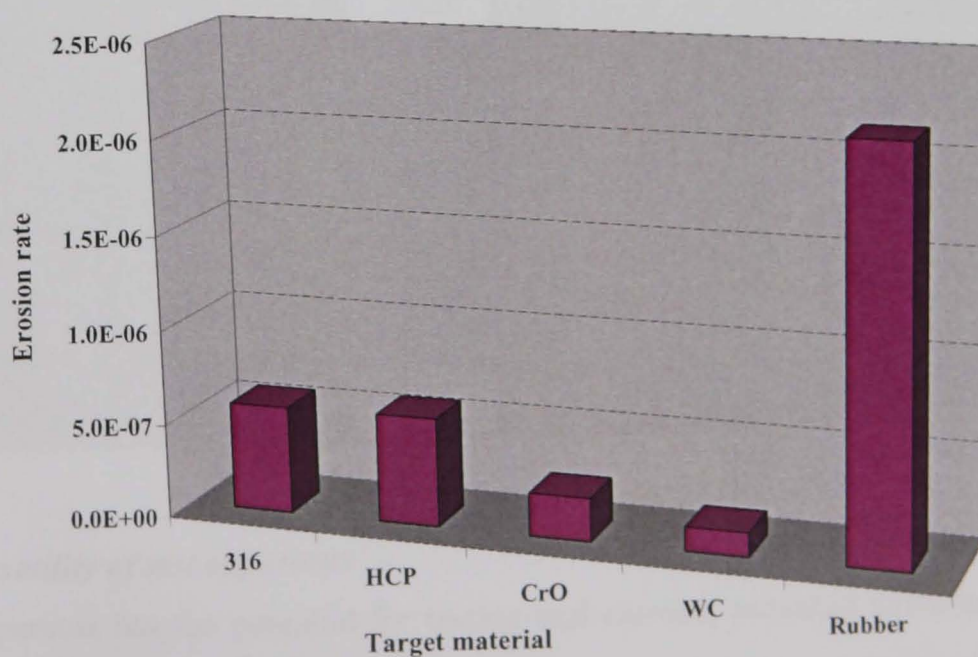
Comparison of standard hard particle laboratory wear tests
with the wear behaviour in a progressive cavity pump

Graph 7.9(a): Erosion rates for the five target materials in units of

- (i) Weight loss g/min
- (ii) Normalised weight loss g/min
- (iii) Gradient of the plot of normalised weight loss (g) vs. time (min)



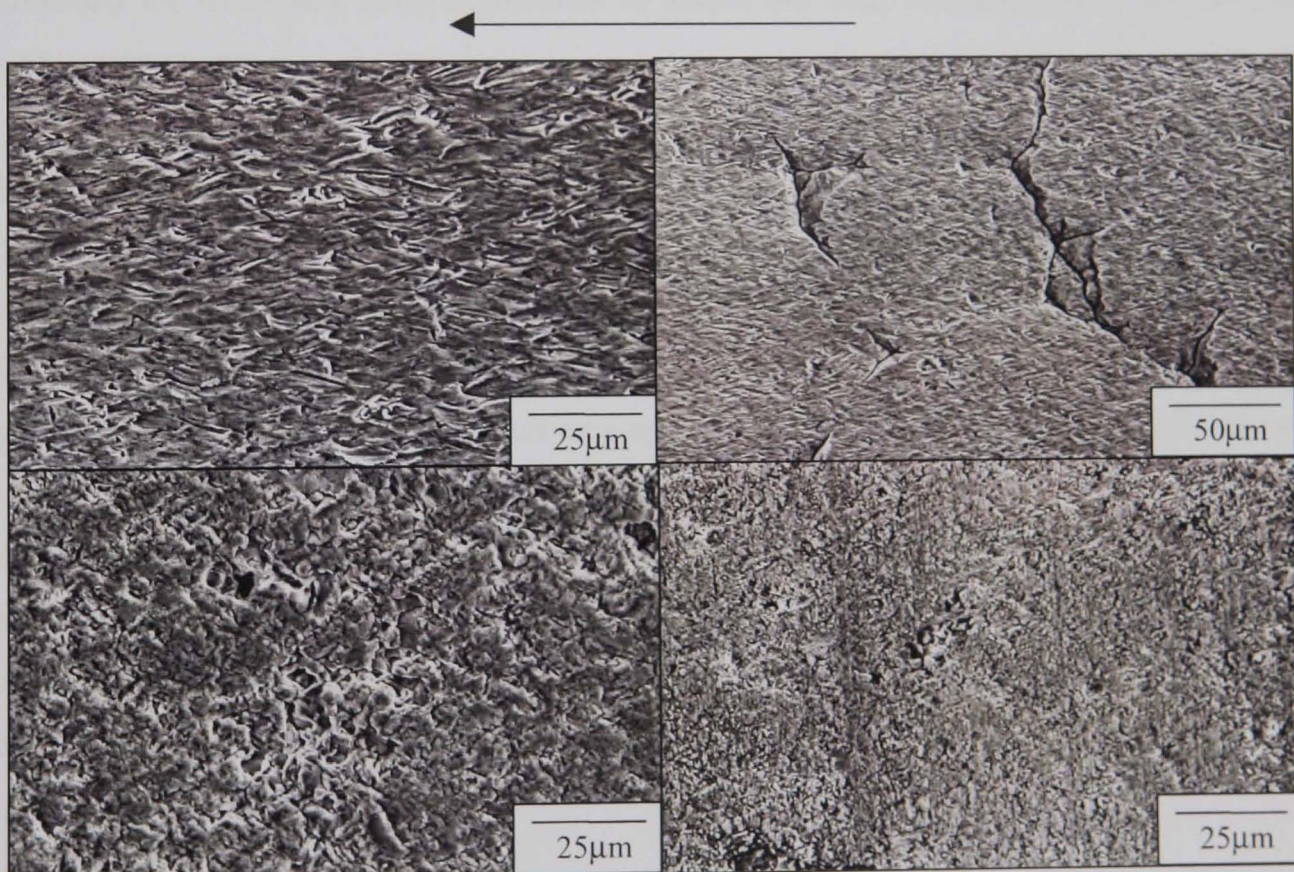
Graph 7.9(b): Erosion rates for the five target materials in units of normalised weight loss (g) per minute, technique (ii)



**Comparison of standard hard particle laboratory wear tests
with the wear behaviour in a progressive cavity pump**

SEM images of the morphologies of the eroded coatings are shown in figure 7.15. A similar wear pattern, as the stainless steel, was observed in the hard chromium plate, although less severe. In addition, large cracks were observed in the plate, figure 7.15 (b), at the opposite end of the sample to the impact zone. These cracks appear to follow the boundaries of the nodule morphology that form during plating and may explain the unexpected low wear rate of the plate. Both the thermally sprayed coatings exhibited similar wear morphologies of a non-directional pattern of pits, which roughened the surface. In the tungsten carbide coatings the pits appeared to have formed in the softer matrix material, leaving the harder carbides exposed. There were no signs of cutting type wear in either of the coatings.

Figure 7.15 : SEM images of the eroded coated samples, by a 0.3% 120 micron silicon oxide slurry at a 30° impingement angle and an impact velocity of 11.9ms^{-1} ; (a) hard chromium plate; (b) cracking in the hard chromium plate; (c) chromium oxide and (d) tungsten carbide. (Arrow indicates direction of impact)



7.6.4 Versatility of test apparatus

The test apparatus has the potential for testing real slurries, provided sufficient quantities are available and concentration levels were low enough to maintain suspension of the particles in the fluid. Initial problems were experienced with the apparatus in producing sufficient velocity to remove material in a practical period of time. This was resolved by reducing the diameter of

the nozzle from 6 mm to 3mm, which doubled the impact velocity. Although it may be necessary to increase the diameter of the nozzle to test slurries containing large particles. It was found that too high a velocity created problems with retaining the deflected slurry within the confines of the tank. At 90° the deflected jet from the target shot directly upwards to a height of 900mm before falling back into the line of the jet and interrupting the stream. As the impact angle tended towards zero the severity of the spray from the deflected jet reduced. It was concluded that a design modification to the sample holder would be necessary to deflect the jet of slurry, from the target, downwards into the slurry. This would contain the slurry more efficiently and increase the impact velocity capability of the apparatus.

7.7 CRITERIA FOR TWO NEW TRIBOMETERS

None of the evaluated hard particle laboratory tests fulfilled all five of the requirements outlined at the beginning of this chapter. However, a better understanding, as to the capability of each laboratory tests and the controlling factors, was gained, enabling recommendations to be proposed for laboratory scale tribometers to assess the wear resistance of progressive cavity pump components.

It has been concluded, from the results of the pump wear study and the evaluation of the hard particle laboratory wear tests, that a single test procedure would not be capable of simulating the wear process in the pumping element. The criteria for the assessment of stator materials was found to be very different than that required for the rotor coatings. Neither of the laboratory abrasion tests produced grooving wear on a similar scale to the macro-grooving observed on the rotors. A possible explanation is the fundamental difference between the relative movement of the contacting surfaces in the laboratory tests, compared with the pumping element. In the pump, the body, which is the rotor, rotates and slides against a stationary counterbody; the stator. Whereas, in the laboratory tests, it is the counterbody which rotates against a stationary body, thus preventing a build up of embedded particles, as observed with the type a wear regime in the stators.

Therefore it is proposed to design two tribometers to individually meet the wear criteria of each of the pumping element components and consequently simplifying the design of the wear test system. By using separate laboratory tests, it eliminates the need, in the rotor assessment, to simulate the true particle behaviour or to use a rubber counterbody.

An important requirement for a test procedure, that is to be used in an industrial environment, is the peripheral equipment needed to analyse the results. For example a scanning electron microscope, would be impractical to include, since most industrial companies are unlikely to have the capital to invest in, or provide access to, such types of equipment. Consequently analysis by weight loss measurements would be the most desirable, with confirmation of wear mechanisms by low magnification optical microscopy.

7.7.1 Test criteria for the assessment of stator materials

The new wear model, proposed in Chapter 6, defines the embedding of particles as the initiation stage in the wear processing. Further damage to the stator was found to occur by repeated embedding of the particles and subsequent coalescence of pits formed as a result of the embedding. Therefore, the criteria for a tribometer for the assessment of stator materials, is not one of abrasion, but of erosion, for which the slurry jet erosion apparatus showed potential. Materials could be tested, at varying angles, using a standard set of test conditions, enabling weight loss measurements to be used, as a simple evaluation technique, to rank the performance of the material to a reference material, such as nitrile rubber. This type of test would evaluate a materials potential of resisting particle impact and subsequent material loss by fatigue, from the continual impingement of particles. It is paramount, however, that the weight loss analysis, is accompanied by a visual inspection, using optical microscopy, as permanent embedding of particles would produce a weight gain, and potentially erroneous data.

7.7.2 Test criteria for the assessment of rotor coatings

It was identified by the wear study, in Chapter 6, that the predominate wear mechanism, which a rotor surface must resist, was two-body abrasion. Prolonged periods of abrasion from the embedded particles in the stator, resulted in coalescence of micro-scratches to produce grooves on a macro-scale, which subsequently damaged the stator. The severity of the abrasion on the rotors was found to be dependent on particle size. Although the evaluated laboratory abrasion tests produced the desired two-body abrasive action, both were also found to be sensitive to particle size, and each of the tests only operated within a specific size range.

A further requirement of the laboratory test was to accelerate the wear analysis duration of the rotor coatings. As discussed, in Chapter 1, tribological testing can be accelerated in several ways. It has been concluded, from the comparison of the dry and wet abrasive conditions on the rubber wheel abrasion test, that removing the lubricant from the tribosystem would significantly increase the severity of the test, whilst maintaining meaningful data. Acceleration by increasing

Comparison of standard hard particle laboratory wear tests with the wear behaviour in a progressive cavity pump

the applied load was not thought to be appropriate, since the potential existed to produce erroneous data when assessing brittle type coatings.

For both of the evaluated abrasion tests, the behaviour of the particles was found to relate to the size of the contact zone and the method by which they were fed into the zone. Consequently, the mechanism of material removal was found to change with particle size. To control the behaviour of the particles, to ensure the required two-body abrasion, fixed particles need to be used for the rotor coating tribometer. However, the disadvantage of fixed particles, would be that the test could not be used to assess the abrasivity of 'real' industrial slurries.

Therefore, it is recommended that the rotor coating assessment tribometer should be a dry pin-on-disk type test, using a fixed abrasive in the form of an abrasive paper. Bonded-abrasive papers are available in a range of particle types and sizes, thus enabling a diverse range of slurries to be simulated. A simple pin geometry is required, of 6 – 10 mm in diameter, and of a suitable length for a fixture. For each test, two pins are required, the ends of which are coated with the sample coating on one and the reference coating, such as hard chromium plate, on the other. Mass loss measurements are used to quantify comparable wear behaviour by the equation:

$$\text{Normalised wear} = \frac{C W_X}{W_R} \quad (7.1)$$

where W_R and W_X are the mass loss of the reference pin and the sample coating, respectively, C is the reference constant, equal to the mean mass loss of the reference pin per unit track length per unit load, for the abrasive type.

7.7.3 Assessment of 'real' slurries

Since the rotor wear was found to be a direct consequence of particle embedding, the assessment of a 'real' slurry should commence with the slurry jet erosion test. This will determine the nature of the particles, within the slurry, for their potential of initiating the wearing process. A standard reference material, such as nitrile rubber, is used as the target material. As with the proposed procedure for the stator material assessment, a reference is used, such as nitrile rubber, eroded by 200 micron silicon oxide slurry, to rank the slurry's abrasivity. Once the response has been determined then a suitable bonded-abrasive paper can be selected, to represent the slurry particles, for the rotor coating assessment.

It should be noted that laboratory scale wear tests can only provide comparative data and can not predict the life of a component. The purpose of the two tribometers is to reduce the assessment time of development materials. However, over a period of time, the tribometers will produce sufficient data on stator materials, rotor coatings and abrasivity of slurries to enable the creation of a database, which can be cross referenced with field trial data to produce real time component life predictions against cost.

7.8 REFERENCES

1. **M. G. Gee**, "Procedure for ball cratering", NPL Report MATC(A)52, March 2001
2. **R. K. Schmid, M. S. Cropper & M. Mohanty**, "*Increasing pump life in abrasive service through state-of-the-art surface protection*", Proc. of 17th Int. Pump Users Symp., 2000, pp 87 - 101
3. **E. Rabinowicz, L. A. Dunn & P. G. Russell**, "*A study of abrasive wear under three-body conditions*", Wear 4, 1961, pp 345 - 355
4. **A. Adachi & I. M. Hutchings** "*Wear-mode mapping for the micro-scale abrasion test*", Submitted to Wear for publication, 2003
5. **R. C. Tucker, Jr. & A. E. Miller**, "*Low stress abrasive and adhesive wear testing*", Selection and use of wear tests for metals, ASTM STP 615, Bayer, R.G., Ed., American Society for Testing and Materials, 1976, pp 68 – 90
6. Private communication with Mono Pumps Ltd.
7. **K. L. Rutherford & I. M. Hutchings**, "*Theory and application of a micro-scale abrasive wear test*", J. Test. Eval. 25, 1997, pp 250 – 260
8. **S. Wirjanupatump & P. H. Shipway**, "*A direct comparison of wet and dry abrasion behaviour of mild steel*", Wear 233 – 235, 1999, pp 65 – 665
9. **P. A. Swanson & R. W. Klann**, "*Abrasive wear studies using wet and dry rubber wheel abrasion tests*", Wear of Materials, 1981, pp 379 – 388
10. Private communication with J. Eaves, The Pump Centre, 05.11.01
11. **P. H. Shipway**, "*The role of test conditions on the micro-abrasive wear behaviour of soda-lime glass*", Wear 233 – 235, 1999, pp 191 – 199
12. **R. I. Trezona & I. M. Hutchings**, "*Three-body abrasive wear testing of soft materials*", Wear 233 – 235, 1999, pp 201 – 221
13. **I. Finnie**, "*Erosion of surfaces by solid particles*", Wear 3, 1960, pp87 - 103

Conclusions & recommendations for further work

8.1 CONCLUSIONS

A new wear model has been proposed to describe the wearing process in the pumping element of a progressive cavity pump operating under purely abrasive conditions. There are several important features to this model;

- (i) the wearing process is initiated by two characteristic wear features in the stator
- (ii) the wear to the rotor develops in distinct bands which follow the contour of the helix
- (iii) the wear to the rotor is a direct consequence of the wear features in the stator
- (iv) the severity of the wear is strongly dependent on particle size
- (v) the wear bands and the seal lines are two distinctly different entities

The new model proposes that the wear process, in the pumping element, is initiated by the creation of two stator wear regimes, identified as type 'a' and 'b', which are two pairs of helical bands, located either side of the centre of the stator minor. The bands consist of a micro-layer texture of cuts/flaps, holes/pits and embedded particles. Continual rotating and sliding movement of the rotor over these regions results in two-body abrasive type wear to the rotors, which generates macro-scale grooves in the rotor if the surface does not have sufficient resistance to prevent the cutting action. The macro-grooves lie in distinct bands along the helix of the rotor scroll. Subsequent damage then occurs to the stator from the sharp edges of the macro-grooves cutting into the soft rubber. The wearing process, once initiated, is self-perpetuating but requires the presence of abrasive particles to initiate.

It is proposed that there are three conditions of wear, whose limits can be defined as $d < x_1$; $x_1 < d < x_2$; $d > x_2$, where d is the nominal particle diameter and x_1 and x_2 are critical particle sizes. For every size of pump, there is a critical particle size range, that will cause maximum wear to the pumping element components, whose upper and lower limits are described by x_1 and x_2 .

The wear rate of the rotor, and the severity of the type 'a' stator wear regime, were found to be strongly dependent on operational speed of the pump, which agrees published data.

However no evidence was found to directly relate fluid velocity or particle velocity with increasing wear rates.

Applying a differential pressure across the pumping element induced an additional wear mechanism of low impingement solid particle erosion, causing a wear process, most commonly described as, 'slip'. The presence of slip appeared to reduce the severity of the type 'a' and 'b' wear regimes in the stator and thus, over a period of time would in fact reduce the amount of grooving wear imposed on the rotor. However any positive effect was found to be counteracted by the additional erosive mode of material removal, occurring across the dynamic seal lines.

Reducing the contact pressure between the rotor and stator was found to have a detrimental effect on both components. It increased the width of, and the amount of particles embedded in, the type 'a' and 'b' stator wear regimes which consequently increased the width of the wear bands on the rotor.

For a rotor surface to prolong the operational life of the pumping element, its primary function is to resist the cutting action of the embedded particles in the stator. Hardness, alone, was found to be an insufficient material property to use as a measure of a coatings ability to resist two-body abrasion.

Whereas classical abrasion theories had limited use in modelling the wear resistance of the rotor surfaces, they were found to be inadequate in describing the whole wearing process of the pumping element, due to the unique interaction of the rotor, stator and abrasive particles. A further model is required to describe the probability of a particle to embed into the stator wall.

The design criteria for two tribometers has been outlined that will specifically meet the unique requirements of the tribological system in the pumping element of a progressive cavity pump. To simulate the stator wear, a slurry jet erosion test is recommended, whilst a dry pin-on-disk is concluded to be suitable for the accelerated assessment of rotor coatings.

8.2 RECOMMENDATIONS FOR FURTHER WORK

8.2.1 *Development of the wear model for progressive cavity pumps*

The new wear model was based upon experimental data from one specific size of progressive cavity pump, for which the upper and lower critical particle sizes were derived. However, a vast size range of progressive cavity pumps is available, with size selection depending upon flow requirements, solid concentration and the size of abrasive particles. Consequently, further work is required to determine whether the critical particle sizes are dependent on the size of the pump, and if so, to quantify the type of relationship. For this it is recommended to pump a range of particles sizes using pumps with rotor minor diameters of 60mm and 100mm, under purely abrasive conditions at operational speeds

The type of progressive cavity pump used in the simulated wear test rig was a single stage with a standard pitch length. To further validate the wear model, it is recommended that wear tests are performed using an extended pitch rotor and stator, and a two- and four-stage pump. To determine the effects of an extended pitch the type 'a' and 'b' stator wear features should be compared to those that were generated under the standard test conditions. To determine how increasing the length of the pump effects particle behaviour, wear tests should be performed against discharge pressure, from 6 to 12 bar for the two-stage pump, and 12 to 24 bar for the four-stage pump, at increments of 2 bar. The stators should then be sectioned at half pitch intervals, and the wear features compared to those from the pressure tests on the single stage pump in this study.

It was demonstrated that the wearing process required the creation of the two helical wear regimes, 'a' and 'b', in the stator and that elimination of these features prevented the process from initiating. Therefore it is recommended to investigate possible ways to prevent, or reduce, the effects, of these two wear regimes, such as 'constant wall thickness' stators, different stator materials or a change in the pumping element geometry.

The severity of the wear on the coated rotors compared to that achieved by the laboratory tests suggests that the loading imposed by the particles, in the pumping element, was far greater than originally thought, based on the assumption that wear is directly proportional to load. The primary load between the rotor and stator was taken as that created by the interference fit between the two components. However, the postulation that a wave is created to accommodate the displaced rubber, potentially changes the loading conditions. Consequently, further investigation is required to determine how the formation of the wave

contributes to the loading conditions at the point of contact between the embedded particles and the rotor.

8.2.2 Development of the tribometers

(i) Stator tribometer

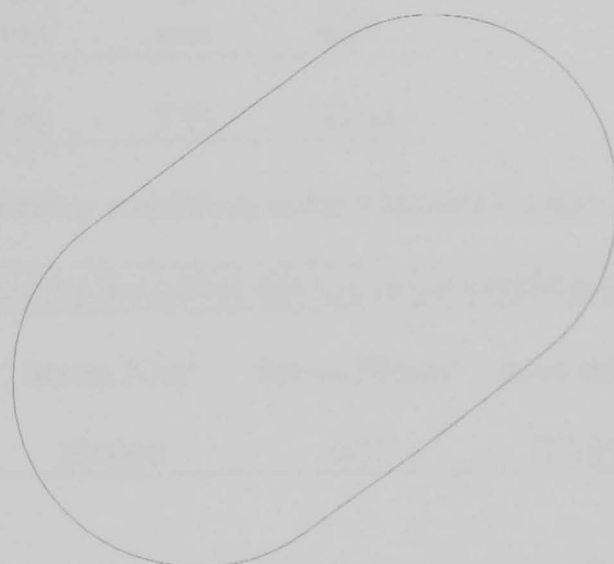
Modifications to the slurry jet erosion test apparatus are necessary to contain the off-spray and the ease at which the rig can be used. The specimen holder needs to be changed so that the off-spray is re-directed downwards and a door inserted into the splash back to enable better access to the specimen holder. These can either be done to the existing equipment or a smaller scale tank and fixtures made to enable the test to be performed within a laboratory environment.

Further evaluation of the variables of impingement angle and impact velocity on nitrile rubber is required to derive a standard test procedure for the assessment of stator materials. The morphology of the generated wear patterns should be examined under a scanning electron microscope and compared with the type 'a' wear regime in the stators tested using the same particle type, to establish the conditions which create similar features.

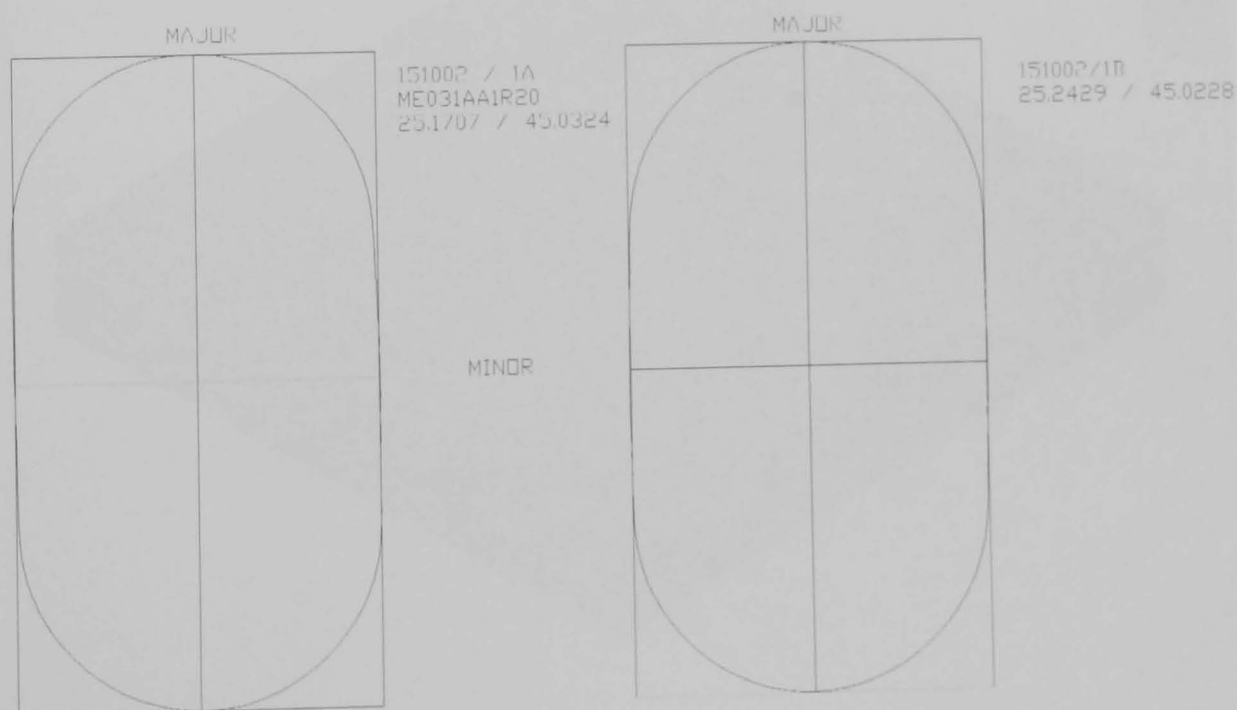
(ii) Rotor tribometer

A pin-on-disk style apparatus is required to be designed and manufactured, with specific care applied to the loading arrangement of the apparatus. Alternatively the apparatus can be purchased from a suitable suppliers, such as Phoenix Technology Ltd.

Appendix A (a): Example of profile of a stator from the Mitutoyo CHN1008 co-ordinate measuring machine



Appendix A (b): Example of an AutoCAD drawing for determining the major and minor dimensions of the stator



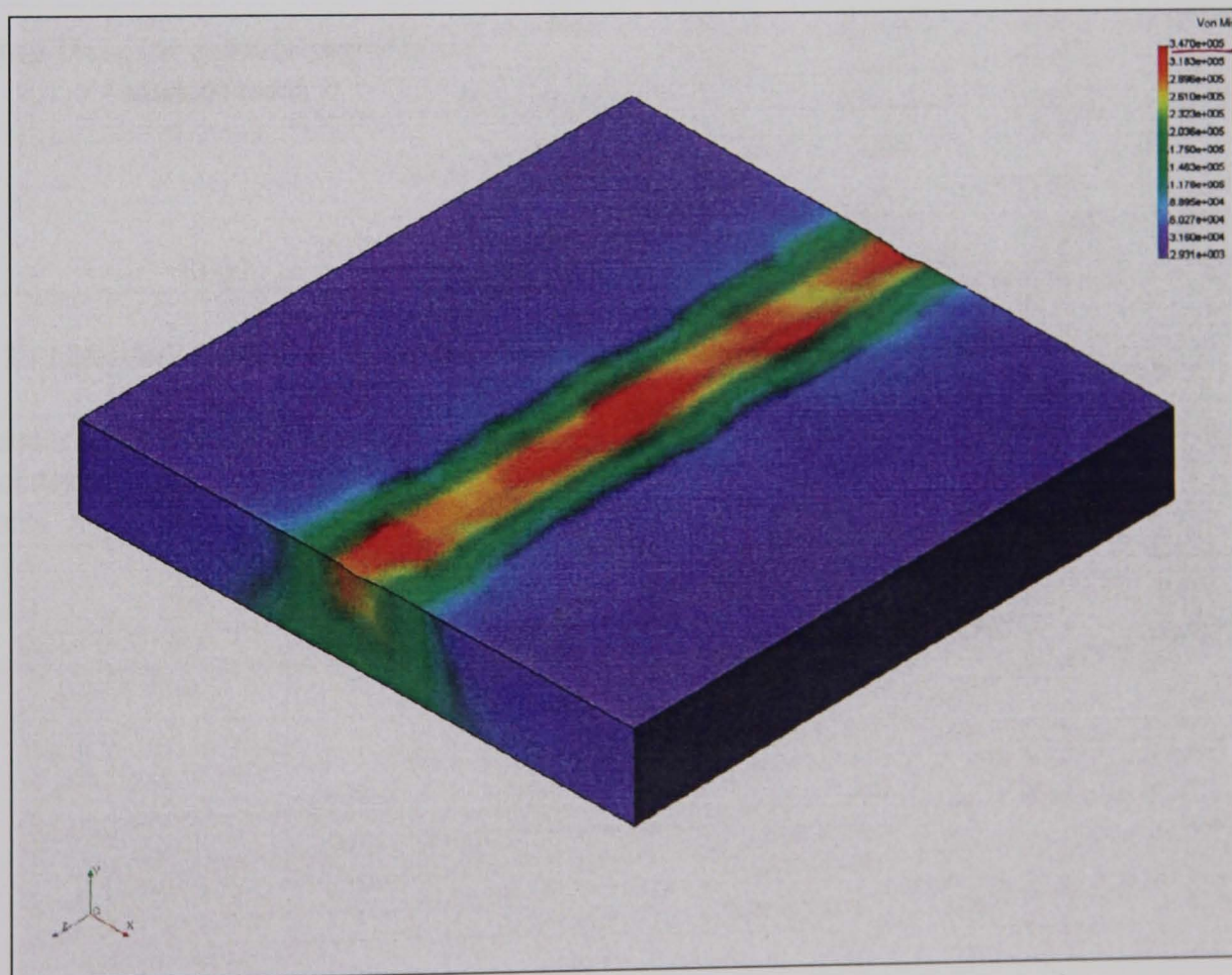
Appendix B: Data for calculating the particle loading conditions*(a) To calculate the contact area for the particle loading model*

Bar Dia D mm	Deflection h mm	Length L mm	Chord s mm	Area A mm ²
26	0.5	100	7.23	723.44

(b) To calculate particle loading conditions using COSMOS computational analysis

Force = resultant load applied by the rubber due to a radial interference of 0.5mm

	Stress N/m ²	Stress N/mm ²	Area mm ²	Force N
Minor	250000	0.25	723.44	180.75

(c) Stress analysis plot of particle loading model, showing stress distribution for a 0.5mm deflection

(d) To calculate particle loading conditions using theoretical derivation

Force = resultant load applied by the rubber due to a radial interference of 0.5mm					
Mk0 Rotor (mm)	Major	35.75	Minor	26	
Stator (mm)	Major	45	Minor	25	
Breakout torque		25000 Nmm			
Rotor major radius		17.875 mm	(Length of maximum moment arm)		
Breakout force		1398.601 N			
Width of seal line		7.37 mm			
Length of seal line		174.6644 mm			
Contact area of ribbons		2574.553 mm ²	(Types a & b)		
Contact area of capsulism seal lines		868.2577 mm ²	(Type c)		
Total contact area		3442.811 mm ²			
Co-efficient of friction		3			
Reaction Force		466.2005 N			
Reaction Stress		0.135413 N/mm ²			
Pump Data for calculating contact area of seals	Ecc	Rotor Pitch	Rotor Scroll Minor Dia	Rotor Scroll Length	Rotor Helical Length
	e (mm)	Pr (mm)	d (mm)	Ls (mm)	Ir (mm)
E031	4.8750	65.0000	26.0000	158.000	174.6644

(e) To calculate particle loading conditions using experimental analysis

Rubber Thickness	Bar Dia D	Deflection h	Length L	Force F	Chord s	Area A	Stress S
mm	mm	mm	mm	N	mm	mm ²	N/mm ²
15	26	0.5	100	272	7.23	723.44	0.38
10	26	0.5	100	475	7.23	723.44	0.66
5	26	0.5	100	808	7.23	723.44	1.12

(f) Load vs. deflection plot for particle loading model at varying rubber thickness '(th)

